2008

Design, Synthesis and Biological Evaluation of a Family of Excitatory Amino Acid Transporter 3 (EAAT3) Preferring Inhibitors

Terri Lynn Mavencamp
The University of Montana

Design, Synthesis and Biological Evaluation of a Family of Excitatory Amino Acid Transporter 3 (EAAT3) Preferring Inhibitors.

By

Terri Lynn Mavencamp

Boston University, Boston, MA, 2003

Dissertation

presented in partial fulfillment of the requirements
for the degree of

Doctor of Philosophy
in Neuroscience

The University of Montana
Missoula, MT

Autumn 2008

Approved by:

Dr. David A. Strobel, Dean
Graduate School

Dr. Christopher S. Esslinger
Department of Biomedical and Pharmaceutical Sciences

Dr. Richard J. Bridges
Department of Biomedical and Pharmaceutical Sciences

Dr. Diana I. Lurie
Department of Biomedical and Pharmaceutical Sciences

Dr. Mark L. Grimes
Division of Biological Science

Dr. Michael P. Kavanaugh
Department of Biomedical and Pharmaceutical Science

Acknowledgments

First I would like to thank my mentor Sean Esslinger, who is the reason I continued my education in science. His excitement and enthusiasm towards chemistry is truly contagious. I can't imagine a more inspiring, understanding mentor. I would also like to thank Rich Bridges who went over papers, grants, abstracts and outlines line by line and always made me feel welcome at group meetings or in his office. Special thanks to the rest of my committee, Mike, Diana and Mark for all of your time and advice. Mike thanks for welcoming me into your lab and sharing your expertise and time.

I would like to thank all of the people who put countless hours towards this project, Fred Rhoderick for doing the assays, David Holley for walking me through the modeling, Sarje Patel for explaining kinetics over, and over again. My wonderful lab mates, Brent Lyda, you're a treasure chest of information and help. Ben your humor and understanding brightened many days. August, what can I say? I miss you since you've gone to the dark side but I'll miss you more in Madison. Mel thanks for all the dinner science sessions-you're the best!

Thanks to my family, my sisters and my best friends, thanks for being there all ways, always. B, my bestest buddy and my true companion, thanks for being the wonderful person you are.

Table of Contents

List of Figures

List of Tables

Manuscripts:

List of Schemes

Manuscripts:

1.1 The Glutamatergic System

L-Glutamate is the primary excitatory neurotransmitter in the mammalian central nervous system (CNS). It is capable of participating in standard fast synaptic communication, as well as in higher order signal processing linked to development, synaptic plasticity, learning and memory (Balazs, Bridges and Cotman, 2006). Excessive concentrations of glutamate can overstimulate the excitatory amino acid (EAA) receptors, leading to cell damage and eventual cell death (excitotoxicity). Excitotoxicity is believed to play key roles in disorders of the CNS including: stroke, epilepsy, spinal cord injury, ALS, and Alzheimer's disease (for reviews see: Rao and Weiss 2004; Won *et al.,* 2002; Malva *et al.,* 2003; Hynd *et al.,* 2004). The primary regulators of extracellular glutamate in the CNS are the excitatory amino acid transporters (EAATs), which are capable of influencing the amount and/or time course that L-glutamate is in contact with the excitatory amino acid (EAA) receptors.

The glutamate-glutamine cycle is a crucial component of neuronal communication (Berl *et al*., 1968). It begins with the packaging of glutamate into vesicles via the vesicular glutamate transporter (VGLUT) (for a review see: Takamori, 2006). Action potentials in the presynaptic neuron cause the concentration of intracellular calcium to increase. The calcium binding protein, calmodulin (CaM) activates CaM Kinase II which phosphorylates synapsin I. Phosphorylation of synapsin I decreases the affinity of this protein for the actin cytoskeleton and/or the vesicles and causes the vesicles to undock.

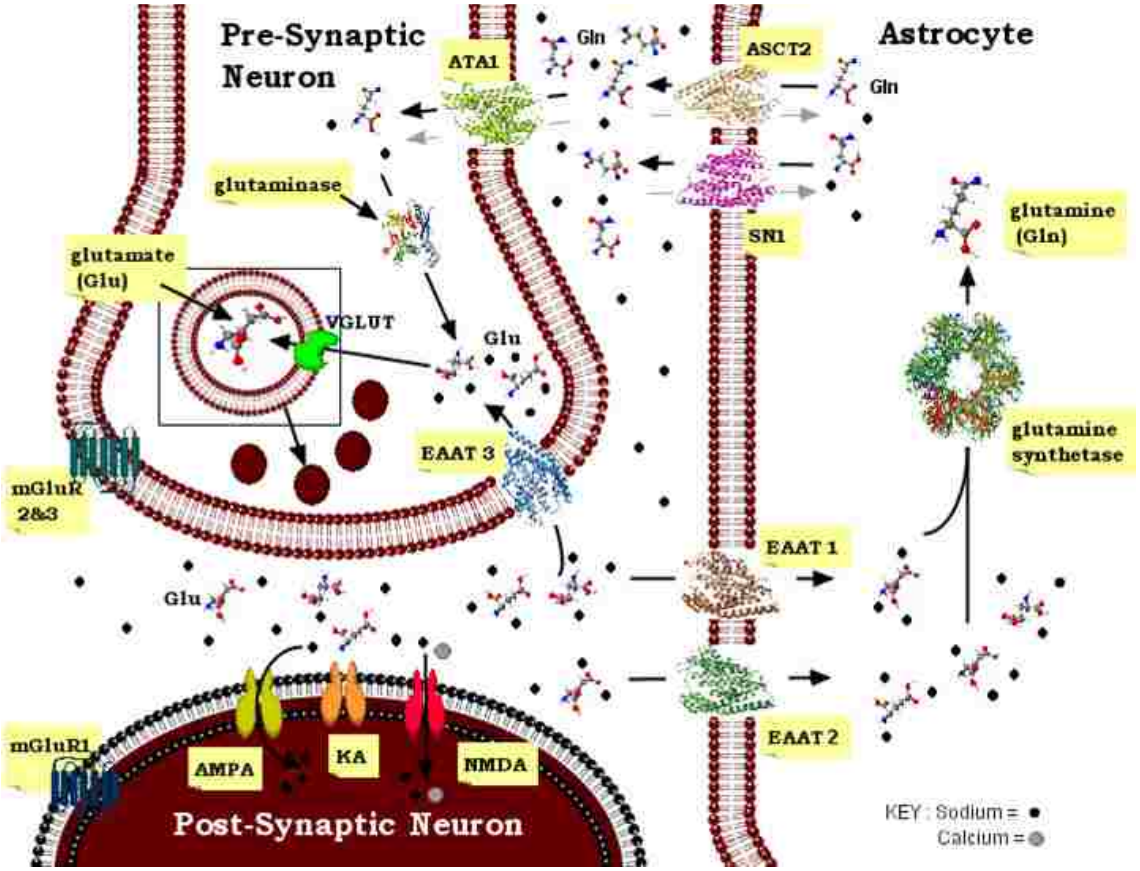

Figure 1. The Glutamatergic Synapse; figure by Brent Lyda of the Esslinger research group.

Simultaneously, calcium causes synaptotagmin, a Ca^{2+} binding protein located on the synaptic vesicle, to prime the vesicle for fusion with the presynaptic membrane. For fusion to occur a trimeric trans-SNARE (soluble *N*-ethylmaleimide-sensitive factor attachment protein receptor) complex must form consisting of the vesicle associated membrane protein (VAMP2 or synaptobrevin) on the synaptic vesicle, and syntaxin-1 and synaptosomal associated protein of 25 KDa (SNAP-25) from the plasma membrane (for a review see: Martens and McMahon, 2008). Upon fusion, the synaptic vesicle membrane is incorporated into the presynaptic membrane and glutamate is released into the synaptic cleft where it can stimulate pre- and postsynaptic glutamate receptors. This translates the chemical signal into an electrical signal either directly by opening ion channels (ionotropic) or indirectly through second messenger systems (metabotropic) (Nakanishi and Masu, 1994).

The EAA receptors are grouped into two categories. The ionotropic receptors AMPA, Kainate and NMDA, named after the selective agonists that act at each receptor: N-methyl-D-aspartate (NMDA), α-amino-3-hydroxy-5-methyl isoxazole-4-propionate (AMPA) and kainic acid (KA) (Figure 2). The metabotropic glutamate receptors mGluR1-5, are G-protein coupled receptors linked to multiple second messenger systems. These two classes of receptors mediate and modulate information transfer at the majority of excitatory CNS synapses (Mayer, 2005; Swanson *et al.,* 2005).

The ionotropic glutamate receptors are a family of heteromeric ligand-gated ion channels that span the plasma membrane. They are believed to mediate the

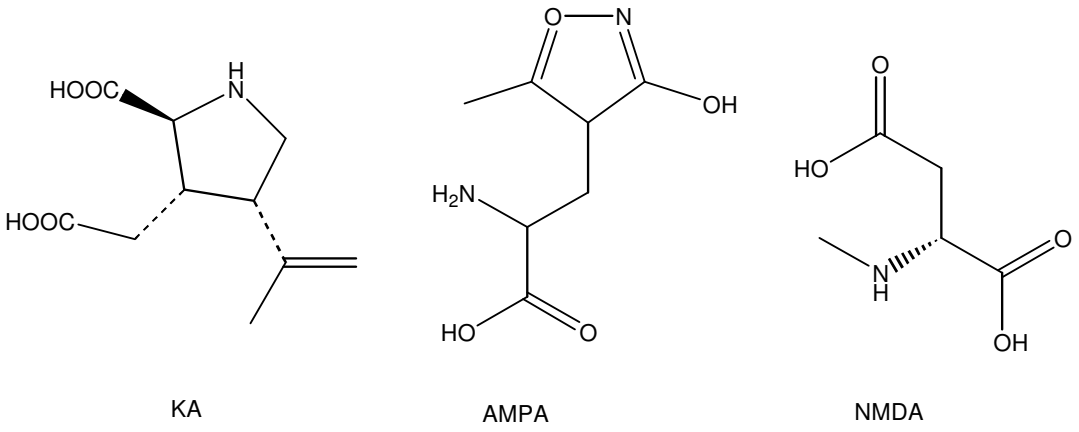

Figure 2. Selective agonists of the glutamate ionotropic receptors.

majority of excitatory neurotransmission in the vertebrate CNS. The binding of L-glutamate causes a conformational change which opens the receptor associated ion channel thereby allowing Na^+ and/or Ca^{2+} to flow into the cell (Armstrong and Gouaux, 2000). If the influx of positive ions sufficiently depolarizes the membrane potential past a critical threshold value of approximately -55mV, measured at the axon hillock, sodium channels open. This allows sodium ions to rapidly enter the cell causing an action potential. Potassium channels, which respond slower than sodium channels restore the membrane potential by allowing potassium to exit the cell. Sodium channels then close, resulting in a short period of hyperpolarization during which the cell is less likely to fire an action potential. The cell then returns to its resting potential of approximately -70 mV.

AMPA and Kainate receptors (AMPARs and KARs) are responsible for mediating fast synaptic transmission (Collingridge *et al.,* 1983; Ganong *et al.,* 1983) and are activated by low frequency stimulation (Davies *et al.,* 1989). AMPARs are responsible for most fast excitatory responses. In addition, the recruitment of AMPARs to the cell surface from an intracellular pool may be an important component of long term potentiation, LTP. LTP is a process whereby synapses become more robust through the insertion of AMPARs into the postsynaptic membrane. This occurs via the calcium/calmodulin dependent protein kinase (CAMKII) which phosphorylates AMPARs in the synaptic membrane. Phosphorylation increases sodium conductance and promotes the migration of AMPARs from intracellular stores to the membrane (Breedlove *et al.,* 2007). This results in the enhancement of AMPAR activation, thereby increasing synaptic current (Luscher *et al.,* 1999; Luthi *et al.,* 1999).

Kainate receptors (KARs) are found throughout the CNS and are present both pre- and post-synaptically. Postsynaptic KARs are believed to carry part of the charge that contributes to the post synaptic response along with AMPARs and NMDA receptors (NMDARs). Presynaptic KARs are hypothesized to regulate neurotransmitter release at inhibitory and excitatory synapses (Rodrigues-Moreno *et al.,* 1997).

The NMDA receptors (NMDARs) contain a Mg^{2+} and a glycine recognition site in addition to a glutamate site. The Mg^{2+} site is situated deep within the channel pore and is removed when the cell is partially depolarized (Flatman *et al.,* 1983) causing NMDARs to respond only after repetitive synaptic activation

(Manabe, 2008). In addition to the removal of the Mg^{2+} block NMDARs require the co-agonist glycine in order to be activated (Johnson and Ascher, 1987). NMDARs are permeable to Ca^{2+}, Na^{+} and K^{+}. The increase in postsynaptic calcium is an important step to activating further processes which may constitute long term potentiation LTP as well as higher cognitive functions such as learning and memory (Cavara and Hollman, 2008).

The metabotropic glutamate receptors are G-protein coupled receptors (GPCRs) of which 8 have been cloned (Nakanishi, 1992; Pin and Duvoisin, 1995). They are subdivided into three groups based on sequence similarity, intracellular signaling mechanisms and pharmacology. Group I mGluRs consist of mGluR1 and mGluR5 and are coupled to phospholipase C-β (PLC-β) and intracellular Ca^{2+} signaling. Group I mGluRs modulate NMDA receptor-mediated synaptic transmission and plasticity and mediate mGluR-dependent plasticity (Cheyne and Montgomery, 2008). Group I mGluRs are primarily expressed at postsynaptic sites. Group II (mGluR2, mGluR3) and group III (mGluR 4,6,7 & 8) inhibit adenylyl cyclase (AC) activity, which results in a decrease in cAMP levels and PKA activity. A decrease in PKA activity is required for the induction of group II mGluR dependent long term depression. Group II mGluRs are expressed both pre- and post-synaptically and Group III mGluRs are expressed primarily at presynaptic sites where they regulate neurotransmitter release (Reviewed in Kim *et al.,* 2008).

In order to prevent overstimulation of the glutamate receptors, which can lead to excitotoxicity, glutamate must be quickly cleared from the synaptic cleft.

This occurs via diffusion or by EAAT mediated substrate uptake (Auger and Attwell, 2000; Huang and Bergles, 2004). The EAATs, of which 5 have been identified to date, are expressed in glial cells (EAAT1 and EAAT2) and in neurons (EAAT3, EAAT4 and EAAT5).

Once glutamate has been transported into the astrocyte by EAAT1 and/or EAAT2, it is converted to the neutral amino acid glutamine by glutamine synthetase. Glutamine can then be transported out of the astrocyte by SNAT3 (SN1), a system N amino acid transporter localized to perisynaptic astrocytes. Glutamine is thought to be transported into the neuron by (SNAT1 & SNAT2), system A transporters, though the localization of these transporters is mainly in the somatodendric domain and rarely axon terminals (Cont and Melone, 2006). In addition, the inability of system A inhibitors to affect basal transmission suggest that transporters not yet identified may be responsible for the uptake of glutamine into the neuron (Kam and Nicoll, 2007).

The glutamatergic system has a central role in excitatory signaling in the CNS. Glutamate levels must be tightly regulated to maintain excitatory signaling as well as to prevent the overstimulation of the glutamate recpetors. Regulation of this system relies on multiple factors, one being the rapid clearance of glutamate from the synaptic cleft by the glutamate transporters.

1.2 Characterization, Localization and Function of the EAATs

Historically, the glutamate transporters have been grouped into three categories depending upon their substrate specificity: the C-4 dicarboxylate transporters found in bacteria, the glutamate/aspartate transporters found in bacteria and eukaryotes and the neutral amino acid transporters also found in bacteria and eukaryotes (Slotboom *et al.,* 1999).

Recently, the glutamate transporters have begun to be classified according to the Human Genome Organization (HUGO) nomenclature. The five glutamate transporters EAAT1-5, which share 50-60% amino acid homology, along with two neutral amino acid transporters ASCT1 and ASTC2, comprise the solute carrier family 1 (SLC1). EAAT1 is encoded by the gene SLC1A3, EAAT2 by SLC1A2, EAAT3 by SLC1A1, EAAT4 by SLC1A6 and EAAT5 by SLC1A7, ASCT1 by SLC1A4 and ASCT2 by SLC1A5 (Kanai and Hediger, 2004).

The five glutamate transporters have been identified by molecular cloning and functional expression. EAAT1-5 have been isolated and cloned from mammalian tissue: GLAST (glutamate and aspartate transporter 1) and GLT1 (glutamate transporter 1) from rat brain (Storck *et al.,* 1992; Pines *et al.,* 1992) and EAAC1 (excitatory amino acid carrier 1) from rabbit small intestine (Kanai & Heidger, 1992). The almost simultaneous cloning of these three transporters was quickly followed by the cloning of the corresponding human homologues by Arriza, who suggested using a standard naming system, the excitatory amino acid transporters (EAATs), of which EAAT1 is the human homologue of GLAST1,

EAAT2 of GLT1 and EAAT3 of EAAC1 (Arriza *et al.*, 1994). Four additional transporters were quickly isolated using homology screening, EAAT4 from the retina, EAAT5 from the cerebellum (Fairman *et al.,* 1995; Arriza *et al.,* 1997), and the two neutral amino acid transporters of the SCL1 family; ASCT1 and ASCT2 (Alanine, Serine and Cysteine Transporters 1 and 2) (Arriza *et al.,* 1994).

The EAATs are found throughout the brain and periphery with enrichment in certain tissues and brain regions depending on the specific EAAT. EAAT1 is expressed throughout the brain with high levels in the heart and skeletal muscle and lower levels in the placenta and lung. EAAT2 expression is largely restricted to the brain with low levels found in the placenta. EAAT3 is expressed throughout the brain with high levels in the kidney and lower levels expressed in the lung, placenta, liver, muscle and heart (Reviewed in Danbolt, 2001).

In the CNS, EAAT1 and EAAT2 are expressed on glial cells and EAAT 3 and EAAT4 on neurons. The glial transporters, EAAT1 and EAAT2 and the neuronal transporter EAAT3 are the primary transporters of synaptic glutamate (Arriza *et al.,* 1994). They are found throughout the brain with enrichment in differing regions.

EAAT1 is the primary transporter of glutamate in the cerebellum where it is found in high levels in Bergmann glia. EAAT1 is also found in lower levels throughout the CNS. Mice deficient in mEAAT1 are susceptible to cerebellar injury and display reduced motor coordination (Watase *et al.,* 1998).

EAAT2 is the dominant glutamate transporter throughout the CNS except in the cerebellum where EAAT1 dominates. EAAT2 expression is particularly

high in the hippocampus, lateral septum, cerebral cortex and the striatum (Lehre *et al.,* 1995; Chaudhry *et al.,* 1995). EAAT2 is found on most astrocytes throughout the CNS, and on all astrocytes in the neocortex, striatum and thalamus. Mice deficient in mEAAT2 are susceptible to lethal spontaneous seizures and acute forebrain injury (Tanaka *et al.,* 1997).

EAAT3 is enriched in the hippocampus, cerebellum and basal ganglia, though the levels of EAAT3 protein are much lower than the other glutamate transporters (Haugeto *et al.,* 1996). EAAT3 has a unique distribution, being found over neuronal bodies and processes as well as presynaptically at GABA terminals (For a review see Nielullon *et al.,* 2006). The localization of EAAT3 to presynaptic GABAergic terminals implicates it as a source of glutamate for GABA synthesis (Sepkuty *et al.,* 2002). The perisynaptic localization of EAAT3 suggests that this transporter helps to regulate spillover, in addition EAAT3 may be the major route for neuronal cysteine uptake (Zerangue and Kavanaugh 1996b; Himi *et al.,* 2003), a necessary precursor for neuronal glutathione synthesis (Aoyama *et al.,* 2006). Glutathione is a major antioxidant, directly linked to the metabolism of nitrosyl oxidants and peroxide (Dringen, 2000). EAAT3 knock-out mice present significantly reduced spontaneous locomotor activity at 12 months of age but otherwise the CNS appears normal. A major dysfunction of EAAT3 knock-out animals is the onset of dicarboxylic aminoaciduria due to the loss of uptake from the renal tubules by EAAT3 (Peghini *et al.,* 1997).

The highest expression of EAAT4 is found in cerebellar Purkinje cells with very low levels expressed in the hippocampus, neocortex, striatum, brain stem and thalamus (Furuta *et al.,* 1997; Reviewed in Danbolt, 2001). EAAT4 is hypothesized to remove extracellular glutamate that is not cleared from the synapse by EAAT1-3 (Mim *et al.,* 2005). In Purkinje cells EAAT1 seems to be the major contributor to the uptake of glutamate from the synaptic cleft and EAAT4 appears to remove low concentrations of glutamate that escape the glial transporters, thereby preventing glutamate spillover to neighboring synapses (Takayasu *et al.,* 2005).

EAAT5 is restricted to the retina where it is found in cone and rod photoreceptor terminals and in axon terminals of rod bipolar cells (Fairman *et al.,* 1995; Rothstein *et al.,* 1994; Arriza *et al.,* 1997; Localization reviewed in detail in Danbolt, 2001). Here, EAAT5 has a unique role and is believed to act as a presynaptic receptor in mouse bipolar cells and may play a major role in controlling the output from these cells (Wersinger *et al.,* 2006).

1.3 Transport Mechanisms and Molecular Structure of the EAATs

It is estimated that glutamate transporters can concentrate glutamate $5x10^6$ fold in cells under physiological conditions (Zerangue and Kavanaugh, 1996a). In order to accomplish this, the EAATs couple the transport of glutamate into the cell to the influx of 3 sodium ions and one proton (for review see; Danbolt, 2001; Kanai and Hediger, 2004). The transporter returns to the extracellular side of the membrane by coupling this movement to the transport of one potassium ion (Zerangue and Kavanaugh, 1996a). In this manner the EAATs harness energy derived from the concentration gradients of sodium and potassium, to import glutamate into the cell and to return to the extracellular side of the plasma membrane.

In addition to the transport current, substrate applied to the EAATs creates a substrate gated anion conductance that is not stochiometrically linked to glutamate transport (Fairman *et al.,* 1995; Wadiche *et al.,* 1995). The anion current is a small component of the EAAT1-3 total current associated with the transporter. In contrast, the current associated with EAAT4 and EAAT5 is almost entirely made up of the anion current. This suggests that the primary role of EAAT4 and EAAT5 may be to regulate cellular excitability via glutamate gated anion channels (Torres-Salazar and Fahlke, 2007).

Advancements in determining the structure of the EAATs has been made through the crystallization of a glutamate transporter homologue from *Pyrococcus horikoshii* (Glt_{ph}), a sodium dependent aspartate transporter, which

shares a 37% amino acid identity with human EAAT2. The transporter homologue was recently crystallized with bound aspartate (closed state) and the glutamate transport inhibitor *threo*-β-benzoylaspartic acid (bound TBOA, open state). An advantage of having crystal structures of the transporter in these two states is the mechanistic information it affords (Yernool *et al.,* 2004; Boudker *et al.,* 2007).

Data suggests that the transporter is a trimer with a bowl shaped basin facing the extracellular space (Figure 3). Three binding sites lay at the bottom of the basin, each gated by two loops. Helical hairpin loop 1 (HP1) acts as the intracellular gate and helical hairpin loop 2 (HP2) acts as the extracellular gate. The substrate binding site is located about 5 Angstroms below the bottom of the aqueous basin buried in a polar cavity formed by the tips of HP1 and HP2, the unwound region of transmembrand 7 (TM7) and polar residues of transmembrane 8 (TM8). HP2, which acts as the extracellular gate is initially in the open position, allowing access of the extracellular solution to the aqueous basin. The authors predict that two sodium ions bind with aspartate, one sodium coupled to HP1, below aspartate, and the other coupled to HP2, above aspartate. The sodium ions are hypothesized to help stabilize the loops. Binding of two sodium ions and substrate induces the HP2 loop to close, giving the "occluded" state. Next, the HP1 loop opens to create an aqueous pathway to the cytoplasm. When HP1 opens, HP2 moves into the space previously occupied by HP1 in order to prevent an open pore thereby allowing "alternating access" from

the extracellular to intracellular sides of the membrane (Yernool *et al.,* 2004; Boudker *et al.,* 2007).

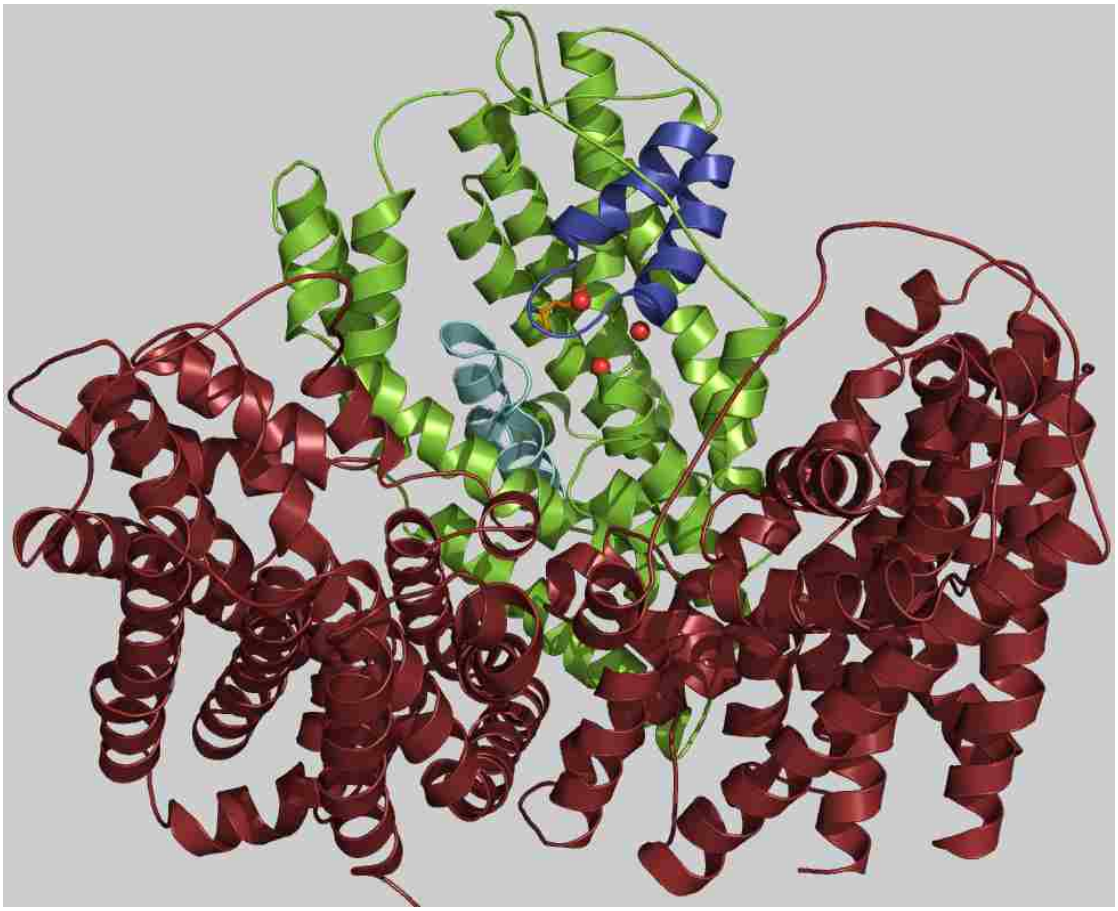

Figure 3. EAAT3 homology model shown with three bound sodium ions and aspartate bound in one of the three active sites.

In addition to structural information, the crystal structure lends insight into the manner in which ligands recognize and bind to the active site. TBOA and aspartate were observed to bind by the same recognition points, thereby validating that TBOA works in a competitive manner, as well as giving credence to the modeling based on the belief that the protein recognizes compounds by at

least 3 points; the α carboxyl group, C1; the distal carboxyl group, C2 and the nitrogen, N (Esslinger *et al.,* 2005). The bulky aromatic group of TBOA is believed to interfere with the closing of HP2, effectually blocking further conformational changes (Boudker *et al.,* 2007). This interference may result in the observed inhibitory acitivity of TBOA. Figure 4 illustrates this point by showing TBOA in the active site of the EAAT3 homology model. The homology model was created by aligning the EAAT3 sequence (Yernool *et al.,* 2004) to the crystal structure coordinates of Glt_{ph} TBOA bound (Boudker *et al.,* 2007).

Valuable information, such as the generation and analysis of EAAT homology models, can be extracted from the Glt_{ph} crystal structures. This information can be used to examine the basic structure of the EAATs as well to determine where changes in amino acids surrounding the binding site may affect substrate binding across the different EAATs. In spite of the wealth of information the EAAT homology models afford, the template from which this information is based upon, *Pyrococcus horikoshii*, remains a generic model of the EAATs. By itself, it is not sufficient to delineate the subtle variations between the individual EAAT binding sites.

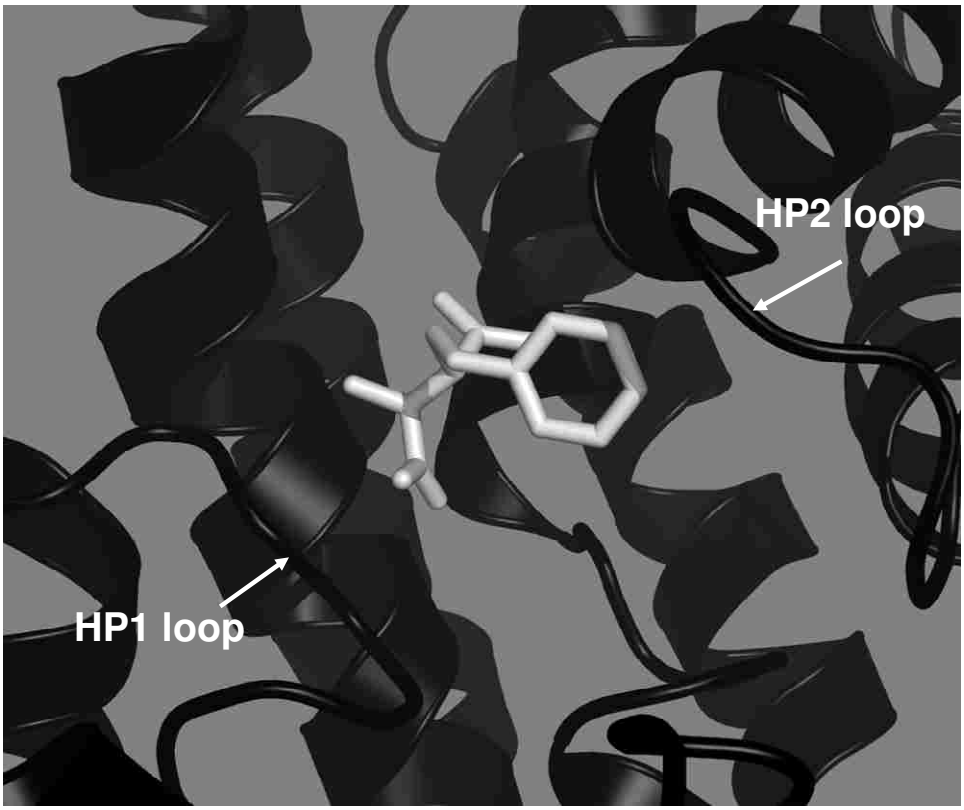

Figure 4. TBOA in the active site of the EAAT3 homology model (threading done by Holley D. and Mavencamp T.).

1.4 Molecular Pharmacology of the EAATs

In order to determine the subtle differences between the individual EAAT subtypes, selective inhibitors can be employed. By examining the structure activity data of compounds at the EAATs, hypotheses about individual binding sites can be formed. These hypotheses can be tested by the synthesis of new analogues designed from the analysis of structure activity data of previous inhibitors. This method aids in elucidating the subtleties of the individual EAAT binding sites and often results in more selective and potent inhibitors with each round of synthesis.

Molecular pharmacology played an important role in the initial characterization of the EAATs. Radiolabeled glutamate was used early on to examine the substrate specificity of the EAATs. It was found that other neurotransmitters did not affect glutamate transport but that L-glutamate, D-aspartate and L-aspartate (Figure 5) are good substrates (Ki = 1-10μM) and that D-glutatmate is not transported (Ferkany and Coyle, 1986; Rauen *et al.,* 1992; Arriza *et al.,* 1994).

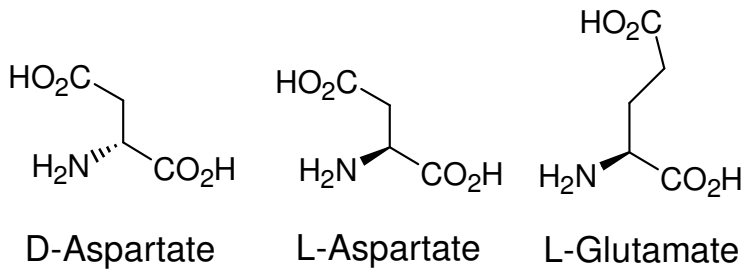

Figure 5. Natural amino acid substrates

The first EAAT inhibitors were mostly developed via simple modifications to known substrates and thus, many showed substrate activity. The downfall of using substrates to characterize the EAATs is that substrates induce heteroexchange, a process whereby exogenously applied substrate induces the efflux of internal substrate. Heteroexchange may increase the amount of glutamate in the synaptic cleft making it difficult to study the role of the EAATs (Shigeri *et al.,* 2004).

One of the first analogues used to characterize glutamate uptake by the EAATs was β-*threo*-hydroxyaspartate (THA) shown in Figure 6 (Fletcher and Johnston, 1991; Bridges and Esslinger, 2005). THA, a competitive substrate of EAAT1-4 and a non-substrate inhibitor of EAAT5, is one template for EAAT inhibitors that has been used as a lead molecule in the development of many potent and selective inhibitors. TBOA, one of the first β-carbon substituted analogues of THA, continues to be the most widely used non-substrate inhbitior of the EAATs. The L-enantiomer of TBOA is the more potent enantiomer with IC_{50} values of 23 μM, 3.8 μM and 7 μM for EAAT1-3, respectively (Shimamoto *et al.,* 1998; Sakaguchi *et al.,* 2004). Modifications to the aryl moiety of TBOA (Figure 6) generally increase the potency over TBOA while retaining non-substrate activity. Replacing the benzyl moiety of TBOA with a naphthyl moiety (L-TNOA1 and L-TNOA2) yields IC_{50} values of 15 μM, 1.3 μM and 4.8 μM for L-TNOA1 and 16 μM, 2.2 μM and 6.5 μM for L-TNOA2 (Shimamoto *et al.,* 2000). To date the most potent TBOA analogue, (2S,3S)-3-{3-[4-[trifluoromethyl)benzoylamino]benzyloxy}aspartate (TFB-TBOA, Figure 6)

displays IC_{50} values of 22 nM, 17 nM and 300 nM for EAAT1-3, respectively (Shimamto *et al.,* 2004).

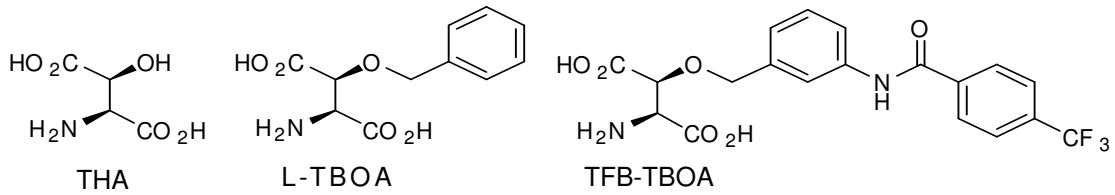

Figure 6. β-threo hydroxy aspartate and derivatives.

Another approach to inhibitor design is to utilize conformationally constrained analogues. This allows for the better prediction of functional group positions as well as decreases the possible binding conformations, which often leads to an increase in selectivity. This method has been shown to be quite robust at enhancing the potency and selectivity of analogues at EAAT2 (Bridges and Esslinger, 2005).

Pyrrolidine dicarboxylate (PDC) and PDC derivatives are conformationally constrained analogues of glutamate similar in structure to dihydrohainate (DHK), an analogue of kainic acid (Figure 7). Kainic acid was isolated in 1953 from red algae in Japan and is a potent, specific agonist of the Kainate Receptor. DHK is an EAAT2 selective non-substrate inhibitor which not surprisingly shows cross reactivity at the Kainate Receptors due to its similarity to KA (Shimamoto *et al.,* 1998).

The PDC derivatives, 2,4 and 2,3 dicarboxylate PDC, were designed as conformationally constrained mimics of glutamate and aspartate, respectively.

The lead molecule, L-trans-2,4 PDC, is a substrate of EAAT1-4 and a non-substrate of EAAT5. When a methyl group is introduced at the 4 position of 2,4 PDC (4-Me-L-trans 2,4 PDC) the compound exhibits increased potency and can no longer be translocated at EAAT2, transforming the substrate to a non-substrate inhibitor. By switching the position of the carboxylate group of L-trans-2,4 PDC from the 4 position to the 3 position (L-trans-2,3 PDC), the selectivity for EAAT2 increases approximately 10 fold (K_i in *Xenous* Oocytes of roughly 12 μM) and displays non-substrate activity at EAAT1-4 (Willis *et al.,* 1996, Bridges *et al.,* 1999). In order to gain insight into the binding site of EAAT2 and in particular to elucidate the differences between substrate and non-substrate inhibitors a pharmacophore model was created. A pharmacophore model is "the ensemble of steric and electrostatic features of different compounds which are necessary to ensure optimal supramolecular interactions with a specific biological target structure and to trigger or to block its biological response" (Langer and Wolber, 2004). An overlay of EAAT2 substrate inhibitors revealed a tight overlap of the α-amine, α-carboxyl and distal carboxyl groups as well as a constrained volume that the backbones occupied within the binding site. When non-substrate EAAT inhibitors were fit onto the model, such as DHK and TBOA, the non-substrate inhibitors aligned with the α-amine, α-carboxyl and distal carboxyl groups but had density outside of the volume taken up by the substrates (Koch *et al.,* 1999; Esslinger *et al.,* 2002; Esslinger *et al.,* 2005). These results suggest that the steric bulk outside of the volume taken up by substrates is responsible for the non-substrate activity.

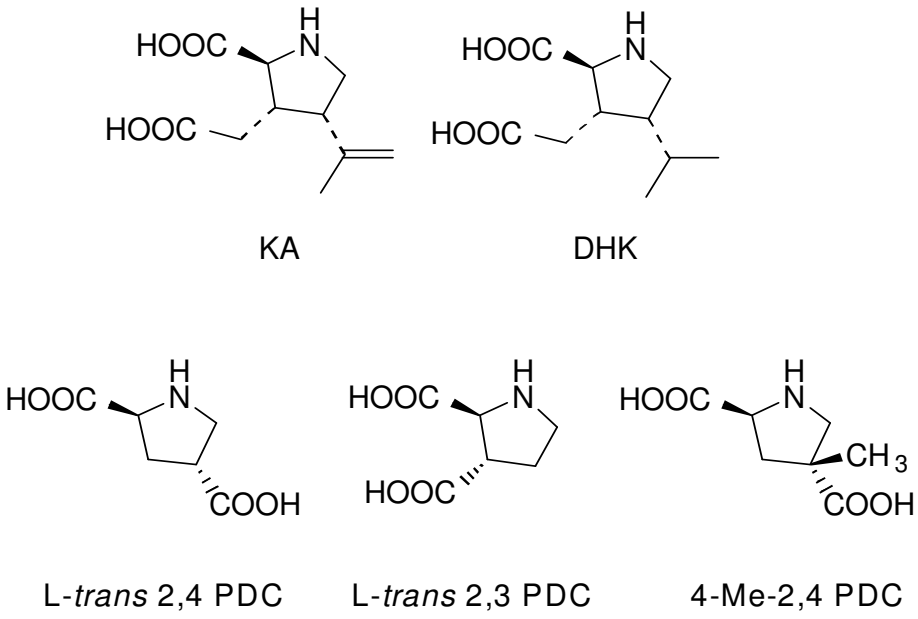

Figure 7. Pyrrolidine dicarboxylates.

In addition to steric bulk, the preferred conformation of the analogue plays an important role in how well the compound will bind to the active site, as well as the ability of the compound to be translocated across the plasma membrane. To address this important issue, Esslinger *et al.,* 2002 synthesized conformationally "locked" analogues of 2,4 PDC. The mimics were designed to capture the most extreme conformations 2,4 PDC may adopt, the folded (pseudo-axial) conformation and the extended (pseudo-equatorial) conformation. The folded conformation was achieved by synthesizing a methyl bridge from carbon 3 and 4 of the pyrrolidine ring (3,4-MPDC). If the methyl bridge is placed between carbon 2 and 4 (2,4 MPDC) the ring is forced into an extended conformation (Figure 8). The biological results from these compounds were striking with 3,4 MPDC acting

as a non-substrate inhibitor with a K_i of roughly 5 µM in rat forebrain synaptosomes and 2,4 MPDC displaying better substrate activity than L-glutamate, as measured by synaptosomal efflux of ^{3}H-D-aspartate (Koch *et al.,* 1999). These results reveal that both conformations effectively bind to the active site but their conformations determine if they are translocated (substrate) or not (non-substrate) across the plasma membrane (Esslinger *et al,* 2002).

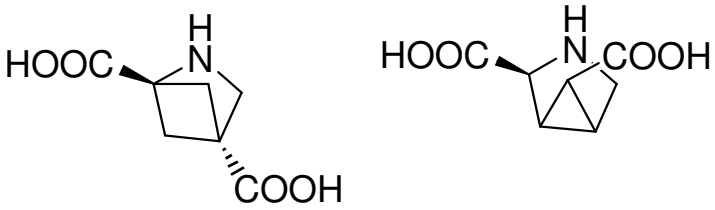

2,4 MPDC 3,4-MPDC

Figure 8. Bridged Pyrrolidines.

In spite of the progress made in the field of glutamate transport inhibitors one problem remains: specificity. It has proven to be very difficult to create inhibitors that show more than modest selectivity. The only EAAT1 inhibitor available to date is L-serine-o-sulfate (L-SOS), an EAAT1 and EAAT3 substrate. The k_i values of L-SOS display modest selectivity for EAAT1: 107 µM, 1157 µM and 150 µM for EAAT1-3, respectively (Bridges *et al.,* 1999; Vandenberg *et al.,* 1998; Arriza *et al.,* 1994).

The most selective and potent EAAT inhibitors are active at EAAT2. This likely follows from EAAT2 being the first EAAT intensely studied due to its prevalence in synaptosomal preparations, the earliest and most common system

used to characterize the EAATs. Two inhibitors that show modest to good selectivity for EAAT2 are DHK and WAY-855 (3-amino-tricyclo[2.2.1.$0^{2.6}$[heptane-1,3-dicarboxylic acid). WAY-855 is an EAAT2 preferring non-substrate inhibitor with IC_{50} values in *Xenopus laevis* oocytes of 125.9 µM, 1.3 µM, and 52.5 µM in EAAT1-3, respectively (Dunlop *et al.,* 2003).

Recently a series of compounds designed to be structurally distinct from other well known inhibitors were synthesized. The compounds were constructed by attaching a lipophilic group to the terminal amine of 2,3 diaminopropionic acid and to the terminal carboxyl of aspartic acid. Both series of compounds are potent, competitive, non-substrate inhibitors of EAAT2. The most potent compound (figure 9a) [N4-[4-(2-bromo-4,5,difluorophenoxy)phenyl]-L-asparagine (WAY 213613) does not interact with metabotropic or ionotropic glutamate receptors and displays an IC_{50} value of about 85nM and a 59 and 45 fold selectivity over EAAT1 and EAAT3 respectively (Greenfield *et al.,* 2005; Dunlop *et al.,* 2005).

In 2006, Greenfield and Dunlop published a review reporting the discovery of a preferential EAAT3 inhibitor, (S)-4-(9H-fluoren-2ylamino)-2-amino-4-oxobutanoic acid (NBI-59159, figure 9b) (Dunlop *et. al.,* 2006). In *Xenopus* oocytes expressing EAAT1-3 this compound acts as a non-substrate inhibitor with IC_{50} values of .212 µM, .055 µM and .023 µM, respectively. In HEK cells expressing EAAT1-3 the compound also displays a preference for EAAT3 yielding IC_{50} values of 1.03 µM, 1.4 µM and .09 µM, respectively (Dunlop *et al*., 2006).

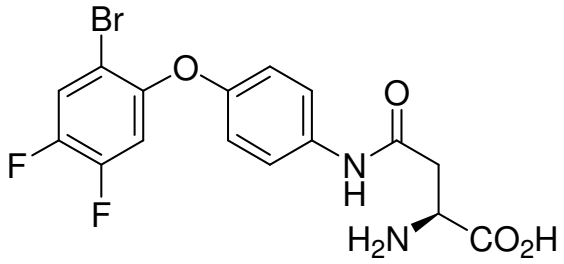

a. WAY-213613

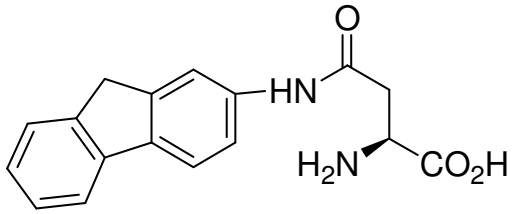

b. NBI-59159

Figure 9. Aspartamide acid analogues displaying preference for EAAT2 (a) and EAAT3 (b).

Based upon previous inhibitors of the EAATs and their corresponding structure activity data, we hypothesize that the conservation of the alpha carboxylate, alpha amine, and distal carboxylate mimic are crucial for protein recognition of the ligand. In addition, we envision that the positioning of a bulky lipophilic group around the backbone will result in increased potency and non-substrate activity of the analogue. By restricting the movement of this lipophilic group in three-dimensional space we suggest that the compounds will show greater selectivity for one EAAT subtype over another. If specific inhibition of one EAAT subtype can be achieved this will aid in the creation of a binding site

map as well as in the elucidation of the EAATs role in CNS function. To achieve the stated goal, the Specific Aims follow a re-iterative strategy of synthesis, assay of activity and molecular modeling.

Specific Aim 1: Design and synthesize L-β-Benzyl Aspartate (described in chapter 2) and L-β-Benzyl Aspartate analogues in order to increase interaction with an adjacent lipophilic domain of EAAT3.

Specific Aim 2: Determine the concentration dependence with which the analogues block ^{3}H-D-aspartate uptake in mammalian C17.2 cells expressing EAAT1, 2 or 3.

Specific Aim 3: Apply the structure activity data generated from Aim 2 to refine the EAAT3 binding site map using advanced computational molecular modeling techniques.

Chapter 2.

The β Substituted Aspartate Analogue L-β-*threo*-Benzyl-Aspartate Preferentially Inhibits the Neuronal Excitatory Amino Acid Transporter EAAT3.

C. Sean Esslinger, Shailesh Agarwal, John Gerdes, Paul A. Wilson, Erin S. Davis, Alicia N. Awes, Erin O'Brien, Teri Mavencamp, Hans P. Koch, David J. Poulsen, Joseph F. Rhoderick , A. Richard Chamberlin, Michael P. Kavanaugh, and Richard J. Bridges

COBRE Center for Structural and Functional Neuroscience, Departments of Biomedical & Pharmaceutical Sciences and Chemistry, University of Montana, Missoula MT, 59812 USA, and the [1]Department of Chemistry, University of California, Irvine CA, 92627 USA

*** Corresponding author:**
Richard J. Bridges
COBRE Center for Structural and Functional Neuroscience
Biomedical and Pharmaceutical Sciences
University of Montana
Missoula, MT 59812
Tel: 406-243-4972
Fax: 406-243-5228
Email: richard.bridges@umontana.edu

ABSTRACT

The excitatory amino acid transporters (EAATs) play key roles in the regulation of CNS L-glutamate, especially related to synthesis, signal termination, synaptic spillover, and excitotoxic protection. Inhibitors available to delineate EAAT pharmacology and function are essentially limited to those that non-selectively block all EAATs or those that exhibit a substantial preference for EAAT2. Thus, it is difficult to selectively study the other subtypes, particularly EAAT1 and EAAT3. Structure activity studies on a series of β-substituted aspartate analogues identify L-β-benzyl-aspartate (L-β-BA) as among the first blockers that potently and preferentially inhibits the neuronal EAAT3 subtype. Kinetic analysis of ^{3}H-D-aspartate uptake into C17.2 cells expressing the hEAATs demonstrate that L-*threo*-β-BA is the more potent diastereomer, acts competitively, and exhibits a 10-fold preference for EAAT3 compared to EAAT1 and EAAT2. Electrophysiological recordings of EAAT-mediated currents in *Xenopus* oocytes identify L-β-BA as a non-substrate inhibitor. Analyzing L-*threo*-β-BA within the context of a novel EAAT2 pharmacophore model suggests: 1) a highly conserved positioning of the electrostatic carboxyl and amino groups, 2) nearby regions that accommodate select structural modifications (cyclopropyl rings, methyl groups, oxygen atoms) and 3) a unique region occupied by the benzyl moieties of L-TBOA, L-β-*threo*-BA and related analogs. It is plausible that the preference of L-β-*threo*-BA and L-TBOA for EAAT3 and EAAT2, respectively, could reside in the latter two pharmacophore regions.

Key Words: Glutamate uptake, transport inhibitors, pharmacophore model

1. INTRODUCTION

The high-affinity, sodium-dependent excitatory amino aid transporters (EAATs) are readily acknowledged as key players in the regulation of extracellular L-glutamate levels in the mammalian CNS (for review see: Danbolt, 2001; Maragakis and Rothstein, 2004; Bridges and Esslinger, 2005). This regulation takes on considerable significance given that L-glutamate is the primary excitatory neurotransmitter in these systems and capable of participating not only in standard fast synaptic communication, but also in the higher order types of signal processing linked to development, synaptic plasticity, learning and memory (for review see multiple chapters in Balazs *et al.,* 2005). Besides its action in neuronal signaling, excessive levels of L-glutamate can also trigger a host of pathological pathways in the CNS through the process of excitotoxicity. In this manner, glutamate-mediated neuronal damage is thought to be a contributing pathological mechanism in both acute CNS injury (e.g., stroke, head trauma, spinal cord injury) and chronic neurodegenerative disease (e.g., amyotrophic lateral sclerosis, Alzheimer's disease, Huntington's disease) (for review see: Choi, 1994; Mattson, 2003; Olney, 2003; Maragakis and Rothstein, 2004). Consequently, the ability of the EAATs to efficiently sequester L-glutamate into neurons and glia, places these integral membrane proteins in a position where they can influence the amount and/or time course with which L-glutamate is in contact with EAA receptors within the context of either normal signaling or pathologic injury.

The EAATs are members of a distinct family sodium-dependent solute carriers (SLC1) that includes five subtypes of glutamate transporter (EAATs 1-5), as well the neutral amino acid transporters ASCT1 and ASCT2 (Kanai and Hediger, 1992; Pines *et al.,* 1992; Storck *et al.,* 1992; Arriza *et al.,* 1994; Fairman *et al.,* 1995; Eliasof *et al.,* 1998; Hediger *et al.,* 2004). While the EAATs share a level of homology of about 50-60% with one another, as well as a dependency on sodium and a high-affinity for L-glutamate (K_m values in the μM range), each exhibits a distinct anatomical and cellular distribution (Furuta *et al.,* 1997; Gegelashvili and Schousboe, 1998; Seal and Amara, 1999; Danbolt, 2001; Maragakis and Rothstein 2004). The presence of distinct EAAT subtypes raises obvious questions regarding potential differences in their physiological roles, especially within the context of excitatory signaling and excitotoxic protection. In turn, such questions highlight the need for selective inhibitors and substrates that could be used to differentiate the EAATs and delineate their individual contributions to glutamate-mediated signaling. Significant advances have been made in generating inhibitors and substrates that can be used to assess EAAT activity with little or no cross-reactivity with EAA receptors, such as L-*trans*-2, 4-pyrrolidine dicarboxylate (L-*trans*-2, 4-PDC) and β-*threo*-benzyloxy-aspartate (TBOA) (Bridges and Esslinger, 2005)). Much of this success has been the direct result of synthetic efforts to produce novel conformationally constrained analogues of glutamate and aspartate (Chamberlin *et al.,* 1998). Limiting the positions that can be occupied by required functional groups (e.g., carboxylate and amino groups) has the potential to both increase potency, as well as reduce

cross-reactivity. It is this same approach that has so effectively been exploited in development of selective agonists and antagonists for the EAA receptors. Additionally, the fact that the functional groups on these rigid and semi-rigid analogues can be accurately mapped in three-dimensional (3D) space allows for the construction of 3D pharmacophore models (Gelin, 1995; Martin, 1998). In this respect, our transporter workgroup has been focused on rigorously probing the structural commonalities and differences amongst EAAT selective ligands (especially EAAT2, see; Esslinger *et al.,* 2002; Bridges and Esslinger, 2005;) through the fabrication of multidimensional superposition pharmacophore models (Perkins and Dean, 1993; Dean and Perkins, 1998; Martin, 1998).

Unfortunately, identifying compounds that readily differentiate among the individual EAAT subtypes has proven to be more elusive than developing analogues that discriminate glutamate transporters from glutamate receptors. The exception to this limitation has been the progress made in pharmacologically delineating EAAT2, particularly within the context of the most commonly studied EAATs 1-3. Thus, glutamate analogues, such as dihydrokainate (DHK), L-*anti-endo*-3,4-methanopyrrolidine dicarboxylate (L-*anti-endo*-3,4-MPDC) (Bridges *et al.,* 1994), *S*-2-amino-3-(3-hydroxy-1,2,5-thiadiazol-5-yl)propionic acid (TDPA) (Brauner-Osborne *et al.,* 2000) and 3-amino-tricyclo[2.2.1.$0^{2.6}$]heptane-1,3-dicarboxylate (WAY-855) (Dunlop *et al.,* 2003) potently and preferentially interact with EAAT2 to a high enough degree that they can be used to distinguish its activity from the other EAAT subtypes. In the instance of the other EAATs, only more subtle indications point to chemical templates that might be used to create

subtype selective blockers. For example, EAAT 1 has the distinguishing feature of being able to effectively use 4-methyl-glutamate and L-serine-O-sulfate as substrates and to exhibit a sensitivity to inhibition by (*R,S*)-2-amino-3-(1-hydroxy-1,2,3-triazol-5-yl)propionate (Arriza *et al.,* 1994; Vandenberg, 1998; Stensbol *et al.,* 2002). Similarly, hints to the potential selectivity of EAAT3 may be traced back to the pioneering characterizations of glutamate uptake, where it was reported that L-aspartate β-hydroxamate was more effective at inhibiting glutamate uptake into neurons than into glia (Roberts and Watkins, 1975). In the present work we carry out a structure activity study on a series of aspartate analogues that have been modified at the β-carbon position. We find that one of these analogues, L-β-benzyl-aspartate, may be among the first transport blockers to be identified that potently and preferentially inhibits the neuronal EAAT3 subtype. Further, molecular modeling studies in which this new inhibitor has been positioned within a current EAAT2 pharmacophore suggest that its specificity of action may be the result of the side chains of L-β-benzyl-aspartate and L-β-TBOA interacting with similar lipophilic residues within the substrate binding domain of the EAATs in addition to distinct residues between EAAT isoforms. These finding represent an important step in developing the reagents that are critically needed to elucidate the physiological roles played by the neuronal EAAT3 glutamate transporter within the processes of excitatory transmission and excitotoxicity.

2. METHODS

2.1. *Chemicals and Reagents*

General cell culture supplies were purchased from Becton Dickinson (Franklin Lakes, NJ), Corning (Corning, NY), and Life Technologies (Grand Island, NY). D-[^{3}H]Aspartic acid was purchased from Dupont NEN (Boston, MA). L-Aspartate, L-β-*threo*-hydroxy-aspartate (L-β-THA), and D,L-*threo*-methyl-aspartate were obtained from Sigma (St. Louis, MO). D,L-□β-*threo*-Benzyloxy-aspartate was obtained from Tocris (Ballwin, MO). L-*trans*-2,3-Pyrrolidine dicarboxylate (L-*trans*-2,3-PDC) was prepared as described (Humphrey *et al.,* 1994). The *cis*-3-methyl-L-*trans*-2,3-PDC (*cis*-3-Me-L-*trans*-2,3-PDC) was prepared in a similar manner by A.R. Chamberlin via methylation of the β-enolate of protected 2,3-PDC, giving a 2:1 mixture of diastereomers from which the desired major isomer was isolated, deprotected, and purified. The synthesis of L-β-benzyl-aspartate was performed by Terri Mavencamp under the mentorship of Dr. Esslinger. The following pharmacological comparisons are included because they provide a basis for interpreting structure activity relationship (SAR) data. This analysis is crucial to both the full evaluation of L-β-BA as well as to the design of a second round of L-β-benzyl aspartate derivatives. The synthesis of L-β-BA begins with L-aspartic acid and utilizes methodology similar to that previously reported (Humphrey *et al.,* 1994). Protection as dimethyl ester using thionyl chloride in methanol, followed by N-tritylation with trityl chloride and triethylamine afforded the protected aspartate derivative. Base promoted

alkylation at the beta carbon afforded a *ca.* 2:1 ratio of diastereomers as distinguished by ^{1}HNMR and correlated to a similar compound previously reported (Humphrey *et al.,* 1994). Deprotection using refluxing 6N HCl followed by ion exchange chromatography afforded the target compound L-β-benzyl aspartate (L-β-BA) as the mixture of diastereomers and aspartate free, as determined by ^{1}HNMR analysis. Optical activity of the mixture ([α]=+29.8^{o}) suggests the alpha carbon stereochemical integrity remained intact. Separation of the two diastereomers by preparative HPLC using a C18 column in 0.1M ammonium acetate buffer pH 6.4 afforded the individual *threo* and *erythro* diastereomers. Full experimental details for these syntheses are reported in Mavencamp et al., 2008. All other chemicals were purchased from Sigma (St. Louis, MO).

2.2. EAAT Expression and Cell Culture

EAAT1, and EAAT3 cDNA were PCR amplified from pBlueScript-hEAAT1 and pBlueScript-hEAAT3 (provided by Dr. M Kavanaugh) using primer pairs (forward; 5'ATAAGGATCCA-TGACTAAAAGCAACGGA3' and reverse 5'TATTGATAT-CCTACATCTTGGTTTCACT3') and (forward: 5'ATAAGGATCCATGGGGAAACCGGCGAGG3' and reverse 5'TATTGATATCCTAGAACTGTGAGGTCTG3') respectively. Each primer pair introduced BamHI sites at the 5' ends and EcoRV sites at the 3' ends of each amplified fragment. The PCR fragments were then subcloned into the BamHI and EcoRV sites within the polylinker of the AAV vector pAM-CAG-WPRE (kindly

provided by Dr. Mathew During, University of Auckland, NZ) to create pAM-CAG-EAAT1-WPRE and pAM-CAG-EAAT3-WPRE. Final clones were confirmed by double stranded sequencing. A 1.9kb EcoRI fragment containing the hEAAT2 cDNA clone was subcloned from pBlueScript-hEAAT2 (Dr. M Kavanaugh) into the EcoRI site of pAM-CAG-WPRE by standard molecular biology techniques to create pAM-CAG-EAAT2-WPRE.

C17.2 cells (obtained from Dr. Evan Snyder, Burnham Inst., La Jolla, CA) between passages 10-20 were seeded at 1 X 10^5 cells/well in 12 well plates and grown in complete DMEM supplemented with 10% fetal bovine serum, 1mM sodium pyruvate, 0.1 mM nonessential amino acids solution, and 0.05% Penicillin-Streptomycin (5,000 units/ml) and Gentamicin sulfate (0.05mg/ml). At 24 hours after plating, cells were transfected using Lipofectamine 2000 Transfection Reagent (Invitrogen, Carlsbad, CA) in a ratio of 4µl of Lipofectamine to 3µg of purified plasmid DNA in accordance with manufacturers instructions. After 24 hours, the relative levels of functional ^{3}H-D-Asp uptake were determined by the method of Martin and Shain (1979 as described below).

2.3. Transporter Activity in C17 Cells

C17.2 cell assays were performed by the Bridges lab. Transfected C17.2 cells were grown in DMEM containing 10% FCS in a humid atmosphere of 5% CO_2. Near-confluent cells (plated at $7x10^4$ -$1x10^5$ cells/well) were rinsed with a physiological buffer (138 mM NaCl, 11 mM D-glucose, 5.3 mM KCl, 0.4 mM KH_2PO_4, 0.3 mM Na_2HPO_4, 1.1 mM $CaCl_2$, 0.7 mM $MgSO_4$, 10 mM HEPES, pH

7.4) and allowed to preincubate at 37°C for 5 min. Uptake was initiated by replacing the pre-incubation buffer with buffer containing ^{3}H-D-aspartate (5-100 µM) and inhibitors (10-100 µM). Following a 5 min incubation, the media was removed by rapid suction and the cells rinsed 3 times with ice-cold buffer. The cells were dissolved in 0.4N NaOH for 24 hours and analyzed for radioactivity by LSC and protein by the BCA (Pierce) method. Transport rates were corrected for background: i.e., radiolabel accumulation at 4°C. Initial studies confirmed that uptake quantified in this manner was linear with time and protein levels and that uptake in untransfected C17.2 cells was indistinguishable from background. Kinetic analyses of the transport inhibitors were carried out using k•cat kinetic computational software (BioMetallics Inc.) to generate Lineweaver-Burk plots with curve-fit weighting based on constant relative error. K_i values were also determined using this software on the basis of a replot of $K_{m,app}$ values.

2.4. Transporter Activity in Xenopus Oocytes

Capped cRNA was transcribed from the human brain glutamate transporter EAAT1-3 cDNAs as described (Arriza at al., 1994). Transcripts were microinjected into *Xenopus* oocytes (50 ng per oocyte) and membrane currents were recorded by the Kavanaugh lab 3-6 days later. Ringer recording solution contained 96 mM NaCl, 2 mM KCl, 1 mM MgCl2, 1.8 mM CaCl2, and 5 mM HEPES (pH 7.4). Two microelectrode voltage-clamp recordings were performed at 22°C with an Axon Instruments GeneClamp 500 amplifier interfaced to a PC using a Digidata 1200 converter controlled using the pCLAMP program suite

(version 6.0; Axon Instruments). Microelectrodes were filled with 3 M KCl solution and had resistances of 0.5 to 2 Mohm. Steady state data were sampled at 1 kHz and low pass filtered at 500 Hz. Data were fitted by least squares using Kaleidagraph v3.0 (Synergy Software) to the Michaelis-Menten function. L-β-BA was applied 10-30 sec before glutamate for competition experiments; recovery from block was complete within 1 min following inhibitor washout.

2.5. *Molecular Modeling*

Computational work was performed by Shailesh Agarwal of the Bridges lab on Silicon Graphics, Inc. (SGI) Octane workstations with R12,000 processors coupled to an SGI Origin 2000 server. The software application suite Sybyl (versions 6.8-7.0), with the Advanced Computation module (Tripos; St. Louis, MO), was used adjunct with the industrially derived stochastic random search algorithm AESOP (Masek, 1998). Molecular databases were prepared in Sybyl formats. Data extracted from the molecular spreadsheets were occasionally exported for sorting and other manipulations in PERL and C code formats that were subsequently automated. Inspections of conformations and multifit superpositions were performed in Sybyl stereoview with CrystalEyes viewers.

The pharmacophore models were constructed as steric-strain, gas-phase derived conformation compositions employing established comprehensive conformational analysis methods (Marshall, 1995; Oprea *et al.,* 1995) with four EAAT2 inhibitor training set ligands, i.e. L-*anti-endo*-3,4-methanopyrrolidine-3,4-dicarboxylate (L-*anti-endo*-3,4-MPDC), *cis*-5-methyl-L-*trans*-2,3-pyrrolidine

dicarboxylate (*cis*-5-Me-L-2,3-*trans*-PDC), (2S,3R,4S)-2-(carboxy-cyclopropyl)glycine (CCG-IV) , and L-β-*threo*-benzyloxy-aspartate (L-TBOA) (for comparative pharmacological properties see Bridges *et al.,* 1999; Bridges and Esslinger, 2005). The important EAAT2 inhibitor classes were carefully considered for inclusion in the training set and those selected satisfied the major criteria of high potency, structural diversity amongst common moieties, and relatively high selectivity, as well as little or no substrate activity.

Conformational space of the EAAT inhibitors was comprehensively searched employing two computational protocols: random search (Tripos Sybyl) and the stochastic technique AESOP (Masek, 1998) (See Figure 1). The random search procedure locates energy minima by randomly adjusting the selected bonds and minimizing the energy of the resulting geometry. Chiral centers, ring closure distances, and energy ranges were checked for consistency. This comparison was based on an RMS match between non-hydrogen atoms in the previously found conformers and the current conformer. Three random searches (or more) were performed on each training set ligand and other test cases. Data from the Sybyl random searches were deposited into a molecular database. AESOP is an alternative stochastic derived program used to search conformational space. It applies high temperature to the molecule (which results in molecule being torqued and tensed), and was set to capture a conformer snapshot every 5 femtoseconds. Temperatures and times were set between 1600-1800 ^{0}K and 60-80K femtoseconds. Data from the AESOP spreadsheets was deposited into the databases established earlier. Subsequently, all

conformers from both search protocols were minimized to zero energy change defining their nearest energy well profile. Conformer database entries were sorted as a function of conformer total energy and cases of degenerate energy profiles were crosschecked as plausible duplicates, based on select distances and angles defined in an exported Molfile spreadsheet. Duplicate or nearly identical conformers (e.g., some non-essential rotamers for TBOA) were eliminated. Some conformations would not have been found if only one conformer search routine had been used.

Four final training set ligand conformational molecular databases were derived. An extended closed form analysis method, which used the conformational data, was developed to select one conformer of each of the four ligands to form the 3D superposition models. To compare one conformation of one ligand to all conformations of each of the remaining three training set ligands, an all-combination comparison regime was used by forming conformational comparison groups (shown as double headed arrows in Fig. 1). For each comparison group, six distinct measures were assessed between each ligand conformer, thus permitting an assessment of molecular similarity. These six measures included the three distances and angles between the α-carboxylate carbon, C1; α-amino nitrogen, N and distal carboxylate carbon, C2 common to each training set ligand (see Figure 4). Additional molecular spreadsheets were also constructed in which *i*) the ether oxygen of L-TBOA and *ii)* the cyclopropyl centroid of L-CCG-IV were substituted for point C2 to consider alterative relative alignments.

The resulting 3.4 X 10^6 conformational comparison groups were analyzed for 3D molecular similarity using a relative difference scoring function (Figure 1), defined as a sum of the average of the four conformations (as per the all-combination regime and denoted as $n_{conformers}$) using absolute value relative difference measurements ($n_{measures}$). Averaging precluded the use of weighting factors. The relative difference comparison measures between the conformers in a group (double headed arrows, Figure 1) included three distance and three angle values. The six conformer-to-conformer measurements were extracted from the molecular database spreadsheets and the calculations of the scoring function values were made. Conformer energies were not used in these calculations, thus making the scoring function energy independent. The comparison group that had a low scoring function value (least amount of differences amongst the six variable conformer measures in 3D space) was identified. Thus, the lower the score the more similar the conformers are to one another, representing molecular similarity of their space groupings. The selected ligand conformer set was brought together with a 1 cal spring constant, and the superposition models were appraised in stereoview using CrystalEyes viewers.

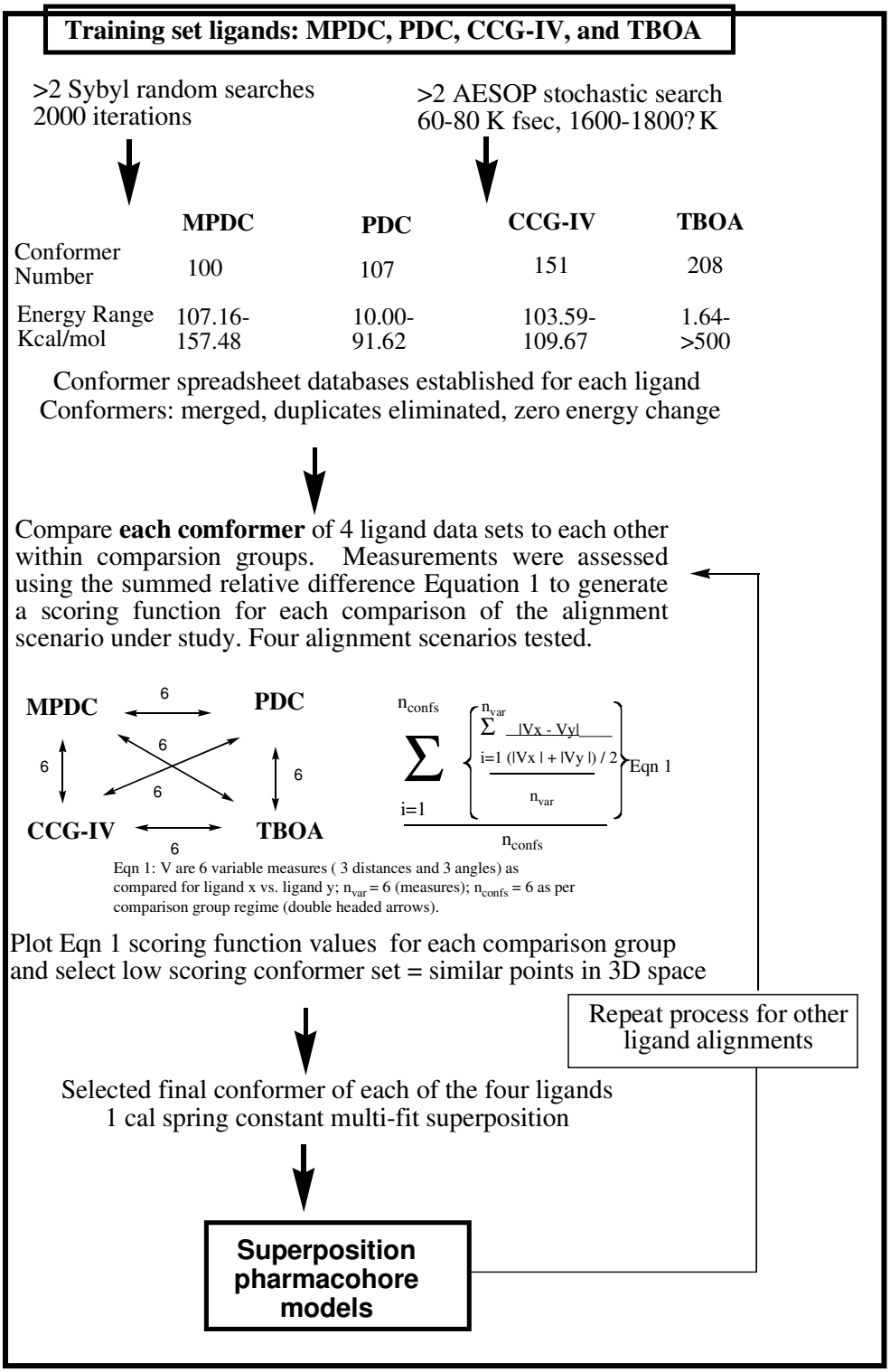

Figure 1. Computational paradigm used to generate the EAAT2 pharmacophore model.

3. RESULTS

3.1. L-threo-Benzyl-aspartate preferentially inhibit the EAAT3 transporter subtype

To delineate the pharmacological specificity of the individual EAATs, the Bridges lab utilized a relatively new expression system that employed C17.2 neuroprogenitor cells and a vector adapted from an Adeno-associated virus (AAV) packaging plasmid (Stone *et al.,* 2005). The vector contains a number of elements that facilitate the expression of the EAATs, including a ubiquitous CAG promoter and a 567 bp woodchuck hepatitis regulatory element (WPRE) that stimulates the expression of intronless viral messages. We and other have observed that the insertion of the WPRE sequence between the stop codon and the poly-A sequence results in a substantial increase in stable transgene expression (Loeb *et al.,* 1999; Paterna *et al.,* 2000). This system proved to be both easy and efficient (approximately 50% transfection), as C17.2 cells transfected 24 hrs after plating with the desired EAAT vector exhibited robust and reproducible levels of activity 48 hrs later. When uptake was quantified with ^{3}H-D-aspartate in untransfected cells, the levels of uptake were indistinguishable from background determined either at 4^{o}C or in the absence of sodium (see Methods, data not shown). In cells expressing the individual subtypes the transport of ^{3}H-D-aspartate exhibited K_M and V_{Max} values (mean ± SEM), respectively, of: 40 ± 4 µM (n ≥ 5) and 501 ± 72 pmol/min/mg protein (n ≥ 5) for EAAT1, 44 ± 3 µM (n ≥ 5) and 1997 ± 270 pmol/min/mg protein (n ≥ 5) for

EAAT2, and 19 ± 3 μM (n ≥ 5) and 334 ± 52 pmol/min/mg protein (n ≥ 5) for EAAT3.

A series of β-substituted aspartate analogues, that included L-benzyl-aspartate (L-BA), were screened at 10 μM and 100μM for the ability to inhibit the uptake of ^{3}H-D-aspartate (25 μM) into C17.2 cells expressing EAAT1, EAAT2 or EAAT3. The data are reported in Table 1 as the mean % of Control (± SEM) measured in the absence of inhibitors. Several of these compounds are well known blockers of the EAATs, (e.g., β-THA, TBOA), and were included in the present study so that structure activity comparisons would be based on assay data collected under identical conditions. Consistent with previous reports (summarized in Bridges *et al.,* 1999) the introduction of a hydroxyl group at the β-carbon of L-aspartate (β-THA) produced a small increase in inhibitory activity when compared to L-aspartate (more easily observed at 10 μM). While the L-enantiomer of THA was used in the present study, earlier work quantifying ^{3}H-L-glutamate uptake into synaptosomes reported that the L- and D enantiomers of THA were approximately equipotent as inhibitors (Robinson *et al.,* 1993). A similarly placed methyl group (D,L-β-*threo*-methyl-aspartate), also produced a level of inhibition essentially equivalent to its unsubstituted counterpart. Significantly, all three of these compounds produced comparable levels of inhibition at each of the three EAAT subtypes.

Compound	Conc.	EAAT1 ^{3}H-D-Asp Uptake (% of Control)	EAAT2 ^{3}H-D-Asp Uptake (% of Control)	EAAT3 ^{3}H-D-Asp Uptake (% of Control)
L-Aspartate 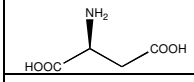	100 µM 10 µM	4 ± 2 (3) 70 ± 9 (3)	16 ± 4 (3) 82 ± 4 (3)	15 ± 3 (3) 87 ± 11 (3)
D,L-β-*threo*-CH_3-Asp 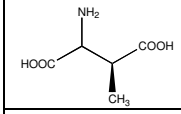	100 µM 10 µM	33 ± 4 (3) 6 5 ± 13 (3)	32 ± 3 (3) 76 ± 4 (3)	42 ± 2 (3) 74 ± 51 (3)
L-β-*threo*-OH-Asp 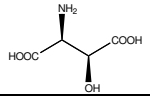	100 µM 10 µM	5 ± 3 (3) 47 ± y (3)	10 ± 3 (3) 53 ± 4 (3)	9 ± 3 (3) 61 ± 7 (3)
L-*trans*-2,3-PDC 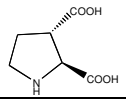	100 µM 10 µM	102 ± 9 (3)	81 ± 5 (3)	89 ± 11 (3)
cis-3-CH_3-L-*trans*-2,3-PDC 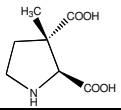	100 µM 10 µM	51 ± 2 (3) 71 ± 5 (3)	12 ± 5 (3) 44 ± 3 (3)	15 ± 2 (3) 63 ± 3 (3)
D,L-β-*threo*-BOA 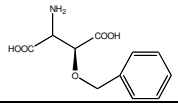	100 µM 10 µM	5 ± 2 (3) 50 ± 4 (3)	2 ± 1 (3) 30 ± 2 (3)	9 ± 3 (3) 53 ± 5 (3)
L-β-Benzyl-Asp 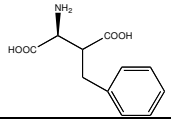	100 µM 25 µM 10 µM	20 ± 4 (3) 50 ± 9 (3) 63 ± 9 (3)	15 ± 3 (3) 39 ± 5 (3) 70 ± 1 (3)	4 ± 2 (3) 20 ± 4 (3) 46 ± 3 (3)
L-β-*threo*-BA 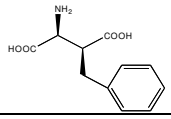	100 µM 10 µM	8 ± 1 (3) 50 ± 3 (3)	9 ± 1 (3) 53 ± 2 (3)	1 ± 1 (3) 30 ± 4 (3)
L-β-*erythro*-BA 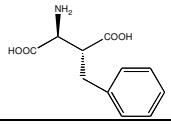	100 µM 10 µM	59 ± 4 (3) 7 9 ± 3 (3)	48 ± 2 (3) 90 ± 5 (3)	14 ± 2 (3) 66 ± 8 (3)

TABLE 1. Inhibitory activity of β-substituted aspartate analogues at EAAT1, EAAT2 and EAAT3.

Embedding L-aspartate into a 5-membered pyrrolidine ring (L-*trans*-2,3-PDC) produced a substantial decrease in the inhibitory activity exhibited at each of the EAATs. This is in marked contrast to the analogous modification to L-glutamate, where L-*trans*-2,4-PDC proved to be a potent inhibitor of each subtype, especially EAAT2 (Bridges *et al.,* 1991; Arriza *et al.,* 1994). Interestingly, however, when a methyl group is introduced at the β-carbon equivalent of L-*trans*-2,3-PDC (i.e., carbon 3), there is a substantial increase in potency as an inhibitor of ^{3}H-D-aspartate uptake. Further, it appears as if *cis*-3-Me-L-*trans*-2,3-PDC, like almost all of the pyrrolidine dicarboxylate-based analogues, preferentially blocks uptake through EAAT2 (Bridges and Esslinger, 2005). A similar pharmacological profile is exhibited by D,L-TBOA, one of the more potent EAAT blockers identified to date (Shimamoto *et al.,* 2000).

L-β-BA stands apart from all of the other aspartate analogues tested in that it more potently inhibited uptake mediated by EAAT3 than either EAAT1 or EAAT2. As reported in Table 1, this effect could be seen at each of the concentrations examined. Thus, in the presence of 25 μM L-β-BA EAAT3 activity (≈ 20% of Control) was about half that observed with EAAT1 (≈ 40% of Control) or EAAT2 (≈ 50% of Control). L-β-BA produced similar levels of inhibition at both EAAT1 and EAAT2 and in each case, it was less than that observed with D,L-TBOA. On the other hand, L-β-BA and D,L-TBOA exhibited comparable levels of inhibition at EAAT3. Direct comparisons of potency, however, must be made cautiously, as L-β-BA was included in this assay as a mixture of its *threo* and *erythro* diaseteromers (i.e., 2:1, respectively), while D,L-TBOA was a mixture of

its L and D enantiomers (1:1, respectively). Prompted by its preferential action at EAAT3, the diastereomers of L-β-BA were separated and tested individually. Similar to the trend observed with THA and TBOA (Shimamoto *et al.,* 2000), the majority of the inhibitory activity resided with the *threo* diastereomer (Table 1).

To calculate Ki values, as well as to verify that L-β-*threo*-BA acts as a competitive inhibitor, more detailed kinetic studies examined the concentration dependence with which the analogue inhibited the uptake of ^{3}H-D-aspartate into C17.2 cells expressing each of the three EAAT subtypes. As illustrated in the Lineweaver-Burk plots depicted in Figure 2, L-β-*threo*-BA blocked uptake of ^{3}H-D-aspartate mediated by EAAT3 in a manner that was consistent with that of a competitive inhibitor. Similar patterns of inhibition were also observed for EAAT1 and EAAT2. The resulting Ki values, reported as mean ± SEM from at least 3 separate kinetic assays for each transporter were found to be: 8.7 ± 2.6 μM for EAAT1, 10.0 ± 2.0 μM for EAAT2 and 0.8 ± 0.2 μM for EAAT3. These findings confirm the results of the initial pharmacological screening and suggest that L-β-*threo*-BA is not only one of the more potent inhibitors of EAAT3 identified to date, but also one that exhibits approximately a 10-fold preference for the EAAT3 compared to EAAT1 and EAAT2.

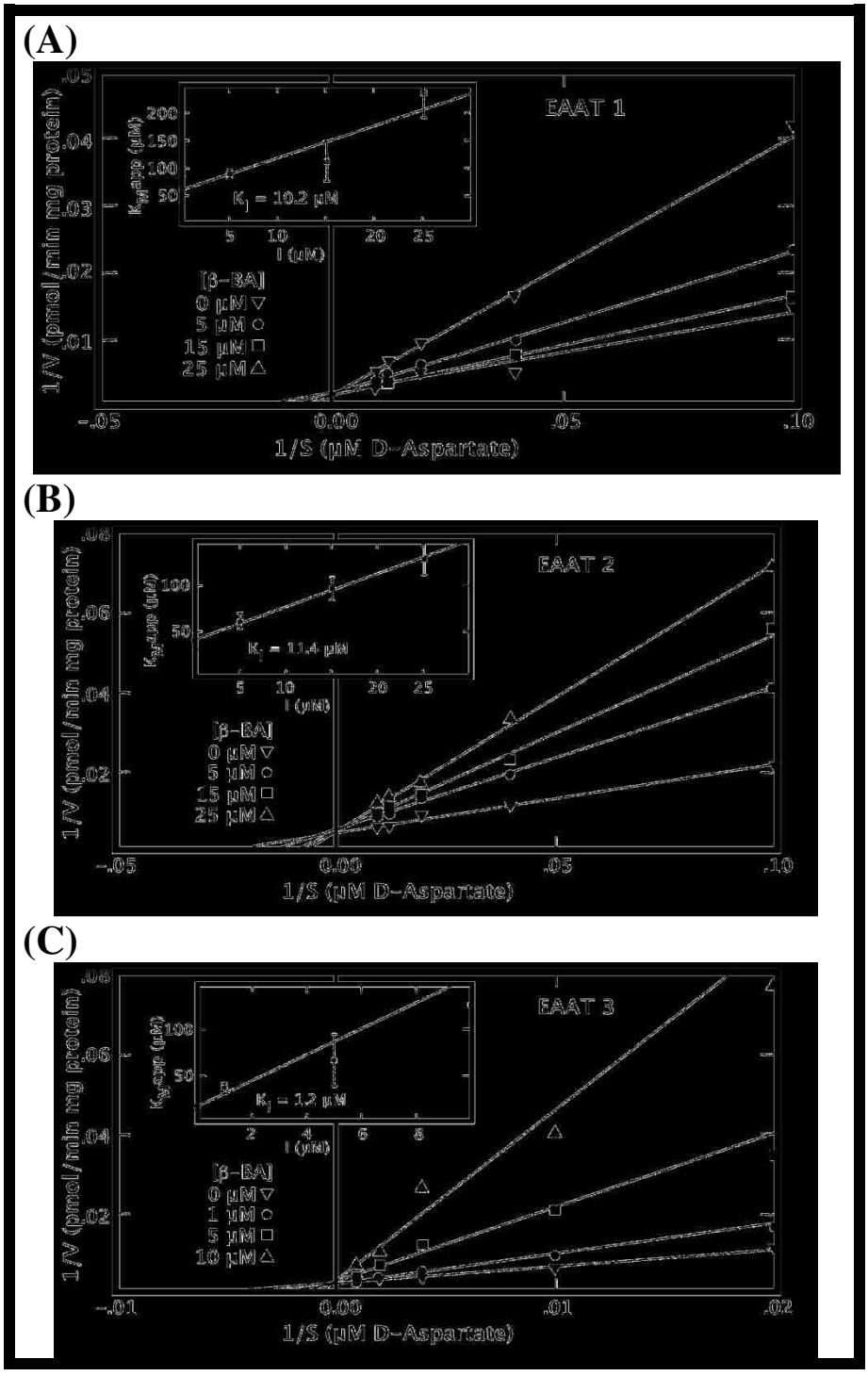

Figure 2. Representative Lineweaver-Burk plots of single experiments demonstrating L-threo-BA as a competitive inhibitor of ^{3}H-D-aspartate uptake by **(A)** hEAAT1, **(B)** hEAAT2 and **(C)** hEAAT3 expressed in C17.2 cells. Data was collected and analyzed as described in Methods and Materials. The inset within each graph shows a replot of K_{Mapp} vs L-threo-BA that was used to determine the indicated K_I value for the depicted experiment. At least three such experiments for each transporter were carried out and averaged to derive the K_I, K_M and V_{Max} values reported in the text.

3.2. L-Benzyl-aspartate is a preferential competitive inhibitor of EAAT3 that does not exhibit substrate activity at any of the EAATs

The actions of L-β-BA, *cis*-3-Me-L-*trans*-2,3-PDC and L-glutamate at human EAAT1, EAAT2 and EAAT3 expressed on *X. laevis* oocytes were examined by the Kavanaugh lab in real time using electrophysiological recording techniques. As the EAAT-mediated co-transport of L-glutamate and its requisite ions is electrogenic, substrate-induced currents serve as a direct measure of the translocation process (Wadiche *et al.,* 1995). This provides a distinct advantage over radiolabeled flux assays, where inhibitory activity is indicative of binding, but does not directly address the issue of whether or not a particular inhibitor also acts as an alternative substrate for the transporter. As illustrated in Figure 3A, the application of L-glutamate (100 μM) to a voltage-clamped oocyte expressing EAAT3 produced the expected inward current. When L-glutamate was co-applied with β-L-BA (2:1 mixture of *threo* and *erythro* diastereomers) the glutamate-induced currents were inhibited in a concentration-dependent manner. Similar curves were produced when *cis*-3-Me-L-*trans*-2,3-PDC was co-applied with L-glutamate (individual traces not shown). The application of either β-L-BA or 3-Me-L-*trans*-2,3-PDC alone did not produce a current. These results are consistent with the ability of the analogue to bind to the glutamate substrate site but not be transported. The concentration dependence with which the analogues blocked these glutamate-mediated currents was also determined. The parallel shifts observed in the dose-response curves for all of the compounds tested with

increasing concentrations of the inhibitors are consistent with competitive inhibition (representative traces shown for β-L-BA at EAAT3, Figure 3B). K_D value were determined using Schild analysis (representative curves for β-L-BA at EAAT1-3 are shown in Figure 3C). As was observed with the radiolabel flux assays, 3-Me-L-*trans*-2,3-PDC exhibited the highest affinity for EAAT2, yielding K_D values at EAAT1, EAAT2 and EAAT3 of 31 µM, 1 µM, and 7 µM, respectively. Schild analysis of β-L-BA, on the other hand, yielded K_D values at EAAT1, EAAT2 and EAAT3 of 12 µM, 9 µM, and 2 µM, once again demonstrating the preferential action of β-L-BA at EAAT3.

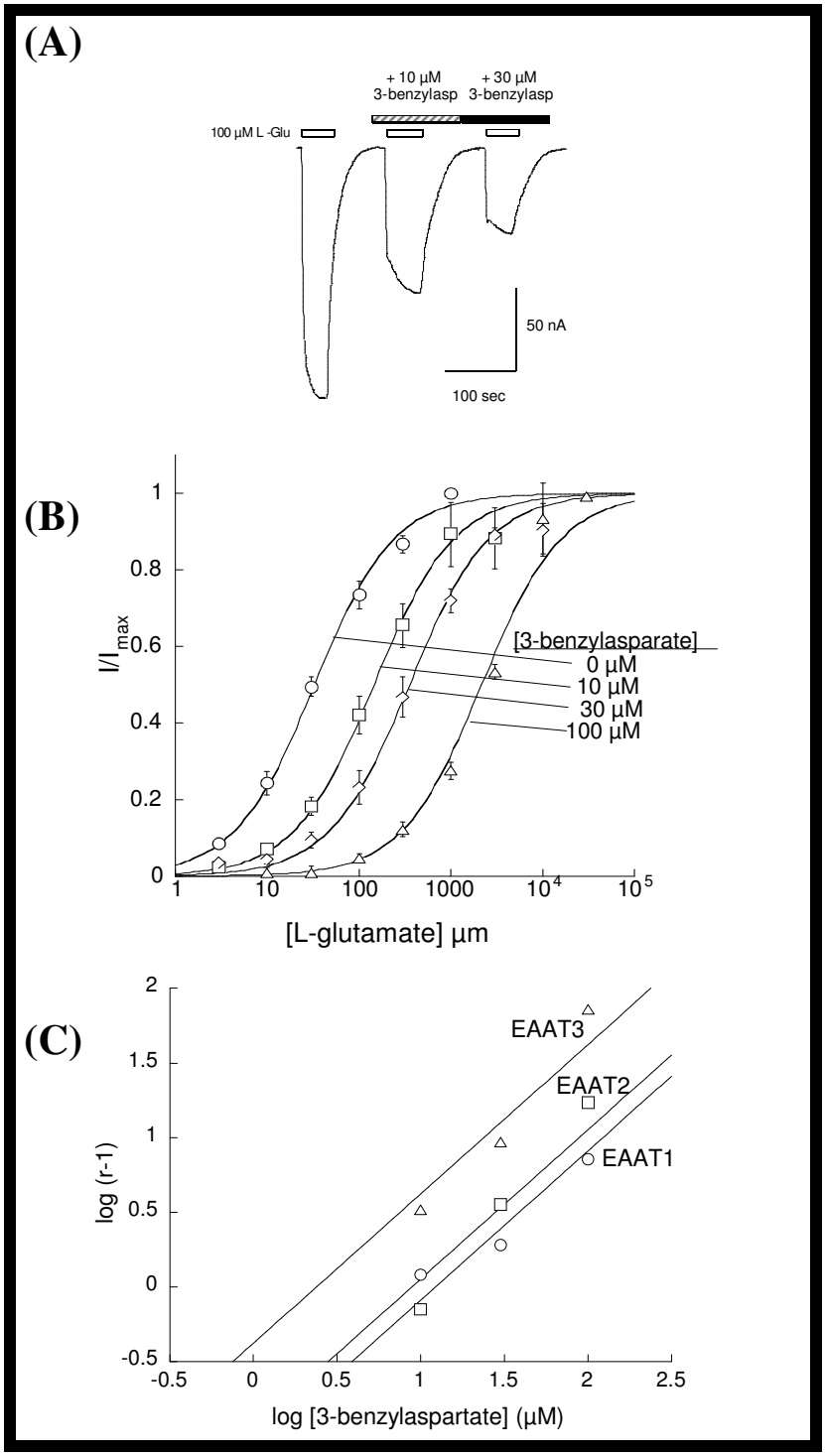

Figure 3. (**A**) Inhibition of hEAAT3 transport by L-β-BA in a representative oocyte voltage-clamped at –30 mV (glutamate and inhibitor applied for the durations indicated by corresponding bars above traces). (**B)** Parallel glutamate dose-response shift with increasing [3-benzylaspartate] is consistent with competitive inhibition. Data points represent mean +/- SEM for 3-5 oocytes. (**C)** Schild analysis of L-β-BA inhibition in analogous competition experiments with EAATs 1,2, and 3 (slope values constrained to 1) gave) yielded K_D values of 12, 9, and 2 µM, respectively.

3.4. Conformational molecular modeling with L-threo-Benzyl-aspartate identifies potential points of divergence between the pharmacophores for EAAT2 and EAAT3.

The molecular modeling was performed by Shailesh Agarwal under the guidance of Dr. Bridges and Dr. Gerdes and is described in the Methods section. The described regimen led to the identification of four plausible pharmacophore models for EAAT2. While the positions of the two carboxylate carbons and the amino nitrogen in L-*anti-endo*-3,4-MPDC and *cis*-5-Me-L-*trans*-2,3-PDC were remarkably aligned in all four models, each differed with respect to the positioning of these same groups in CCG-IV and L-TBOA. The model shown in Figure 4 was selected from among the four because it afforded the best alignments of both carboxylate groups, the amino moieties, and the carbon backbone. The other models, which were based upon the superpositioning of *i*) the ether-O of L-TBOA at the C2 carboxylate position, *ii*) the centroid of the cyclopropyl ring of L-CCG-IV at the C2 carboxylate position, or *iii*) both, were discounted because they resulted in an inappropriate positioning of the carbon backbone and/or relevant side chains. For example, when the centroid of the cyclopropyl ring of L-CCG-IV was superpositioned on the C2 carboxylate position, the carbon backbone markedly deviated outside the bounds defined by the other analogues. The model that was selected as the most plausible EAAT2 pharmacophore (and used to evaluate the selectivity of L-β-*threo*-BA, see Discussion) is shown in Figure 4, with critical distances and angles between the various functional groups listed in an inset. The model conformer energy profiles

were: L-*anti-endo*-3,4-MPDC, 107.16 -157.48 Kcal/mol; cis-5-Me-L-*trans*-2,3-PDC, 10.00-91.62 Kcal/mol; CCG-IV, 103.59-109.67 Kcal/mol and L-TBOA, 1.64->500 Kcal/mol. The almost identical positioning of the two carboxylate Cs among the inhibitors suggests a very regimented interaction (i.e., electrostatic) between these groups and corresponding residues in the binding. Another notable feature of this pharmacophore is the planar arrangement of the α-C, β-C, amino-N and distal carboxylate-C atoms (i.e., x-y plane of the graphical representation shown in Figure 4). The positioning of the cyclopropyl ring of CCG-IV and L-*anti-endo*-3,4-MPDC, as well as the inhibitory activity observed when this ring is replaced with a cyclohexenyl group (see analogues in (Denton *et al.,* 2002)), suggest a unique role for possible Π bond-like interactions with the protein. Lastly, the area delineated by the phenyl ring highlights regions facilitating lipophilic interactions between the analogues and transporter binding site.

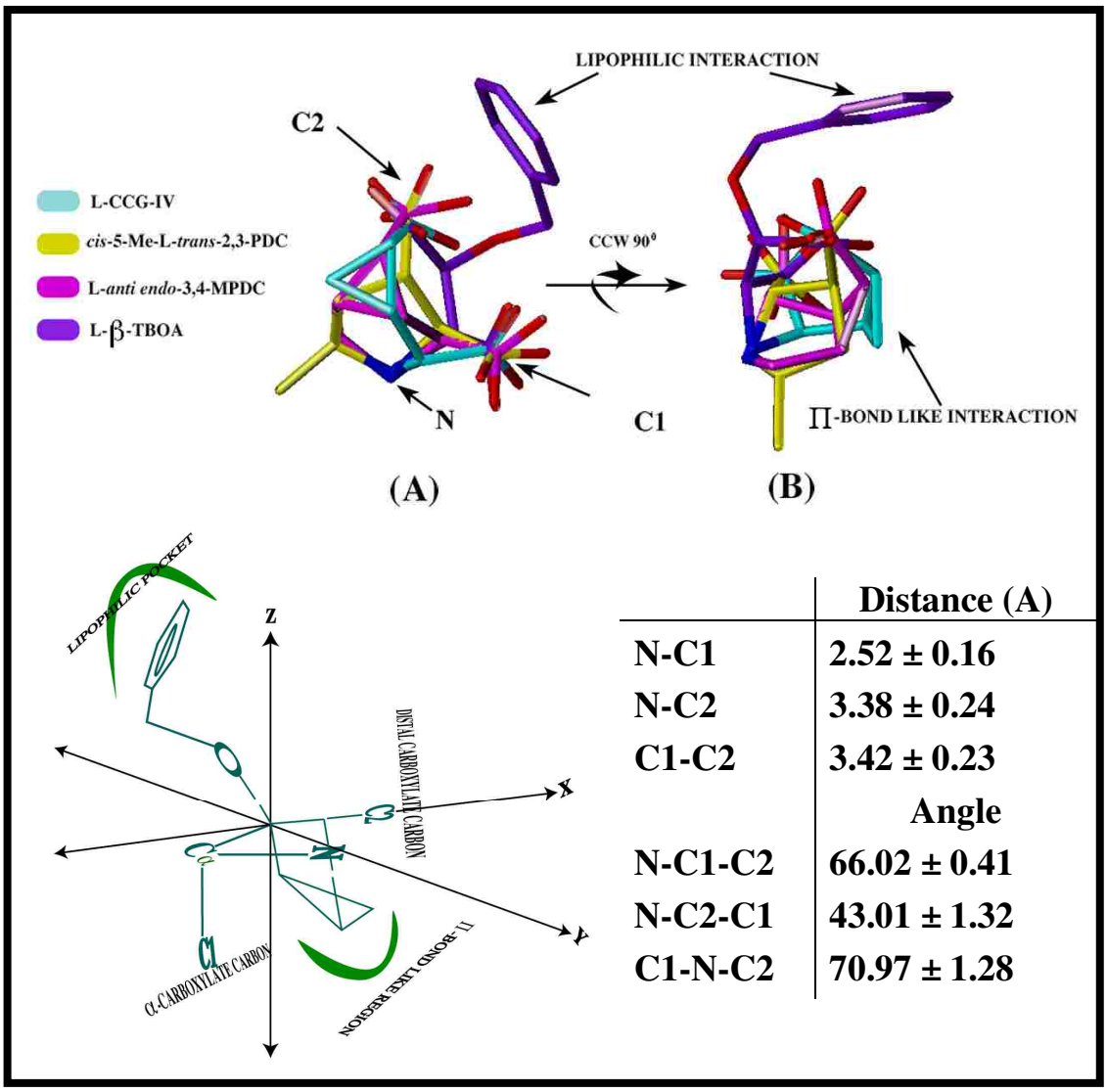

	Distance (A)
N-C1	2.52 ± 0.16
N-C2	3.38 ± 0.24
C1-C2	3.42 ± 0.23
	Angle
N-C1-C2	66.02 ± 0.41
N-C2-C1	43.01 ± 1.32
C1-N-C2	70.97 ± 1.28

Fig 4. EAAT2 Binding-Site Pharmacophore Model. Views **(A)** and **(B)** of the superpositioned (1cal spring constant), color-coded four training-set ligands that highlight the spatial placements of the amino nitrogen (N), α-carboxyl carbon (C1) and the distal carboxyl carbon (C2), along with other key structural features. A graphical representation depicting the averaged position of these structural features is also shown, with the averaged specific angle and distance measurements reported in the inset.

4. DISCUSSION

The ability to pharmacologically manipulate EAAT activity, and thereby assess its potential contribution to given processes, such as shaping an excitatory post synaptic signal or affording excitotoxic protection, is dependent upon the development of potent and selective inhibitors. Indeed, transport inhibitors such as L-*trans*-2,4-PDC and TBOA have been used to differentiate those synaptic connections in which EAATs likely contribute to signal shaping or termination (e.g., excitatory inputs on cerebellar Purkinje neurons) from those where uptake may not play such a role (e.g., excitatory signaling in CA1 hippocampal pyramidal neurons) (Isaacson and Nicoll, 1993; Sarantis *et al.,* 1993; Barbour *et al.,* 1994; Wadiche and Jahr, 2001). These or similar inhibitors have also been employed to demonstrate that compromised EAAT activity increases the likelihood and/or extent of excitotoxic damage (Robinson *et al.,* 1993; Rothstein *et al.,* 1993). Significantly, the compounds presently available for such applications have been limited to those that non-selectively block all of the EAATs or those that exhibit a substantial preference for EAAT2, thus leaving in question the specific contributions of EAAT1 and EAAT3. In the present work we identify L-β-BA as one of the first EAA analogues that inhibits EAAT3 activity more potently than it does EAAT1 or EAAT2. This effect was observed with EAATs expressed in two different cells systems, *Xenopus* oocytes and C17.2 neuroprogenitor cells, where, in each case, its mechanism of inhibition was confirmed as competitive. Consistent with the actions of the other β-substituted aspartate-based inhibitors, the *threo* configuration proved to be the more potent

diastereomer, exhibiting a sub-micromolar K_i at EAAT3 representative of about a 10-fold preference for the subtype. L-β-BA did not induce currents in oocytes expressing EAAT3 (or any of the EAATs), though it did block glutamate-mediated currents, further delineating its action as a non-substrate inhibitor.

The actions of L-β-BA are similar to those of TBOA in several respects. Significantly, each is a relatively effective inhibitor of all three EAAT subtypes, yet L-β-BA exhibits a preferential activity at EAAT3, while reports of TBOA activity have typically reported a preference for EAAT2 (Shimamoto *et al.,* 2004). While the observed 10-fold preference of L-β-*threo*-BA for EAAT3 is not sizeable enough to be classified as an EAAT3-specific inhibitor, its action raises interesting questions regarding what properties it has in common with other inhibitors of EAATs1-3 and what might be the basis for increased activity at EAAT3. Phrased another way, can L-β-BA and TBOA provide any insight into where the pharmacophores (and consequently the structural domains of the transporters) for EAAT2 and EAAT3 diverge? Given the lack of EAAT3-preferring ligands compared to those selective for EAAT2 and our previous SAR-modeling studies of EAAT2, we have begun to examine these issues by analyzing L-β-BA within the context of an EAAT2 pharmacophore model.

The EAAT2 pharmacophore model was constructed (see Methods for details) using four potent competitive non-substrate EAAT2 inhibitors that were as structurally diverse as possible. As shown in Figures 4 and 5, the nearly equivalent superposition of the three selected electrostatic bearing moieties (the two carboxyl groups and the amine moiety) of the training set ligands (as well as

in L-β-*threo*-BA) in 3D space suggests that these regions may define a critical ligand triad that serves as an initial recognition group plane. Thus, the electrostatic triad might initially interact with a limited collection of complimentary residues located at the EAAT protein binding site, most likely in combination with select ions. Additionally, other structural properties beyond this electrostatic configuration may serve to influence more subtle pharmacological properties, such as substrate versus non-substrate activity, potency, and EAAT subtype selectivity. In this respect, three additional regions exclusive of the carboxyl and amino functionalities are found within distinctive regions of 3D model space. The region occupied by introduction of a hydroxyl group (L-β-THA), methyl group (*cis*-3-Me-L-*trans*-2,3-PDC) or most prominently the extended arm of a benzyloxy group (TBOA) at the β-carbon of aspartate suggests the presence of a lipophilic pocket, consistent with our earlier work (Esslinger *et al.,* 2002), or a related region of lipophilic protein contacts near the initial recognition binding site residues. The sheer size of aromatic rings that appears to be tolerated at the binding site (i.e., see the recently described series of TBOA analogs in Shimamoto *et al.,* 2004) support the notion of regional protein contacts (e.g., along various transmembrane residues) rather than a distinctive lipophilic pocket. Some of these same residues may also interact with a methyl group of *cis*-4-methyl-L-*trans*-2,4-PDC. Interestingly, the addition of the methyl moiety to L-*trans*-2,4-PDC has little effect on potency, but converts this substrate into a non-substrate inhibitor of EAAT2 (Esslinger *et al.,* 2002). Taken together with the activity of TBOA, this suggests that interaction with these domains may

determine whether or not a bound ligand can be translocated. The orientation of this lipophilic domain relative to the carboxyl-carboxyl-amine group triad may occur in two ways, as suggested by the L-BOA *erythro* and *threo* stereoisomer, (see Figure 5B). Since the *threo* form exhibits greater potency, it is thought that the benzyl group projected within this model orientation (Figures 4 and 5) presents a ligand motif that is more favorable for complimentary interaction with residues at the binding site. Another feature of L-TBOA that may come into play is the arm linking the phenyl group to the aspartate backbone. Thus, the regio- and stereochemical placement of the ether oxygen of L-TBOA is suggestive of possible H-bonding at the binding site, potentially conferring enhanced ligand potency and/or influencing L-TBOA selectivity. The close 3D proximity of the two cyclopropyl rings of MPDC and CCG-IV are suggestive of a Π-bond like character to the region shown in Figure 4B that may also influence binding. Consistent with this proposition, the cyclohexenyl-based inhibitor structurally similar to the CCG class of compounds also shows increased selectivity for EAAT-2 (Denton *et al.,* 2002). Lastly, the unique regio- and stereochemical placement of the methyl group of *cis*-5-Me-L-*trans*-2,3-PDC, away from the benzyl extension of L-TBOA (or L-β-BA), points to the possibility of an additional region where modest lipophilic groups are tolerated. It remains less clear whether this area is a distinct lipophilic pocket associated with the EAAT protein (s).

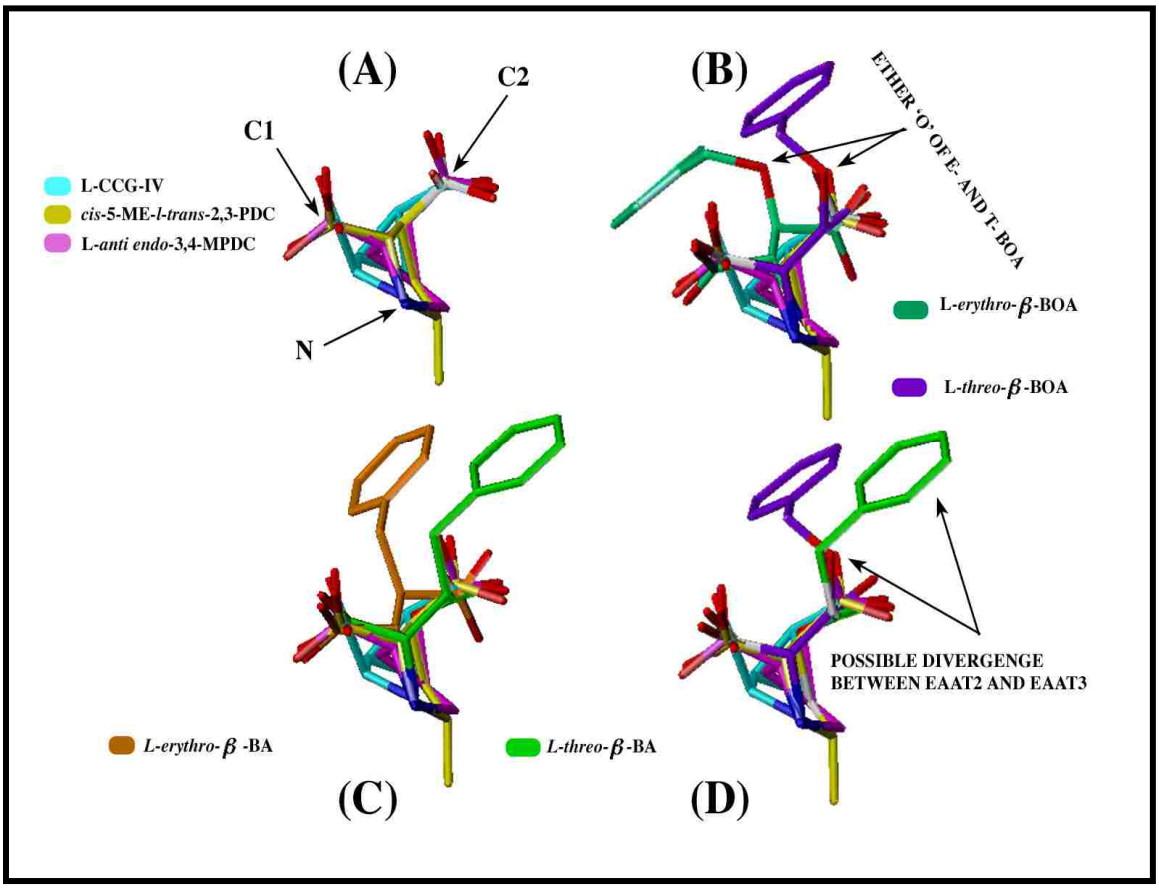

Fig 5. Assessment of conformations and activities of L-β-*threo*-BOA, L-β-*erythro*-BOA, L-β-*threo*-BA and L-β-*erythro*-BA against the EAAT2 binding-site pharmacophore. The pharmacophore model is shown in **(A)** without either TBOA or L-β-BA. In **(B)** the superposition (1cal spring constant) of L-β-*threo*- and L-β-*erythro*-BOA with the model illustrating the better fit of aspartyl backbone of the *threo* diastereomer with other aligned molecules, in addition to the distinct placements of the ether 'O' and the benzyl group that might influence the potency and selectivity for this inhibitor at EAAT2. A similar conclusion is reached regarding L-β-*threo*-BA, when the two diastereomers of the L-β-BA are compared **(C).** The superposition of L-β-*threo*-BOA and L-β-*threo*-BA with the model **(D)** suggesting that possible points of divergence between the EAAT2 and EAAT3 pharmacophores may include subtle differences in the size, location and/or orientation of the aromatic ring or in the oxygen atom present in the linking group of L-β-*threo*-BOA, but not L-β-*threo*-BA.

Similar analyses for the novel L-β-BA analogue (Figure 5), leads to the conclusion that the benzyl group of the more potent *threo* diastereomer is locating to similar regions as its L-TBOA conformer counterpart. This suggests that like EAAT2, EAAT3 proteins may accommodate these lipophilic groups to various extents, providing ligand-protein residue contacts lending to their respective potency profiles. The subtype selectivity, however, indicates that there are differences between the ways in which L-β-*threo*-BA and L-TBOA bind more favorably to EAAT3 and EAAT2, respectively. One underlying factor may reside in subtle difference in the size, location and/or orientation of the aromatic ring with respect to the lipophilic residues on the transporters. It is also interesting to consider that the specificity may be a result of the aromatic ring linkage to the aspartyl backbone relative to the protein residues that interact with this ligand region. Thus, the oxygen atom of L-TBOA may be preferentially hydrogen bonding with a residue in EAAT2, whereas within EAAT3 there may be reduced hydrogen bonding, yet preserved lipophilic contacts. Conversely, the carbon linking atom of the benzyl aspartate ligand is devoid of hydrogen bonding opportunity within the EAAT 2 binding domain, yet, may interact favorably with a lipophilic side chain residue within EAAT3 binding region. Hence, selectivity for one EAAT relative to another may be driven by both favorable and unfavorable ligand-protein residue side chain interactions involving the ligand benzyl group linking region.

Collectively, the superposition model coupled to ligand potency and selectivity data results in the following distinctive pharmacophore region map: 1)

a discrete three point area (triad) that is comprised of the electrostatic carboxyl and amino groups that are conserved in space across substrates and inhibitors and may be essential for initial ligand protein recognition, 2) areas nearby this electrostatic group triad that can accommodate select structural modification (e.g., cyclopropyl ring, methyl groups, and oxygen atoms), and 3) the unique 3D region consumed by the pendant benzyl ring moieties of L-TBOA, L-β-*threo*-BA and related analogs. These first two model regions suggest there exists an intimate and highly ordered region of the EAAT protein binding domain that may be associated with initial ligand recognition. Conversely, the area that accommodates the pendant benzyl groups is distinct and extended from the initial ligand recognition site, and also is more tolerant of steric bulk (e.g., additional aromatic rings and functional groups). It is particularly notable in this respect that the recent report of a crystal structure for a eukaryotic glutamate transporter homologue may now set the stage for the potential integration of emerging structural models of the EAATs (Yernool *et al.,* 2004; Kanner and Borre, 2002) with proposed pharmacophore models. From a functional perspective, the benzyl appended ligands may lend to greater lipophilic ligand-protein contacts thereby enhancing potency, but at a loss in the ability of the transporter to translocate the compound. Based on the comparison of these model details relative to the profiles described for the ligands in Table 1, it appears that respective preferential action of L-β-*threo*-BA and L-TBOA at EAAT3 and EAAT2, likely resides in the latter two distinctive pharmacophore regions, and in particular, a function of atom type (oxygen or carbon) extending

from the β-aspartyl backbone position. All of these SAR details are valuable for the subsequent design of more refined EAAT inhibitor ligands. Since the stereochemically defined pendant aromatic region is a more tolerant one, it is this area of the pharmacophore model that we are currently exploring to develop additional inhibitors to differentiate among the EAAT subtypes.

ACKNOWLEDGEMENT

The authors wish to thank M. Beckman and S. Patel for their insightful advice in the preparation of this manuscript. This work was supported in part by NINDS NS30570 (RJB), NINDS NS1R1536405 (J.M.G.), NINDS NS27600 (ARC), NINDS NS33270 (MPK) and NCRR COBRE RR15583 (RJB, J.M.G., C.S.E., M.P.K.).

Chapter 3.

Synthesis and preliminary pharmacological evaluation of novel derivatives of L-β-*threo*-benzylaspartate as inhibitors of the neuronal glutamate transporter EAAT-3.

Terri L. Mavencamp, Joseph F. Rhoderick, Richard J. Bridges**, C.Sean Esslinger**

Abstract

A series of β-benzylaspartate derivatives were prepared from N-trityl-L-aspartate dimethyl ester and evaluated as inhibitors of neuronal glutamate transporter EAAT3. The result of the structure-activity studies suggest that the position occupied by the aromatic ring of β-benzylaspartate within the binding site of EAAT3 may be different from that occupied by comparable groups in previously identified inhibitors, such as L-*threo*-benzyloxy aspartate (TBOA). Further, halogen substitutions at the 3-postition of the aromatic ring of β-benzylaspartate can increase the potency with which the analogues inhibit EAAT3.

1. Introduction

L-Glutamate is the most abundant excitatory neurotransmitter in the mammalian CNS and, as such, contributes to neuronal signaling and cognitive function through its activation of a wide variety of ionotropic and metabotropic excitatory amino acid (EAA) receptors (Balazs, R., Bridges, R. J. and Cotman, 2006). If extracellular glutamate concentrations in the CNS become excessive, it can lead to the over-activation of EAA receptors and the triggering of numerous neuropathological pathways (Balazs, R., Bridges, R. J. and Cotman, 2006; Hynd *et al.,* 2004; Foster and Kemp, 2006). Termed excitotoxicity, glutamate-mediated neuronal injury is believed to contribute to CNS pathology in acute insults (ischemia, traumatic injury), as well as chronic neurological disorders (e.g., ALS, Alzheimer's disease, epilepsy, and Huntington's disease). Excitatory amino acid transporters (EAATs) present on neurons and glia play a critical role in regulating extracellular levels of glutamate and are thereby positioned to influence: *i*) the access of neurotransmitter to synaptic and extrasynaptic EAA receptors, *ii*) the recycling of the neurotransmitter and *iii*) the accumulation of excitotoxic levels of glutamate (Danbolt, 2001; Bridges and Esslinger, 2005). The expression of EAATs has also been found to be altered in neurological disorders such as epilepsy, ischemia, spinal cord injury, amyotrophic lateral sclerosis (ALS), Alzheimer's and schizophrenia (Beart and O'Shea, 2007). Much of our understanding of the function of the EAATs has been dependent upon the development of substrates and inhibitors with which to probe transporter function and the physiological consequences of decreased activity.

Five distinct glutamate transporters (EAATs 1-5) have been identified by molecular cloning that, along with the sodium-dependent neutral amino acid transporters ASCT1-2, comprise a novel gene family (i.e., SLC1 in the Human Genome Organization HUGO nomenclature) (Hediger *et al.,* 2004). Uptake through the EAATs occurs via an alternate access mechanism that is electrogenic and driven by ionic gradients across the cell membrane. In this manner, the transport of one molecule of glutamate into a cell is stoichiometrically coupled to the import of three Na^+ ions and one H^+, and to the counter transport of one K^+ (Zerangue and Kavanaugh, 1996). While the EAATs share a similar mechanisms and ionic dependence, each exhibits a distinct localization (Danbolt, 2001). EAAT1 and EAAT2 are primarily considered to be glial transporters that exhibit a preferential distribution in the cerebellum and forebrain, respectively. In contrast EAAT3 is present on neurons and is enriched in forebrain areas. EAAT4 is localized to purkinje neurons in the cerebellum and EAAT5 is restricted to the retina. To a large degree the EAATs can be pharmacologically distinguished from one another based upon the comparative actions of a number of substrates and inhibitors, although EAAT2 stands alone with respect to readily available, well-characterized subtype-selective inhibitors (Bridges and Esslinger, 2005; Kanner *et al.,* 2001). Not surprisingly, considerable effort has been focused on the development of inhibitors that can be used to selectively modulate the activity of the other individual transporters.

Toward this goal our laboratories prepared L-β-benzylaspartate (L-β-BA) and identified it as one of the few EAAT inhibitors that exhibits a marked

selectivity for EAAT3 (Esslinger *et al.,* 2005). The more potent enantiomer, L-*threo*-β-benzylaspartate ((2*S*,3*S*) 3-benzylaspartate, L-*t*-β-BA), shows an approximate 10-fold preference for blocking EAAT3 compared to either EAAT1 or EAAT2 in C17.2 cells expressing the human isotypes. This contrasts with activity of the closely related and widely used inhibitor L-*threo*-benzyloxy aspartate (TBOA) which has been reported to more potently inhibit the activity of EAAT2 than EAAT3 (Shimamoto *et al.,* 2000; Shimamoto *et al.,* 2004; Humphrey *et al.,* 1994). In the present study a new series of L-β-benzylaspartate derivatives has been prepared from the easily accessible precursor N-trityl-L-aspartate dimethyl ester. The analogues were evaluated as inhibitors of ^{3}H-D-aspartate uptake in C17.2 neuroprogenitor cells transiently transfected to express human EAAT3. We report that structure activity profile of these inhibitors is quite different from TBOA-based analogues suggesting that subtle variations in size, substituents and orientation of the aromatic ring appended to the β-position of aspartate can noticeably influence activity at the EAATs. In particular, substitutions at the 3-position of the aromatic ring of L-*t*-β-BA are most favorable for imparting potency at EAAT3.

2. Results and Discussion

2.1. Preparation of β-substituted Aspartates

The starting material N-trityl-L-aspartate dimethyl ester (**2**) was prepared following a general procedure. The aspartate dimethyl ester was formed using thionyl chloride in methanol. N-Tritylation is achieved with triphenylmethyl chloride and triethylamine (Zervas and Theodorpoulos, 1956). The resulting starting material was purified by two subsequent crystallizations from methanol. The triphenylmethyl protecting group was chosen due to ease of preparation, mild deprotection conditions, and the protection against alpha-carbon deprotonation it imparts to the molecule to avoid alpha-racemization (Scheme 1).

Initially, beta addition was achieved by the addition of lithium hexamethyldisilyl amide (LiHMDS, 2 equivalents in THF) to a 1M solution of **2** in anhydrous THF at -32℃ under inert atmosphere. This was followed by quenching with the desired substituted-benzylic bromide (2-3 equivalents) and allowing the temperature to rise to 0℃ (Humphrey, 1994). Substituted-benzylic bromides are shown in Table 2 as R, A-J. The reaction was terminated by the addition of 2N ammonium chloride. This produced a mixture of **3**, *SS:SR* with *SR* as the major component in a 1:2 to 1:1 mixture of diastereomers. This was verified by detailed NMR analysis and compared to similar systems with similar reaction conditions reported that were accompanied by in-depth stereochemical determinations (Fernandez-Megia *et al.,* 1994).

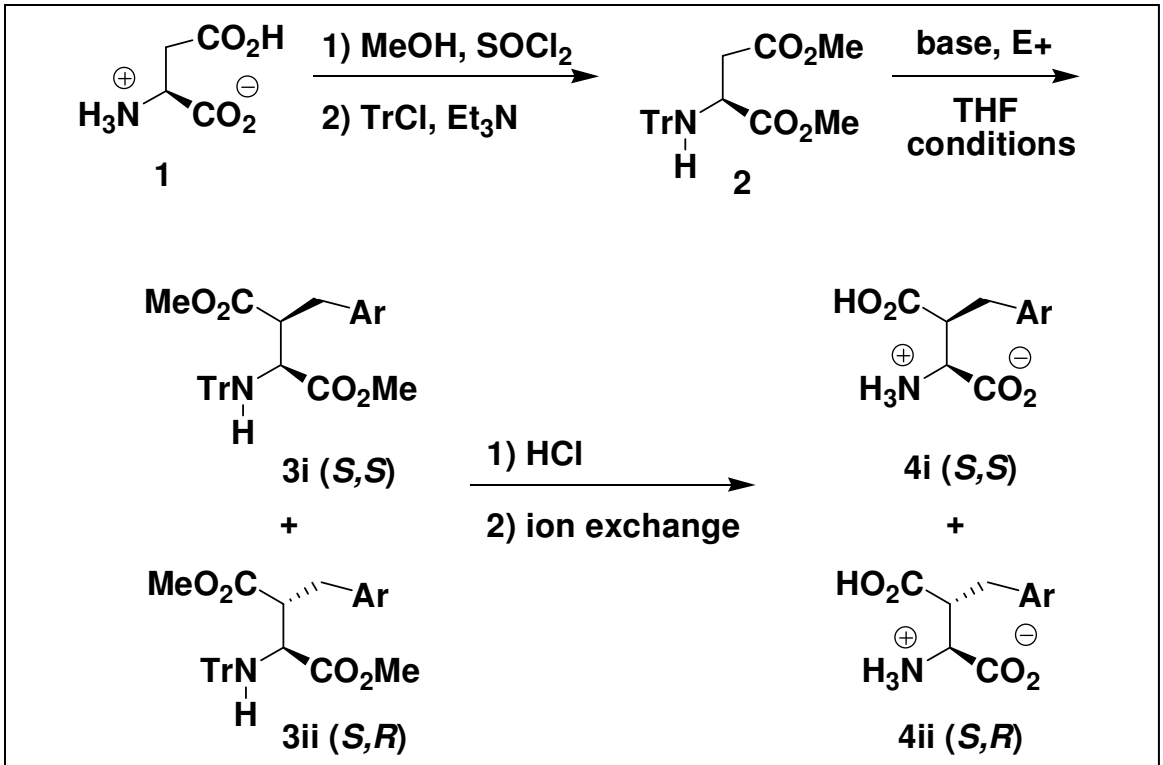

Scheme 1. Synthesis of β-benzyl aspartates. Tr = triphenyl methyl. See Table 1 and Experimental Section for base, E+, and conditions.

N-Protecting group + additives	Temp ℃	Base: E+	Time of rxn (hrs)	E+	S,S : S,R (i:ii)	% yield
1. Trityl	-35→0	2:2 LiHMDS	4	3F	1:2	57%
2. Trityl	-55	2:2 LiHMDS	6	3F	1:11	55%
3. Trityl	-55→0	2.5:3 LiHMDS	6	3F	1:2	65%
4. Trityl DMPU	-55	2:3 LiHMDS	21	3Cl	3:1	74%
5. Trityl	-65	2:2 LiHMDS	21	3Cl	1:11	68%
6. Trityl	-65	2:3 LiHMDS	21	3Cl	1:11	76%
7. Trityl	-55	2.1:2.3 KHMDS	21	3Nitro	99:1	51%
8. Trityl	-55	2.1:2.3 KHMDS	21	3F	99:1	58%
9. Trityl	-55→0	2.1:2.3 KHMDS	21	3Br	2.5:1	88%

Table 1. Conditions used and results obtained in the benzylation reactions. S,S:S,R ratios as determined by ^{1}H NMR.

Compound	R-group 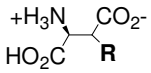	EAAT3 Uptake ^{3}H-D-Asp (25 µM) (% of Control)	Compound	R-group 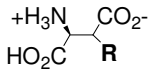	EAAT3 Uptake ^{3}H-D-Asp (25 µM) (% of Control)
L-β-Benzyl-asp **4A**		4 ± 2	L-β-3-Br-benzyl-asp **4F**	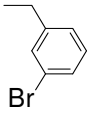	8 ± 3
L-β-Benzyl-asp ***S,S*-4i**		1 ± 1	L-β-3-F-benzyl-asp **4G**	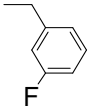	0 ± 0
L-β-Methyl-2-napthyl-asp **4B**	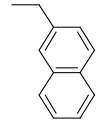	68 ± 6	L-β-4-F-benzyl-asp **4H**	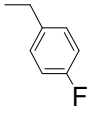	7 ± 3
L-β-3,5 Dimethyl-benzyl-asp **4C**	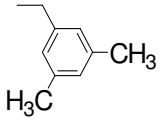	36 ± 7	L-β-3-Nitro-benzyl-asp **4I**	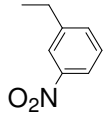	29 ± 5
L-β-3-Methyl-benzyl-asp **4D**	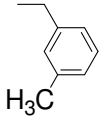	33 ± 3	L-β-4-Nitro-benzyl-asp **4J**	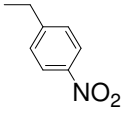	65 ± 8
L-β-2,6-Dichloro-benzyl-asp **4E**	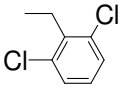	86 ± 5			

Table 2. Percent of control uptake in the presence of L-β-benzyl aspartate derivatives (control uptake with no inhibitor present is 100%). C17.2 Cells assayed for their ability to block 25µM ^{3}H-D aspartate uptake in the presence of 100µM inhibitor, n≥3. Inhibitors in an approximate 1:1 ration of (S,S) : (S,R) unless specified.

HPLC separation of L-β-BA diastereomers **4A** gave NMR spectra consistent with previous reports of similar aspartate syntheses (Humphrey *et al.,* 1994; Fernandez-Megia *et al.,* 1994; Hanessian *et al.,* 1998; Sakaguchi *et al.,* 2004). At this step, yields of the mixture ranged from 13.5% to 87% following chromatography. Yields generally improved with greater equivalents of substituted-benzylic bromide, Table 1: **5** vs. **6**, as well as higher temperatures, **2** vs. **3**, though diastereoselectivity decreased with increasing temperature. We found that the ratio of *SS:SR* increases to 1:11 if the temperature is decreased to -55℃ and quenched at this cold temperature (entries 5 and 6, Table 1). If the reaction temperature is allowed to rise to 0℃ after addition of substituted-benzylic bromide the ratio of *SS:SR* decreases to 1:2 to 1:1. Interestingly we found that adding DMPU to the starting material reverses the stereochemistry to give *SS:SR* in a 3:1 mixture of diastereomers (Hanessian *et al.,* 1998).

When KHMDS was used in place of LiHMDS we observed a switch in diastereoselectivity similar to that observed by Humphrey *et al.,* with N-benzyl-N-9-phenylfluoren-9-yl dimethyl aspartate (Humphrey *et al.,* 1994). We propose that Li complexes tightly to the enolate but may be forming a loose cyclic chelate between the enolate oxygen and the nitrogen (Figure 1), similar to that suggested by Fernàndez-Megía and Sardina (Fernàndez-Megía *et al.,* 1994). This is supported by the decrease in selectivity observed at higher temperatures, as well as the reversal of diastereoselectivity observed upon addition of DMPU.

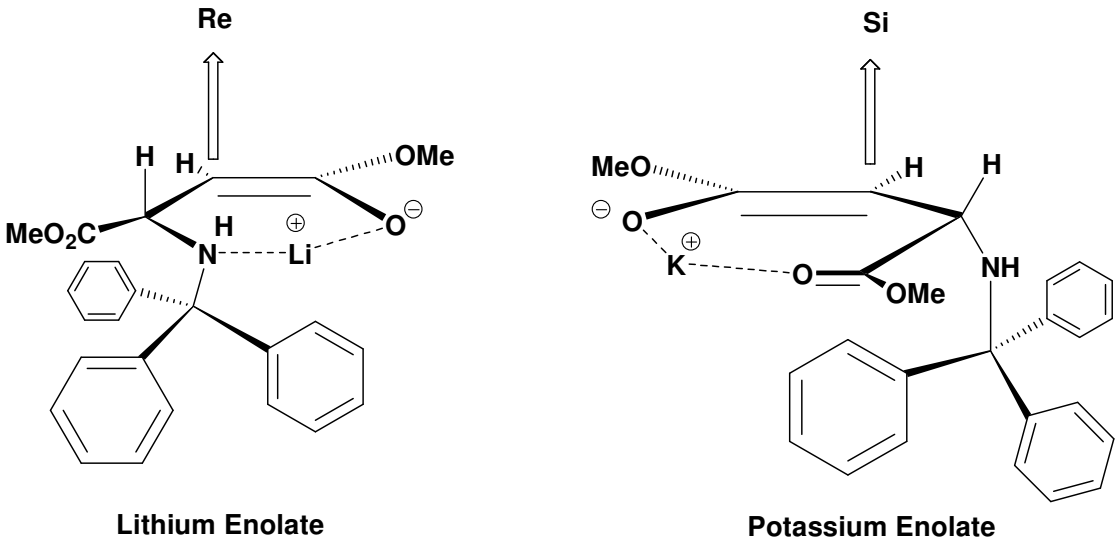

Figure 1. Low temperature chelation controlled diastereomeric outcome of enolates using lithium and potassium bases.

This reversal of selectivity suggests that the metal is being complexed by DMPU, thereby disrupting the nitrogen oxygen chelate and allowing the molecule more rotational flexibility. This would increase the probability that the Si face is open for attack. We hypothesize that potassium forms a cyclic enolate - α-ester chelation as previously proposed (Humphrey *et al.,* 1994; Fernàndez-Megía *et al.,* 1994), giving the (*S,S*) product (Figure 1).

Deprotection was achieved by heating the alkylated product (**3**) in 6N HCl to afford the chloride salt of the product. The reaction was then neutralized to a pH of 7, loaded on an anion exchange resin (acetate form, 10g resin per gram product), and eluted using a gradient of 1-5N acetic acid. The zwitterion was obtained by concentrating the ninhydrin positive fractions followed by chasing the product with deionized water several times. Alternatively, the product can be precipitated out of ethyl acetate then water to give final product.

2.2. Inhibitory Activity at EAAT3

The compounds were evaluated in collaboration with the Bridges lab as inhibitors of EAAT3. This was achieved by quantifying their ability to reduce the uptake of ^{3}H-D-asparate in standard competition assays[10]. In each instance the analogues (SS:SR ratio of an approximately 1:1) were added simultaneously with the radiolabel to achieve a final concentration of 100 µM and 25 µM, respectively. The results are summarized in Table 2 as % of Control activity, *i.e.,* uptake in the absence of any inhibitor. The replacement of the benzyl group on L-β-BA with a napthyl moiety (**4B**) resulted in a marked reduction of inhibitory activity.

Interestingly, when an analogous substitution is made with L-TBOA to produce L-*threo*-β-(1-napthyl)methyloxaspartate (L-TNOA1) and L-*threo*-β-(1-napthyl)methyloxaspartate (L-TNOA2), the inhibitory activity was retained (or increased) as reflected by a decrease in the IC_{50} with which the compounds blocked the uptake of ^{14}C-glutamate into COS-1 cells expressing EAAT3 (i.e., L-TBOA, 7.0 μM; L-TNOA1, 4.8 μM; L-TNOA2, 6.5 μM) (Shimamoto *et al.,* 2000). This would suggest that the proposed lipophilic regions adjacent to the substrate binding domain on EAAT3 with which the benzyl groups of either L-TBOA or L-*t*-β-BA interact, can only accommodate a larger napthyl group when its orientation is dictated by the methoxy linkage of TBOA and not the methylene linking group of L-*t*-β-BA. Recent structural insight into these substrate binding domains has emerged from crystallographic studies in which the archaeal aspartate transporter Glt_{ph} from *Pyrococcus horikoshii* has been crystallized in the presence of either L-aspartate or L-TBOA (Boudker *et al.,* 2007). It was concluded that the binding site is positioned between two hairpin loops that extend from opposite sides of the membrane and likely participate in the gating of substrate movement. While non-substrate inhibitors such as L-TBOA or L-*t*-β-BA can fit into this site normally occupied by L-glutamate, interaction with nearby lipophilic residues in the vicinity of the HP2 loop may preclude subsequent conformational movements that are necessary for substrate translocation, such as the closure of the external HP2 gate or providing access of external sodium to its requisite binding site. Interestingly, the ability of an inhibitor to interact with EAAT3 in this manner may increase its potency as an inhibitor, but decrease its

ability to act as an alternative substrate. Comparisons between the naphthyl derivatives of L-TBOA or L-β-BA, suggest, however, that the exact placement of the aromatic rings within the binding site of EAAT3 is probably distinct and may additionally point to structural differences between the EAAT3 and EAAT2 subtypes.

The addition of a methyl (**4D**) or nitro (**4I**) group to the 3 position of of L-β-BA, as well as a methyl group to both the 3 and 5 positions (**4C**), resulted in a retention of some inhibitory activity, although to a lesser degree than found in the parent molecule (e.g. about 30% of Control uptake vs. 4%). Again, this may be indicative of a more constrained binding arena surrounding the aromatic ring of L-β-BA when compared to L-TBOA. In contrast to these compounds, the di-substitution of chloro groups at the 2 and 6 position (**4E**) produced an almost complete loss of inhibitory activity. In this instance the decreased ability to bind to EAAT3 may be attributable to steric clashes with the transporter itself or, given the locations on the aromatic ring, between the substituents and the carbon backbone of aspartate when it assumes the requisite conformation for binding. Comparisons among additions made at the 3 position revealed a rank order of inhibitory activity of: methyl (**4D**) ≈ nitro (**4I**) < bromo (**4F**) < fluoro (**4G**). Lastly, L-β-3-F-BA (**4G**) and L-β-4-F-BA (**4H**) inhibited EAAT3-mediated uptake to a similar or greater extent than observed with either L-β-3-Br-BA or the parent L-β-BA. This would be consistent with the steric argument that the lipophilic region interacting with the benzyl group of L-β-BA in the binding site of EAAT3 is spatially confined, as well as reflect the ability of fluoro groups to favorably

interact with both regional sidechain R groups and backbone peptide bonds (Muller *et al.,* 2007).

To illustrate the diastereomeric preference of EAAT3 for ligand binding as well as highlight the diastereoselectivity of the benzylation reaction depending on base used, the individual diastereomers ***(S,S)*4Gi** and ***(S,R)*4Gii** of L-β-3-F-BA **4G** were synthesized and evaluated as inhibitors of EAAT3. Competitive binding curves were obtained using ^{3}H-D-asparate at 1μM and varying the concentration of inhibitor (Figure 2). Curve fitting using GraphPad Prism 4.0 software to the equation Y = 1/(1+10^(X-logIC_{50})), where Y is the fractional % of control and X is the log[Inhibitor] in M, IC_{50} values were obtained for the two diastereomers. As reported previously, the (*S,S*) diastereomer is the more potent (Esslinger *et al.,* 2005; Shimamoto *et al.,* 2000), and in this case ***(S,S)*4Gi** exhibits a 10-fold higher affinity for EAAT3 than ***(S,R)*4Gii**.

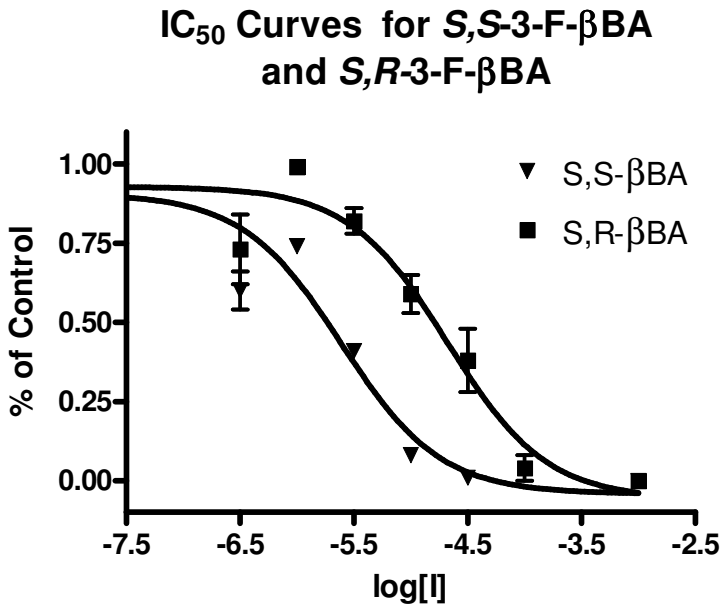

Figure 2. IC_{50} curves for (*S,S*)-3-F-β BA and (*S,R*)-3-F-β BA with [^{3}H-D-aspartate] = 1 µM. (*S,S*) 3-F-βBA IC_{50} = 2.46+/-0.9 µM (*S,R*)-3-F-β BA IC_{50} = 21.1+/-9.2 µM (IC_{50} +/- SEM).

2.3 Molecular Modeling

The recently published crystallographic study in which L-TBOA is bound to the archaeal aspartate transporter Glt_{ph} provides a strategy to conformationally compare these two inhibitors (Boudker *et al.,* 2007). The similarities are readily apparent when the bound conformation of L-TBOA is extracted from crystal structure and overlaid with a computationally minimized (Esslinger *et al.,* 2005) conformation of L-*threo*-β-BA (Figure 3). While the aromatic rings are positioned in a similar direction it also appears that the benzyl group of L-*threo*-β-BA is considerably closer to the carbon backbone of the amino acid than that of L-TBOA. In this respect the aromatic rings of the two analogues are likely interacting with subtly different lipophilic regions within the binding domain on EAAT3. Our SAR data would suggest that the in the instance of L-*threo*-β-BA, this region of the protein is less accommodating of steric bulk than the comparable region delineated by L-TBOA. Further, it is tempting to speculate that the ability of L-*threo*-β-BA to interact with these portions of the binding site may be a factor in its selectivity for EAAT3.

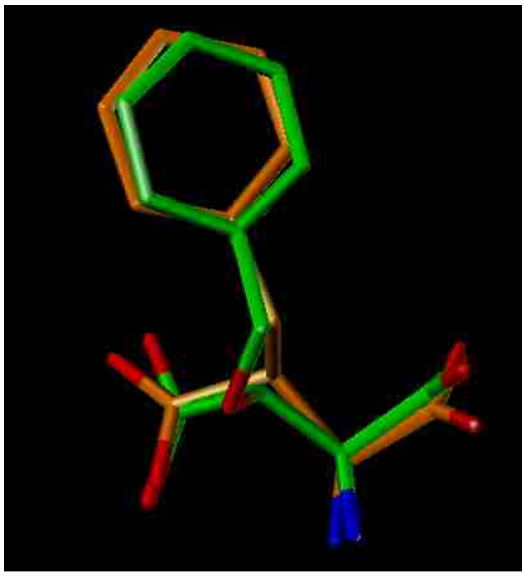

Figure 3a. Overlay of L-TBOA and L-*threo*-β-BA using the bound conformation of L-TBOA and similar conformation of L-*threo*-β-BA. Viewed by looking down perpendicular to the plane of the aromatic ring.

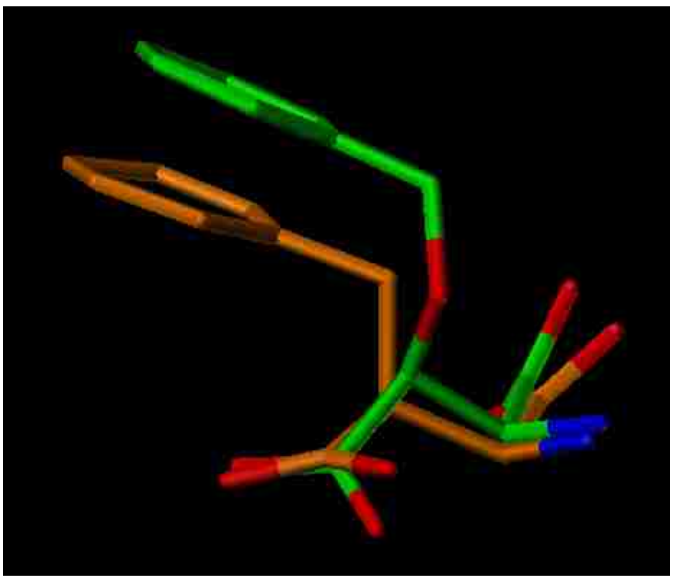

Figure 3b. Overlay of L-TBOA and L-*threo*-β-BA using the bound conformation of L-TBOA and similar conformation of L-*threo*-β-BA. Viewed by looking parallel to the plane of the aromatic ring.

3. Conclusions

A series of L-β-benzylaspartate derivatives have been prepared from N-trityl-L-aspartate dimethyl ester in which diastereomeric control was achieved using either lithium hexamethyldisilazide to yield predominantly the (2*S*,3*R*) adduct in one example or potassium hexamethyldisilazide to yield predominantly the (2*S*,3*S*) adduct in one example and evaluated as inhibitors of the neuronal glutamate transporter EAAT3. SAR data, including the inactivity of L-β-methyl-2-napthyl-aspartate (**4B)** and the increased activity of L-β-3-F-benzylaspartate relative to the lead analogue L-β-benzylaspartate, suggest a confined interaction between lipophilic domains of EAAT3 and the aromatic moiety of L-β-benzylaspartate that is distinct from previously characterized inhibitors, such as L-TBOA. These finding will be further explored in pursuit of more potent and selective ligands for the EAAT subtypes.

4. Experimental Section

In order to verify the purity and composition of the compounds product analysis was performed by high resolution mass spectrometry. Intermediates were treated with trifluoroacetic acid prior to mass spectrometry to remove the trityl group so the signal of the molecular ions could be detected. Proton and carbon NMR were taken on a Varian 400 MHz NMR in $CDCl_3$, D_2O or DMSO with TMS as the internal standard. NMRs were reported as mixtures of SS:SR with each diastereomer being identified where possible. Diastereomers on carbon NMR are indicated in parentheses where carbon peaks of each molecule are resolved. Chirality was verified by optical rotation on a Perkin-Elmer 241 Polerimeter in 1N HCl unless otherwise specified in a 1.0dm tube. Reagents were purchased from Sigma (St. Louis, MO) and were used without further purification. Microanalyses were performed for C, H, and N (Midwest Microlab, Indianapolis, IN) and were within ± 0.4% of theoretical values. Compounds showing potency equal to or greater than L-β-Benzyl-Aspartate (approximate 1:1 S,S:S,R mixture) were resolved by semi-preparative reverse phase HPLC. The detection method was a Waters 486 tunable absorbance detector set at 254 nm.

4.1. N-tritylamino dimethyl ester aspartate (2)

L(+)-Aspartic acid (26 g, 100 mmol) was stirred in a round bottom flask in a 1M solution of Methanol (200 ml). Thionyl chloride (22 ml, 140 mmol) was added dropwise. The solution was stirred at room temperature for 48 hours. The

resulting dimethyl ester aspartate hydrochloride was washed 3 times with methanol, 3 times with methylene chloride, 2 times with toluene and once with water. The dimethyl ester aspartate was then suspended in methylene chloride (200ml) and dried with magnesium sulfate. Triphenyl methyl chloride (53 g, 95 mmol) was added followed by the dropwise addition of triethyl amine (83.6 g, 300 mmol). The reaction was stirred overnight then diluted with ether and filtered through a silica plug with a 30/70 solution of ethyl acetate/hexanes. The filtrate was concentrated and rinsed 2 times with methylene chloride and recrystalized from methanol to yield N-tritylamino dimethyl ester aspartate **2** (70%). ^{1}H NMR (400 MHz, $CDCl_3$) δ: 7.54-7.48 (m, 6H), 7.32-7.15 (m, 9H), 3.77-3.71 (m, 1H), 3.69 (s, 3H), 3.28 (s, 3H), 2.99-2.91 (s, 1H), 2.73-2.62, (m, 1H), 2.58-2.48 (m, 1H). ^{13}C NMR (100 MHz, $CDCl_3$) δ: 173.86, 170.95, 145.61, 128.71, 127.83, 126.48, 71.13, 53.63, 51.91, 51.71, 40.16. $[\alpha]^{21}_{D}$ = 13.3° (ethyl acetate).

4.2. General procedure for alkylation:

Compound **2** was placed in a flame dried round bottom flask equipped with a stir bar. 1 M anhydrous THF was added under argon and the reaction was super-cooled. Once cooled 1M LiHMDS in THF (2-3 equivalents) was added via needle and syringe. After approximately 20 minutes the desired substituted-benzylic bromide (2-3 equivalents) was added. The temperature was then allowed to rise to 0ºC (unless specified) and the reaction was stirred until quenched (4-24 hours) with 2N NH_4Cl. Water and ethyl acetate (or ether) were added for separation. The water layer was subsequently washed three times

and the organic layers were combined and concentrated. Flash chromatography, when needed, through silica gel using hexane:ethyl acetate in an approximate 85:15 ratio gave the desired protected substituted benzylaspartate in good to moderate yields.

4.3. N-tritylamino dimethyl ester β-benzylaspartate (3a)

To **2** (1.55 g, 3.84 mmol) in 1M THF under Argon at -23°C was added LiHMDS (9.6 ml, 11.53 mmol). After 15minutes benzyl bromide (1.15 ml, 9.6 mmol) was added and temperature allowed to rise to 0ºC at which time it was stirred for a subsequent 2.5 hours. The reaction was quenched and ether was added for separation followed by a silica plug (85:15 Hexanes:ethyl acetate) (82.7%: 1.57 g). ^{1}H NMR (400 MHz, $CDCl_3$) δ : 7.57-7.48 (m, 6H), 7.32-7.20 (m, 14H), (3.94-3.90 (m, .5 H, S,S), 3.75-3.72 (m, .5 H, S,R)), (3.65 (s, 1.5H, S,S), 3.60 (s, 1.5H, S,R)), (3.28 (s, 1.5H, S,S), 3.23 (s, 1.5H, S,R)), 3.19-2.88 (m, 3H). ^{13}C NMR (100 MHz, $CDCl_3$) δ: 172.77, 172.51, 145.43, (139.15, 138.96), 129.12, 128.72, 127.71, 126.40, 126.22, (71.07, 70.93), (58.11, 57.67), 52.82, (51.65, 51.95), (51.53, 51.48), (34.05, 33.47). HRMS m/e calcd. for $C_{13}H_{17}NO_4^+$ 252.1236, found 252.1225.

4.4. N-tritylamino dimethyl ester β-2-napthylmethyl-aspartate (3b)

To **2** (2.5 g, 6.2 mmol) in 1M THF under Argon at -35°C was added LiHMDS (18.6 mmol). 20 minutes later 2-napthyl methyl bromide was added (3.4 g, 15.5 mmol) as a solid all at once. Temperature was allowed to rise to 0ºC, at which time it was stirred for an additional 4 hours before being quenched with 2N NH_4Cl (9 ml). Ethyl acetate was added for separation, followed by silica column 85:15

hexane:ethyl acetate (1.68 g, 50%). ^{1}H NMR (400 MHz, $CDCl_3$) δ : 7.84-7.74 (m, 3 H), 7.66-7.59(m, 1 H), 7.47-7.43 (m, 7H), 7.37-7.29 (m, 1 H), 7.18-7.26 (m, 8H), 7.16-7.11(m, 1 H), 7.09-6.99 (m, 1 H) (3.91-3.87 (m, .4H, S,S), 3.73-3.70 (m, .6H, S,R)), (3.61 (s, 1.2 H, S,S), 3.56 (s, 1.8 H, S,R)), (3.27 (s, 1.2 H, S,S), 3.22 (s, 1.8 H, S,R)), 3.19-2.90 (m, 3H). ^{13}C (100 MHz, $CDCl_3$) δ: 173.20, 172.93, 145.76, 135.32, 133.38, 129.80, 129.07, 129.01, 128.93, 128.19, 128.08, 128.04, 127.96, 127.00, 126.81, 126.72, 126.64, (71.41, 71.31), 60.63, 52.98, 52.02, 49.66, 34.30. HRMS m/e calcd. for $C_{17}H_{20}NO_4^+$ 302.1392, found 302.1388.

4.5. N-tritylamino dimethyl ester β-3,5 dimethyl-benzylaspartate (3c)

To 2 (3.2 g, 8.02 mmol) in 1M THF under Argon at -55°C was added LiHMDS (24 mmol). 20 minutes later 3,5 dimethyl benzyl bromide was added (6.4 g, 32.1 mmol) as a solid all at once. Temperature was allowed to rise to 0ºC, at which time it was stirred for an additional 1.5 hours before being quenched with 2N NH_4Cl (12 ml). Ethyl acetate was added for separation, followed by silica column 85:15 hexane:ethyl acetate (61%, 3.9 g). ^{1}H NMR (400 MHz, $CDCl_3$) δ : 7.47 (m, 6H), 7.29-7.20 (m, 9H), 6.85-6.76 (m, 3H), (3.86-3.83 (m, .66 H, S,S), 3.72-3.68 (m, .33H, S,R)), (3.63 (s, 1H, S,S), 3.60 (s, 2H, S,R)), (3.25 (s, 1H, S,S), 3.20 (s, 2H, S,R)), 3.03-2.74 (m, 3H), (2.29 (5 H app. singlet, S,S), 2.17 (1H app. singlet S,R)). ^{13}C (100 MHz, $CDCl_3$) δ: (173.05, 172.96), (172.80, 172.69), 145.52, (139.05, 138.93), (137.78, 137.69), (128.81, 128.69), 127.93, 127.87, 127.78, 127.17, 126.72, 126.58, 126.48, 126.37, (71.16, 70.93), (58.19, 57.79), (52.86, 52.77), (51.78, 51.72), (51.65, 51.60), (33.93, 33.36), 21.21. HRMS m/e calcd. for $C_{13}H_{18}NO_4^+$ 280.1549, found 280.1540.

4.6. N-tritylamino dimethyl ester β-3 methyl-benzylaspartate (3d)

To **2** (1.86 g, 4.61 mmol) in 1M THF under Argon at -30℃ was added LiHMDS (13.8 mmol) slowly. 20 minutes later 3 methyl benzyl bromide was slowly added (1.56 ml, 11.5 mmol). Temperature was allowed to rise to 0ºC, at which time it was stirred for an additional 4 hours before being quenched with 2N NH_4Cl (7 ml). Ethyl acetate was added for separation, followed by silica column 85:15 hexane:ethyl acetate (1.05 g, 45%). ^{1}HNMR (400 MHz, $CDCl_3$) δ: 7.48-7.45 (m, 7H), 7.32-7.13 (m, 10H), 7.03-6.93 (m, 2H), (3.86-3.81 (m, .66H, S,R), 3.68-3.64 (m, p. obsc., .33H, S,S)), (3.63 (s, 1H, S,S), 3.59 (s, 2H, S,R)), (3.24 (s, 1H, S,S), 3.19 (s, 2H, S,R)), 3.08-2.77 (m, 3H), (2.33 (s, 2H, S,R), 2.30 (s, 1H, S,S)). ^{13}CNMR (100 MHz, $CDCl_3$) δ: 172.99, 172.74, 145.55, 139.15, 139.01, 129.71, 128.83, 127.81, 126.51, 125.82, (71.16, 70.98), (58.19, 57.79), (52.89, 52.86), (51.84, 51.77), (51.71, 51.65), (34.02, 33.46), 21.38. HRMS m/e calcd. for $C_{14}H_{19}NO_4^+$ 266.1392, found 252.1225.

4.7. N-tritylamino dimethyl ester β-2,6 dicloro-benzylaspartate (3e)

To **2** (4.35 g, 10.78 mmol) in 1M THF under Argon at -35℃ was added LiHMDS (32.3 mmol). After stirring at -35℃ for 15 minutes, 2,6-diclorobenzyl bromide was added by removing the septa and quickly adding the dry reactant (6.47 g, 26.95 mmol). Temperature was allowed to rise to 0ºC, at which time it was stirred for an additional 5 hours before being quenched with 2N NH_4Cl (15 ml). Ethyl acetate was added for separation. No starting material was observed by TLC and NMR showed disappearance of starting material with no breakdown to aspartic acid. ^{1}HNMR (400 MHz, $CDCl_3$) δ: 7.53-7.49 (m, 6H), 7.29-7.15 (m,

11H), 7.10-7.06 (m, 1H), (3.94-3.90 (m, .5H, S,R), 3.78 (m, .5H, S,S)), (3.63 (s, 1.5H, S,S), 3.62, (s, 1.5H, S,R)), 3.55-3.38 (m, 2H), (3.20 (s, 1.5H, S,S), 2.19 (s, 1.5H, S,R)), 3.06-3.02 (m, 1H). ^{13}CNMR (100 MHz, $CDCl_3$) δ: (172.72, 172.51), (172.31, 172.17), 145.46, 135.75, 135.29, 134.90, 129.40, 128.84, 127.74, 127.22, 127.02, 126.42, 126.34, (71.25, 70.90), (58.08, 57.70), (51.86, 51.74), (51.68, 51.60), (50.11, 49.25), (30.28, 29.62). HRMS m/e calcd. for $C_{13}H_{15}Cl_2NO_4^+$ 320.0456, found, 320.0441.

4.8. N-tritylamino dimethyl ester β-3 bromo-benzylaspartate (3f)

To **2** (2.27 g, 5.63 mmol) in 1M THF under Argon at -35℃ was added LiHMDS (16.9 mmol) slowly. 20 minutes later 3-bromo-benzyl bromide was added (3.5 g, 14.1 mmol) as a solid all at once. Temperature was allowed to rise to 0ºC, at which time it was stirred for an additional 2.5 hours before being quenched with 2N NH_4Cl (5 ml). Ethyl acetate was added for separation, followed by silica column 85:15 hexane:ethyl acetate (56%, 1.8 g). Spectra S,R, separated via column chromatography. S,R comes off first followed by S,S. Spectra reported for S,R ^{1}HNMR (400 MHz, $CDCl_3$) δ: 7.46-4.44 (m, 5H), 7.34-7.29 (m, 5H), 7.26-7.08 (m, 9H), 3.86-3.82 (m, 1H), 3.58 (s, 3H), 3.21 (s, 3H), 2.99-2.78 (m, 3H). ^{13}CNMR (100MHz, $CDCl_3$) δ: 173.04, 172.55, 145.68, 141.96, 132.15, 130.16, 129.72, 129.05, 128.11, 127.85, 126.82, 122.63, 71.34, 58.32, 52.77, 51.96, 33.21. HRMS m/e calcd. for $C_{13}H_{16}BrNO_4^+$ 330.0341, found 330.0336.

4.9. N-tritylamino dimethyl ester β-3 fluoro-benzylaspartate (3g)

To **2** (.5 g, 1.24 mmol) in 1M THF under Argon at -35℃ was added LiHMDS (2.5 ml) slowly. 20 minutes later 3-fluoro-benzyl bromide was slowly added (.304 ml, 2.40 mmol). Temperature was allowed to rise to 0ºC, at which time it was stirred for an additional 4 hours before being quenched with 2N NH_4Cl (3 ml). Ethyl acetate was added for separation, followed by silica column 85:15 hexane:ethyl acetate (57%, .363 g). ^{1}HNMR (400 MHz, $CDCl_3$) δ: 7.47-7.43 (m, 6H), 7.32-7.18 (m, 10H), 6.98-6.83 (m, 3H), (3.86-3.82 (m, .66H, S,R), 3.64-3.60 (m, .33H, S,S)); (3.64 (s, 1H, S,S), 3.59 (s, 2H, S,R)); (3.25 (s, 1H, S,S), 3.20 (s, 2H, S,R)); 3.05-2.87 (m, 3H). ^{13}CNMR (100 MHz, $CDCl_3$) δ: 173.04, 172.64, 161.81, 145.86, 142.09, 130.02, 129.05, 128.11, 126.82, 124.82, (116.13, 115.91), (113.62, 113.41), 71.32, 58.30, 52.86, 52.08, 51.99, 33.33. HRMS m/e calcd. for $C_{13}H_{16}FNO_4^+$ 270.1142, found 270.1141.

4.10. N-tritylamino dimethyl ester β-3 fluoro-benzylaspartate (3g, *S,S*)

Trityl aspartate (.555 g, 1.38 mmol) was placed in a flame dried round bottom flask equipped with stir bar. Anhydrous THF (5.5 ml) was added under argon and reaction was cooled to -35℃. Once cooled 20% KHMDS in THF (3.2 ml) was slowly added, 20 minutes later 3-Floro benzyl bromide was slowly added (.39 ml, 3.16 mmol). The reaction was stirred for an additional 21 hours before being quickly quenched with 2N NH_4Cl (4 ml). Separate by adding water and ethyl acetate. Wash water layer two more times with ethyl acetate, combine organic layers and concentrate. Purification by chromatography on silica gel using ethyl acetate and hexanes 15:85 gave product in 58% yield (.407 g).

^{1}HNMR (400MHz, $CDCL_3$) δ: 7.51-7.46 (m, 7H), 7.27-7.20 (m, 11H), 7.00-6.86 (m, 1H), 3.69 (s, 3H), 3.64-3.60 (p.obsc. m, 1H-α), 3.28 (s, 3H), 2.95 (m, 1H-β); (2.69-2.65 (m, 1H), 2.54-2.50 (m, 1H,). ^{13}CNMR (100MHz, $CDCl_3$) δ: 173.04, 172.64, 161.81, 145.86, 142.09, 130.02, 129.05, 128.11, 126.82, 124.82, (116.13, 115.91), (113.62, 113.41), 71.32, 58.30, 52.86, 52.08, 51.99, 33.33.

4.11. N-tritylamino dimethyl ester β-3 fluoro-benzylaspartate (3g. *S,R*)

Trityl aspartate (.5 g, 1.24 mmol) was placed in a flame dried round bottom flask equipped with stir bar. Anhydrous THF (5 ml) was added under argon and reaction was cooled to -55℃. Once cooled LiHMDS in THF (2.5 ml) was slowly added, 20 minutes later 3-Floro benzyl bromide was slowly added (.3 ml, 2.48 mmol). The reaction was stirred for an additional 21 hours before being quickly quenched with 2N NH_4Cl (4 ml). Separate by adding water and ethyl acetate. Wash water layer two more times with ethyl acetate, combine organic layers and concentrate. Purification by chromatography on silica gel using ethyl acetate and hexanes 15:85 gave product in 55% yield (.35 g). ^{1}HNMR (400MHz, $CDCL_3$) δ: 7.51-7.46 (m, 6H), 7.31-7.27 (m, 9H), 7.22 (d, 1H, J=7.33), 7.00 (d, 1H, J=7.33), 6.94-6.92 (m, 2H), 3.95 (m, .1H, S,S), 3.68 (m, .9H, S,R), 3.65 (s, .3H, S,S), 3.60 (s, 2.7H, S,R,), 3.27 (s, .3H, S,S), 3.22 (s, 2.7H, S,R), 3.08-2.85 (m, 3H).

4.12 N-tritylamino dimethyl ester β-4-fluoro-benzylaspartate (3h)

To **2** (.536 g, 1.33 mmol) in 1M THF under Argon at -30℃ was added LiHMDS (2.66 mmol) slowly. 20 minutes later 4-fluoro-benzyl bromide was added (.33 ml, 2.66 mmol) dropwise. Temperature was allowed to rise to 0ºC, at which time it

was stirred for an additional 2 hours before being quenched with 2N NH_4Cl (6 ml). Ethyl acetate was added for separation, followed by silica column 85:15 hexane:ethyl acetate (.517 g, 76%). (Found: C, 75.06; H, 6.00; N, 2.74 $C_{32}H_{30}FNO_4$ requires C, 75.13; H, 5.91; N, 2.74). ^{1}H NMR (400 MHz, $CDCl_3$) δ: 7.48-7.44 (m, 6H), 7.29-7.15 (m, 9H), 7.13-7.05 (m, 2H), 6.99-6.89 (m, 2H), (3.86-3.82 (m, .5H, S,R), 3.69-3.65 (m, .5H, S,S)), (3.63 (s, 1.5H, S,S), 3.58 (s, 1.5H S,R)), (3.24 (s, 1.5H, S,S), 3.19 (s, 1.5H, S,R)), 3.09-2.78 (m, 3H). ^{13}C NMR (100 MHz, $CDCl_3$) δ: (172.83, 172.78), 172.51, (172.71, 160.28), 145.44, (134.85, 134.82), (134.65, 134.62), (130.45, 130.38), (130.35, 130.27), 128.77, 128.65, 127.78, 126.52, 126.42, (115.26, 115.20), (115.05, 115.01), (71.13, 70.99), (58.05, 57.52), 53.00, (51.89, 51.75), (51.72, 51.65), (33.26, 32.67).

4.13. N-tritylamino dimethyl ester β-3-nitro-benzylaspartate (3i)

To **2** (3.546 g, 8.8 mmol) in 1M THF under Argon at -23°C was added LiHMDS (26.4 mmol) slowly. 20 minutes later 3-nitro-benzyl bromide was added (4.7 g, 21.97 mmol) as a solid all at once. Temperature was allowed to rise to 0ºC, at which time it was stirred for an additional 4 hours before being quenched with 2N NH_4Cl (13 ml). Ethyl acetate was added for separation, followed by silica column 85:15 hexane:ethyl acetate (13.5%, .64g). ^{1}H NMR (400 MHz, $CDCl_3$) δ: 8.20-8.10 (m, 3H), 8.07-8.04 (m, 1H), 7.60-7.17 (m, H), (3.95-3.90 (m, .75H, S,R), 3.76-3.70 (m, .15H, S,S)), (3.66 (s, .45H, S,S), 3.63, (s, 2.55H, S,R)), (3.28 (s, .45H, S,S), 3.25 (s, 2.55H, S,R)), 3.08-2.98 (m, 3H), 2.91 (s, .75H), 2.88 (s, .25H). ^{13}C (100 MHz, $CDCl_3$) δ: 172.68, 182.36, 145.32, 135.47, 135.40, 129.81, 129.25, 128.77, 128.63, 128.33, 128.18, 127.93, 127.87, 126.99, 126.69, 126.55,

123.88, 123.75, 121.64, 121.56, 71.23, (57.99, 57.59), 52.25, 52.12, 51.92, (33.71, 32.70). HRMS *m/e* calcd for $C_{13}H_{16}N_2O_6^{+\cdot}$ 297.087, found 297.1076.

4.14. N-tritylamino dimethyl ester β-3-nitro-benzylaspartate (3i, S,S)

Trityl aspartate (.5 g, 1.34 mmol) was placed in a flame dried round bottom flask equipped with stir bar. Anhydrous THF (5 ml) was added under argon and the solution was cooled to -55℃. Once cooled KHMDS (20% in THF, 2.6 mmol) was slowly added, 20 minutes later 3-nitro-benzyl bromide was added (.634 g, 2.9 mmol) as a solid all at once. The reaction was stirred for an additional 21 hours before being quenched with 2N NH_4Cl (6 ml). Ethyl acetate was added for separation. The water layer was washed two more times and the organic layers were concentrated down for separation on silica in 15% ethyl acetate, 85% hexanes (51%, .34 g). ^{1}H NMR (400 MHz, $CDCl_3$) δ: 8.26-8.00 (m, 1H), 7.52-7.37 (m, 4H), 7.52-7.16 (m, 15H), 3.63 (s, 3H), 3.58 (m, 1H β), 3.30 (s, 3H), 3.27-3.25 (m, 1H α), 3.22-3.15 (m, 2H), 3.03-2.94 (m, 2H). ^{13}C (100 MHz, CDCl3) δ: 172.36, 145.34, 141.06, 135.47, 129.01, 128.77, 128.63, 127.87, 127.66, 126.55, 123.75, 121.64, 71.23, 57.59, 52.24, 52.10, 51.91, 33.71.

4.15. N-tritylamino dimethyl ester β-P-nitro benzylaspartate (3j)

Compound **2** (3.123 g, 7.74 mmol) in 1 M anhydrous THF under argon was cooled to -40℃. Once cooled 1M LHMDS (23.2 mmol) was added. After 20 minutes P-nitro benzyl bromide, dissolved in anhydrous THF, was added (4.18 g, 19.35 mmol). The temperature was then allowed to rise to 0ºC and the reaction was stirred for 4 hrs at which time the reaction was quenched with 2N NH_4Cl

(10ml). Water and ether were added for separation. The water layer was subsequently washed three times and the ether layers were combined and concentrated down. Chromatography through silica gel (90% hexanes 10% ethyl acetate and .5% triethyl amine), methylene chloride was for easier loading to give (3.63g, 87.0%) as a yellow solid. ^{1}H-NMR (400 MHz, $CDCl_3$) δ: (8.14(d, 1.55 H, S,R, J=8.06), 8.08 (d, .44H, S,S, J=8.06)), 7.43 (dd, 6H, J=7.33, 8.79), 7.34 (d, 2H, J=8.79), 7.28 (dd, 2H, J=7.33), 7.26 (m, 2H), 7.26 (d, 1.55H, S,R, J=8.06), 7.22 (d, .44H, S,S, J=8.06), 7.21 (d, 2H, J=7.33), 7.19, (d, 1H, J=7.33). 3.90-3.87 (m, .8H, S,R), (3.63 (s, .65H, S,S), 3.57 (s, 2.33H, S,R)), (3.25 (s, .65H, S,S), 3.24 (d, 2.33H, S,R)), 3.03-2.94 (m, 3H). ^{13}C (100 MHz, $CDCl_3$) δ: 172.65, 171.98, 145.34, 129.83, 128.77, 127.92, 126.69, 123.62, 58.03, (52.25; 51.92), (32.94, 30.88). HRMS m/e Calcd for $C_{13}H_{16}N_2O_6^+$, 297.087, found 297.1076.

4.16. N-tritylamino dimethyl ester β-3-chloro benzylaspartate

Trityl aspartate (.50 g, 1.2 mmol) was placed in a flame dried round bottom flask equipped with stir bar. Anhydrous THF (5 ml) was added under argon and the solution was cooled to -65°C. Once cooled 1M LHMDS in THF (2.5 ml) was slowly added, 20 minutes later 3-cloro-benzyl bromide was added (.47 ml, 3.6 mmol) at which time the reaction was stirred for an additional 21 hours before being quenched with 2N NH_4Cl (6 ml). Ethyl acetate was added for separation. The water layer was washed two more times and the organic layers were concentrated down for separation on silica in 15% ethyl acetate, 85% hexanes (63%, .654 g). ^{1}H NMR (400 MHz, $CDCl_3$) δ: 7.46-7.42 (m, 6H), 7.25-7.22 (m,

7H), 7.19-7.16 (m, 5H), 7.06-7.05 (m, 1H), (3.85-3.83 (m, 1H), (3.61 (s, .3H, S,S), 3.56 (s, 2.7, S,R)), (3.23 (s, .3H, S,S), 3.19 (s, 2.7, S,R)), 3.02-2.78 (m, 3H). ^{13}C (100 MHz, $CDCl_3$) δ: 173.10, 172.66, 146.81, 145.37, 141.31, 134.05, 129.59, 128.93, 128.74, 127.81, 127.13, 126.54, 71.02, 58.00, 52.48, 51.77, 51.71, 32.94. HRMS *m/e* calcd. for $C_{13}H_{16}ClNO_4^+$ 286.0846, found 286.0840.

4.17. General Procedure for Deprotection:

The protected β-substituted aspartate was taken up in 6N HCl and refluxed for 3-12 hours. The reaction was then diluted with water and washed three times with ether. The water layer was concentrated and neutralized with NH_4OH and loaded onto an Ag 1X 8 acetate form ion exchange resin in the ratio of 1g product to 10g resin. The product was eluted with varying concentrations of acetic acid from .1 to 5N. Product came off around 2N. Water was lyophilized 2-3 times to remove the acetic acid.

4.18. β-Benzylaspartate (4A)

The protected benzyl aspartate (1.496 g) was taken up in 6N HCl and refluxed for 3 hours. Product came off at 2N as indicated by NMR (8.6 %, .058 g). ^1H NMR (400 MHz, D_2O) δ: 7.32-7.21 (m, 2H), 7.25-7.21 (m, 3H), (4.04 (d, .25H, S,S, J=3.88), 3.96 (d, .75H, S,R, J=3.88)), (3.40 (ddd .75H, S,R, J=3.88, 6.47, 9.06), 3.24 (ddd, .25H, S,S, J=3.88, 6.47, 9.06)) 3.09-3.01 (m, 1H), 2.95-2.89 (m, 1H). ^{13}C (100 MHz, $CDCl_3$) δ: 172.69, 169.64, (139.69, 138.69), 129.07, 128.42,

126.54, (54.85, 52,91), (49.66, 47.87), (33.46, 32.99). HRMS m/e calcd. for $C_{11}H_{14}NO_4^+$ 224.0923, found 224.0923. $[\alpha]^{21}_D$ = +29.8°.

4.19. *S,S* L-β-Benzylaspartate (4A)

The solvent system comprised of a buffered solution of ammonium acetate and water (0.1 M at pH 6.4). Reversed phase C18 3u analytical and 10u semi-prep columns were used with a retention time for *S,S* being 2.59 minutes and 16.00 minutes, respectively and for *S,R* 3.19 minutes and 21.00 minutes, respectively. ^{1}H NMR (400MHz, D_2O) δ: 7.29-7.25 (m, 2H), 7.21-7.17 (m, 3H), 3.89 (d, 1H, J=3.24), 2.99 (ddd, 1H, J=3.24, 4.53, 11.00), 2.79-2.66 (m, 2H). ^{13}C NMR (400MHz, D_2O) δ: 22.00, 33.46, 49.41, 55.96, 126.96, 128.96, 139.02, 176.693. *S,S*: $[\alpha]^{25}_D$ = +14.11.

4.20. β-2 Napthylmethylaspartate (4B)

The protected β-alkylated aspartate (1.68 g, 3.09 mmol) was taken up in 6N HCl and refluxed for 4 hours. Ethyl ether was added for separation; the water layer was washed 3 times and concentrated. Product crashes out of solution upon neutralization with NaOH. The pH was adjusted to about 12 and precipitated out of methanol (.5g, 51%). ^{1}HNMR (400MHz, D_2O) δ: 7.83-7.78 (m, 3H), 7.66 (app.singlet, 1H), 7.47-7.35 (m, 3H), 3.60 (m, 1H, S,S), 3.27-3.25 (m, 1H, S,R), 3.03-2.94 (m, 1H), 2.86-2.83 (m, 1H), 2.69-2.60 (m, 1H). ^{13}CNMR (100MHz, DMSO) δ: (172.93. 172.82), (170.44, 170.12), 136.99, 133.65, 132.50, 129.93, 129.29, 128.29, 128.13, 127.70, 127.50, 126.65, 126.11, (55.27, 53.18) (50.54,

48.62), (33.53, 31.39). 18.27 = acetic acid. HRMS m/e Calcd for $C_{15}H_{16}NO_4^+$ 349.9889, found 349.9902. $[\alpha]^{21}_D$ = +9.8.

4.21. β-3,5 Dimethyl-benzylaspartate (4C)

The protected β-alkylated aspartate (1.29 g, 2.47 mmol) was taken up in 6N HCl and heated for 24 hours at 70°C. Ethyl ether was added for separation; the water layer was washed and concentrated. NH_4OH was added to adjust the pH to 7 and loaded onto an anion exchange resin. Product came off at 2N (.032 g, 8%). ^{1}H NMR (400 MHz, D_2O) δ: (6.92 (app. Singlet, .67H, S,R.); 6.91 (app. Singlet, .33H, S,R)), (6.88 (1.33H, app. Singlet, S,R,); 6.87 (.66H, app singlet, S,S)), (4.08-4.07 (m, .33H, S,S), 4.00-3.99 (m, .66H, S,R)), (3.45-3.40 (m, .66H, S,R), 3.26-3.21 (m, .33H, S,S)), 3.05-2.98 (m, 1H), 2.89-2.81 (m, 1H), (2.18 (br singlet, 5H), 2.12 (br singlet, 1H S,S)). ^{13}C (100MHz, D_2O) δ: (172.54,172.07), (169.43,169.37), (138.52,138.20), (137.34,137.14), (128.05,127.87; 126.78, (52.68,52.36), (47.90,47.46), (34.23, 32.03), 21.00. HRMS m/e calcd. for $C_{13}H_{18}NO_4^+$ 252.1236 found 252.1230. $[\alpha]^{21}_D$ = +34.8°.

4.22. β-3 Methyl-benzylaspartate (4D)

The protected β-alkylated aspartate (.9 g, 1.77 mmol) was taken up in 6N HCl and heated for 24 hours at 70°C. Ethyl ether was added for separation; the water layer was washed and concentrated. NH_4OH was added until the pH reached 6. THF was added for solubility and the product was loaded onto an Ag 1X 8 acetate form ion exchange resin in the ratio of 1g product to 10g resin. Product was eluted with varying concentrations of acetic acid from .1 to 5N in a 4:1 ratio of water:THF. Product comes off around 2N. (.0765 g, 18.3%). ^{1}HNMR

(400MHz, D_2O) δ: 7.24-7.19 (m, 1H), 7.11-7.05 (m, 3H), (4.14-4.13 (m, .36H, S,S), 4.09-4.08 (m, .64H, S,R)), (3.52-3.47 (m, .64H, S,R), 3.31-3.28 (m, .36H, S,S)), 3.12-3.07 (m, 1H), 2.98-2.88 (m, 1H), 2.25 (s, 3H). ^{13}CNMR (100MHz, $CDCl_3$) δ: 174.89, 170.46, 139.13, 137.49, 129.78, 128.96, 127.93, 126.06, 52.86, (47.55, 46.88), (33.76, 33.65), 20.47. HRMS m/e calcd. for $C_{12}H_{16}NO_4^+$ 238.1079, found 238.1079. $[\alpha]^{21}_D$ = +7.8° (in DI H_2O, adjusted to 7.5 with NaOH).

4.23. β-2,6 Dicloro-benzylaspartate (4E)

The protected β-alkylated aspartate was dissolved in THF and 6N HCl and refluxed for 5 hours. The reaction was washed with ethyl acetate and the water layers were combined and concentrated. The reaction was neutralized to pH 5 using NaOH, loaded onto an anion exchange resin and eluted with 4:1 H_2O:THF mixture followed by a gradient of acetic acid prepared from concentrated acetic acid in the same 4:1 H_2O:THF ratio to give a gradient from .1N to 5N. Product was isolated from 2N and 5N acetic acid (1g, 37.2%). ^{1}HNMR (400MHz, D_2O) δ: 7.37-7.32 (m, 2H), 7.21-7.14 (m, 1H), (4.05 (m, .4H, S,S), 3.96 (m, .6H, S,R)), 3.47-3.33 (m, 2H), 3.24-3.21 (m, .6H), 3.12-3.09 (m, .4H).. ^{13}CNMR (100MHz, $CDCl_3$) δ: 171.75, 169.40, 135.23, 134.03, 129.18, 128.37, 52.80, 46.16, 28.07. HRMS m/e calcd. for $C_{11}H_{12}Cl_2NO_4^+$ 320.0456, found 320.0441. $[\alpha]^{21}_D$ = +31.7°.

4.24. β-3 Bromo-benzylaspartate (4F)

The protected β-alkylated aspartate(.5 g, .873mmol) was taken up in 6N HCl and heated for 24 hours. Ethyl ether was added for separation; the water layer was washed 3 times and concentrated. NH_4OH is added until the pH is 7.

THF is added for solubility and is loaded onto an Ag 1X 8 acetate form ion exchange resin in the ratio of 1g product to 10g resin. Product is eluted with varying concentrations of acetic acid from .1 to 5N in a mixture of water:THF in a ratio of 4:1. Product comes off around 2N. Lyophilize off water 2-3 times to remove the acetic acid (.1 g, 38.5%). ^{1}HNMR (400 MHz, DMSO) δ: 7.47 (m, 1H), 7.41-7.38 (m, 1H), 7.28-7.22 (m, 2H), 4.01 (br s, .85H, α S.S) 3.82, (br s, .15H, α S,R), 3.25-3.21 (m, .15H, β S,R), 3.12-3.10 (m, .85H, β S,S), 3.04-3.00 (m 1H), 3.28-2.74 (m, 1H). ^{13}CNMR (100MHz, DMSO) δ: 171.80, 169.23, 141.69, 131.65, 130.42, 129.27, 128.22, 121.52, 52.68, (48.16, 47.35, β C), (31.62, 30.76, CH_2), acetic acid 21.15, 172.33. HRMS m/e calcd for $C_{11}H_{13}BrNO_4^+$ 302.0028, found 302.0014. $[\alpha]^{21}_D$ = +26.9°.

4.25. β-3 Fluoro-Benzylaspartate (4G)

The protected β-alkylated aspartate (.678 g, 1.33 mmol) was taken up in 6N HCl and heated for 24 hours at 70°C. Ethyl ether was added for separation; the water layer was washed 3 times and concentrated. NH_4OH was added until the pH reached 7 and loaded onto an ion exchange resin where product comes off around 2N (.115 g, 36.2%). ^{1}H NMR (400 MHz, DMSO) δ: 7.34-7.29 (m, 1H), 7.08-6.99 (m, 3H), (3.99 (d, .33H, S,S, J=4.40), 3.88 (d, .66H, S,R, J=4.40)), (3.33 (ddd, .66H, S,R, J=4.40, 6.59, 9.52), 3.20 (ddd, .33H, S,S, J=4.40, 5.86, 10,26)), 3.08-2.86 (m, 2H). ^{13}C (100 MHz, DMSO) δ: (172.54, 171.89), 169.17, (163.18, 160.77), (141.60, 141.53), (130.15, 130.03, 129.94), 125.05, (115.63, 115.42), (113.31, 113.16, 112.94), (52.97, 52.48), (48.89, 47.25), (33.70, 32.03,

30.65). HRMS *m/e* for $C_{11}H_{13}FNO_4^+$ calcd. 242.0829, found 242.0834. $[\alpha]^{21}_D$ = +40°.

The mixture of diasteromers was resolved by HPLC as well as synthetically prepared in ratios of 99:1, S,S:S,R and 11:1 S,R:S,S. For HPLC resolution the solvent system comprised of a buffered solution of ammonium acetate and water (0.1 M at pH 6.4). Reversed phase C18 3u analytical and 10u semi-prep columns were used with a retention time for *S,S* being 2.3 minutes and 18.48 minutes, respectively and for *S,R* 2.8 minutes and 27.22 minutes, respectively.

4.26. β-3 Fluoro-Benzylaspartate (4G, S,S)

^{1}H NMR (400 MHz, D_2O) δ: 7.30-7.26 (m, 1H), 7.06-6.94 (m, 3H), 3.94 (m, 1H), 3.08-3.05 (m, 1H), 2.88-2.81 (m, 1H), 2.77-2.73 (m, 1H). ^{13}C (100 MHz, DMSO) δ: 178.20, 172.02, 164.62, 162.21, 143.35, 131.50, 126.19, 116.81, 114.49, 56.53, 49.31, 33.91. $[\alpha]^{21}_D$ = +18.3°

4.27. β-3 Fluoro-Benzylaspartate (4G, S,R)

^{1}H NMR (400 MHz, D_2O) δ: 7.32-7.25 (m, 1H), 7.05-6.95 (m, 3H), 3.64-3.59 (m, 1H), 3.07-3.02 (m, 1H), 2.96-2.88 (m, 2H). ^{13}C (100 MHz, DMSO) δ: 179.81, 172.63, 163.22, 160.81, 140.12, 129.93, 125.11, 115.43, 112.90, 52.68, 49.74, 28.22. $[\alpha]^{21}_D$ = +38.23°

4.28. β-4 Fluoro-benzylaspartate (4H)

The protected β-alkylated aspartate (.457 g, .893 mmol) was taken up in 6N HCl and heated for 24 hours at 75°C. Ethyl ether was added for separation; the water layer is washed and concentrated. NH_4OH is added until the pH reached 7. THF 1:7 ratio was added for solubility and loaded onto an Ag 1X 8 acetate form ion exchange resin. Product is eluted with varying concentrations of acetic acid in a mixture of water:THF in a ratio of 4:1. Product comes off at 2N and 5N acetic acid. Lyophilize off water 2-3 times to remove the acetic acid (.156, 73%). Found C, 53.48; H, 4.83; N, 5.60; $C_{11}H_{11}FNO_4$ 1/3 H2O requires C, 53.66; H, 4.78; N, 5.69. ^{1}HNMR (400 MHz, D_2O) δ: 7.26-7.20 (m, 2H), 7.06-7.00 (m, 2H), (3.98 (d, .5H, S,S, J=3.24), 3.88 (d, .5H, S,R, J=3.24)), (3.31 (ddd, .5H, S,R, J=3.24, 7.12, 9.71), 3.18 (ddd, .5H, S,S, J=3.24, 5.18, 9.06)), 3.05-2.84 (m, 2H). ^{13}CNMR (100 MHz, D_2O) δ: (176.21, 176.00), (172.29, 171.81), (163.01, 162.93), (160.60, 160.53), (133.80, 133.39), (130.72, 130.68), (130.65, 130.59), (115.69, 115.58), (115.47, 115.37), 54.74, (48.19, 48.03), (33.82, 32.82). $[\alpha]^{21}_D$ = +116.6° in DI H_2O adjusted to 7.5 with NaOH.

4.29. β-3 Nitro-benzylaspartate (4l)

The protected β-alkylated aspartate (.24 g, .446 mol) was taken up in 6N HCl and heated for 24 hours at 65°C. Ethyl ether was added for separation; the water layer was washed and concentrated. NH_4OH was added until the pH reached 7. THF was added for solubility and loaded onto an ion exchange resin. Product was eluted with a mixture of water:THF in a ratio of 4:1. Product came off around 2N. Lyophilized off water 2-3 times to remove the acetic acid (.022 g, 18.4%). Product was sparingly insoluble in H_2O. ^{1}H NMR (400 MHz, D_2O) δ: 8.13-8.06

(m, 2H), 7.67-7.61 (m, 1H), 7.54-7.48 (m, 1H), (3.99 (d, .6H, S,S, J=3.88), 3.87 (d, .4H, S,R, J=3.88)), (3.30 (ddd, .4H, S,R, J=3.88, 5.18, 9.17), 3.21 (ddd, .6H, S,S, J=3.88, 5.18, 9.06)), 3.11-3.05 (m, 1.4H), 2.97 (d,, .45 H, J=5.18) 2.94 (d, .25H, J=5.18). ^{13}C (100 MHz, DMSO) δ: (173.92, 172.48), (169.50, 168.75), (146.79, 146.56), 139.37, 136.19, (131.76, 130.60), (123.72, 123.55), (122.23, 122.02), 52.92, 48.83, 29.69. HRMS *m/e* calcd for $C_{11}H_{13}N_2O_6$ 269.0774, found 269.0779. $[\alpha]^{21}_D$ = + 2.7° in DI H_2O adjusted to 7.5 with NaOH. $[\alpha]^{21}_D$ = -20°.

4.30. β-3 Nitro-benzylaspartate (4I, S,S)

The protected β-alkylated aspartate(.325 g, .603 mmol) is taken up in 6N HCl with a little acetone and heated for 24 hours at 65°C. The reaction is then concentrated down, washed with water 2 times and placed under vacuum. Ethyl acetate is added and product precipitates out, white powder. For ease this was centrifuged down for 10 minutes at 4000 rpm and the supernant poured off. The precipitate was dissolved in a small amount of water from which it almost immediately crashed out as white crystals. This is washed with water and concentrated down 2 more times (.045 g, 28%). ^1H NMR (400 MHz, D_2O) δ: 8.10 (s, 1H), 8.06 (d, 1H, J=8.06), 7.64 (d, 1H, J=7.33), 7.50 (t, 1H, J=8.06,7.33), 4.13 (1H, α), 3.40-3.36 (m, 1H, β), 3.28-3.23 (m, 1H), 3.11-3.06 (m, 1H). ^{13}C (100MHz, D_2O) δ: 172.28, 169.29, 147.75, 141.07, 136.05, 129.69, 123.67, 121.64, 52.79, 47.28, 33.85.

4.31. β-para nitro benzylaspartate (4J)

The protected β-alkylated aspartate (1.35 g, 2.51 mmol) was placed in a round bottom flask with 6N HCl and THF, to dissolve. Reaction was refluxed for three hours then washed with ethyl acetate. The ethyl acetate layer was washed 2 more times and the aqueous layer was concentrated down. 7.4g AgX1-8 resin 200-400mesh size was loaded into a column and washed with two columns of water. Product was loaded and the column was washed with a gradient of acetic acid from .1N to 5N. Faction's 1-5 are lyophilized down (.378 g, 56%). ^{1}H-NMR (400 MHz, D_2O) δ: 8.04-8.00 (m, 2H), 7.39-7.34 (m, 2H), (3.99-3.88 (d, .65H, S,S), 3.92-3.91 (d, .35H, S,R)), (3.35-3.33 (m, .35H, S,R), 3.23-3.22 (m, .65H, S,S)), 3.12-2.91 (m, 2H). ^{13}CNMR (100MHz, D_2O) δ: (178.86,178.41), (173.37,172.64), (147.30,146.96), (146.42,146.35), (129.92,129.83), (123.86,123.80), (55.73,55.67), (49.40,48.99), (36.12,33.29). HRMS m/e Calcd for $C_{11}H_{14}N_2O_6^+$ calcd. 252.1236, found 252.1225. $[\alpha]^{21}_D$ = +18.52°.

4.32. β-3 Chloro-benzylaspartate S,R

^{1}H-NMR (400 MHz, D_2O) δ: 7.30-7.24 (m, 3H), 7.18-7.17 (m, 1H), (3.96 (app. d, .07H, S,S), 3.81 (app. d, .93H, S,R)), (3.27-3.22 (m, .91H, S,R), 3.15-3.10 (m, .09H, S,S)), (3.02-2.89 (m, 1.9H, S,R), 2.83-2.79 (m, .1H, S,S). ^{13}CNMR (100MHz, D_2O) δ: 172.01, 169.34, 141.26, 132.73, 130.06, 128.65, 127.75, 126.34, 52.44, 49.61, 32.14. $[\alpha]^{21}_D$ = +25.7°.

4.33 EAAT3-Mediated transport in C17.2 cells

EAAT3 was transiently expressed in C17.2 cells (obtained from Dr. Evan Snyder, Burnham Inst., La Jolla, CA) using an AAV-based vector (kindly provided by Dr. Mathew During, University of Auckland, NZ) pAM-CAG-EAAT3-WPRE as previously described (Esslinger *et al.,* 2005). Cells between passages 10-20 were seeded at 5 X 10^4 cells/well in 12 well plates and grown in complete DMEM supplemented with 10% fetal bovine serum, 1mM sodium pyruvate, 0.1 mM nonessential amino acids solution. At 24 hours after plating, cells were transfected using FuGENE6 Transfection Reagent (Roche, Indianapolis, IN) in a ratio of 4µl of FuGENE6 to 3µg of purified plasmid DNA in accordance with manufacturers instructions. The cells were used in transport assays 24 hours following transfection as described by Esslinger *et al.,* 2005. Briefly, transfected C17.2 cells were grown in DMEM containing 10% FCS in a humid atmosphere of 5% CO_2. Near-confluent cells (plated at 5x10^4 cells/well) were rinsed with a physiological buffer (138 mM NaCl, 11 mM D-glucose, 5.3 mM KCl, 0.4 mM KH_2PO_4, 0.3 mM Na_2HPO_4, 1.1 mM $CaCl_2$, 0.7 mM $MgSO_4$, 10 mM HEPES, pH 7.4) and allowed to preincubate at 37°C for 5 min. Uptake was initiated by replacing the pre-incubation buffer with buffer containing ^{3}H-D-aspartate (25µM) and inhibitors at the concentrations indicated. Following a 5 min incubation, the media was removed by rapid suction and the cells rinsed 3 times with ice-cold buffer. The cells were dissolved in 0.4N NaOH for 24 hours and analyzed for radioactivity by LSC and protein by the BCA (Pierce) method. Transport rates were corrected for background: i.e., radiolabel accumulation at 4°C. Initial studies confirmed that uptake quantified in this manner was linear with time and protein

levels and that uptake in untransfected C17.2 cells was indistinguishable from background.

5. Acknowledgements

The authors wish to thank J. Gerdes, M. Kavanaugh, S. Patel, C.M. Thompson, and T. Denton for their insightful advice regarding the studies presented in this manuscript. Molecular modeling studies were conducted in the Molecular Computational Core Facility of the Center for Structural and Functional Neuroscience and HRMS were obtained in the Proteomics and Mass Spec. Core Facility of the Center for Structural and Functional Neuroscience. This work was supported in part by NINDS NS30570 (RJB), NINDS NS045704 (CSE) and NCRR COBRE RR15583 (RJB, CSE).

Chapter 4.

L-β-Benzyl-aspartate derivatives; pharmacological characterization and computational evaluation of a novel class of preferential EAAT3 inhibitors.

Terri Mavencamp, Joseph F. Rhoderick, David Holley, John Gerdes, Michael Kavanaugh, C. Sean Esslinger and Richard J. Bridges

Abstract

Derivatives of L-β-benzyl aspartate were prepared and characterized for the ability to inhibit ^{3}H-D-aspartate uptake into hEAAT1-3 expressing C17.2 cells. This series comprises one of the first families of EAAT3 preferring inhibitors identified to date. The three most potent compounds contain a halogen substitution at the 3-position of the aromatic ring. IC_{50} values at EAAT1-3 have been determined for L-β-3- (bromo-, chloro- and fluoro-) benzyl aspartate. IC_{50} values of the most potent, L-β-3-fluoro-benzyl aspartate are 7.50 µM ± 2.12, 5.56 µM ± 0.65 and .1.95 µM ± 0.37 respectively. Potency decreases when substitutions are made at the 4-postition as well as with increasing size of the substituent. Computational modeling and analysis of structure activity data suggest the area the aromatic moiety of L-β-benzyl aspartate derivatives probe is 1) 3-dimentionally confined, 2) more tolerant of substitutions at the 3 and 5 positions than the 4 position, 3) at least partially distinct from the area probed by L-TBOA and 4) more accessible in the EAAT3 protein than EAAT1 and EAAT2.

1. Introduction

Glutamate is the major excitatory neurotransmitter in the mammalian central nervous system (CNS). It is capable of participating in standard fast synaptic communication as well as in higher order signal processing linked to development, synaptic plasticity, learning and memory (for review see: Balaz *et al*., 2006). The interaction of glutamate with the ionotropic and metabotropic glutamate receptors mediates signal transmission, yet overstimulation of these receptors has been shown to result in excitotoxic conditions that could result in cell death. This is believed to play a key role in disorders of the CNS such as stroke, epilepsy, spinal cord injury, ALS, and Alzheimer's disease (for reviews see: Rao and Weiss 2004; Won *et al*., 2002; Malva *et al*., 2003; Hynd *et al*., 2004). The excitatory amino acid transporters (EAATs), clear glutamate from the synaptic cleft, thereby influencing the amount and/or time course that L-glutamate is in contact with the excitatory amino acid (EAA) receptors.

Five glutamate transporters have been identified by molecular cloning and functional expression and share about 50-60% homology at the amino acid level. EAAT1-5 along with two neutral amino acid transporters comprise the sodium dependent solute carrier family (SLC1) and are referred to as: EAAT1(GLAST), EAAT2(GLT-1), EAAT3(EAAC1), EAAT4, EAAT5, ASCT1 and ASCT2 (Storck *et al*., 1992; Pines *et al.,* 1992; Kanai & Heidger, 1992; Arriza *et al*., 1994; Fairman *et al.,* 1995; Arriza *et al.,* 1997; Kanai and Hediger, 2004).

Advancements in determining the structure of the EAATs have been made through the crystallization of a transporter homologue from *Pyrococcus horikoshii,* Glt_{ph}. Data suggests that the transporter is a trimer with a bowl shaped basin facing the extracellular space. Three binding sites lay at the bottom of the basin, 1 per monomer. Each site is covered by two helical hairpins (HP1 and HP2) extending from opposite sides of the membrane (Yernool *et al.,* 2004). The transporter homologue was recently crystallized with bound aspartate (closed state) and bound L-β-*threo*-benzyloxy-aspartate (TBOA) (open state). TBOA and aspartate were observed to bind by the same recognition points. This validates that TBOA works in a competitive manner and gives credence to modeling based on the belief that the protein recognizes compounds by at least 3 points, the α carboxyl group, C1; the distal carboxyl group, C2 and the nitrogen, N. The authors predict that two sodium ions bind with aspartate, one sodium coupled to the hairpin loop on the intracellular side HP1 and the other coupled to the hairpin loop on the extracellular side, HP2, of the protein. The bulky aromatic group of TBOA is believed to interfere with the closing of HP2; not allowing the second sodium to

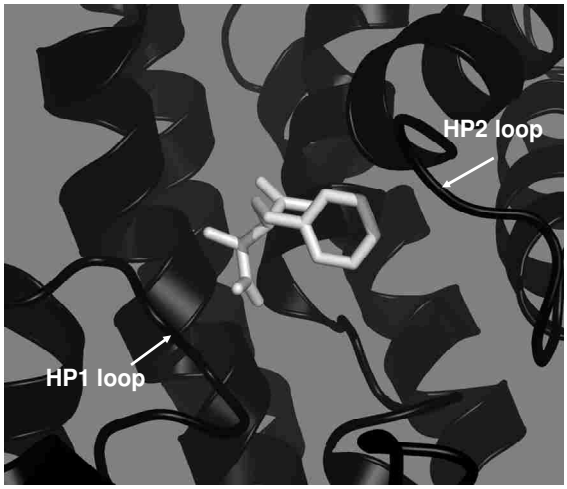

Figure 1. TBOA in the active site of the EAAT3 homology model.

bind thereby effectually blocking further conformational changes (Boudker *et al.,* 2007).

Amino acid residues positioned to make numerous protein-substrate interactions in Glt_{ph} are also present in the EAATs. Functional studies of Asp444 and Arg447 in EAAC1 support the importance of these residues in substrate binding. Asp444 is conserved among members of the SCL1 family but is replaced by a serine in the dicarboxylic acid transporters DctA. When Asp444 is mutated in EAAC1, even to similar residues such as glutamate, almost complete loss of transport is observed (Teichman and Kanner, 2007). This suggests that the ligand amine group is engaging in key hydrogen bonds to Asp444.

Another residue shown to be crucial for transport is Arg447. Arg447 is conserved in eukaryotic and bacterial glutamate transporters as well as in DctA, but is not conserved in the two neutral amino acid transporters ASCT1 and ASCT2. Arg447 is involved in binding the substrate distal carboxylate group, C2. Mutation of Arg447 to a neutral or negative amino acid residue abolishes transport of L-glutamate and D- and L-aspartate but leaves cysteine transport intact, converting the transporter to a neutral amino acid transporter (Bendahan *et al.,* 2000).

Due to the high degree of conservation among amino acid residues implicated in substrate binding, the development of inhibitors that act selectively at one EAAT over another is an ongoing challenge. Recently important advancements have been made by the addition of two potent EAAT2 preferring non-substrate inhibitors. WAY-855 (3-amino-tricyclo[2.2.1.$0^{2.6}$[heptane-1,3-

dicarboxylic acid) and WAY-213613 (S)-2-amino-4-(4-(2-bromo-4,5-difluorophenoxy)phenylamino)-4oxobutanoic acid (Figure 2). WAY-855 and WAY-213613 display potent activities at EAAT2 (1.3 μM and .08 μM, respectively and a 40 and 46 fold preference for EAAT2 over EAAT3) (Dunlop *et al*., 2003; Dunlop *et al*., 2005).

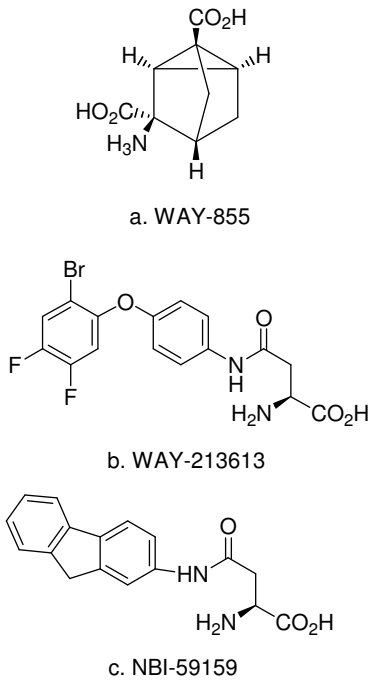

Figure 2. Aspartamide acid analogues displaying preference for EAAT2 (a,b) and EAAT3 (c).

An EAAT3 preferring compound was synthesized that belongs to the same class of compounds as WAY-213613, (S)-4-(9H-fluoren-2ylamino)-2-amino-4-oxobutanoic acid (NBI-59159). One major difference between NBI-59159 and WAY-213613 is the fused ring system found in the EAAT3 preferring compound versus the phenoxy benzene ring structure in the EAAT2 preferring compound (Figure 2). NBI-59159 displays non-substrate activity In *Xenopus* oocytes expressing EAAT1-3 (inhibitory IC_{50} values of 212 nM, 55 mM and 23 nM respectively) and in HEK cells expressing EAAT1-3 (inhibitory IC_{50} values of 1.03 μM, 1.4 μM and 0.09 μM, EAAT1-3 respectively) (Dunlop *et al*., 2006).

Prior to the reporting of the above compounds, our laboratories published the characterization of one of the first preferential EAAT3 inhibitors, L-β-benzyl-aspartate (L-β-BA). Kinetic analysis of ^{3}H-D-aspartate uptake into C17.2 cells

expressing the hEAATs demonstrated that L-*threo*-β-BA is the more potent diastereomer (Ki values 9 μM for EAAT1, 10.0 μM for EAAT2 and 0.8 μM for EAAT3), acts competitively, and exhibits a 10-fold preference for EAAT3 compared to EAAT1 and EAAT2. Electrophysiological recordings of substrate mediated currents in *Xenopus* oocytes expressing EAATs identified L-β-BA as a non-substrate inhibitor. It was initially hypothesized, prior to publication of the Glt_{ph} crystal structure, that the observed EAAT3 preference was due to 1) the highly conserved positioning of the α carboxyl group, C1; the distal carboxyl group, C2 and the nitrogen, N, 2) nearby regions that accommodate select structural modifications (cyclopropyl rings, methyl groups, oxygen atoms) and 3) a unique region occupied by the benzyl moieties of L-TBOA, L-β-*threo*-BA and related analogs.

In this chapter we present the in vitro pharmacological characterization of a family of novel analogues of L-β-BA prepared by enolate addition of a lipophilic head group to protected aspartate (Mavencamp *et al.*, 2008). The compounds were assayed for their ability to inhibit D-[^{3}H] aspartic acid uptake into C17.2 cells. We found that the L-β-BA scaffold presents a unique opportunity to build a family of EAAT3 preferring molecules. Modeling studies were carried out in which select compounds were docked into an EAAT3 homology model using the program GOLD. The results from the docking studies suggest L-β-BA and derivatives bind in a manner distinct from TBOA due to the absence of the oxygen on the β-substituent.

2. Methods

2.1 Chemicals and reagents

General cell culture supplies were purchased from Becton Dickinson (Franklin Lakes, NJ), Corning (Corning, NY), and Life Technologies (Grand Island, NY). D-[^{3}H]Aspartic acid was purchased from Dupont NEN (Boston, MA). L-Aspartate. D,L-β-*threo*-Benzyloxy-aspartate was obtained from Tocris (Ballwin, MO). The syntheses of L-β-benzyl-aspartate derivatives were performed as described in (Mavencamp *et al*., 2008).

2.2 EAAT Expression and Cell Culture

C17.2 cells (obtained from Dr. Evan Snyder, Burnham Inst., La Jolla, CA) between passages 10-20 were seeded at 1 X 10^5 cells/well in 12 well plates and grown in complete DMEM supplemented with 10% fetal bovine serum, 1mM sodium pyruvate, 0.1 mM nonessential amino acids solution, and 0.05% Penicillin-Streptomycin (5,000 units/ml) and Gentamicin sulfate (0.05mg/ml). At 24 hours after plating, cells were transfected using Transfection Reagent (Roche, Molecular Biochemicals) in a ratio of 4µl of FuGene to 3µg of purified plasmid DNA in accordance with manufacturer's instructions. After 24 hours, the relative levels of functional ^{3}H-D-Asp uptake were determined by the method of Martin and Shain (1979 as described below).

2.3 Transporter Activity in C17 Cells

Transfected C17.2 cells were grown in DMEM containing 10% FCS in a humid atmosphere of 5% CO_2. Near-confluent cells (plated at $7x10^4$ - $1x10^5$ cells/well) were rinsed with a physiological buffer (138 mM NaCl, 11 mM D-glucose, 5.3 mM KCl, 0.4 mM KH_2PO_4, 0.3 mM Na_2HPO_4, 1.1 mM $CaCl_2$, 0.7 mM $MgSO_4$, 10 mM HEPES, pH 7.4) and allowed to preincubate at 37°C for 5 min. Uptake was initiated by replacing the pre-incubation buffer with buffer containing ^{3}H-D-aspartate (5-100 µM) and inhibitors (10-100 µM). Following 5 min incubation, the media was removed by rapid suction and the cells rinsed 3 times with ice-cold buffer. The cells were dissolved in 0.4N NaOH for 24 hours and analyzed for radioactivity by LSC and protein by the BCA (Pierce) method. Transport rates were corrected for background: i.e., radiolabel accumulation at 4°C. Initial studies confirmed that uptake quantified in this manner was linear with time and protein levels and that uptake in untransfected C17.2 cells was indistinguishable from background. Dose response curves for IC_{50} determination were prepared for the three most potent compounds. Concentrations of inhibitors were selected to span 2 log units above and below the estimated $IC_{50.}$ ^{3}H-D-aspartate was included at 1 µM (Shimamoto *et al.*, 2004; Dunlop *et al.*, 2005). IC_{50} values were determined using Kalidegraph and fit to the equation y = 1-(m0/(m2+m0)) where 1 is the maximum, m0 is the concentration of inhibitor and m2 is the IC_{50} value.

2.4 Computational Modeling

Human EAAT3 sequence (obtained from GenBank, http://www.ncbi.nlm.nih.gov) was aligned with the Protein Data Bank (PDB) sequences for an archaeal homologue (GltPh ,2NWW.pdb) according to Yernool, *et al.,* 2004; Boudker *et al.*, 2007. The EAAT3 homology model was constructed by threading the aligned sequence along 2NWW coordinates using the SwissProt server (http://swissmodel.expasy.org//SWISS-MODEL.html). The resulting model was optimized through local energy minimizations of regions with high steric and electrostatic interference using the AMBER7 force field in the Tripos SYBYL7.3 platform. Representations of TBOA, 2-NOA, BA, 2-napth, and 3-F-BA were docked using GOLD (http://www.ccdc.cam.ac.uk/) into the EAAT3 model. Each of the top twenty poses for each of four separate docking runs were evaluated for their capacity to hydrogen bond with EAAT3 R447 and D444 residues. The top ranked poses determined by GOLDScore were incorporated into the homology model and visualized using PyMol1.0.

3. Results

3.1 L-β-Benzyl Aspartate derivatives preferentially inhibit the EAAT3 transporter subtype.

To delineate the pharmacological specificity of the individual EAATs, the Bridges Lab employed the same expression system as was used to characterize *L-β*-benzyl aspartate*,* C17.2 neuroprogenitor cells and a vector adapted from an

Adeno-associated virus (AAV) packaging plasmid (Stone *et al.,* 2005; Esslinger *et al*., 2005).

A series of L-β-substituted aspartate analogues, that included L-β-benzyl-aspartate (L-β-BA), were screened by Fred Rhoderick of the Bridges lab, at 100 μM for the ability to inhibit the uptake of ^{3}H-D-aspartate (25 μM) into C17.2 cells expressing EAAT1, EAAT2 or EAAT3. L-β-BA and L-β-BA derivatives were included in the assays as approximate 2:1 mixtures of their *threo* and *erythro* forms (2S,3S and 2S,3R). The data are reported in Table 1 as the mean % of Control (± SEM) measured in the absence of inhibitors. D,L-TBOA and L-β-methyl aspartate were included in the present study so that structure activity comparisons would be based on assay data collected under identical conditions.

L-β-Methyl aspartate is approximately equipotent at the three EAATs, with a statically non-significant preference for EAAT3. Consistent with literature reports, D,L-TBOA, a well know EAAT blocker preferentially inhibits EAAT2. In accord with L-β-methyl aspartate and D,L-TBOA, L-β-benzyl aspartate utilizes β substitution on the aspartate backbone. It was recently shown that L-β-BA is a preferential EAAT3 inhibitor. In agreement with what is observed for TBOA, the *threo* diasteromer of L-β-BA was shown to be more active than the *erythro* diasteromer.

It can be seen from Table 1 that all of the L-β-BA analogues synthesized show a preference for EAAT3 except for 2,6-dichloro benzyl aspartate, entry 16, which shows very little activity at any of the transporters. In general, substitutions made at the 3 position were more potent than those at the 4

position. This is illustrated by comparing L-β-3-nitro-BA with L-β-4-nitro-BA, entries 10 and 14. L-β-3-Nitro-BA inhibits uptake to roughly 30% of control, about twice the inhibition as seen with L-β-4-nitro-BA (*ca.* 65% of control). Similarly, L-β-3-floro-BA completely inhibits ^{3}H-D-aspartate uptake at 100 µM, while the 4-floro substitution inhibits uptake to about 9% of control (entries 9 and 13 respectively). Adding a substituent to the symmetrical position, 5 of the aromatic ring does not appear to affect potency or selectivity. L-β-3-Methyl-BA, entry 11, inhibits uptake at EAAT3 to about 33% of control and at EAAT1 and EAAT2 to about 70% of control. When an additional methyl group is introduced to the 5 position (L-β-3,5-dimethyl-BA, entry 12) inhibitory activity is not significantly effected. In general, smaller substituents showed greater potency. This is most easily observed among the 3-substituted halogen derivatives, entries 6-9. The halogens have similar physical characteristics but range in size from the small fluoro to the large iodo. The size of the substitutions is reflected in the potency of inhibition, ranging from complete inhibition of uptake at EAAT3 to about 20% inhibition for L-β-3-iodo-BA. A striking example of a decrease in potency with an increase in size can be observed with 1-and 2- β substituted naphthyl aspartates (L-β- 1 & 2-NA) (entries 18 and 19). Both compounds show a large reduction in potency from BA. In contrast, 1 and 2 naphthyl analogues of TBOA, *threo*-β-(1-naphthyl)-methoxyaspartate and *threo*-β-(2-naphthyl)-methoxyaspartate (TNOA-1 and TNOA-2), exhibit a slight increase in potency over the parent compound TBOA (Shimamoto et al., 2000).

Cmpd. #	Compound (100 µM)	EAAT1 ^{3}H-D-Asp Uptake (% of Control)	EAAT2 ^{3}H-D-Asp Uptake (% of Control)	EAAT3 ^{3}H-D-Asp Uptake (% of Control)
1	L-Aspartate 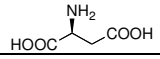	4 ± 2	16 ± 4	15 ± 3
2	L-β-Methyl-Asp 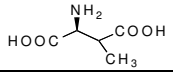	43 ± 8	49 ± 6	32 ± 15
3	D,L-β-*threo*-Benzyloxy-Asp (TBOA) 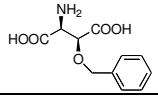	5 ± 2	2 ± 1	9 ± 3
4	L-β-Benzyl-Asp (BA) 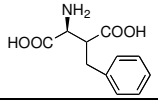	20 ± 4	15 ± 3	4 ± 2
5	L-β-*threo*-BA 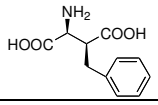	8 ± 1	9 ± 1	1 ± 1
6	L-β-3-Iodo-BA 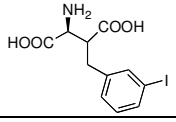	50 ± 6	64 ± 3	19 ± 6
7	L-β-3-Bromo-BA 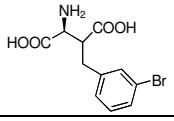	45 ± 6	22 ± 5	8 ± 3
8	L-β-3-Chloro-BA 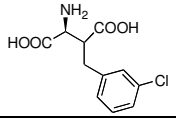	21 ± 7	23 ± 2	7 ± 4
9	L-β-3-Fluoro-BA 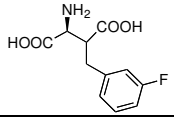	11 ± 1	23 ± 3	0 ± 0

Table 1. Inhibitory activity of β-substituted aspartate analogues at EAAT1, EAAT2 and EAAT3, all experiments were done a minimum of 3 times with the exception of 4-F-BA.

Cmpd #	Compound (100 µM)	EAAT1 ^{3}H-D-Asp Uptake (% of Control)	EAAT2 ^{3}H-D-Asp Uptake (% of Control)	EAAT3 ^{3}H-D-Asp Uptake (% of Control)
10	L-β-3-Nitro-BA 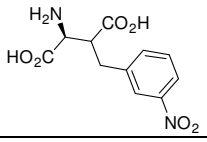	62 ± 8	75 ± 6	29 ± 5
11	L-β-3-Methyl-BA 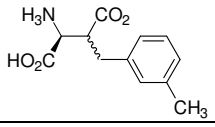	60 ± 4 (3)	48 ± 3	33 ± 1
12	L-β-3,5-Dimethy-BA 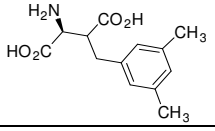	72 ± 4	69 ± 7	36 ± 7
13	L-β-4-Fluoro-BA 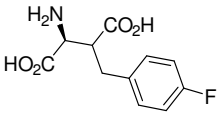	21 (2)	40 (2)	9 (2)
14	L-β-4-Nitro-BA 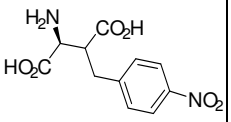	80 ± 7	82 ± 12	65 ± 8
15	L-β-4-Amino-BA 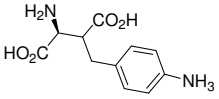	57 ± 2	57 ± 4	21 ± 3
16	L-β-2,6-Dichloro-BA 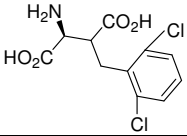	76 ± 1	100 ± 6	86 ± 5

Table 1. cont.

Cmpd #	Compound (100 µM)	EAAT1 ^{3}H-D-Asp Uptake (% of Control)	EAAT2 ^{3}H-D-Asp Uptake (% of Control)	EAAT3 ^{3}H-D-Asp Uptake (% of Control)
17	L-β-1-Napthyl-Benzyl-Asp 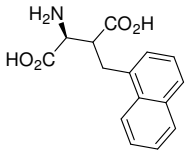	84 ± 5	92 ± 6	60 ± 4
18	L-β-2-Napthyl-Benzyl-Asp 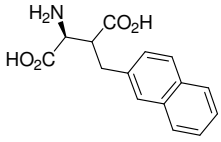	99 ± 6	92 ± 13	68 ± 6

Table 1. cont.

3.2. IC_{50} determination for L-β-3-Cl-, 3-Br- and 3-F- benzyl aspartate.

Structures of L-β-3-cloro-benzyl aspartate, (L-β-3-Cl-BA), L-β-3-bromo-benzyl aspartate (L-β-3-Br-BA) and L-β-3-floro-benzyl aspartate (L-β-3-F-BA) are shown in Table 2. IC_{50} values were determined by the Bridges lab for the three compounds at EAATs 1, 2 and 3 in C17.2 cells expressing the human EAAT1-3 in the presence of 1 μM ^{3}H-D-aspartate. The compounds were evaluated as mixtures of their *threo* and *erythro* (S,S:S,R) forms in an approximate 2:1 ratio. IC_{50} values were below 10 μM at EAAT3 for all three compounds, IC_{50} values for EAAT1 and EAAT2 are also presented in Table 2 with log concentration response curves shown in Figure 3. L-β-3-Cl-BA is the most selective of the compounds with an approximate 4 and 5 fold preference for EAAT3 over EAATs 1 and 2 respectively, 3-BrBA is 9 and 2 times more selective and L-β-3-F-BA is 4 and 3 times more selective for EAAT3 over EAAT1 and EAAT2 respectively. L-β-3-F-BA is the most potent of the compounds with an IC_{50} value at EAAT3 of 1.95 ±.37 μM.

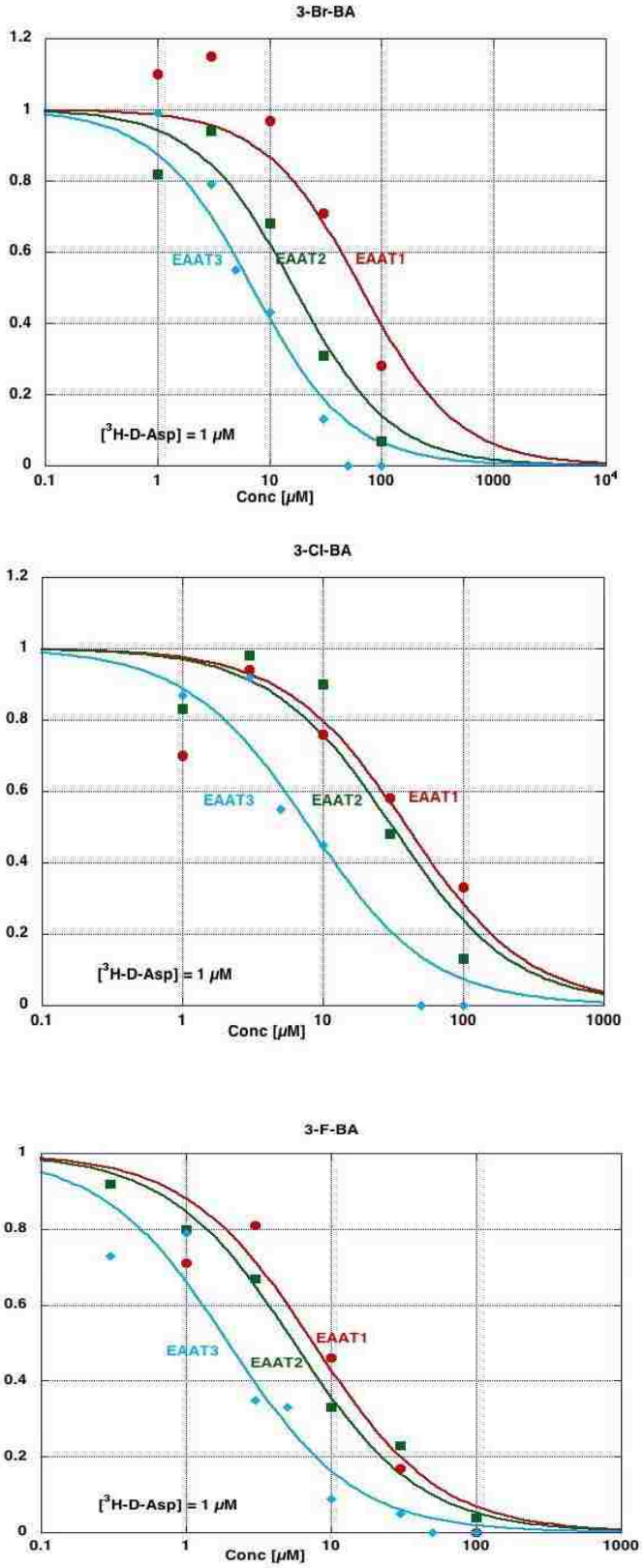

Figure 3. Log concentration response curves for the effects of 3-Br-, 3-Cl- and 3-F-BA on ^{3}H-D-aspartate uptake in C17.2 cells expressing hEAAT1 (●), hEAAT2 (■) and hEAAT3 (♦). Data are expressed as the percent of control uptake measured in the absence of inhibitors and represent the mean ± SEM from at least three independent experiments.

Compound	EAAT1	EAAT2	EAAT3
		μM	
L-β-3-Bromo-Benzyl Aspartate 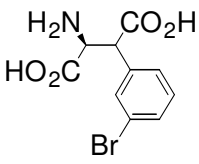	65.1 ± 25.9	16.5 ± 4.06	7.04 ± 1.33
L-β-3-Chloro-Benzyl Aspartate 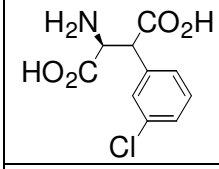	39.6 ± 15.4	31.3 ± 10.1	8.03 ± 2.15
L-β-3-Floro-Benzyl Aspartate 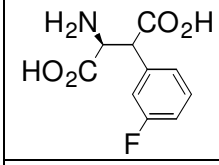	7.50 ± 2.12	5.56 ± 0.65	1.95 ± 0.37

Table 2. IC_{50} values for the inhibition of ^{3}H-D-aspartate uptake by hEAAT1-3 expressed in C17.2 cells.

3.3 Computational studies.

Computational studies were carried out in collaboration with Dave Holley in the Gerdes lab. Inhibitors L-β-3-F-BA, L-β-BA, L-β-2-naphthyl aspartate (L-β-2-NA), TBOA and the naphthyl derivative of TBOA, *threo*-β-(2-naphthyl)-methoxyaspartate (TNOA-2) (Shimamoto *et al.*, 2000) were docked in an EAAT3 protein homology model based on the crystal structure of TBOA bound Glt_{ph} using the program GOLD (Boudker *et al.*, 2007). In order to attempt correct evaluations of different poses we took a heuristic approach that incorporated known hydrogen bonding interactions involving Arg447 and Asp444 shown to be critical for affinity and transport (Teichman and Kanner, 2007; Bendahan *et al.,* 2000).

TBOA docked into the EAAT3 model aligned with the alpha carboxyl, amine and distal carboxyl of TBOA bound in the Glt_{ph} crystal structure and was able to achieved H-bonding interactions with Arg447 and Asp444. Arg447 H-bonds between docked TBOA (dark blue) and TBOA in the crystal structure (light blue) are shown in figure 4. In order to emphasize the H-bonding interactions between Arg447 and the ligand, H-bonding interactions between the alpha carboxyl group and Asp444 were not highlighted, though these hydrogen bonds were formed. Docked poses of TBOA revealed an interesting ability of the ether group to substitute for the distal carboxyl in the H-bond interaction with Arg447. In addition to acting as a substitute for the distal carboxyl the ether group was observed to participate in H-bonding interactions of the distal carboxyl with

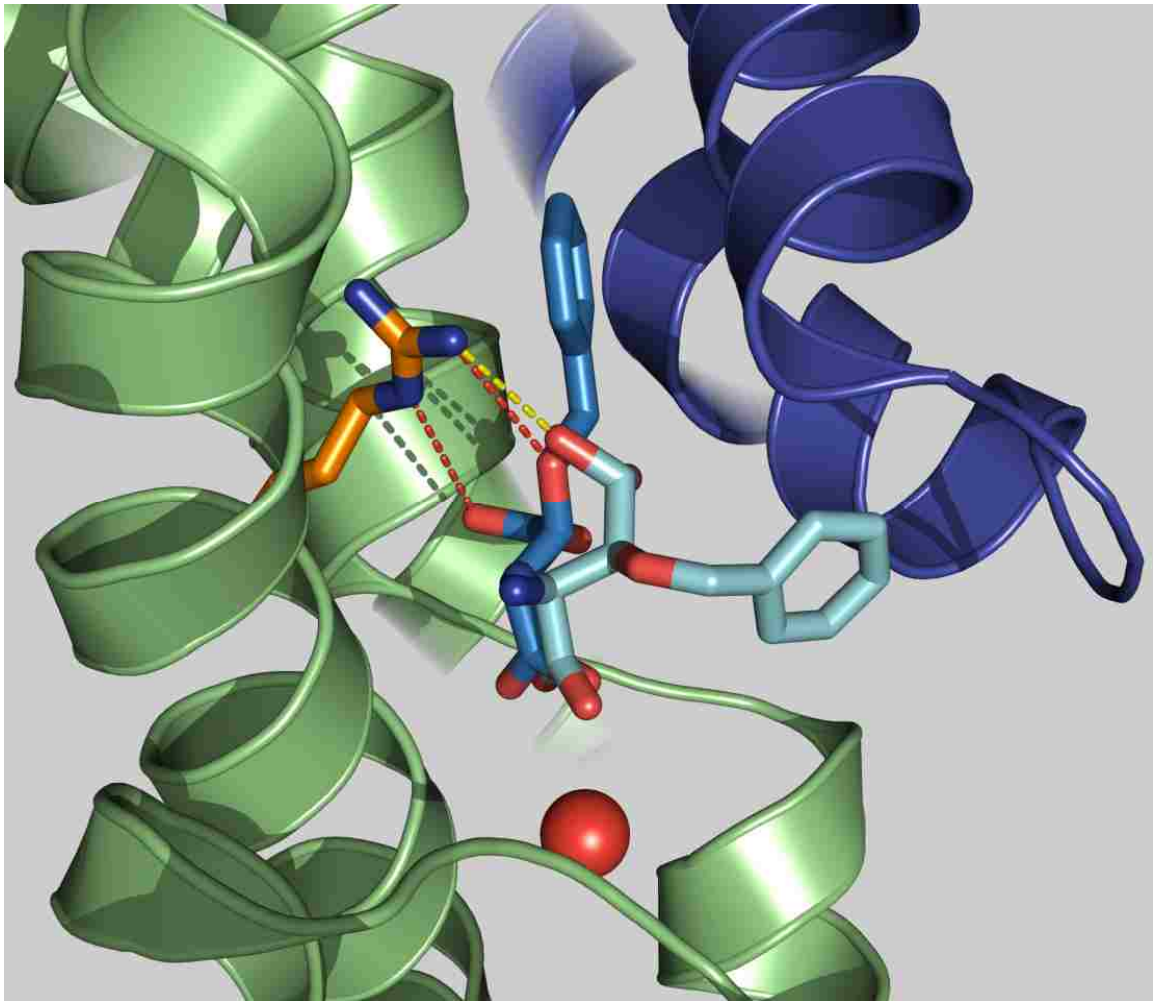

Figure 4. TBOA from the crystal structure TBOA-Glt_{ph} is shown in light blue and TBOA docked by GOLD into the EAAT3 model is shown in dark blue.

Arg447. Figure four illustrates the ability of the distal carboxyl group and/or the ether of TBOA to hydrogen bond with Arg447, red dashed line. This is complementary to the crystal structure which shows interaction of the distal carboxyl group and Arg447, yellow dashed line. Docked poses placed the aromatic portion of TBOA in a lipophilic pocket near Leu408 and Met411 in hair pin loop 2 (HP2) and Tyr365 in trans membrane 7 (TM7) in a distinct position from the crystal structure.

Of the three L-β-BA analogues, docked poses of L-β-3-F-BA and L-β-BA met the criteria for correct orientation as described above (figure 5). Docked poses of L-β-2-NA revealed that H-bonding interactions with either the distal carboxyl group and Arg447 or the alpha amine group and Asp444 predominately occurred. Simultaneous H-bonding interactions were rarely observed. On the infrequent occasions that both H-bonding interactions were achieved, the GoldScore was much lower than the scores observed for the other compounds.

In order to determine potential differences between the mechanisms for binding between the TBOA structures and the L-β-BA structures we docked the naphthyl derivative of TBOA, TNOA-2. In agreement with what was observed for L-β-2-NA, TNOA-2 rarely made H-bonding interactions with both the distal carboxyl group and Arg447 and the alpha amine group and Asp444. Significantly TNOA-2 could form simultaneous H-bonds between the ligand alpha amine and Asp444 and between the ligand ether and Arg447, effectively supplanting the distal carboxyl interactions (figure 6).

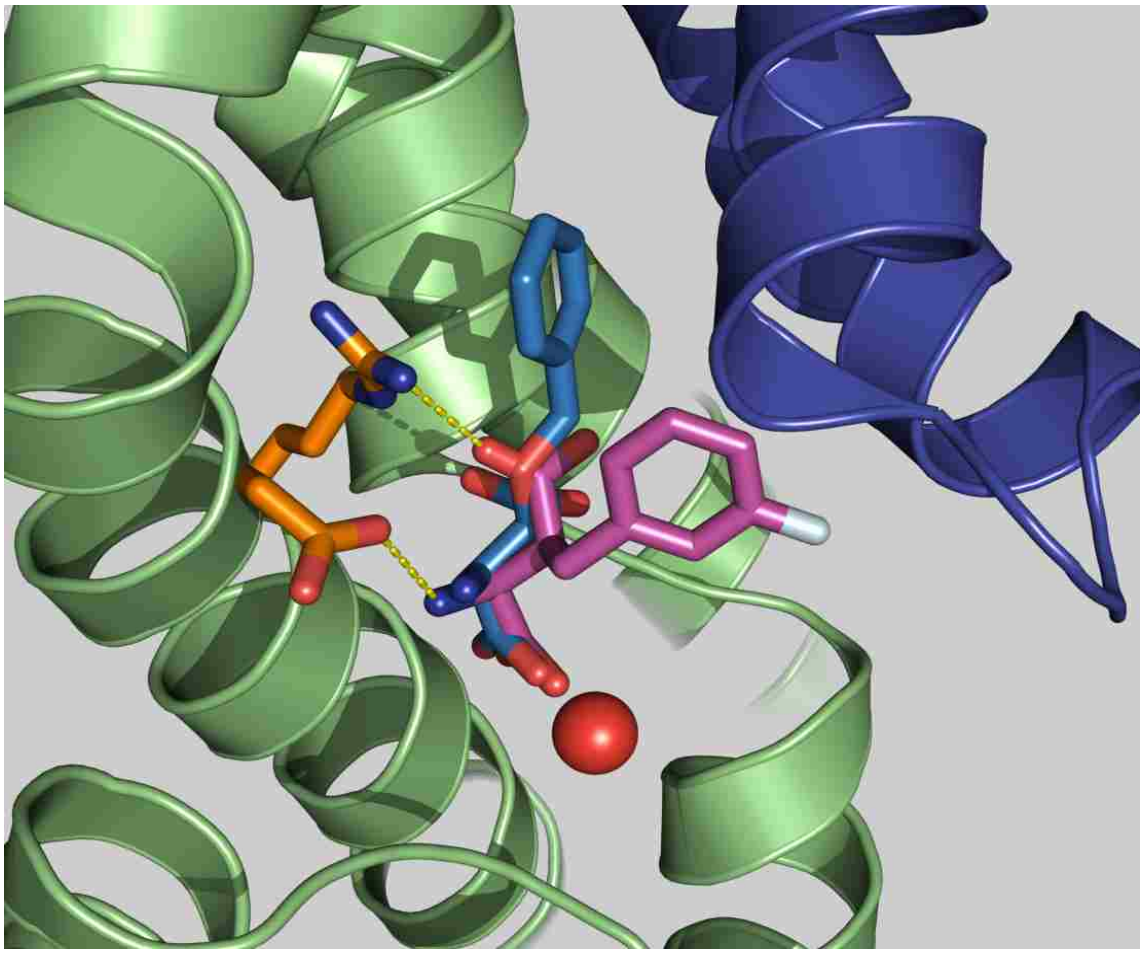

Figure 5. Docked TBOA, shown in dark blue and L-β-3-F-BA, shown in pink, in the active site of the EAAT3 model. H-bonding interactions shown for L-β-3-F-BA with Asp444 and Arg447 are shown in yellow.

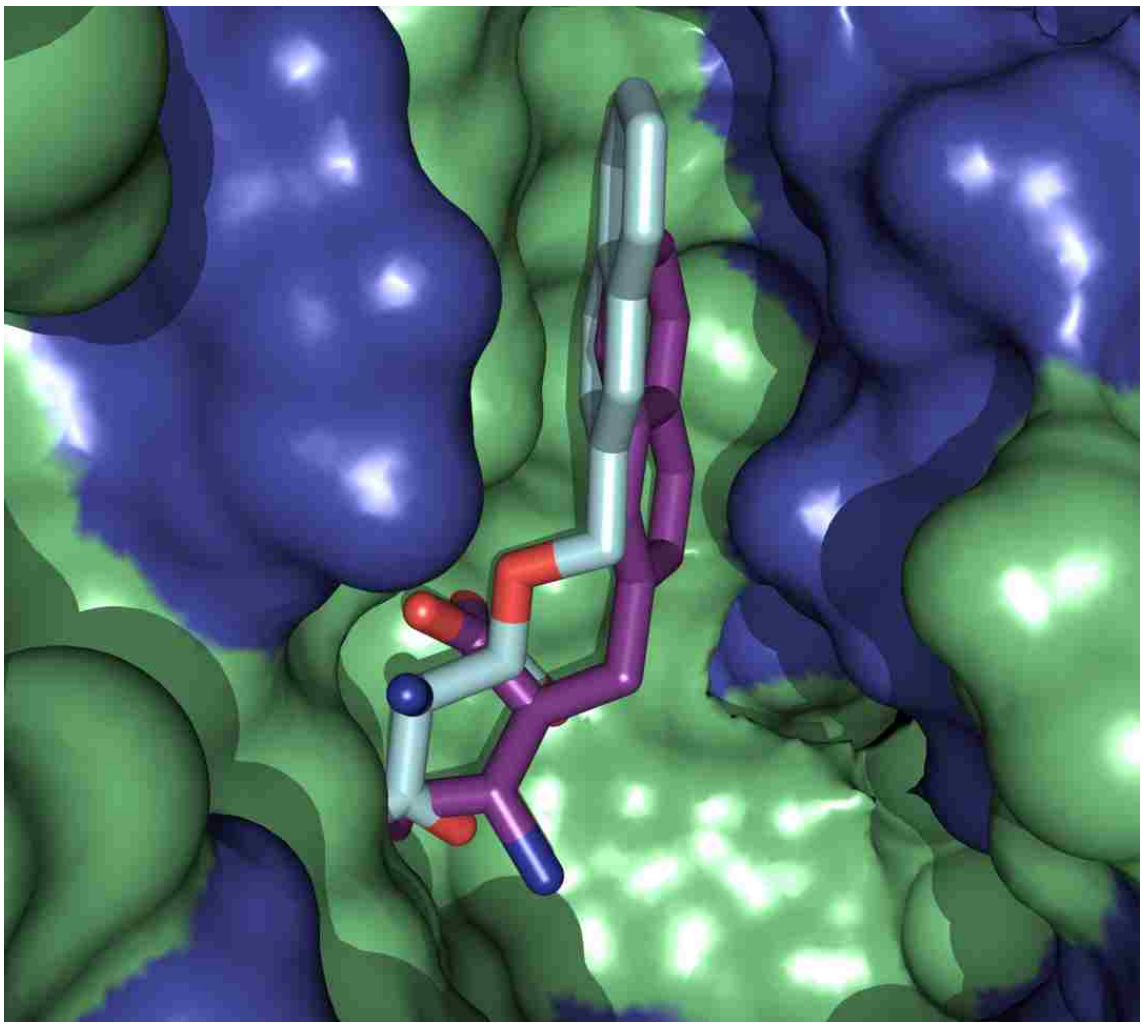

Figure 6. L-β-2-NA (purple) and TNOA-2 (light blue) in the active site of the EAAT3 model. The amine group of L-β-2-NA, shown in blue, is positioned away from Asp444 and cannot make the necessary H-bond interaction.

4. Discussion

In the present study we introduce one of the first known set of compounds displaying a consistent preference for EAAT3. The data was evaluated pharmacologically and computationally and results suggest the reason for the observed selectivity is due to necessary H-bonding interactions of L-β-BA with key residues in the binding site. These interactions position the aromatic moiety in a specific area of the protein which is more accessible in EAAT3.

Pharmacological data lent insight to the physical characteristics of the binding site, particularly the area that supports the aromatic moiety of L-β-BA and L-β-BA derivatives. Two reliable trends were observed among the analogues: decreased potency with larger substituents and a consistent preference for EAAT3 compared to EAAT1 and EAAT2. Dramatic reductions in potency were observed for the largest additions made to the aspartate backbone e.g., 1- and 2-β naphthyl aspartate (L-β- 1- and 2-NA). Significantly, 1- and 2-substituted naphthyl TBOA derivatives (TNOA-1 and -2) show an increase in potency from the original benzyl analogue (TBOA) (Shimamoto *et al.*, 2000), reinforcing the conclusion that the area BA analogues probe is, at least partially, distinct from the area probed by TBOA analogues. Substitutions that positions the ring away from the aspartate backbone are not tolerated (L-β-2,6-dichloro BA) within the transporter binding sites (EAAT1-3). This may be due to steric clashes with the protein when the aromatic moiety is forced into a different configuration. There appears to be more room in the lipophilic pocket for substitutions at the 3 and 5

positions than at the 4 position of the aromatic ring. This is supported by the loss of activity when comparing 3 and 4 substitutions (L-β-3- and 4-F-BA; L-β-3 and 4-nitro-BA). The retention of activity observed for L-β-3,5-dimethyl-BA compared to L-β-3-methyl-BA further suggests that there is more area in the lipophilic pocket to tolerate small groups at the 3 and 5 positions than at the 4 position. Small hydrophobic substituents were found to be optimal at the C-3 position on the benzene ring. The most potent and selective compound of this series, L-β-3-fluoro-BA (L-β-3-F-BA), shows similar potency and selectivity as L-β-BA. The fluoro- substitution increases the lipophilicity of the aromatic ring while imparting a small amount of steric bulk. This can be compared to larger substitutions, such as the less potent iodo derivative, which also increase the lipophilicity of the aromatic moiety but with greater steric bulk. This emphasizes the importance of both the size and position of the substitutions, as well as the consistent trend among EAAT inhibitors of increased potency with increased lipophilicity.

Computational analysis suggests that the difference in selectivity observed between L-β-BA analogues and TBOA analogues is likely due to the positioning of the aromatic moiety within the protein. It has been suggested that the positioning of the aromatic moiety is affected by essential H-bonding interactions between the ligand α-amine and Asp444 and the ligand distal carboxyl group and Arg447 (Teichman and Kanner, 2007; Bendahan *et al.,* 2000). We hypothesize that the wide range of inhibitory activity observed with TBOA lies in the ability of the ether group to substitute for the distal carboxylate in H-bonding interactions with Arg447. This allows the aromatic region to be placed in an area of the

protein that appears to be capable of tolerating more steric bulk. BA and its derivatives do not have an H-bond acceptor positioned to make this key interaction. Therefore the aromatic region of BA is forced into a lipophilic pocket which is more accessible in EAAT3, but which is 3-dimentionally confined and can only tolerate a limited amount of steric bulk. We tested this hypothesis by docking ligands into an EAAT3 homology model using the program GOLD. GOLD is a computational program that optimizes the position of the ligands in the binding site by giving the ligands maximal flexibility while allowing the protein partial flexibility. The poses are scored by GoldScore which is optimized for the prediction of ligand binding positions and takes into account factors such as van der Waals energy, H-bonding energy and ligand torsion strain (From Gold Support Online; http://www.ccdc.cam.ac.uk/products/life_sciences/gold/faqs/scientific_faq.php).

L-β-2-NA and TNOA-2 (L-TNOA-2 is slightly more potent at EAAT1-3 than L-TBOA) present a unique opportunity to explore differences between the binding sites of the EAAT3 and EAAT2 proteins. The only structural difference between these two compounds is the presence of an ether group on the β-substituent of TNOA-2. As expected from TBOA docking exercises, the ether group in TNOA-2 allowed for H-bonding interactions with Arg447, while the ligand α-amine H-bonded to Asp444. The distal carboxyl of TNOA-2 rarely achieved H-bonding interactions while the α-amine was engaged in H-bonding interactions with Arg444. Larger groups appear to have more difficulty making these H-bond interactions as supported by L-β-2-NA and TNOA-2, which rarely achieve them.

We propose that TNOA-2 maintains potency and wide spectrum inhibitory activity at the EAATs due to the ability of the ligand to make this key interaction between Arg447 and the ether of the β-substituent. This substitution allows the ligand to place the naphthyl ring in the larger lipophilic pocket, in a more favorable binding orientation. Interestingly (2S,3S) ethyl phenyl aspartate, a TBOA derivative with a carbon replacing the oxygen on the β-substituent is slightly less potent an inhibitor than TBOA, but shows a 2 fold preference for EAAT3 over EAAT2 (Sakaguchi et al., 2004). This lends credence to the idea that the absence of the ether on the β-substituent places the aromatic moiety into a defined area of the protein, an area which is more accessible in EAAT3. We suggest that the reasons our docked poses of TBOA were different from the crystal structure may be attributed to: differences in the transporters and/or the crystal structure captured one of multiple binding orientations TBOA may achieve. We hypothesize that the docked orientation of TBOA may be preferred in the EAATs and that when the aromatic moiety is larger, such as with the naphthyl (TNOA-2), the position shown in our docking studies is the only position TNOA-2 may take.

A space filling model of TBOA and L-β-BA docked in the active site of EAAT3 (figure 7) further illustrates these points. Figure 7 illustrates the lipophilicity of the regions the benzyl moieties of TBOA and L-β-BA reside in (hydrophobic residues are shown in blue). The lipophilic region the benzyl group of TBOA is placed in appears larger than the area the benzyl group of L-β-BA resides in. In support of the pharmacological data, examination of figure 7 suggests that there is more room to support substitutions at the 3 and 5 positions

than the 4 position. Results from the docking studies support the hypothesis that L-β-BA has a specific manner in which it can interact with the protein and a restricted area in which the benzyl moiety is tolerated. We suggest these points explain the selectivity observed among L-β-BA and L-β-BA derivatives.

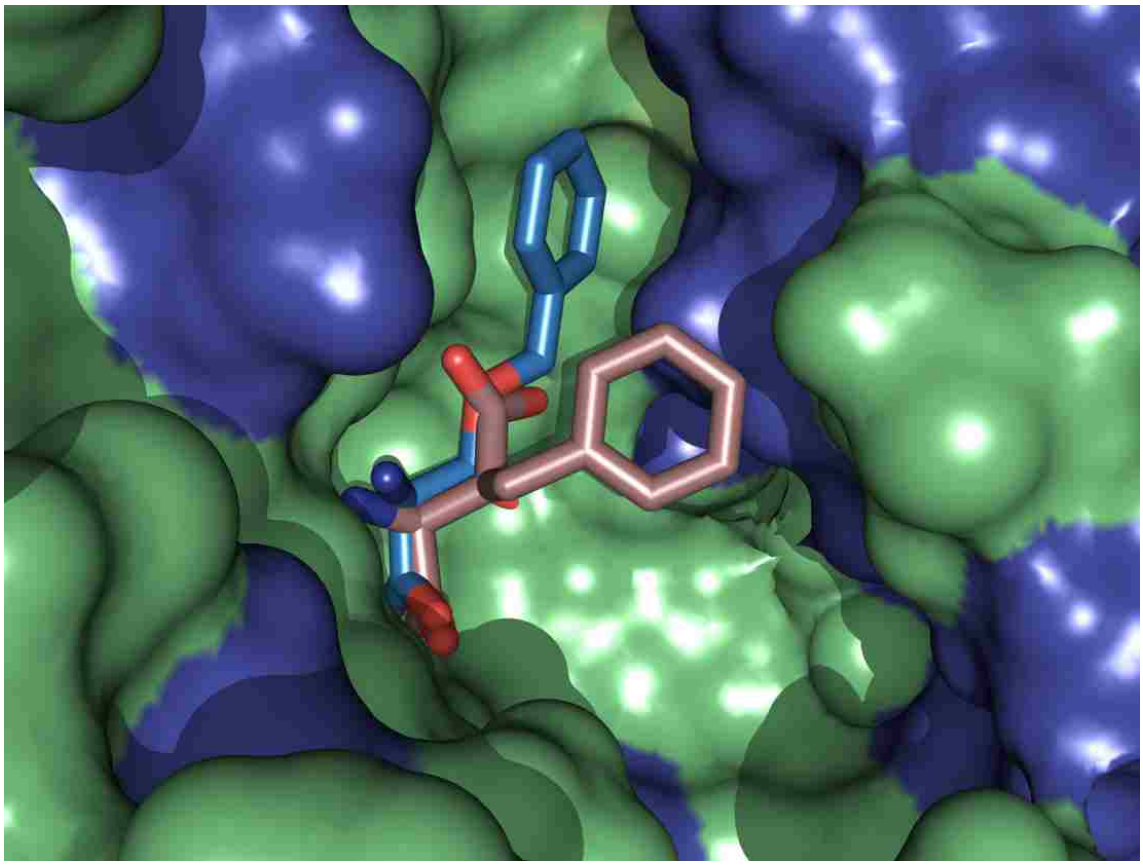

Figure 7. Space filling model of TBOA (blue) and L-β-BA (light pink) docked in the binding site of the EAAT3 model. Hydrophobic residues are shown in blue. The HP2 loop is along the right side of the picture.

5. Conclusions

This work describes the synthesis and the initial characterization of the biological activity of one of the first identified EAAT3 selective inhibitors, L-β-benzyl aspartate. L-β-BA was synthesized in an approximate 2:1 ratio of diasteromers (*threo*:*erythro*), using base promoted enolate addition (Mavencamp *et al.,* 2008). Kinetic analysis of ^{3}H-D-aspartate uptake into C17.2 cells expressing the hEAATs demonstrated that L-*threo*-β-BA is the more potent diastereomer (Ki values of 9 μM for EAAT1, 10.0 μM for EAAT2 and 0.8 μM for EAAT3), acts competitively, and exhibits a 10-fold preference for EAAT3 compared to EAAT1 and EAAT2. Electrophysiological recordings of EAAT-mediated currents in *Xenopus* oocytes further identified L-β-BA as a non-substrate inhibitor. Thus, the analogue binds to the transporter but is not translocated as a substrate. The structure of L-β-benzyl aspartate is similar to TBOA, a well known wide spectrum EAAT inhibitor with a preference for EAAT2. This allows L-β-BA to be directly compared to TBOA, presenting an excellent opportunity to examine subtle differences between the EAAT3 and EAAT2 binding sites. L-β-BA differs from TBOA by the absence of an oxygen atom on the β-substituent. Two hypotheses can be drawn from the analysis of the structure activity data with respect to TBOA. The positioning of the aromatic group of L-β-BA in the protein binding site is different from that of TBOA due to the absence of the oxygen on the β-substituent and/or the difference in length of the β-arm. The selectivity observed for L-β-BA is due to the unique positioning of

the aromatic group in the protein binding site, which appears to be better tolerated in EAAT3 than in EAAT1 and EAAT2.

L-β-BA derivatives were designed and synthesized to answer key questions about the binding site. 1) The steric tolerance of the binding site was probed by making larger aromatic substitutions to the aspartate backbone, as well as by varying the sizes of substitutions on the benzene ring. 2) The lipophilicity of the pocket was examined by making substitutions to the ring that both increased and decreased the lipophilicity. 3) Substitutions to the ring were made that could act as a H-bond donor or as an acceptor. 4) Substitutions were made in different positions around the aromatic ring to help determine the topology of the lipophilic pocket.

The L-β-β-BA derivatives showed a consistent preference for EAAT3, suggesting that the protein region the compounds probe is more accessible in the EAAT3 protein than in the EAAT1 and EAAT2 proteins. In addition, the derivatives revealed that the EAAT3 lipophilic pocket occupied by L-β-BA is likely smaller than that occupied by TBOA and that it could not tolerate much steric bulk over that of the benzene ring. The lipophilicity of the binding pocket was determined to be important due to the increase in potency observed for substituents which increased the lipophilicity of the aromatic ring over those which decreased lipophilicity. Substitutions to the aromatic ring suggested that H-bonding interactions between the ligand aromatic group and the protein were not likely playing a determinative role in selectivity or potency. The three dimensional constraints of the pocket were determined by substitutions to the

aromatic ring in both the 3 and 5 positions as well as the 4 position. Pharmacological results suggest that the pocket expands in the direction of the 3 and 5 positions but is constrained in the region probed by 4-substitutions.

The most potent and selective L-β-BA derivative, L-β-3-F-BA, highlights these conclusions about the EAAT3 binding site. The 3-fluoro substitution resulted in an analogue displaying increased potency and selectivity over L-β-BA. This is hypothesized to be due to the increase in lipophilicity of the aromatic ring by a small substitution at the preferred 3-position.

Historically, selective, conformationally constrained analogues were used to gain insight into the EAAT binding sites. An EAAT2 pharmacophore model was constructed using the low energy conformations of well known EAAT2 non-substrate inhibitors and overlaying three main ligand groups the protein is hypothesized to recognize: α-amine, α-carboxyl and distal carboxyl group. Potential differences between the EAAT2 and EAAT3 binding sites could be elucidated by overlaying an EAAT3 preferring inhibitor (L-β-BA) onto the EAAT2 pharmacophore model and observing points of diversion. It was immediately obvious that the aromatic regions of L-β-BA and TBOA were in different areas due to the oxygen in the TBOA β-substituent and/or in the one atom longer arm of TBOA (Esslinger *et. al.,* 2005). A crystal structure of the EAAT homologue, Glt_{ph}, was recently published, with both aspartate and TBOA bound in the binding site (Yernool *et al.,* 2004; Boudker *et al.,* 2007). From the crystal structure an EAAT3 homology model could be constructed by overlaying the EAAT3 sequence onto the crystal structure of Glt_{ph} with TBOA bound. From the

homology model, the program GOLD could be utilized to optimize the position of ligands in the active site.

Docking studies performed using the program GOLD revealed distinct conformations with which L-β-BA and TBOA analogues may bind in the active sites. These studies suggest that the lipophilic moiety of TBOA analogues reside in a distinct area from the aromatic moiety of L-β-BA analogues. This different placement appears to be due to the ability of the ether group of TBOA to substitute for crucial H-bonding interactions in the active site typically made by the distal carboxylate of analogues. In contrast, L-β-BA binds in the active site in a distinct manner due to the absence of alternate atoms (*i.e.* ether) with which to form key H-bonding interactions in the active site. This forces the aromatic ring of L-β-BA into an area of the protein that, as suggested by pharmacological data, is more available in the EAAT3 protein than in EAAT1 or EAAT2. The docking studies suggest areas within the EAAT2 and EAAT3 proteins which may be exploited to design more selective and potent inhibitors. Both the pharmacophore model and the conclusions from the docking studies will be modified as more results become available, increasing the accuracy with which the models dictate new synthesis.

An important future direction of this work is to characterize the separated diastereomers: L-β- *threo*- and *erythro*-3-F-BA. In light of the results from *threo*- and *erythro*-BA, we hypothesize that the *threo* form of L-β-3-F-BA will be the more potent diastereomer and preliminary data suggests that this is the case.

More detailed assays of the *threo* and *erythro*-diasteromers are currently underway.

The next generation of EAAT3 inhibitors can be designed from comparisons of the current EAAT2 and EAAT3 binding site models. An intriguing approach is to design a compound capable of probing both the lipophilic pocket that the benzyl group of TBOA resides and the lipophilic pocket that the benzyl group of L-β-BA probes. An increase in potency would be predicted to occur due to the enhanced lipophilic interactions of the TBOA like aromatic group. Selectivity would be maintained by the benzyl aspartate like aromatic group that probes the lipophilic pocket hypothesized to be unique to EAAT3. Due to the small size of the proposed lipophilic pocket in EAAT3, smaller substitutions may be beneficial, such as L-β-3-amine-BA. Symmetrical substitutions to the aromatic ring may show an increase in selectivity, L-β-3,5-diamine-BA and L-β-3,5-difluoro-BA could be synthesized to test this hypothesis. Larger aromatic substitutions with more flexibility may be advantageous as they are less rigid and could possibility avoid steric interactions with the HP2 loop that are predicted to occur between L-β-naphthyl-BA and the EAAT3 protein. Dibenzyl ring systems in place of the benzyl ring, such as diphenyl methane, or rings connected by an ether linkage such as diphenyl ether which is commercially available as the electrophile; 1-(bromomethyl)-3-phenoxybenzene, may increase the potency and selectivity of L-β-BA for EAAT3.

In addition to the synthesis of new compounds it is important to test L-β-BA and L-β-BA derivatives for cross reactivity. In particular, it is crucial to

determine if L-β-BA is interacting with the metabotropic and ionotropic glutamate receptors. Cross reactivity with the ionotropic EAA receptors is not anticipated due to the similar template of L-β-BA and TBOA, which did not display cross reactivity (Shimamoto *et al.*, 2002). To verify this hypothesis receptor binding assays could be performed.

It is anticipated that this group of L-β-BA derivatives will be useful in investigating the role that EAAT3 plays in glutamate uptake as related to shaping the postsynaptic signal. Additionally, L-β-BA could be used as a tool to elucidate the role of EAAT3 in various physiological roles, such as learning and memory, as well as in pathophysiological states such as those observed in ischemia and schizophrenia.

Preceding the syntheses of EAAT selective inhibitors, both EAAT knock-out and EAAT antisense animals were utilized to study the physiological role of the EAATs. EAAT3 knock-out mice present significantly reduced spontaneous locomotor activity at 12 months as measured in an open-field monitoring chamber. The EAAT3 knock-out mice do not show neuronal loss or motor incoordination in rotorod testing, and learning appears unimpaired in water maze testing. A major dysfunction of EAAT3 knock-out animals is the onset of dicarboxylic aminoaciduria due to the loss of uptake from the renal tubules by EAAT3 (Peghini *et al.,* 1997). The reason for the mild CNS deficits of knock-out mice may be due to compensation by other glutamate transporters during development. This is supported by behavioral abnormalities observed in antisense treated animals including staring-freezing episodes and electrographic

(EEG) seizures (Sepkuty *et al.,* 2002). Administration of an EAAT3 specific inhibitor to adult mice would help clarify the effect of decreased EAAT3 on learning and coordination as well as on the potential to induce seizures, neuronal damage or dicarboxylic aminoaciduria. These results are particularly important when considering the use of EAAT3 inhibitors as potential therapies. The consequences of EAAT3 inhibition, particularly over long periods, are not clear and need to be evaluated before therapeutic applications can be seriously considered.

Due to the availability of EAAT2 specific inhibitors, more is known about the role of EAAT2 in glutamate uptake than any other EAAT. From these studies we can conclude that EAAT2 uptake plays a role in shaping the postsynaptic signal when the synapse is tightly ensheathed by glial cells and the volume of the synapse is restricted. The EAAT2 preferring inhibitors, DHK and WAY-855, have been utilized to assess the role of EAAT2 in clearing glutamate from the synaptic cleft. When DHK was used to selectively inhibit EAAT2, a threefold increase in the amplitude of mGluR1 mediated EPSCs from oriens-lacunosum molecular interneurons in hippocampal slices was observed. In contrast, when TBOA was used to block the EAATs a greater than 15 fold increase in the EPSCs was observed suggesting a prominent role for EAAT1 and/or EAAT3 (Huang *et al.,* 2004). In agreement with the results gained from DHK, the more potent, selective EAAT2 inhibitor WAY-855 did not cause excitotoxicity in rat hipppocampal slices, but when TBOA was applied significant neuronal death was observed (Selkirk *et al*., 2005).

Due to the lack of EAAT3 selective inhibitors, the role of EAAT3 in shaping the excitatory post synaptic response among excitatory circuits in varying parts of the brain is not as clearly defined as for EAAT2. In the past the role of EAAT3 was determined by studying the role of EAAT2 and comparing this to the effects of blocking all of the EAATs then ascribing the difference to EAAT1 and/or EAAT3. This was further followed up by experiments done in knock out EAAT1 and EAAT3 animals (Huang *et al.*, 2004; Selkirk *et al.,* 2005). Now that EAAT3 selective inhibitors are available, the contribution of EAAT3 to variables such as the duration, amplitude and decay of the post synaptic response could be directly examined using electrophysiological techniques. Glutamate uptake by the EAATs is the main mechanism by which glutamate is cleared from the synaptic cleft in brain regions that are tightly ensheathed by glial cells. Hence, one would be expect the time course of the postsynaptic response to be prolonged by EAAT3 transport inhibition (Overstreet *et al.,* 1999). In contrast, brain regions where glutamate clearance is mainly attributed to diffusion, uptake blockers would not be expected to show significant changes in the duration of the postsynaptic responses (Isaacson and Nicoll, 1993). In addition, it would be of interest to determine if EAAT3 contributes to the presynaptic neuronal pool of glutamate. If EAAT3 did contribute to this pool, blocking EAAT3 might be expected to change the probability of release as measured by paired pulse ratios.

Glutamate that escapes the synaptic cleft has been shown to affect neighboring synapses. This phenomenon is termed spillover (Scanziani *et al.,*

1997; Kullman and Asztely, 1998). The perisynaptic localization of EAAT3 on neurons implicates EAAT3 in controlling the extent of spillover, and thus the extent to which glutamate stimulates receptors outside of the synaptic cleft. Spillover of glutamate from excitatory mossy fibers has been shown to inhibit GABA release by activating presynapic mGluRs on inhibitory interneuron axons within the cerebellar glomerulus and the hippocampus. This may be a way of sharpening the output of select cells by inhibiting neighboring boutons. (Vogt and Nicoll, 1998; Mitchell and Silver, 2000). Blocking EAAT3 may increase the inhibition of GABA release by allowing more glutamate to stimulate the presynaptic mGluRs. This could be measured directly with the use of an EAAT3 selective inhibitor.

The localization of EAAT3 to presynaptic GABA neurons led to the hypothesis that EAAT3 played a role in GABA synthesis. In order to test the role of EAAT3 in GABA synthesis, rats were administered EAAC1 antisense oligonucleotides which resulted in a 60% decrease in EAAC1 expression. Behavioral abnormalities, including staring-freezing episodes and electrographic seizures, were observed along with a decrease in miniature inhibitory post synaptic currents (mIPSCs) in whole cell patch clamp recordings of CA1 pyramidal neurons and a 50% loss of hippocampal GABA levels (Sepkuty *et al*., 2002). These results suggest that EAAT3 plays a significant role in controlling the amount of GABA in the hippocampus. An EAAT3 blocker offers a direct method with which to examine the role of EAAT3 in GABA synthesis and release. In addition, an EAAT3 blocker could directly and reversibly block EAAT3 to

determine the time course with which blocking EAAT3 decreases GABA synthesis as well the time course to recover full GABA activity after the EAAT3 blocker is removed.

Long term potentiation (LTP) is the cellular basis for learning and memory (Larkman and Jack, 1995; Bennett, 2000). LTP works by strengthening synapses either presynaptically, by increasing the probability of release or postsynaptically, by altering the sensitivity of the cell to glutamate (Kawamura *et al.*, 2004). Contextual fear conditioning is a form of learning in which fear is associated with a neutral stimulus and learning can be measured by the ability of the neutral stimulus to elicit fear. LTP and contextual fear conditioning increase the uptake of glutamate from the synaptic cleft and increase the membrane expression of EAAT3. These results suggest that the uptake of glutamate by EAAT3 may be a component of plasticity at glutamatergic synapses (Levenson *et al.,* 2002). This hypothesis could be tested *in vivo* with animal models administered an EAAT3 selective inhibitor and submitted to fear conditioning. Fear conditioning could be accomplished by administering electrical shocks associated with a neutral stimulus and measuring freezing behavior 24 hours later when the neutral stimulus was administered. An EAAT3 blocker administered before fear conditioning would be predicted to decrease freezing behavior, which would suggest a learning impairment. *In vitro* experiments may help elucidate the mechanism responsible for the learning impairment. Levenson induced LTP by high frequency stimulation (HFS) of the Schaffer-collateral pathway in the hippocampus and observed an increase in the uptake of

glutamate and in the membrane expression of EAAT3 as measured by western blots. He predicted that decreasing diffusion to inhibitory presynaptic mGluRs, and/or to limiting NMDA activation to prevent toxicity may be the reason for the increase in transport activity (Levenson *et al*., 2002). Our development of an EAAT3 blocker provides a strategy to determine if LTP is affected by blocking EAAT3.

One area where EAAT3 inhibitors may be therapeutically useful is in alleviating damage during brain ischemia. Brain ischemia is an important therapeutic target as it is the third cause of death in industrialized countries. Glutamate release contributes to neuronal damage observed during ischemia and is hypothesized to be due, in part, to the reversal of the EAATs, particularly EAAT3 (Rossi *et al.,* 2000). The reversal of the EAATs has been observed under conditions of ATP depletion or elevated extracellular potassium levels (Anderson *et al.,* 2001). The cytosolic concentration of glutamate in neurons is approximately 10mM, much higher than the 3mM observed in glial cells. This suggests that EAAT3 is more likely to release glutamate than a glial transporter (Camacho and Massieu, 2006). Of the glial transporters EAAT1 is a more likely candidate than EAAT2. EAAT2 does not appear to run in reverse, as supported by the EAAT2 knock down rats which undergo transient middle cerebral artery occlusion (MCAO) and display more damage. These results suggest that EAAT2 aids in clearing glutamate from the synaptic cleft during ischemia. Administration of an EAAT3 inhibitor post transient MCAO and examination of the damage as

marked by infarct volume, brain edema and mortality would answer many important questions about the role of EAAT3 in ischemia.

EAAT3 inhibitors are emerging as potential pharmaceuticals in the development of novel antipsychotics. The glutamate hypofunction model states that the positive, negative and cognitive symptoms of schizophrenia are associated with reduced stimulation of NMDA. This is supported by the application of NMDA antagonists, which produce schizophrenia like symptoms and are used as a model of schizophrenia. From these observations it can be hypothesized that Increasing stimulation of NMDA may alleviate symptoms of schizophrenia. If EAAT3 controls the amount of glutamate available to stimulate NMDA receptors this indicates it as a potential drug target. Consistent with this is altered EAAT3 levels in persons with schizophrenia as well as in rats and persons treated by antipsychotic medications (McCullumsmith and Meador-Woodruff, 2002; Schmitt *et al.*, 2003). The EAAT3 inhibitor, NBI-59159, displays an approximate 5 and 40 fold selectivity over EAAT2 and EAAT1. This compound was shown to decrease amphetamine-stimulated locomotor activity in mice (Dunlop and Marquis, 2006). Further support of the role of EAAT3 inhibition in decreasing amphetamine-stimulated locomotor activity is the application of a selective EAAT2 inhibitor WAY-855 which did not influence amphetamine-stimulated locomotion (Dunlop and Marquis, 2006). Because the 5 fold selectivity reported for NBI-59159 over EAAT2 is less than the selectivity observed for L-β-*threo*-BA and derivatives of L-β-BA, it would advantageous to compare the results from Dunlop and Marquis with results obtained from

administration of L-β-*threo*-BA and/or L-β-*threo*-3-F-BA to amphetamine stimulated mice.

In summary, the excitatory amino acid transporters (EAATs) play a central role in regulating extracellular glutamate levels in the Central Nervous System (CNS). These uptake systems are capable of influencing the amount and/or time course with which L-glutamate is in contact with the EAA receptors. Among five identified isoforms, EAAT3 is the most abundant subtype present on neurons and is widely expressed throughout the forebrain and cerebellum. The synthesis of selective inhibitors and the creation of a binding site model will aid in elucidating the roles of EAAT3 in CNS function. EAAT3 has been implicated in a variety of both physiological and pathophysiological processes including long term potentiation, schizophrenia, neurodegeneration and ischemia. Its roles however, remain undefined, due to the lack of reagents with which to selectively modulate its activity. Specifically, work in our laboratories has led to the first EAAT3 preferring inhibitor and the first family of EAAT3 preferring inhibitors. We suggest that these analogues will serve as excellent tools with which to study the specialized roles of EAAT3 in the CNS.

References:

Anderson CM, Bridges RJ, Chamberlin AR, Shimamoto K, Yasuda-Kamatani Y, Swanson RA. 2001. Differing effects of substrate and non-substrate transport inhibitors on glutamate uptake reversal. *J. Neurochem.* **79(6):**1207-16.

Aoyama, K., S. W. Suh, A. M. Hamby, J. Liu, W. Y. Chan, Y. Chen and R. A. Swanson 2006. Neuronal glutathione deficiency and age-dependent neurodegeneration in the EAAC1 deficient mouse. *Nat Neurosci* **9(1):** 119-26.

Armstrong and Gouaux. 2000. Mechanisms for Activation and Antagonism of an AMPA-sensitive Glutamate Receptor Crystal Structures of the GluR2 ligand binding core. *Neuron*. **28(1):** 165-181.

Arriza, J. L., W. A. Fairman, J. I. Wadiche, G. H. Murdoch, M. P. Kavanaugh and S. G. Amara 1994. Functional comparisons of three glutamate transporter subtypes cloned from human motor cortex. *J Neurosci* **14(9):** 5559-69.

Arriza, Eliasof, Kavanaugh, Amara 1997. Excitatory amino acid transporter 5, a retinal glutamate transporter coupled to a chloride conductance. *Proc Natl. Acad. Sci. USA* **(94)8**:4155-60.

Auger, C. and D. Attwell 2000. Fast removal of synaptic glutamate by postsynaptic transporters. *Neuron* **28(2):** 547-58.

Balazs, Bridges and Cotman, 2006. Excitatory Amino Acid Transmission in Health and Disease. *Oxford University Press.*

Barbour, B., Keller, B.U., Llano, I., Marty, A., 1994. Prolonged presence of glutamate during excitatory synaptic transmission to cerebellar Purkinje cells. *Neuron*. **12**:1331-1343.

Beart, P. M.; O'Shea, R. D. 2007**.** Transporters for L-glutamate: an update on their molecular pharmacology and pathological involvement. *Br. J. Pharmacol.* **150(1)**: 5-17.

Bendahan, A., Armon, A., Madani, N., Kavanaugh, M.P. and Baruch I. Kanner 2000. Arginine 447 plays a pivotal role in substrate interactions in a neuronal glutamate transporter. *J. Biol. Chem.*, **275(48):** 37436-37442.

Bennett MR. 2000. The concept of long term potentiation of transmission at synapses. *Prog Neurobiol.* **60(2):** 109-37.

Berl, S., Nicklas, W.J., Clarke, D.D., 1968. Compartmentation of Glutamic Acid Metabolism in Brain Slices. *J. Neuroch*. **(15):** 131-140.

Boudker, Olga; Ryan, Renae; Yernool, Dinesh; Shimamoto, Keiko; Gouaux, Eric 2007. Coupling Substrate and ion binding to extracellular gate of a sodium-dependent aspartate transporter. *Nature* **(445)**: 387-393.

Brauner-Osborne, H., Hermit, M.B., Nielsen, B., Krogsgaard-Larsen, P., Johansen, T.N., 2000. A new structural class of subtype-selective inhibitor of cloned excitatory amino

acid transporter, EAAT2. *Eur. J. Pharmacol*. **406**:41-44.

Breedlove et. al., 2007. *Biological Psychology,* Fifth Edition, published by Sinauer Associates. Sinauer Associates and Sumanas, Inc.

Bridges, R. J., M. S. Stanley, M. W. Anderson, C. W. Cotman and A. R. Chamberlin 1991. Conformationally defined neurotransmitter analogues. Selective inhibition of glutamate uptake by one pyrrolidine-2,4-dicarboxylate diastereomer. *J Med Chem.* **34(2):** 717-25.

Bridges, R. J., F. E. Lovering, H. Koch, C. W. Cotman and A. R. Chamberlin 1994. A conformationally constrained competitive inhibitor of the sodium-dependent glutamate transporter in forebrain synaptosomes: L-anti-endo-3,4-methanopyrrolidine dicarboxylate. *Neurosci Lett* **174(2):** 193-7.

Bridges, R.J., Kavanaugh, M.P., Chamberlin, A.R., 1999. A pharmacological review of competitive inhibitors and substrates of high-affinity, sodium-dependent glutamate transporters in the central nervous system. *Curr. Pharm. Des*. **5:**363-379.

Bridges, R. J. and C. S. Esslinger 2005. The excitatory amino acid transporters: pharmacological insights on substrate and inhibitor specificity of the EAAT subtypes. *Pharmacol Ther* **107(3):** 271-85.

Camacho A, Massieu L. 2006. Role of glutamate transporters in the clearance and release of glutamate during ischemia and its relation to neuronal death. *Arch Med Res.* **37(1)*:***11-18

Cavara N.A. and Hollman M. 2008. Shuffling the deck anew: how NR3 tweaks NMDA receptor function. *Mol. Neurobiol*. **38(1):**16-26.

Chamberlin, A.R., Koch, H.P., Bridges, R.J., 1998. Design and synthesis of conformationally constrained inhibitors of high-affinity, sodium-dependent glutamate transporters. In: Amara, S.G. (Ed.), Neurotransmitter Transporters, Vol. 296. Academic Press, San Diego, CA. 175-189.

Chaudhry F.A., Lehre K.P., van Lookeren Campagne M., Ottersen O.P., Danbolt N.C., Storm-Mathisen J., 1995. Glutamate transporters in glial plasma membranes: highly differentiated localizations revealed by quantitative ultrastructural immunocytochemistry. *Neuron*. **15(3)**:711-20.

Cheyne J.E., Montgomery J.M., 2008. Plasticity-dependent changes in metabotropic glutamate receptor expression at excitatory hippocampal synapses. *Mol Cell Neurosci.* **37(3)**:432-9.

Choi, D.W., 1994. Glutamate receptors and the induction of excitotoxic neuronal death. *Prog. Brain Res.* **100**:47-51.

Cont and Melone 2006. The glutamate commute. *Neurochemical International.* **48(6-7):**459-464.

Coolingridge, G.I., Kehl, S.J. and McLennan, H. 1983. Excitatory Amino Acids in synaptic transmission in the Schaffer Collateral-Commissural pathway of the rat hippocampus. *J. Physiol*. **334**:33-46.

Crino, P. B., H. Jin, M. D. Shumate, M. B. Robinson, D. A. Coulter and A. R. Brooks-Kayal 2002. Increased expression of the neuronal glutamate transporter (EAAT3/EAAC1) in hippocampal and neocortical epilepsy. *Epilepsia* **43(3):** 211-8.

Danbolt 2001. Glutamate uptake. *Prog. Neurobiol*. **65:**1-105.

Davies, S.N., Lester, R.A.J., Reyman, K.G., Collingridge, G.L., 1989. Temporally distinct pre- and postsynaptic mechanisms maintain LTP. *Nature* **338**: 500-503.

Dean, P.M., Perkins, T.D., 1998. Calculation of three-dimensional similarity. In: Martin, Y.C., Willett, A. (Eds.), Designing Bioactive Molecules, Three-Dimensional Techniques and Applications. American Chemical Society, Washington, DC, 199-220.

Dener, Zhang, and Rapoport. An Effective Chirospecific Synthesis of (+) Pilocarpine from L-aspartic Acid. 1993 *J. Org. Chem.* **58**: 1159-1166.

Denton, T.T., Seib, T., Bridges, R.J., Thompson, C.M., 2002. Synthesis and preliminary evaluation of trans-3-4-conformationally-restricted glutamate and pyroglutamate analogues as novel EAAT2 inhibitors. *Bioorg. Med. Chem. Lett.* **12**:3209-3213.

Denton, Xiaodong, Cashman 2005. 5-Substituted, 6-Substituted, and Unsubstituted 3-Heteroaromatic Pyridine Analogues of Nicotine as Selective Inhibitors of Cytochrome P-450 2A6. *J. Med. Chem.* **48:** 224-239.

Dringen, R. 2000. Metabolism and functions of glutathione in brain. *Prog Neurobiol* **62(6):** 649-71.

Dunlop, J., S. Eliasof, G. Stack, H. B. McIlvain, A. Greenfield, D. Kowal, R. Petroski and T. Carrick 2003. WAY-855 (3-amino-tricyclo[2.2.1.02.6]heptane-1,3-dicarboxylic acid): a novel, EAAT2-preferring, nonsubstrate inhibitor of high-affinity glutamate uptake. *Br J Pharmacol* **140(5):** 839-46.

Dunlop, J., H. B. McIlvain, T. A. Carrick, B. Jow, Q. Lu, D. Kowal, S. Lin, A. Greenfield, C. Grosanu, K. Fan, R. Petroski, J. Williams, A. Foster and J. Butera 2005. Characterization of novel aryl-ether, biaryl, and fluorene aspartic acid and diaminopropionic acid analogs as potent inhibitors of the high-affinity glutamate transporter EAAT2. *Mol Pharmacol.* **68(4):** 974-82.

Dunlop, J. and Butera, J.A. 2006. Ligands targeting the excitatory amino acid transporters (EAATs). *Curr Top Med Chem*. **6(17):**1897-906.

Dunlop and Marquis, K., 2006. Glutamate transport inhibitors as targets for treating psychosis. *Drug Discovery Today: Therapeutic Strategies*. **3(4)**: 533-537.

Dunn, Haner and Rapoport. Stereoselective Synthesis of 2,3-Diamino Acids. 2,3-Diamino-4-phenylbutanoic Acid. 1990. *J. Org Chem*. **55**: 5017-5025.

Eliasof S.H., McIlvain H.B., Petroski R.E., Foster A.C., Dunlop J. 2001. Pharmacological characterization of threo-3-methylglutamic acid with excitatory amino acid transporters in native and recombinant systems. *J. Neurochem.* **77(2)**:550-7.

Eliasof, S.H., Arriza, J.L., Leighton, B.H., Kavanaugh, M.P., Amara, S.G., 1998. Excitatory amino acid transporters of the salamander retina: identification, localization, and function. *J. Neurosci*. **18 (2)**, 698-712.

Esslinger, C., J. Titus, H. Koch, R. Bridges and A. Chamberlin 2002. Methylation of L-trans-2,4-pyrrolidine dicarboxylate converts the glutamate transport inhibitor from a substrate to a non-substrate inhibitor. Bioorg. Med. Chem. **10(11):** 3509-15.

Esslinger, C. S., S. Agarwal, J. Gerdes, P. A. Wilson, E. S. Davis, A. N. Awes, E. O'Brien, T. Mavencamp, H. P. Koch, D. J. Poulsen, J. F. Rhoderick, A. R. Chamberlin, M. P. Kavanaugh and R. J. Bridges 2005. The substituted aspartate analogue L-*threo*-β-Benzyl aspartate preferentially inhibits the neuronal excitatory amino acid transporter EAAT3. *Neuropharmacology* **49:**850-861.

Esslinger, C. S., K. A. Cybulski and J. F. Rhoderick 2005. Ngamma-aryl glutamine analogues as probes of the ASCT2 neutral amino acid transporter binding site. *Bioorg Med Chem* **13(4):** 1111-8.

Fairman W.A., Vandenberg R.J., Arriza J.L., Kavanaugh M.P., Amara S.G. 1995. An excitatory amino acid transporter with the properties of a ligand gated chloride channel. *Nature* **375**:599-603.

Ferkany J., Coyle J.T. 1986. Heterogeneity of sodium-dependent excitatory amino acid uptake mechanisms in rat brain. *J Neurosci Res* **16**:491-503.

Fernandez-Megia, P.; Sardina. 1994. On the Stereoselectivity of the Reaction of N-(9-Phenylfluoren-9-yl)aspaartate Enolates with Electrophiles. Synthesis of Enantiomerically Pure 3-Hydroxy-, 3-Amino-, and 3-Hydroxy-3-methylaspartates. *J. Org. Chem* **. 59**:643-7652.

Flatman, Schwindt, Crill, Strafstrom. 1983. Multiple Actions of NMDA on cat neocortical neurons in vitro. *Brain Research*. **266:1**:169-73.

Fletcher E.J., Johnston G.A.R. 1991. Regional heterogeneity of L-glutamate and L-aspartate high-affinity uptake systems in the rat CNS. *J Neurochem.* **57**:911-914.

Foster A., Kemp J. 2006. Glutamate- and Gaba- based CNS therapies. *Curr Opin Pharmacol.* **6:**7-17.

Fournier K.M., Gonza´ lez M.I., and Robinson M.B., 2004. Rapid trafficking of the neuronal glutamate transporter, EAAC1: evidence for distinct trafficking pathways differentially regulated by protein kinase C and platelet-derived growth factor. *J. Biol. Chem.* **(33):**34505-13.

Furuta A., Martin L. J., Lin C. L. G., Dykes-Hoberg M and Rothstein J. D. 1997. Cellular and synaptic localization of the neuronal glutamate transporters excitatory amino acid transporter 3 and 4. *Neuroscience*, **81(4):**1031-1042**.**

Ganong, A.H., Lanthorn, T.H., and Cotman, C.W., 1983. Kynurenic Acid inhibits synaptic and other amino acid induced responses in the rat hippocampus and spinal cord. *Brain Research*. **273**:170-174.

Gegelashvili, G., Schousboe, A., 1998. Cellular distribution and kinetic properties of the high-affinity glutamate transporters. *Brain Res. Bull*. **45(3)**: 233-238.

Gelin, B.R., 1995. Current approaches in computer-aided molecular design. In: Reynolds, C.H., Holloway, M.K., Cox, H.K. (Eds.), Computer Aided Molecular Design. American Chemical Society, Washington, DC, pp. 1-13.

Greenfield A, G. C., Dunlop J, McIlvain B, Carrick T, Jow B, Lu Q, Kowal D, Williams J, Butera J. 2005. Synthesis and biological activities of aryl-ether-, biaryl- and fluorene-aspartic acid and diaminopropionic acid analogs as potent inhibitors of the high-affinity glutamate transporter EAAT- 2. *Bioorganic and Medicinal Chemistry Letters*: **15:**4985-4988.

Grewer C., Watzke N., Wiessner M., Raven T., 2000. Glutamate translocation of the neuronal glutamate transporter EAAC1 occurs within milliseconds. P*NAS USA* **97:**9706-9711.

Hanessian, Margarita, Hall and Luo, 1998. 1,2-Asymmetric Inductin in Dianionic Allyolation Reactions of Amino Acid Derivatives-Synthesis of Functionally Useful, Enantiopure Aspartates and Constrained Scaffolds. *Tet. Let*. **39**: 5883-5886.

Haugeto O., Ullensvang, Levy, Chaudhry, Honore, Nielsen, Lehre and Danbolt 1996. Brain Glutamate Transporter Proteins Form Homomultimers. *The Journal of Biological Chemistry* **271(44)**: 27715-27722.

Hediger, M. A.; Romero, M. F.; Peng, J. B.; Rolfs, A.; Takanaga, H.; Bruford, E. A. 2004. *Pflugers Arch. Eur. J. Physiol.* **447**: 465-468.

Himi T, Ikeda M, Yasuhara T, Nishida M, Morita I. 2003. Role of neuronal glutamate transporter in the cysteine uptake and intracellular glutathione levels in cultured cortical neurons. *J Neural Transm.* **110(12):**1337-48.

Huang, Y. H. and D. E. Bergles 2004. Glutamate transporters bring competition to the synapse. *Current Opinion in Neurobiology* **14(3):** 346-352.

Humphrey, Bridges, Hart and Chamberlin 1994. 2,3-pyrrolidinedicarboxylates as neurotransmitter conformer mimics: enantioselective synthesis via chelation-controlled enolate alkylation. *J. Org. Chem.* **59:** 2467-2472.

Hynd, M. R., H. L. Scott and P. R. Dodd 2004. Glutamate-mediated excitotoxicity and neurodegeneration in Alzheimer's disease. *Neurochem Int* **45(5):** 583-95.

Isaacson, J.S., Nicoll, R.A., 1993. The uptake inhibitor L-trans-PDC enhances responses to glutamate but fails to alter kinetics of excitatory synaptic currents in the hippocampus. *J. Neurophysiol.* **70**: 2187-2191.

Jardetzky, O. 1966. Simple Allosteric Model for Membrane Pumps. *Nature* (**211**): 969-970.

Johnson and Ascher 1987. Glycine potentiates the NMDA response in cultured mouse brain neurons. *Nature* **325(6104)**:529-531.

Kam and Nicoll 2007. Excitatory Synaptic Transmission Persists Independent of Glutamate Glutamine Cycle. *J. Neuro.* **27:34:**9192-9200.

Kanai, Y., and Hediger, M.A. 2004. The glutamate/neutral amino acid transporter family SLC1: molecular, physiological and pharmacological aspects. *Eur J Physiol*. **447**:469-479.

Kanai, Y., Hediger, M.A., 1992. Primary structure and functional characterization of a high-affinity glutamate transporter. *Nature* **360**: 467-471.

Kanner, B.I., Borre, L., 2002. The dual function glutamate transporters structure and molecular characterization of the substrate-binding sites. *Bioorg. Med. Chem.* **10**: 3509-3515.

Kanner, B. I.; Kavanaugh, M. P.; Bendahan, A. 2001. Molecular characterization of substrate-binding sites in the glutamate transporter family. *Biochem. Soc. Trans* **29**:707-710.

Kawamura Y, Manita S, Nakamura T, Inoue M, Kudo Y, Miyakawa H. 2004. Glutamate release increases during mossy-CA3 LTP but not during Schaffer-CA1 LTP. *Eur J Neurosci.* **19(6):**1591-600.

Kim C.H., Lee J., Lee J.Y., Roche K.W. 2008. Metabotropic glutamate receptors: phosphorylation and receptor signaling. *J Neurosci Res*. **86(1):**1-10.

Koch, H.P., Kavanaugh, M.P., Esslinger, C.S., Zerangue, N., Humphrey, J.M., Amara S.G., Chamberlin A.R., Bridges, R.J. 1999. Differentiation of Substrate and Nonsubstrate Inhibitors of the High-Affinity, Sodium-Dependent Glutamate Transporters. *Mol. Pharma.* **56:**1095-1104.

Langer, T. and Wolber, G. 2004. Pharmacophore definition and 3D searches. *Drug Discovery Today.* **1(3):** 203-207.

Larkman, A.U., Jack J.J. 1995. Synaptic plasticity: hippocampal LTP. *Curr Opin Neurobiol.* **(3):**324-34.

Leary G.P., Stone E.F., Holley D.C., Kavanaugh M.P., 2007. The glutamate and chloride permeation pathways are colocalized in individual neuronal glutamate transporter subunits. *J Neuro*. **11**:2938-3942.

Lee, G, Huang Y, Washington J.M, Briggs N.W, Zuo Z. 2005. Carbamazepine enhances the activity of glutamate transporter type 3 via phosphatidylinositol, 3-kinase. *Epilepsy Research* **66:**145-153.

Lehre K.P., Levy L.M., Ottersen O.P., Storm-Mathisen J., Danbolt N.C. 1995. Differential expression of two glial glutamate transporters in the rat brain: quantitative and immunocytochemical observations. *J Neurosci.* **15(3:1)**:1835-53.

Lerma, 2005. Kainate receptor physiology. *Current Opnion in Pharmacology*. **6**(1): 89-97.

Levenson J, Weeber E, Selcher JC, Kategaya LS, Sweatt JD, Eskin A. 2002 Long-term potentiation and contextual fear conditioning increase neuronal glutamate uptake. *Nat Neurosci*. **5(2):**155-61.

Loeb, J.E., Cordier, W.S., Harris, M.E., Weitzman, M.D., Hope, T.J., 1999. Enhanced expression of transgenes from adeno-associated virus vectors with the woodchuck hepatitis virus posttranscriptional regulatory elements: implications for gene therapy. *Hum. Gene Ther.* **10**: 2295-22305.

Lüscher C, Xia H, Beattie EC, Carroll RC, von Zastrow M, Malenka RC, Nicoll RA. 1999. Role of AMPA receptor cycling in synaptic transmission and plasticity. *Neuron*. **24(3)**:649-58.

Lüthi A, Chittajallu R, Duprat F, Palmer MJ, Benke TA, Kidd FL, Henley JM, Isaac JT, Collingridge GL. 1999. Hippocampal LTD expression involves a pool of AMPARs regulated by the NSF-GluR2 interaction. *Neuron*. **24(2)**:389-99.

Malva, J. O., A. P. Silva and R. A. Cunha 2003. Presynaptic modulation controlling neuronal excitability and epileptogenesis: role of kainate, adenosine and neuropeptide Y receptors. *Neurochem Res.* **28(10):**1501-1515.

Manabe, T., 2008. Molecular Mechanisms for Memory Formation. *Brain and Nerve.* **60(7):** 705-715.

Maragakis, N.J., Rothstein, J.D., 2004. Glutamate transporters: animal models to neurologic disease. *Neurobiol. Dis.* **15**: 461-473.

Marshall, G.R., 1995. Molecular modeling in drug design. In: Wolff, M.E. (Ed.), Burger's Medicinal Chemistry and Drug discovery. Wiley, New York, pp. 573-659.

Martin, Y.C., 1998. Pharmacophore mapping. In: Martin, Y.C., Willett, A. (Eds.), Designing Bioactive Molecules, Three-Dimensional Techniques and Applications. *American Chemical Society, Washington, DC*. 121-148.

Martens S and McMahon HT, 2008. Mechanisms of membrane fusion: disparate players and common principles. *Nat Rev Mol Cell Biol.* **9(7)**:543-556.

Masek, B.B., 1998. ASEOP, A Molecular Mechanics Program. Zenica Inc., Wilmington, DE.

Mattson, M.P., 2003. Excitotoxic and excitoprotective mechanisms: abundant targets for the prevention and treatment of neurodegenerative disorders. *Neuromol. Med.* **3(2):** 65-94.

Mavencamp T.L., Rhoderick J.F., Bridges R.J., C. Sean Esslinger. 2008 Synthesis and preliminary pharmacological evaluation of novel derivatives of L-β-*threo*-benzylaspartate as inhibitors of the neuronal glutamate transporter EAAT3. *Bio. Org. and Med. Chem.* **16(16)**:7740-8.

Mavencamp, T., J.F Rhoderick, G. Leary, M.P. Kavanaugh, R. Bridges, C.S. Esslinger 2007. Characterization of novel L-β-benzyl aspartate derivatives at the Excitatory Amino Acid Transporters, EAAT1-3. In preparation.

Mayer, M. L. 2005. Glutamate receptor ion channels. *Curr Opin Neurobiol* **15(3):** 282-8.

McCullumsmith, R.E. and Meador-Woodruff, J.H., 2002. Striatal excitatory amino acid transporter transcript expression in schizophrenia, bipolar disorder and major depressive disorder. *Neuropsychopharmacology* **26**: 368-375.

Mendenhall and Smith 1973. 2-Nitrocarbazole. *Organic Syntheses*. **5: 829**

Mennerick, Shen, Xu, Benz, Tanaka, Shimamoto, Isenberg, Krause, Zorumski 1999. Substrate turnover by transporters curtails synaptic glutamate transients. *J. Neuroscience* **19:**9242-51.

Mitchell S.J., Silver R.A. 2000. GABA spillover from single inhibitory axons suppresses low-frequency excitatory transmission at the cerebellar glomerulus. *J Neurosci*. **1;20(23):**8651-8.

Mim C., Balani P., Raven T., Grewer C. 2005. The glutamate transport subtypes EAAT4 & EAATs1-3 transport glutamate with dramatically different kinetics and voltage dependence but share a common uptake mechanism. *J Gen Physiol*. **126(6)**: 571-589.

Nakanishi 1992. Molecular diversity of glutamate receptors and implications for Brain function. *Science* **258**:597-603.

Nakanishi S., Masu M. 1994. Molecular diversity and functions of glutamate receptors. *Annual Review of Biophysics and Biomolecular structure*. **23**:319-348.

Neyman S., Manahan-Vaughan D., 2008. Metabotropic glutamate receptor 1(mgluR1) & 5(mGluR5) regulate late phases of LTP and LTD in the hippocampal CA1 region in vitro. *Eur. J. Neurosci*. **27(6)**: 1345-1352.

Nieoullon, A., B. Canolle, F. Masmejean, B. Guillet, P. Pisano and S. Lortet 2006. The neuronal excitatory amino acid transporter EAAC1/EAAT3: does it represent a major actor at the brain excitatory synapse? *J Neurochem*. **98:** 1007-1018.

O'Kane, R.L., Vina, J.R., Simpson, I., Hawkins, R.A. 2004. Na+ dependent neutral amino acid transporters A, ASC, and N of the blood brain barrier: mechanisms for neutral amino acid removal. *Am. J. Physiol. Endocrinol Metab*. **287**: E622-E629.

Olney, J.W., 2003. Excitotoxicity, apoptosis and neuropsychiatric disorders. *Curr. Opin. Pharmacol.* **3(1)**: 101-109.

Onishi, Y., D. Ogawa, M. Yasuda and A. Baba 2002. Direct conversion of carbonyl compounds into organic halides: indium(III) hydroxide-catalyzed deoxygenative halogenation using chlorodimethylsilane. *J Am Chem Soc* **124(46):** 13690-1.

Oprea, T.I., Ho, C.M., Marshall, G.R., 1995. De novodesign, ligand construction and prediction of affinity. In: Reynolds, C.H., Holloway, M.K., Cox, H.K. (Eds.), Computer Aided Molecular Design. American Chemical Society, Washington, DC, pp. 64-81.

Overstreet LS, Kinney GA, Liu YB, Billups D, Slater NT. 1999. Glutamate transporters contribute to the time course of synaptic transmission in cerebellar granule cells. *J. Neurosci.* **1;19(21):**9663-73

Parr, Boehlein, Dribben, Schuster, Richards, 1996. Mapping the Aspartic Acid Binding Site of Escherichia coli Asparagine Synthetase B Using Substrate Analogs. *J. Med. Chem*. **39**:2367-2378.

Parr, Dribben, Norris, Hinds and Richards, 1999. 1,2-Asymmetric induction in dianionic functionalization reactions of L-aspartic acid diesters. *J. Chem. Soc., Perkin Trans*. **1:**1029-1038.

Paterna, J.C., Moccettii, T., Mura, A., Feldon, J., Bueler, H., 2000. Influence of promoter and WHV post-transcriptional regulatory element on AAV-mediated transgene expression in rat brain. *Gene Ther*. **15**: 1304-1311.

Peghini, Pietro, Janzen, Julia and Stoffel, Wilhelm. 1997. Glutamate transporter EAAC-1-deficient mice develop dicarboxylic aminoaciduria and behavioral abnormalities but no neurodegeneration. *The EMBO Journal* **16**(13): 3822–3832.

Perkins, T.D., Dean, P.M., 1993. An exploration of a novel strategy for superposing several flexible molecules. *J. Computer-Aided Mol. Des*. **7**: 155-172.

Pin, J.P. & Duvoisin, R. 1995. The metabotropic glutamate receptors: structure and functions. *Neuropharmacology* **34**:1-36.

Pungpo, P. and S. Hannongbua (2000). Three-dimensional quantitative structure-activity relationships study on HIV-1 reverse transcriptase inhibitors in the class of dipyridodiazepinone derivatives, using comparative molecular field analysis. *J Mol Graph Model* **18(6)**: 581-90, 601.

Rao, V. L., A. Dogan, K. G. Todd, K. K. Bowen, B. T. Kim, J. D. Rothstein and R. J. Dempsey 2001a. Antisense knockdown of the glial glutamate transporter GLT-1, but not the neuronal glutamate transporter EAAC1, exacerbates transient focal cerebral ischemia-induced neuronal damage in rat brain. *J Neurosci* **21(6):** 1876-83.

Rao, V. L., K. K. Bowen and R. J. Dempsey 2001b. Transient focal cerebral ischemia down-regulates glutamate transporters GLT-1 and EAAC1 expression in rat brain. *Neurochem Res.* **26(5):** 497-502.

Rao, S. D. and J. H. Weiss 2004. Excitotoxic and oxidative cross-talk between motor neurons and glia in ALS pathogenesis. *Trends Neurosci.* **27(1):** 17-23.

Rauen T., Jeserich G., Danbolt N.C., Kanner B.I. 1992. Comparative analysis of sodium dependent L-glutamate transport of synaptosomal and astroglial membrane vesicles from mouse cortes. *FEBS Lett.* **312**:15-20.

Roberts, P.J., Watkins, J.C. 1975. Structural requirements for the inhibition for L-glutamate uptake by glia and nerve endings. *Brain Res*. **85**:120-125.

Robinson, M.B., Sinor, J.D., Dowd, L.A., Kerwin, J.F., 1993. Subtypes of sodium-dependent high -affinity L-[^{3}H]glutamate transport activity: pharmacologic specificity and regulation by sodium and potassium. *J. Neurochem.* **60:**167-179.

Rodríguez-Moreno, A., Herreras, O. and Lerma, J., 1997. Kainate receptors presynaptically downregulate GABAergic inhibition in the rat hippocampus. *Neuron* **19**:893–901.

Rossi, D. J., T. Oshima and D. Attwell 2000. Glutamate release in severe brain ischaemia is mainly by reversed uptake. *Nature* **403(6767):** 316-21.

Rothstein, J.D., Jin, L., Dykes-Hoberg, M., Kuncl, R.W., 1993. Chronic inhibition of glutamate uptake produces a model of slow neurotoxicity. *Proc. Natl. Acad. Sci. USA* **90:** 6591-6595.

Rothstein JD, Martin L, Levey AI, Dykes-Hoberg M, Jin L, Wu D, Nash N, Kuncl RW 1994. Localization of Neuronal and Glial Glutamate Transporters. *Neuron* **3:**713-25**.**

Sakaguchi K., Yamamoto M., Kawamoto T., Yamada T., Shinada T., Shimamoto K., Ohfune Y. 2004. Synthesis of optically active β-alkyl aspartate via [3,3] sigmatropic rearrangementofα-acyloxytrialkylsilane.*Tet.Let.* **45(30)**:5869-5872.

Sarantis, M., Ballerini, L., Miller, B., Silver, R.A., Edwards, M., Attwell, D., 1993. Glutamate uptake from the synaptic cleft does not shape the decay of the non-NMDA component of the synaptic current. *Neuron*. **11**: 541-549.

Scanziani M., Salin P.A., Vogt K.E., Malenka R.C., Nicoll R.A. 1997. Use-dependent increases in glutamate concentration activate presynaptic metabotropic glutamate receptors. *Nature*. **13;385(6617):**630-4

Schmitt, A., Zink, M., Petroianu, G., May, B., Braus, D.F., Henn, F.A. 2003. Decreased gene expression of glial and neuronal glutamate transporters after chronic antipsychotic treatment in rat brain. *Neuro. Let.* **347:** 81-84.

Seal, R.P., Amara, S.G., 1999. Excitatory amino acid transporters: a family in flux. *Annu. Rev. Pharmacol. Toxicol.* **39**: 431-456.

Selkirk J.V., Nottebaum L.M., Vana A.M., Verge G.M., Mackay K.B., Stiefel T.H., Naeve G.S., Pomeroy J.E., Petroski R.E., Moyer J., Dunlop J., Foster A.C. 2005. Role of the GLT-1 subtype of glutamate transporter in glutamate homeostasis: the GLT-1-preferring inhibitor WAY-855 produces marginal neurotoxicity in the rat hippocampus. *Eur J Neurosci.* **21(12):**3217-28.

Sepkuty, Cohen, Eccles, Rafiq, Behar, Ganel, Coulter, Rothstein 2002. A Neuronal Glutamate Transporter Contributes to Neurotransmitter GABA Synthesis and Epilepsy. *The Journal of Neuroscience* . **22(15):**6372-6379.

Shashidharan, P., G. W. Huntley, J. M. Murray, A. Buku, T. Moran, M. J. Walsh, J. H. Morrison and A. Plaitakis1997. Immunohistochemical localization of the neuron-specific glutamate transporter EAAC1 (EAAT3) in rat brain and spinal cord revealed by a novel monoclonal antibody. *Brain Res*. **773(1-2):** 139-48.

Shigeri, Y., Seal, R.P., Khimamoto K. 2004. Molecular pharmacology of glutamate transporters, EAATs and VGLUTs. *Br. Research Reviews.* **45**:250-265.

Shimamoto K, Lebrun B, Yasuda-Kamatani Y, Sakaitani M, Shigeri Y, Yumoto N, and Nakajima T 1998. DL-threo-β-Benzyloxyaspartate, a potent blocker of excitatory amino acid transporters. *Mol Pharmacol.* **53**:195-201.

Shimamoto, K., Y. Shigeri, Y. Yasuda-Kamatani, B. Lebrun, N. Yumoto and T. Nakajima 2000. Syntheses of optically pure beta-hydroxyaspartate derivatives as glutamate transporter blockers. *Bioorg Med Chem Lett* **10(21):** 2407-10.

Shimamoto, K., R. Sakai, K. Takaoka, N. Yumoto, T. Nakajima, S. G. Amara and Y. Shigeri 2004. Characterization of novel L-threo-beta-benzyloxyaspartate derivatives, potent blockers of the glutamate transporters. *Mol Pharmacol.* **65(4):** 1008-15.

Slotboom, D. J., W. N. Konings and J. S. Lolkema 1999. Structural features of the glutamate transporter family. *Microbiol Mol Biol Rev* **63(2):** 293-307.

Smart, B.E., 2001. Fluorine substituent effects (on bioactivity). J. of Fluorine Chemistry **109(1)**: 3-11.

Stensbol, T.B., Uhlmann, P., Morel, S., Eriksen, B.L., Felding, J., Kromann, H., Hermit, M.B., Greenwood, J.R., Brauner-Osborne, H., Madsen, U., Junager, F., Krogsgaard-Larsen, P., Begtrup, M., Vedso, P., 2002. Novel 1-hydroxyazole bioisosteres of glutamic acid. Synthesis, protolytic properties, and pharmacology. *J. Med. Chem.* **45(1)**: 19-31.

Stone, I.M., Lurie, D.I., Kelley, M.W., Poulsen, D.J., 2005. Adeno-associated virus mediated gene transfer to nair cells and support cells of the murine cochlea. *Mol. Ther.* **11(6)**: 843-848.

Storck, T., Schulte, S., Hofmann, K., Stoffel, W., 1992. Structure, expression, and functional analysis of a Na(+)-dependent glutamate/aspartate transporter from rat brain. *Proc. Natl. Acad. Sci. USA*. **89**: 10955-10959.

Swanson, C. J., M. Bures, M. P. Johnson, A. M. Linden, J. A. Monn and D. D. Schoepp 2005. Metabotropic glutamate receptors as novel targets for anxiety and stress disorders. *Nat Rev Drug Discov* **4(2):** 131-44.

Swanson 2006. Neuronal glutathione deficiency and age dependent neurodegeneration in EAAC1 deficient mouse. *Nature Neuroscience*. **9(1)**:119-126

Takamori, S. 2006. VGLUTs: 'exciting' times for glutamatergic research? *Neuro. Research.* **55(4):**343-51

Takayasu Y., Iino M., Kakegawa W., Maeno H., Watase K., Wada K., Yanagihara D., Miyazaki T., Komine O., Watanabe M., Tanaka K., Ozawa S.. 2005. Differential roles of glial and neuronal glutamate transporters in Purkinje cell synapses. *J Neurosci.* **25(38):**8788-93.

Tanaka K, Watase K, Manabe T, Yamada K, Watanabe M, Takahashi K, Iwama H, Nishikawa T, Ichihara N, Kikuchi T, Okuyama S, Kawashima N, Hori S, Takimoto M, Wada K. 1997. Epilepsy and exacerbation of brain injury in mice lacking the glutamate transporter GLT-1. *Science*. **276(5319):**1699-702.

Teichman, S. and Kanner, B.I. 2007. Aspartate-444 is essential for productive substrate interactions in a neuronal glutamate transporter. *J Gen Physiol.* **129(6)**:527–539.

Torres-Salazar D. and Fahlke C., 2007. Neuronal Glutamate Transporters Vary in Substrate Transport Rate but Not in Unitary Anion Channel Conductance. *J. Of Biological Chemistry*. **282(48):**34719-34726.

Vandenberg RJ, Mitrovic AD, Chebib M, Balcar VJ, Johnston GA. 1997. Contrasting modes of action of methylglutamate derivatives on the excitatory amino acid transporters, EAAT1 and EAAT2. *Mol Pharmacol*. **51(5)**:809-15.

Vandenberg, R.J., 1998. Molecular pharmacology and physiology of glutamate transporters in the central nervous system. *Clin. Exp. Pharmacol. Physiol*. **25**: 393-400.

Vogt K.E., and Nicoll, R.A. 1998. Glutamate and γ-aminobutyric acid mediate a heterosynaptic depression at mossy fiber synapse in the hippocampus. *Proc. Natl. Acad. Sci.* **96:** 1118-1122.

Wadiche, J.I., Jahr, C.E., 2001. Multivesicular release at climbing fiber-Purkinje cell synapses. *Neuron*. **32(2)**: 301-313.

Wadiche J.I., Amara S.G., and Kavanaugh M.P. 1995. Ion fluxes associated with excitatory amino acid transport. *Neuron* **15**:721-728.

Wadiche, J. I. and M. P. Kavanaugh (1998). Macroscopic and microscopic properties of a cloned glutamate transporter/chloride channel. *J Neurosci.* **18(19):** 7650-61.

Watase K, Hashimoto K, Kano M, Yamada K, Watanabe M, Inoue Y, Okuyama S, Sakagawa T, Ogawa S, Kawashima N, Hori S, Takimoto M, Wada K, Tanaka K. 1998. Motor discoordination and increased susceptibility to cerebellar injury in GLAST mutant mice. *Eur J Neurosci.* **10(3)**:976-88.

Watzke, N. and C. Grewer (2001). The anion conductance of the glutamate transporter EAAC1 depends on the direction of glutamate transport. *FEBS Lett.* **503(2-3):** 121-5.

Wersinger E., Schwab Y., Sahel J.A., Rendon A., Pow D.V., Picaud S., Rous M.J. 2006. *J. Physiol.* **577**: 221-234.

Willis C.L., Humphrey J.M., Koch H.P., Hart J.A., Blakely T., Ralston L., Baker C.A., Shim S., Kadri M., Chamberlin A.R., Bridges R.J. 1996. L-trans-2,3-pyrrolidine dicarboxylate: characterization of a novel excitotoxin. *Neuropharmacology*. **35(5)**:531-9.

Won SJ, Kim and Gwag. 2002. Cellular and Molecular Pathways of Ischemic Neuronal Death. *Journal of Biochem and Molec Biol.* **35(1):** 67-86.

Yernool, D., Boudker, O., Jin, Y. and Gouaux E. 2004. Structure of a glutamate transporter homologue from Pyrococcus horikoshii. *Nature* **431**:811-818.

Zerangue N, Kavanaugh MP, 1996a. Flux coupling in a neuronal glutamate transporter. *Nature* **383:** 634-7.

Zerangue, N., and Kavanaugh, MP 1996b. Interaction of L-cysteine with a human excitatory amino acid transporter. *J Physiol*. **493:** 419-423.

Zerangue, N., and Kavanaugh, MP 1996c. ASCT2 is a neutral amino acid exchanger with chloride channel activity. *J. Biol. Chem.* **271**: 27991-27994.

Zervas, L.; Theodorpoulos, D. *J.* 1956. N-Tritylamino Acids and Peptides. A New Method of Peptide Synthesis. *J. Am. Chem. Soc.*, **78**: 1359.

Appendix A:

History of 1,2-asymmetric induction

The synthesis of unnatural amino acids has assumed an important role in a variety of pharmacological systems. This has created a demand for stereo-controlled methodologies based on amino acids. 1,2-asymmetric induction in the alkylation of aspartic acid ester enolates is one area that has received considerable attention.

In 1990 Dunn et al., studied the regioselective β-benzylation of N-phenylfluorenyl 2,3 diester (α-tert-butyl, β-methyl) at the β-carbon with KHMDS and benzyl bromide at -78°C. This reaction yielded 2S,3S : 2S,3R (S,S:S,R) in a 2:1 ratio. The ratio of diastereomers can be affected by a number of factors. One way to increase the diasteromeric yield is to increase the reactivity of the electrophile. Consistent with this observation the ratio of S,S:S,R increased to 7:1 when the electrophile was switched from benzyl bromide to benzyl iodide. Dener et al., 1993, also used the N-phenylfluorenyl protecting group (2,3 diester-α-methyl, β-methyl) aspartate, alkylation at the β-carbon with ethyl triflate and got a 2:1 SS:SR ratio. After optimizing the mole percents of base and ethyl triflate the ratio increased to 18:1, displaying the importance of the stoichiometry of the base and electrophile to substrate (Dener et al., 1993).

β-addition of N-phenylfluorenyl 2,3 diester (α-methyl, β-methyl) was used for hydroxylation using MoOPH with KHMDS at -78 - -65 °C and got SS:SR in a

3:1 ratio. LHMDS reversed this ratio to 1:8 and adding DMPU and HMPU reversed this to 8:1 and 11:1 respectively. (Fernandez-Megia, 1994)

Altering the N-protecting group to replace both amine hydrogen atoms by adding an N-benzyl group to the amine in addition to the N-phenylfluorenyl group increased the stereoselectivity to 30:1 at -23 ℃. Complications arose with this scheme as the methyl ester could not be hydrolyzed without epimerization at C-3 (Dunn *et al.*, 1990).

In order to correct this the β-methyl ester was replaced with a β-benzyl ester and diasteromeric ratios at -23℃ decreased to 12:1 and 25:1 using benzyl bromide and benzyl iodide respectively. In contrast alkylation of dibenzyl amine gave almost no diastereoselectivity (Dunn *et al.*, 1990).

Substituting methyl for t-butyl as the α-ester protecting group dramatically affected the diasteromeric outcome. N-phenylfluorenyl 2,3 diester (α-methyl, β-benzyl) aspartate gave ratios of 1:1.5 S,S to S,R at -23℃ with either benzyl bromide or benzyl iodide, interestingly the preference for S,R was reversed when the temperature was decreased to -78℃ to 2.5:1 (Denner et al., 1993).

A paper by Humphrey *et al.*, 1994 describes the diastereoselective β-alkylation of the D-isomer, N-benzyl phenylfluorenyl, 2-3 diester (α-methyl, β-methyl) aspartate. Enolate formation with KHMDS at -23 ℃ favored formation of the R,R diastereomer in excess of 50:1. Interestingly, Humphrey also observed that switching the base to LiHMDS reverses this selectivity to 1:50 (R,R:R,S).

The N-protecting group, carbobenzyloxy with LiHMDS as a base at -78℃ gave diasteromeric ratios of 3:1, S,S:S,R (Parr et. al. 1996). Interestingly with

N-Pro. Group	Base	E+	Ester protecting Groups	SR:SS ratio	Temp	Paper
PhF	KHMDS	BnBr	α -t Bu β-CH_3	1:2	-78	Dunn, 1990
PhF	KHMDS	BnI	α -t Bu β-CH_3	1:7	-78	Dunn, 1990
BnPhF	KHMDS (2)	BnBr (2)	α -t Bu β-CH_3	1:30	-20	Dunn, 1990
BnPhF	KHMDS	BnBr	α -t Bu β-Bn	1:12	-23	Dunn, 1990
BnPhF	KHMDS	BnI	α -t Bu β-Bn	1:25	-23	Dunn, 1990
BnPhF	KHMDS	BnBr/bnI	α - Bn β-Bn	1:1.6	-23	Dunn, 1990
BnPhF	KHMDS	BnBr/BnI	α - CH_3 β-Bn	1.5:1	-23	Dunn, 1990
BnPhF	KHMDS	BnI	α - CH_3 β-Bn	1:2.5	-78	Dunn, 1990
BnPhF	KHMDS	BnBr	α - CH_3 β-CH3	1:50	-23	Humphrey, 1994
BnPhF	LiHMDS	BnBr	α - CH_3 β-CH3	50:1	-23 -78	Humphrey, 1994
CBZ	LiHMDS +DMPU\HMPA	Cycloheyn yl Bromide	α - CH_3 β-CH3	75:25	-78	Hanessian, 1998
CBZ	LiHMDS +DMPU \HMPA	Cycloheyn yl Bromide	α–TMSE β-CH_3	99:1	-78	Hanessian 1998
CBZ	LiHMDS	MeI	α -t Bu β-CH_3	1:3	-78	Parr, 1996
PhF	KHMDS	Ethyl triflate	α - CH_3 β- CH_3	1:18	-75-0	Dener 1992
PhF	KHMSD	MoOPH	α - CH_3 β- CH_3	1:3	-78 – -65	Fernandez-Megia, 1994
PhF	LiHMDS	MoOPH	α - CH_3 β- CH_3	8:1	-78 – -65	Fernandez-Megia, 1994
PhF	LDA	MoOPH	α - CH_3 β- CH_3	1:2	-78 – -65	Fernandez-Megia, 1994
PhF	LiHMDS DMPU	MoOPH	α - CH_3 β-CH3	1:8	-78 – -65	Fernandez-Megia, 1994
PhF	N-BuLi/LHMDS	MoOPH	α - CH_3 β-CH3	20:1	-78 – -65	Fernandez-Megia, 1994
PhF	N-BuLi/LiHMDS +HMPA	MoOPH	α - CH_3 β-CH3	1:2	-78 – -65	Fernandez-Megia, 1994

Table 1. Diasteromeric control of 1,2 asymmetric induction as reported in the literature.

DMPU or HMPA as a co-solvent/additive S,R formation was favored over S,S, 75:25 to 99:1, S,R;S,S (Hanessian, 1998).

Attempts to improve these results were also performed using various solvents (ethyl ether, toluene) as well as additives (HMPA or DMPU), which modify the enolate aggregation state. Another important factor is the temperature, maintaining the reaction at a temperature below -50°C has been shown to improve 1,2-asymmetric induction. An interesting issue stemming from reaction temperature is the way in which the reaction is quenched. Parr *et al.*, 1999, found that a mixture of diasteromeric products resulted from quenching their 1,2 asymmetric induction reaction by pouring an aqueous acid solution into the reaction at a low temperature followed by warming. Conversely, If they poured the cold reaction into an aqueous acid solution they obtained a single diastereomer.

Appendix B:

Synthetic Schemes of β-substituted Aspartates:

This appendix describes the synthesis used to prepare the β-substituted analogues. In particular the details not covered in chapter two of this dissertation are covered including failed schemes, abandoned synthetic routes as well as the reasoning behind the routes chosen.

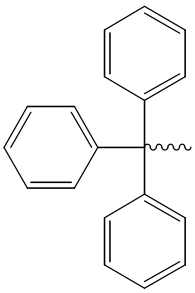

Figure 2. Triphenylmethyl protecting group.

Protecting groups:

Trityl:

The N-triphenylmethyl protecting group was initially chosen for the ease of which large amounts of starting material can be prepared as well as for its large size which was hypothesized to protect from alpha racemization (for preparation see chapter 2 methods). This protection from alpha racemization is observed at temperatures below 0℃, as reactions carried out at temperatures exceeding 0℃ yield racemic products.

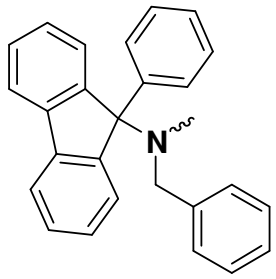

Figure 3. Benzyl phenyl fluorenyl protecting group

Benzyl phenyl fluorenyl:

For preparation of N-benzyl phenyl fluorenyl dimethyl ester aspartate see Humphrey *et al*., 1994.

Carbobenzyloxy:

The CBZ-Carbobenzyloxy protecting group was also used. N-CBZ-L-aspartate dimethyl ester was prepared by dissolving aspartate in 3M sodium hydroxide, adding toluene then 1.5 equivalents benzyl chloroformate drop wise. The reaction was stirred for 24 hours at a pH greater than 10, the pH was adjusted with NaOH when necessary. The reaction was then acidified with 6N HCl to a pH of about 1, extracted into ethyl acetate, washed with brine, dried with magnesium sulfoxide, filtered and rotovaped. Esterification is achieved by adding 1.4 equivalents thionyl chloride drop wise to the starting material in methanol and allowing the reaction to proceed for 48 hours. The product does not crystallize so concentration by rotary evaporation followed by chasing with methanol, methylene chloride, toluene and hexane is sufficient to remove excess solvents and water.

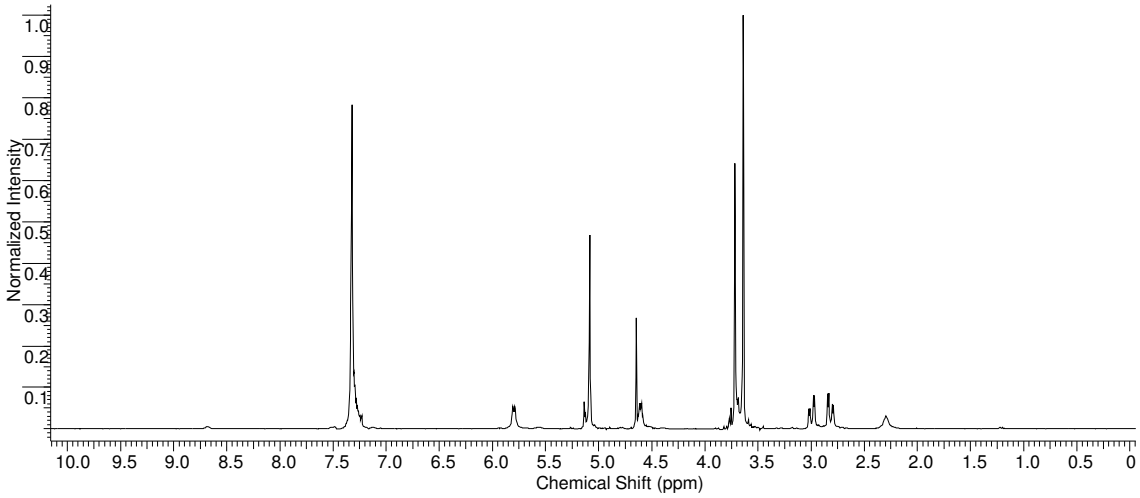

Figure 4. Carbobenzyloxy protecting group.

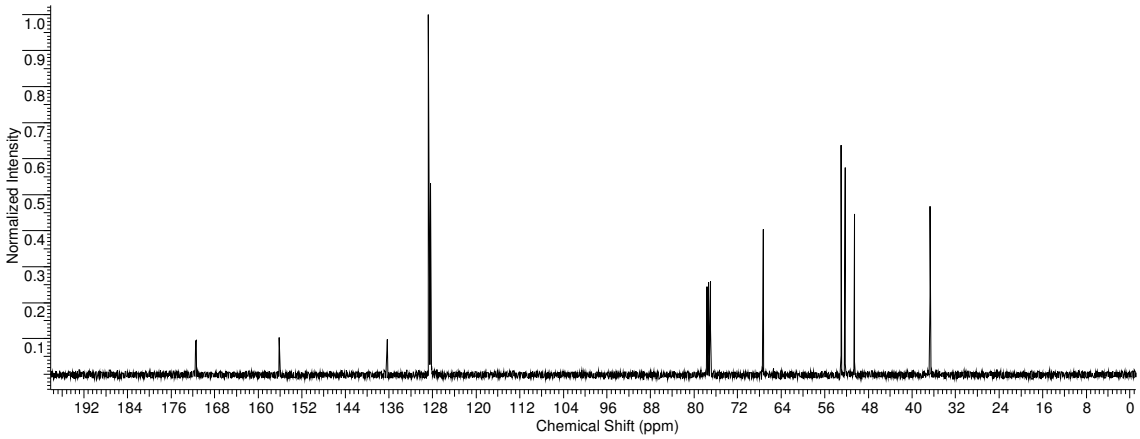

CBZ sm: ^{1}H NMR (400 MHz, $CDCl_3$) δ: 7.38-7.28 (m, 5H), 5.81-5.78 (m, 1H), 4.65-4.60 (m, 1H), 3.72 (s, 3H), 3.64 (s, 3H), 3.02-2.97 (m, 1H), 2.84-2.80 (m, 1H). ^{13}C (100 MHz $CDCl_3$) δ: 171.17, 171.05, 155.82, 136.00, 128.42, 128.10, 128.01, 67.00, 52.71, 51.95, 50.22, 36.34.

Alkylation of N-CBZ-dimethyl ester with 3-cloro benzyl bromide, LiHMDS + DMPU :

In an oven dried round bottom flask with stir bar 3.6 equivalents of LiHMDS and 3ml DMPU were cooled to -55℃ under argon. .513g N-CBZ-dimethyl ester was added in 12 ml THF slowly by a syringe. About 2 hours later 3 equivalents of 3-cloro-benzyl bromide was slowly added and the reaction proceeded for 21 hours when it was quenched with 10 ml of 10% HCl, the reaction rose to room temperature and was extracted into ethyl acetate and concentrated for separation on a silica column (.2mg, 27%)

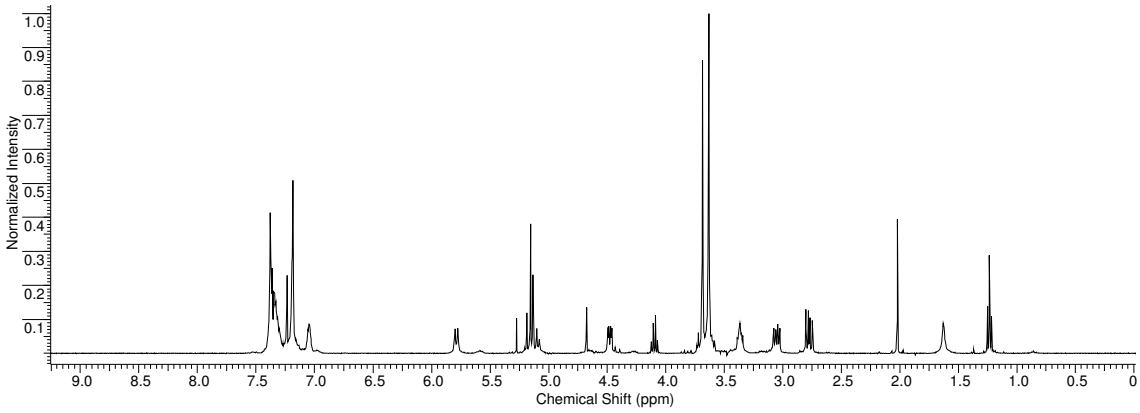

^{1}H NMR (400 MHz, $CDCl_3$) δ: 7.38-7.16 (m, 9H), 5.19-5.08 (m, 2H), 4.49-4.46 (m, 1H), 3.69 (s, 3H), 3.63 (s, 3H), 3.39-3.34 (m, 1H), 3.08-3.03 (m, 1H), 2.80-2.75 (m, 1H).

Deprotection of N-CBZ-dimethyl ester β-3-cloro-benzyl-aspartate

Hydrogenation of starting material (.2g) in ethanol with acetic acid (.25ml) and Palladium on Carbon (.15g) under 50 psi for 25 hours did not remove the CBZ protecting group. The NMR was messy and hard to define.

Alkylation of N-CBZ-dimethyl ester with 4-bromo-benzyl bromide

The alkylation was carried out in the presence of DMPU, 2.1 equivalents of LiHMDS and 3 equivalents of 4-benzyl bromide in the manner described for alkylation of N-CBZ-dimethyl ester with 3-cloro-benzyl bromide (58%)

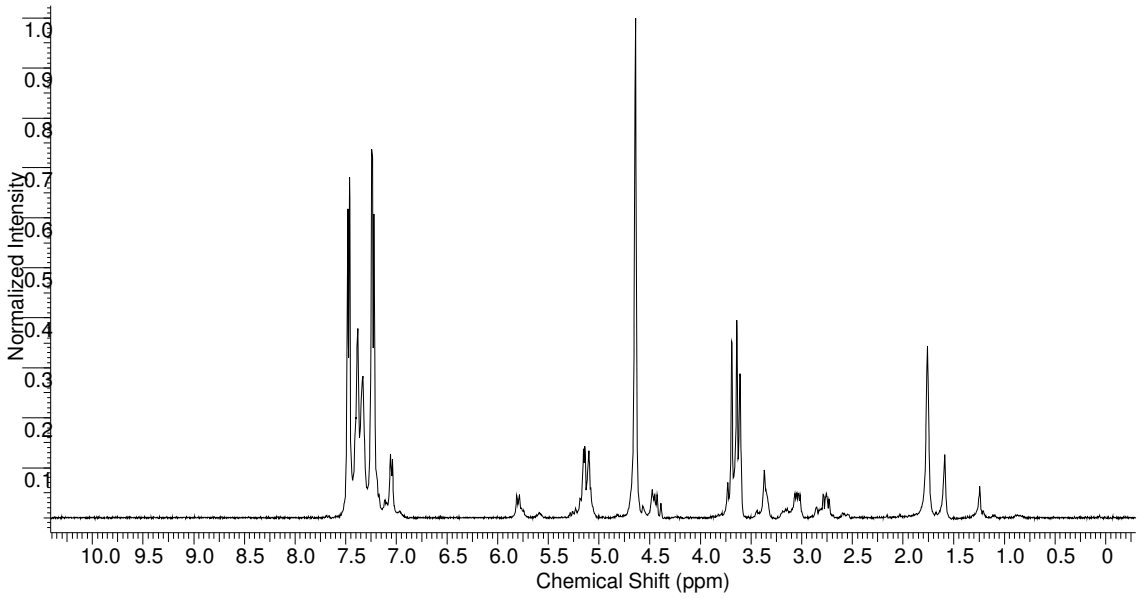

Deprotection of N-CBZ-dimethyl ester β-4-bromo-benzyl-aspartate

Deprotection under the conditions given for N-CBZ 3-cloro-benyl aspartate did not go to completion. The resultant material from the hydrogenation was taken on and deprotected with 6N HCl for 24 hours. The water layer was extracted with ethyl acetate and product was precipitated out of water. NMR was too messy to assign peaks to.

Benzyl Phenyl fluorenyl: N-BPF-dimethyl ester-3-F-Benzyl-Aspartate

In a dry round bottom flask, .5g of N-BPfl-dimethyl aspartate was dissolved in 5 ml THF. 2M KHMDS was added drop wise at -23℃. 20 minutes later 3-floro-benzyl bromide was added drop wise and the reaction proceeded for 53 hours at which time it was quenched with 8ml saturated NH_4Cl. The product was extracted into ether. Organic layers were combined washed with brine and subsequently concentrated. The product was isolated on a silica column to give a 16% yield.

Deprotection of N-BPF-dimethyl ester-3-F-Benzyl-Aspartate

To N-BPF-dimethyl ester-3-F-Benzyl-Aspartate (.1g, .166mm) in methylene chloride (2ml) and ethyl acetate (2ml) concentrated HCl and methanol (15ml) were added with 10% palladium on carbon (.1g). Hydrogenation under 52 psi for 24 hours followed by filter through celite and heated to 65℃ for 24 hours followed by washing with ethyl acetate and concentration of the aqueous layer yielded an absolute mess, yellow gooey layer that was incomprehensible by NMR.

Deprotection of N-trityl-L-β-substituted aspartate dimethyl ester

The most commonly used deprotection scheme was to heat the alkylated intermediate in 6N HCl for 24 hours at about 80℃. The aqueous layer was then washed with ether to remove trityl chloride and concentrated to give the chloride salt of the product. Next an anion exchange resin was used in the ratio of 1:10 product:resin, weight:weight and eluted with varying fractions of acetic acid from .1N to 5N with product coming off from 1N to 5N. This method resulted in yields from 8% to 73%.

Another deprotection scheme was to de-tritylate with 1N HCl in ethanol, heat 1-2 minutes in a water bath, evaporate ethanol and triturate with ether. With N-trityl diester p-nitro benzyl aspartate to diester p-nitro benzyl aspartate the yield was 37% with this method. Next the alkylated product can be added to a 2N solution of LiOH or KOH in ethanol, stirring at room temperature for 30

minutes. As the product is de-methylated it crashes out of solution. The problem we encountered with this method is that both methyl groups are often not saponified and the yields are very low, less than10%.

The easiest deprotection scheme is to deprotect in 6N acid at 80℃ and concentrate down the sample, rotovap off excess HCl by 2-3 water rinses and dried on the high vac. Next the product is precipitated out of ethyl acetate (sample must be very dry and free of excess Cl^-) followed by precipitation from water. With this method yields are consistently higher, 75%, though some product is lost due to incomplete removal of methyl peaks even at reaction times greater than 30 hours.

Aromatic ring transformations

3-Nitro Benzyl Bromide: aldehyde to bromide

3nitro benzaldehyde was transformed to 3 nitro benzyl alcohol using 1 equivalent sodium borohydride in ethanol. The reaction was stirred at room temperature until starting material spot disappeared by TLC (30/70 Ethyl acetate/Hexanes). The reaction was quenched by adding ammonium chloride (saturated), extracted with ethyl acetate and dried over magnesium sulfate. 3-nitro benzyl alcohol was transformed to 3-nitro benzyl bromide under argon by adding dry ether and drop wise addition of 1 equivalent phosphorous tribromide (PBr_3). The reaction was monitored by TLC (50/50 ethyl acetate/hexane). Cold water was added drop wise to quench the reaction. The product was extracted into ether and washed with brine then filtered through a silica plug.

3-methoxy Benzyl Bromide

3 methoxy benzyl alcohol was transformed to 3 methoxy benzyl bromide using the same procedure as for 3 nitro benzyl alcohol.

2-benzyl fluorenyl

Attempts to synthesize 2-benzyl fluorenyl from 2-fluorenyl aldehyde started with the successful transformation of 2-fluorenyl aldehyde to 2 fluorenyl alcohol. This was acheived by a standard reduction in ethanol and addition of sodium borohydride and quenching with water. The reaction was worked up by extracting product into ethyl acetate layer, yield 90%.

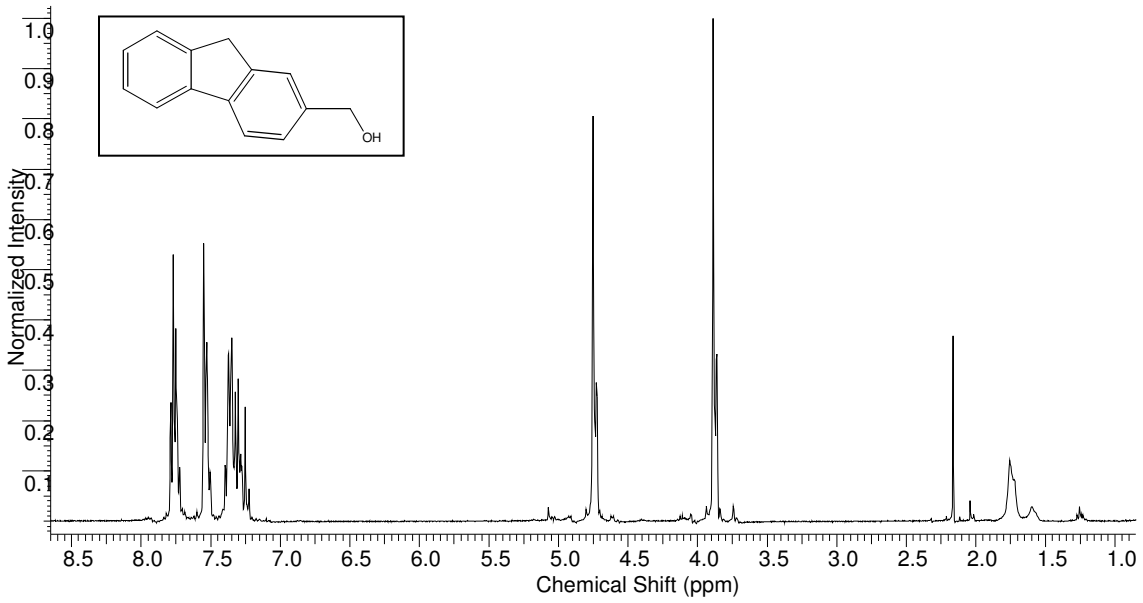

^{1}H NMR (400 MHz, CDCl3) δ: 7.32-7.25 (m, 1H), 7.79-7.73 (m, 2H), 7.55-7.50 (m, 2H), 7.40-7.22 (m, 3H), 4.74 (m, 2H), 3.86 (m, 2H), 1.74 (m, 1H).

Attempts to convert the alcohol moiety to bromine were achieved using phosphorous tribromine in methylene chloride at -10℃ under argon. The reaction appeared to proceed as indicated by the disappearance of the alcohol proton at 1.74.

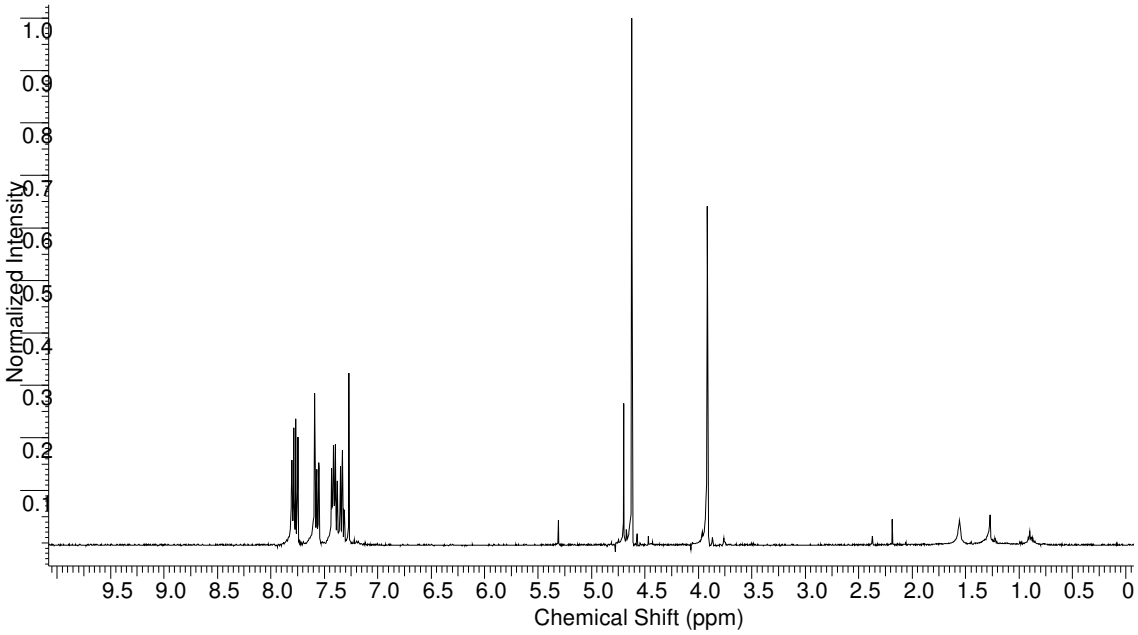

^{1}H NMR (400 MHz, CDCl3) δ: 7.80-7.75 (m, 2H), 7.59-7.55 (m, 2H), 7.43-7.31 (m, 3H), 4.62 (s, 2H), 3.92 (s, 2H).

Alkylations of N-Trityl dimethyl ester aspartate with LiHMDS base

Alkylation with 3-methoxy benzyl bromide

Alkylation with 3-methoxy benzyl bromide proved to be extremely difficult. The reaction was allowed to proceed for 2 hours with 2 and 1.5 equivalents of base and electophile respectively. There appeared to be a product spot above the starting material on TLC using 30/70 ethyl acetate/hexanes, but upon work up this spot could not be positively identified as product.

3-methoxy benzyl bromide was converted to 3-methoxy benzyl iodide by the addition of 10 equivalents of sodium iodide to 3-methoxy benzyl iodide in acetone. The reaction was allowed to reach room temperature and stir overnight. This method showed very light staining under the starting material spot via TLC that may have been product. After deprotection and ion exchange no product was isolated.

Another method used to attempt alkylation was to tosylate the three methoxy benzyl alcohol using tosyl chloride. This method was also unsuccessful though it could have been due to the age of tosyl chloride and the storage conditions; outside of a desiccator.

In addition to tosylate the mesolate was made from 3-methoxy benzyl alcohol and chloromesolate. This was performed in a dry round bottom flask in 1M dry methylene chloride, 2 equivalents pyridine were added and 1.5 equivalents of chloromesolate. The reaction was diluted with ether, washed with 1N HCL, dried with magnesium sulfate and roto-vaped with ether. When alkylation was attempted no appreciable product was discerned.

Alkylation with cinnamyl chloride

Alkylation with cinnamyl chloride began by the conversion of the chloride to iodide via sodium iodide and acetone. The alkylation reaction did not proceed below 0℃, and above it yielded racemic product.

Alkylation with phenyl ethyl bromide

The alkylation ran for 5 hours at 0℃ with 3 equivalents base and 2.5 equivalents electrophile gave no product. The starting material was converted from phenyl ethyl bromide to phenyl ethyl iodide employing the same reaction conditions as described for 3-methoxy benzyl bromide, this yielded a faint spot above starting material by TLC that was not taken on.

The mesolate was then made from benzyl ethyl alcohol and chloro-mesolate. This was performed in a dry round bottom flask in 1M dry methylene chloride. 2 equivalents of pryidine were added and 1.5 equivalents of chloromesolate. The reaction was diluted with ether, washed with 1N HCL, dried with magnesium sulfate and rotovaped with ether. When alkylation was attempted no appreciable product was discerned.

Finally triflouoro methyl sulfonic acid was reacted with phenethylalcohol to form trifluoromethyl sulfonic leaving group. This was achieved by adding a solution of trifluoromethylsulfonic (1.4eq) acid in dry chloroform (3 eq) to a solution of pyridine and phenethylalcohol (.8eq) on ice under argon. The transfer was difficult due to using a needle and getting it jammed, perhaps from moisture, I may have only transferred about 70% of the solution. A cannula may have been easier. A precipitate was formed upon addition and the clear supernant was concentrated with argon and taken up in dry THF for the next (alkylation) step. The alkylation was carried out with 3.5 equivalents of LiHMDS and 2.5 equivalents of phenethyltrifluoromethylsulfonic acid. The phenethyltrifluoromethylsulfonic acid was difficult to transfer due to extreme

insolubility in THF, sonication did not solubilize it so I had to crush it up and transfer it to the reaction via a needle. Reaction proceeded for 4 hours. By TLC, reaction appears to have gone but upon separation by silica column no product could be discerned.

2-Nitro Benzyl Bromide

Reaction carried out with 2.5 equivalents of base and 3.5 equivalents of 2-nitro Benzyl bromide. The reaction went for 4.5 hours at what time no alkylation appeared to occur.

Propargyl Bromide

Reaction carried out with 3 equivalents LiHMDS and 2.5 equivalents of propargyl bromide. At 4.5 hours at 0℃ no reaction could be observed by TLC. Propargly bromide was old and may have been wet explaining the lack of product.

2-benzyl fluorenyl

Unfortunately attempts to alkylate N-trityl-diester aspartate with 2-benzyl fluorenyl were unsuccessful.

Additives to Alkylation

Manganese bromide (MnBr2) 1.4 equivalents added to starting material in THF, 3 equivalents LiHMDS and 2.5 equivalents BnBr. Reaction proceeded

about 60% in 5 hours at -30℃. Unfortunately at this time additives were only used with the aim of increasing yields not for effects on diasteromeric control.

DMPU

DMPU was added to alkylations with CBZ (Appendix A; Hanessian, 1998; Fernandez-Megia, 1994) and trityl. Alkylation of N-trityl-dimethyl ester aspartate with 3-benzyl bromide gave yields of 74% post silica column in a 1:3 ratio of *threo:erythro* (Mavencamp *et al.*, 2008). Though DMPU does affect diasteromeric control and often increases ratios, it is very difficult to remove, causing problems during deprotection and requiring an ion exchange column for a clean final sample.

Diasteromeric Enrichment Procedure

Diasteromeric enrichment can be achieved by heating the mixture in a small amount of water (compound will not be dissolved) much as you would approach a crystallization procedure. Heat for about 20 minutes until no more material dissolves. The material is then hot-filtered and dried. This gives an approximate 11:1 enrichment of *threo:erythro* or S,S:S,R even when starting with a mixture of mostly *erythro*.

2,3 diester N-trityl asparatate conversion to 2, ester 3 amino, N-trityl aspartate

Conversion from the distal carboxyl group to the amine was achieved by heating the starting material (.130g) in 3.3 ml methanol and 1 ml concentrated NH4OH to about 80℃ in a pressure tube for 3 days. Product is extracted into ethyl acetate and concentrated then taken up in 6N HCl for deprotection.

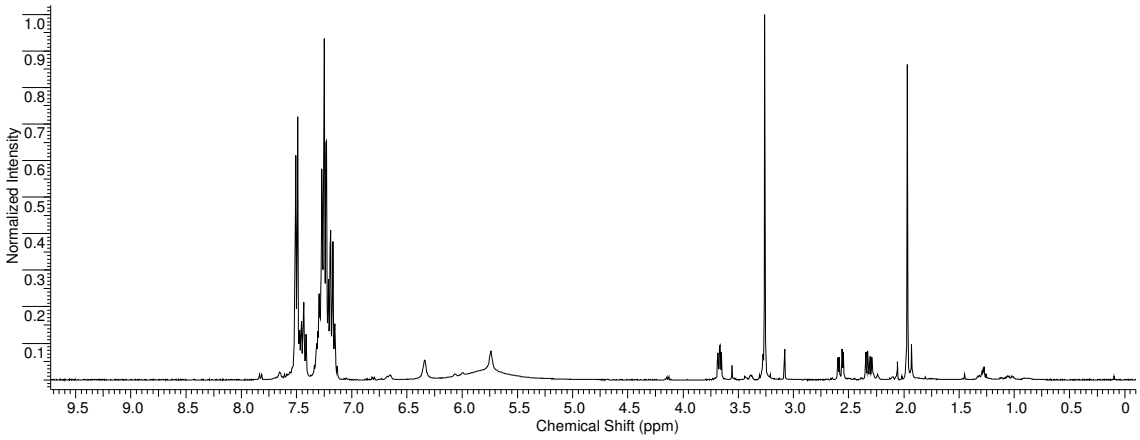

^{1}H NMR (400 MHz, CDCl3) δ: 7.51-7.30 (m, 5H), 7.29-7.16 (m, 10H), 3.63-3.66 (m, 1H), 3.26 (s, 3H), 2.60-2.55 (m, .5H), 2.34-2.31 (m, .5H), 1.95-1.93 (m, 1H).

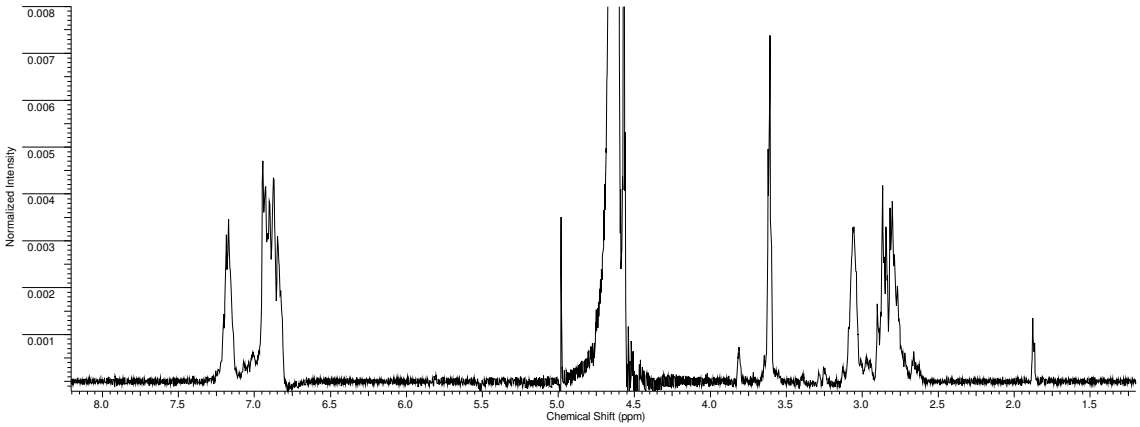

^{1}H NMR (400 MHz, D_20) δ: 7.20-7.17 (m, .8H), 6.94-6.85 (m, 2H), 3.62 (s, 1H), 3.09-3.05 (m, .6H), 2.90-2.78 (m, 1.4H).

There may be residual trityl in the final product or another impurity may be a small amount of starting material in with the amide.

Appendix C. NMR Spectra of Synthesized Compounds.

4.1. N-tritylamino dimethyl ester aspartate (2)

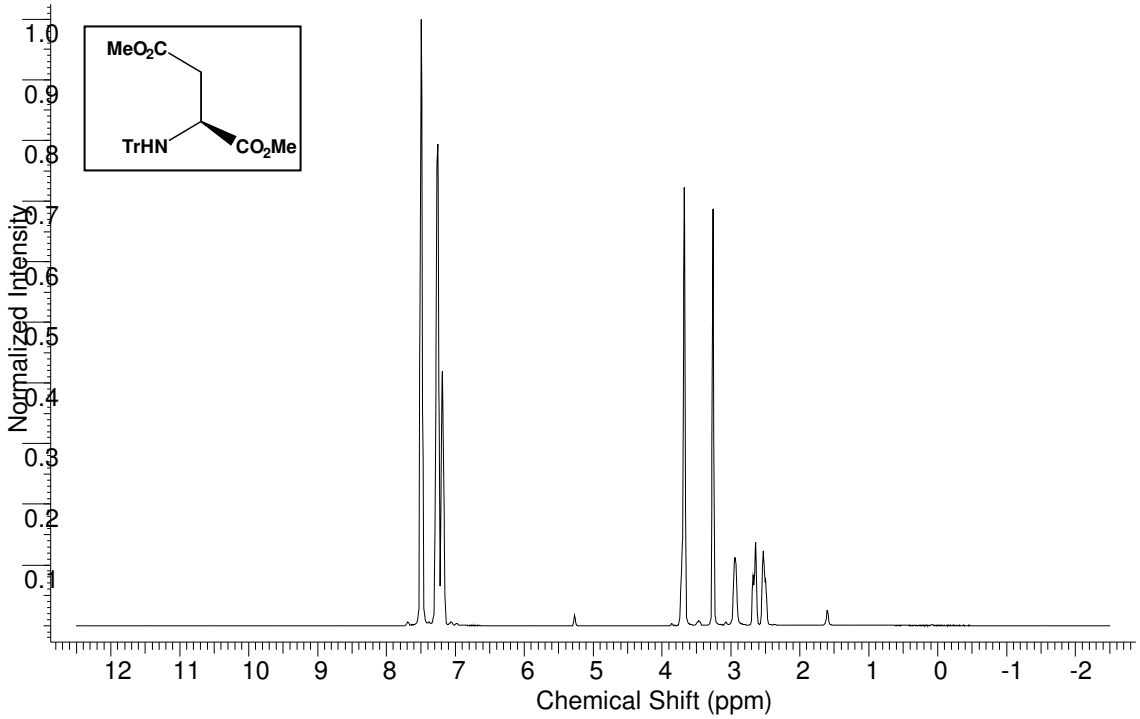

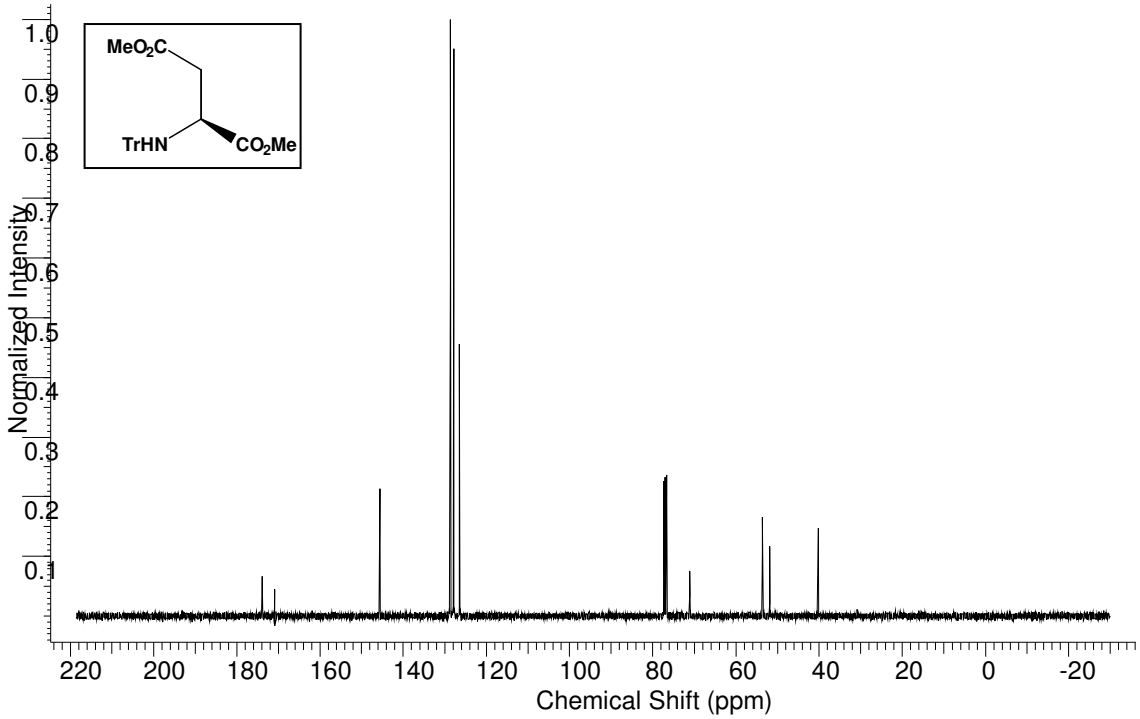

4.3. N-tritylamino dimethyl ester β-benzyl aspartate (3a)

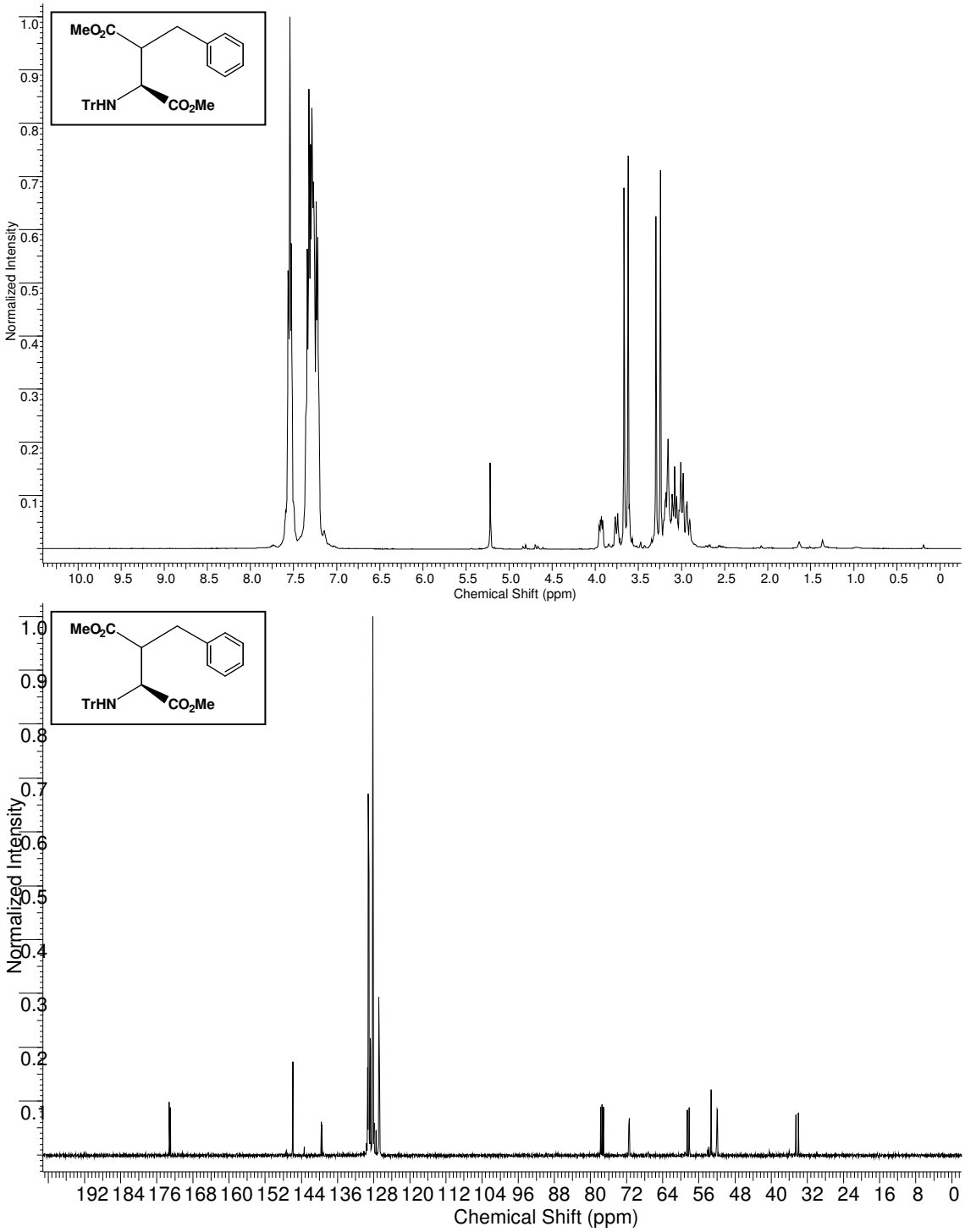

4.4. N-tritylamino dimethyl ester β-2-napthyl methyl aspartate (3b)

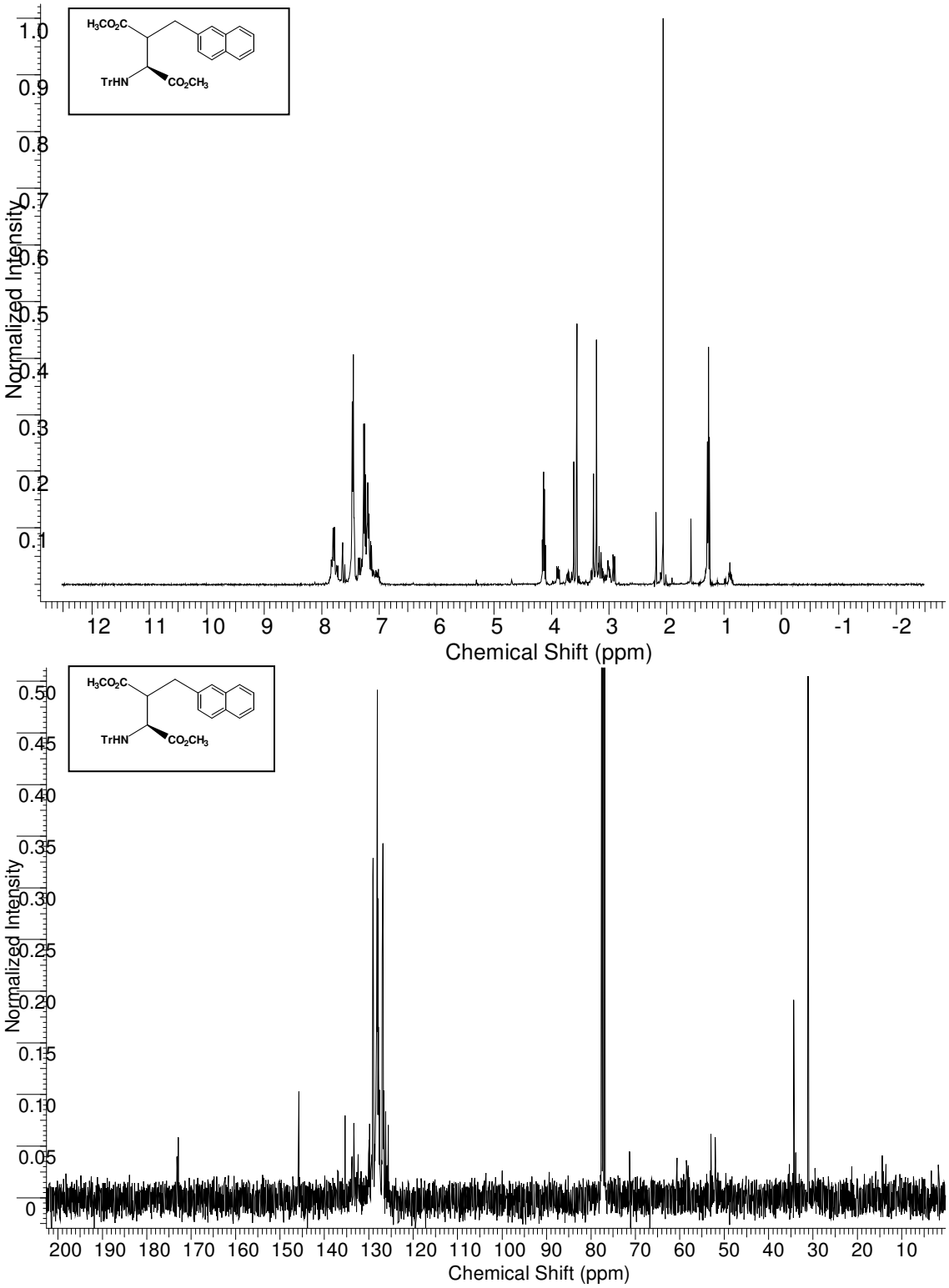

4.5. N-tritylamino dimethyl ester β-3,5 dimethyl-benzyl aspartate (3c)

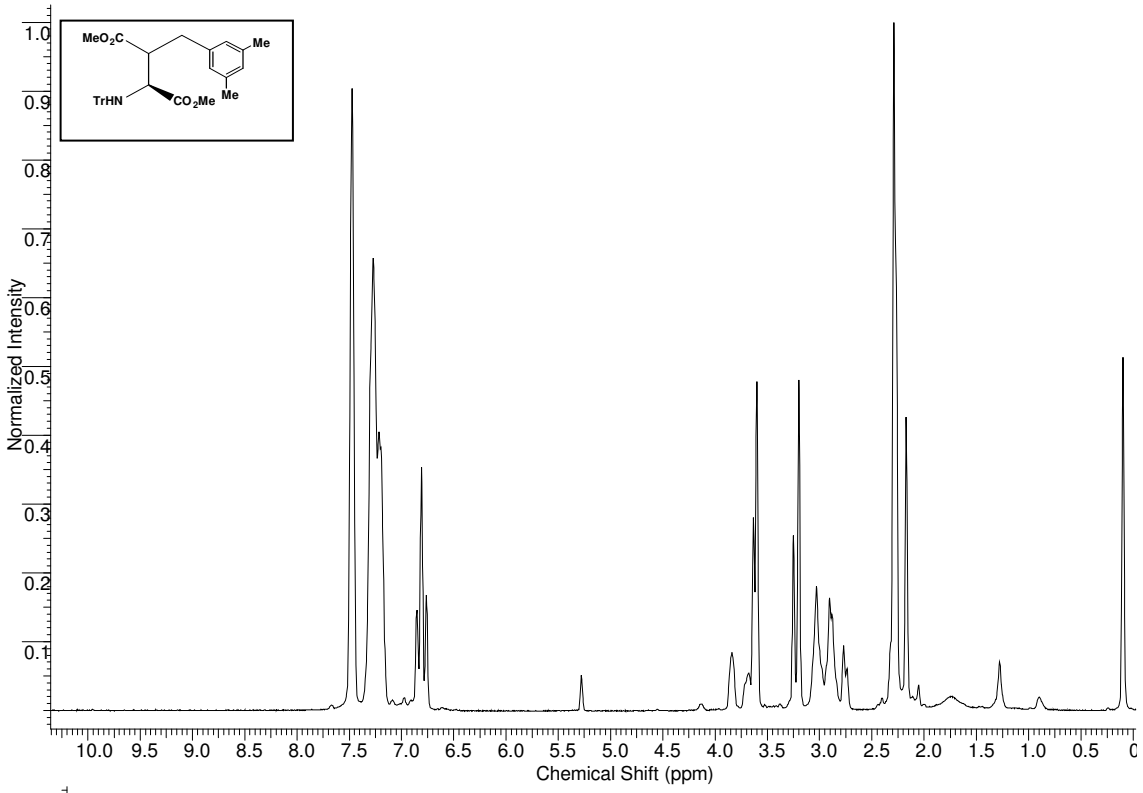

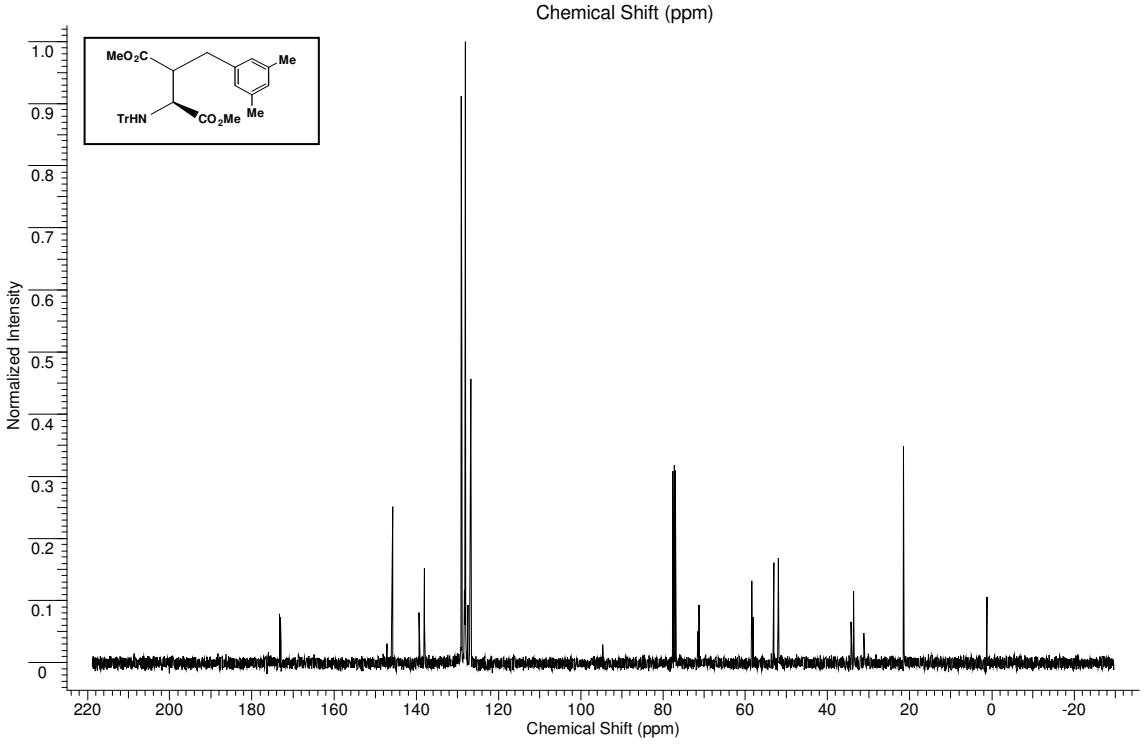

4.6. N-tritylamino dimethyl ester β-3 methyl-benzyl aspartate (3d)

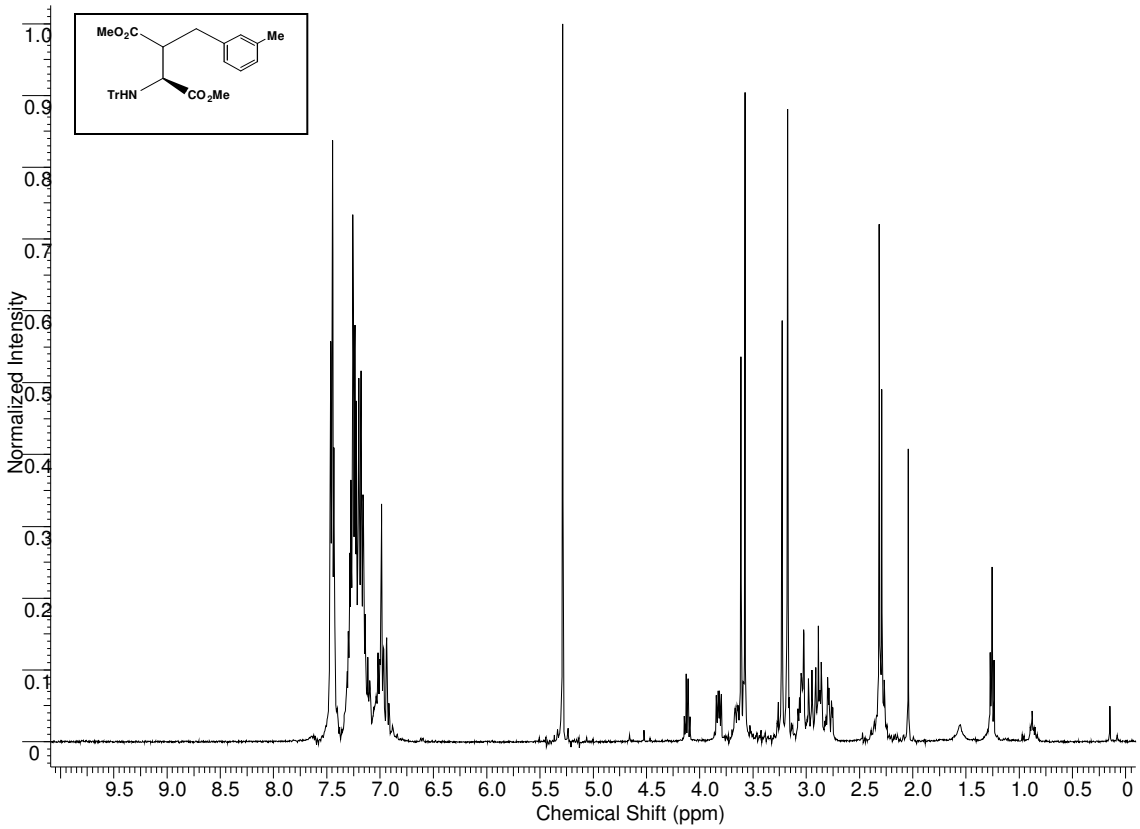

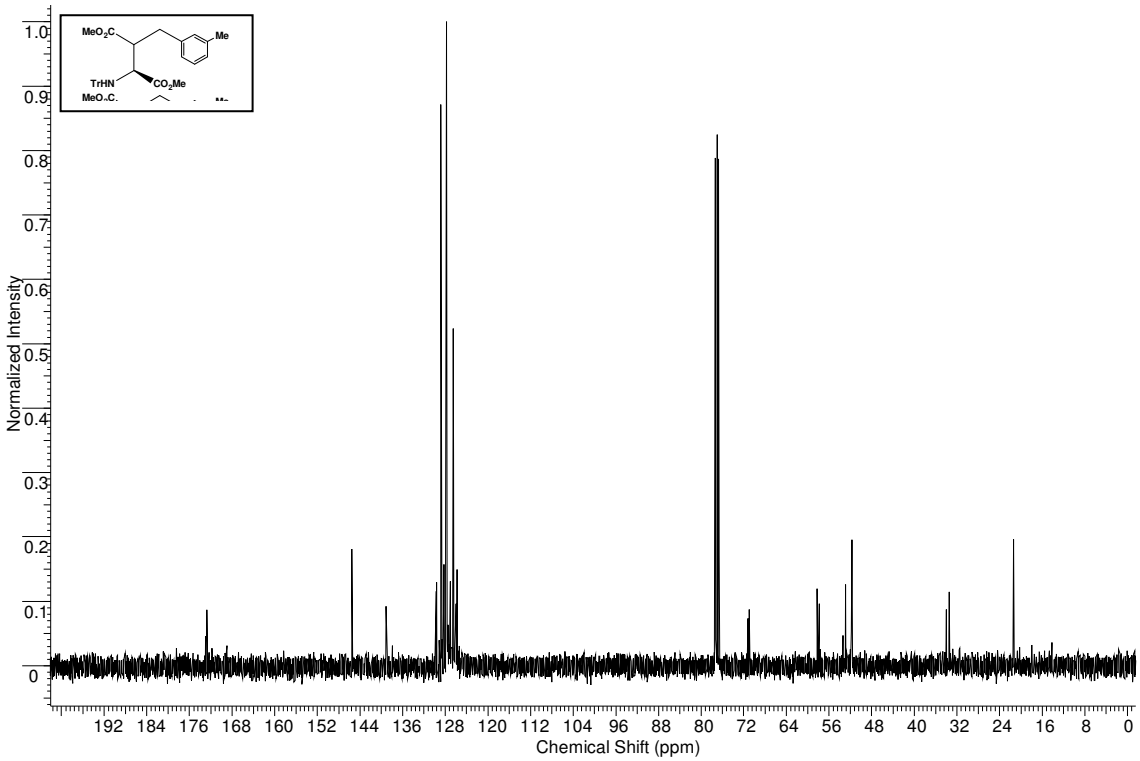

4.7. N-tritylamino dimethyl ester β-2,6 dicloro-benzyl aspartate (3e)

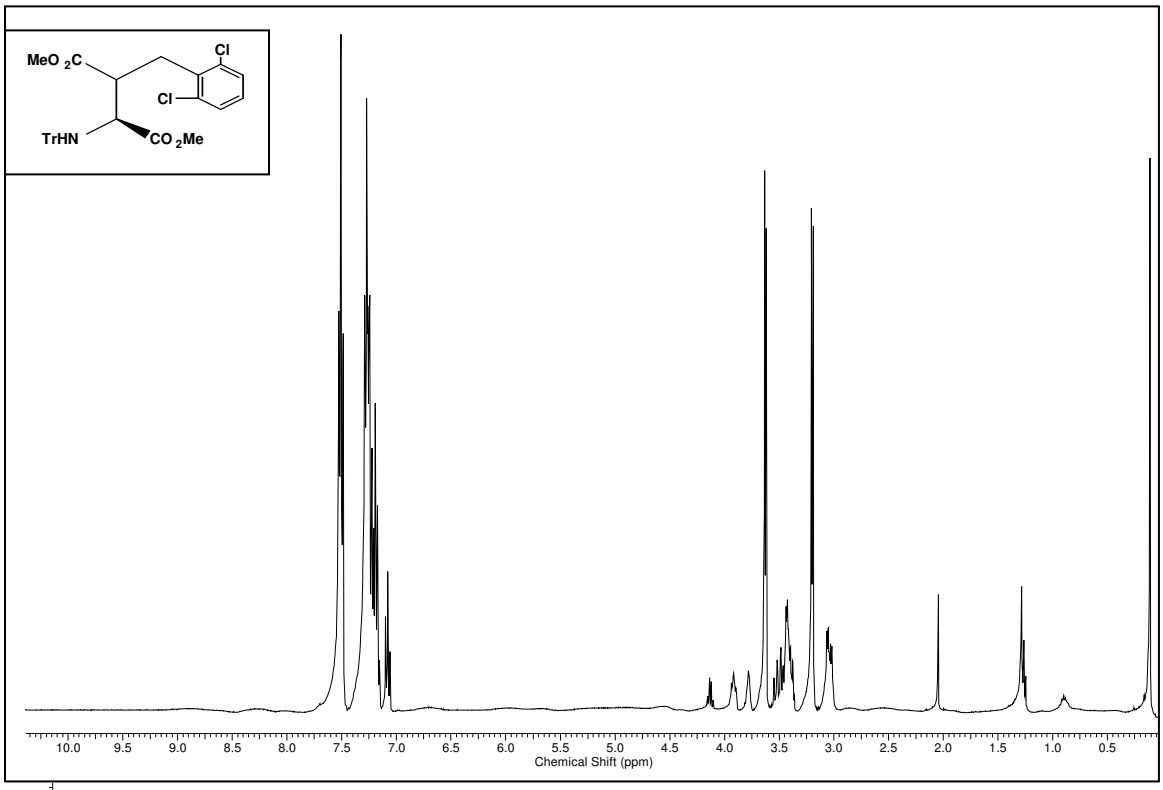

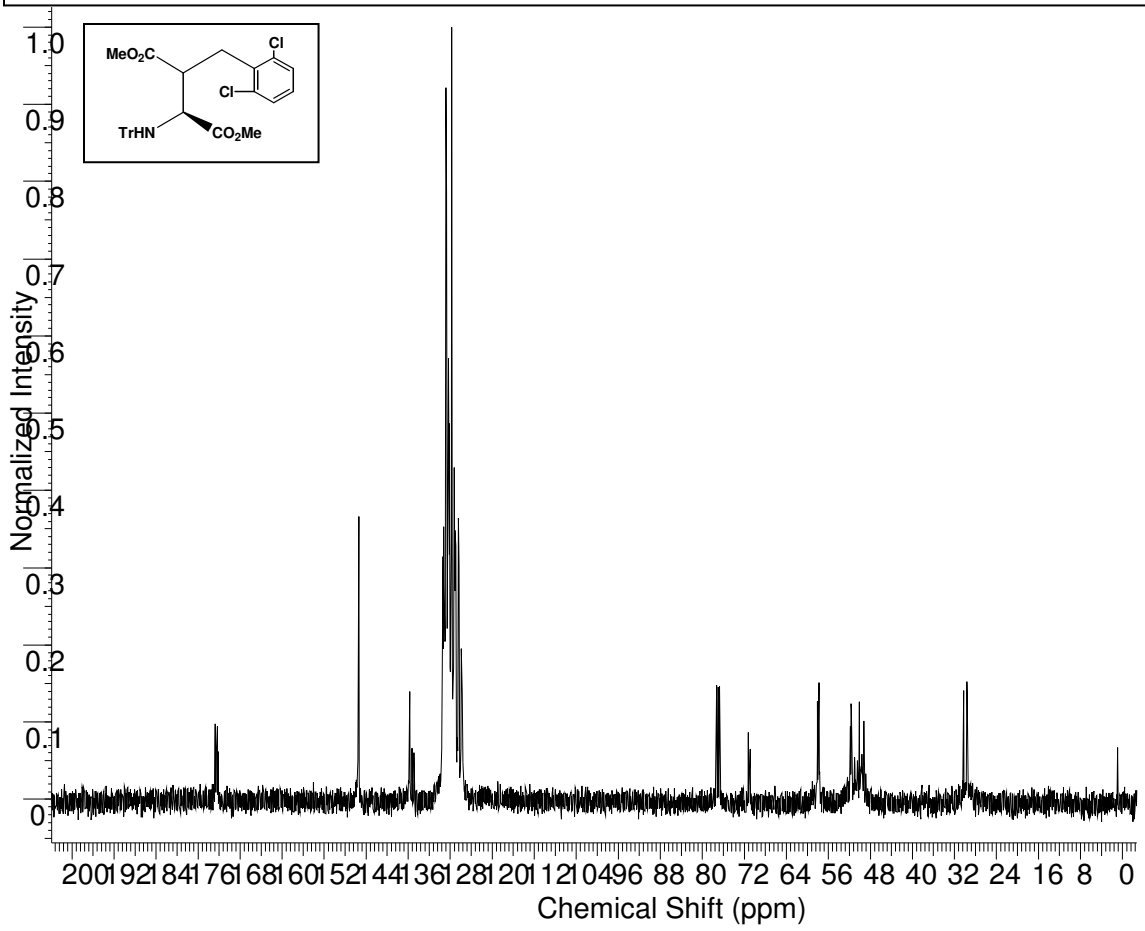

4.8. N-tritylamino dimethyl ester β-3 bromo-benzyl aspartate (3f)

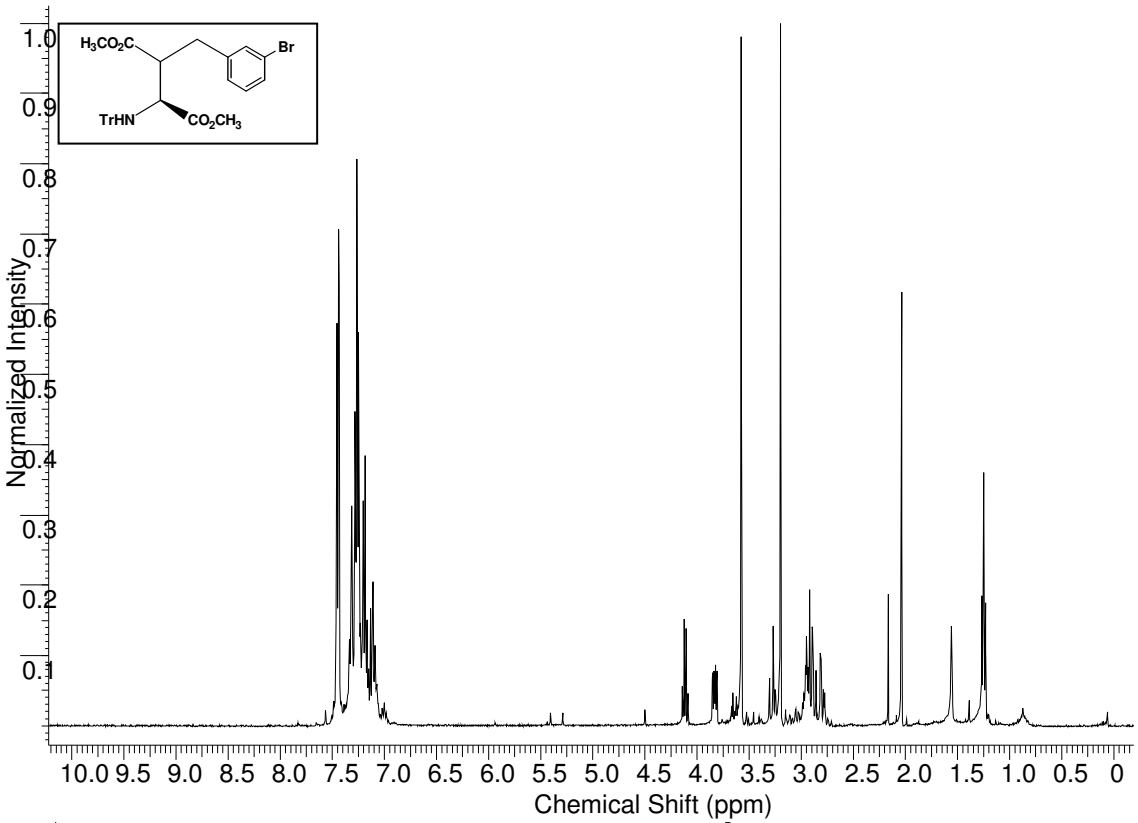

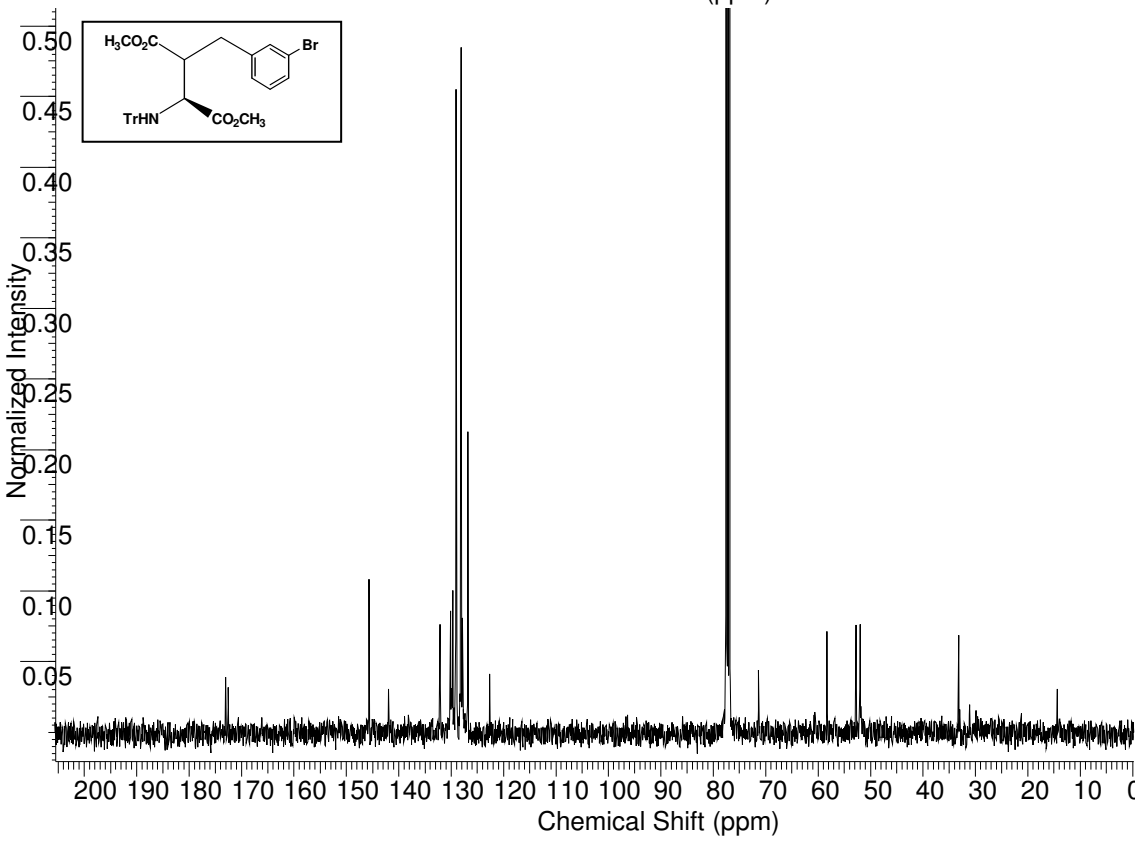

4.9. N-tritylamino dimethyl ester β-3 fluoro-benzyl aspartate (3g)

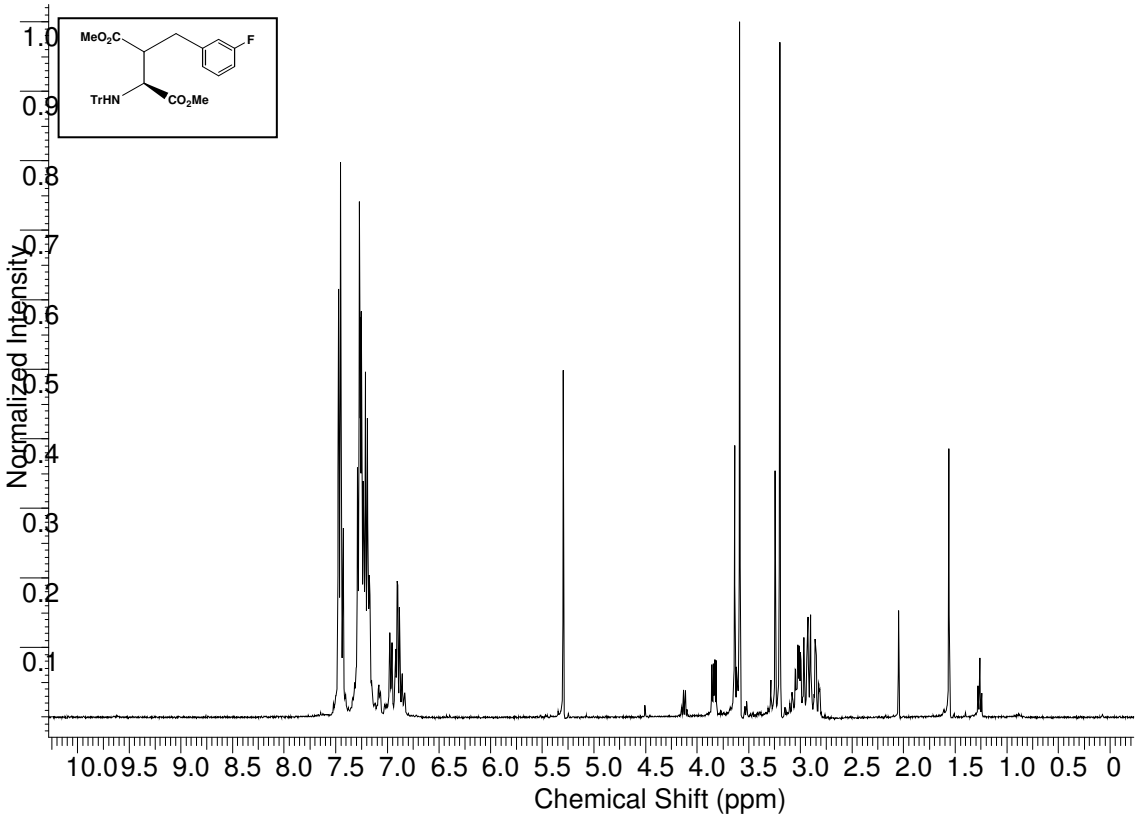

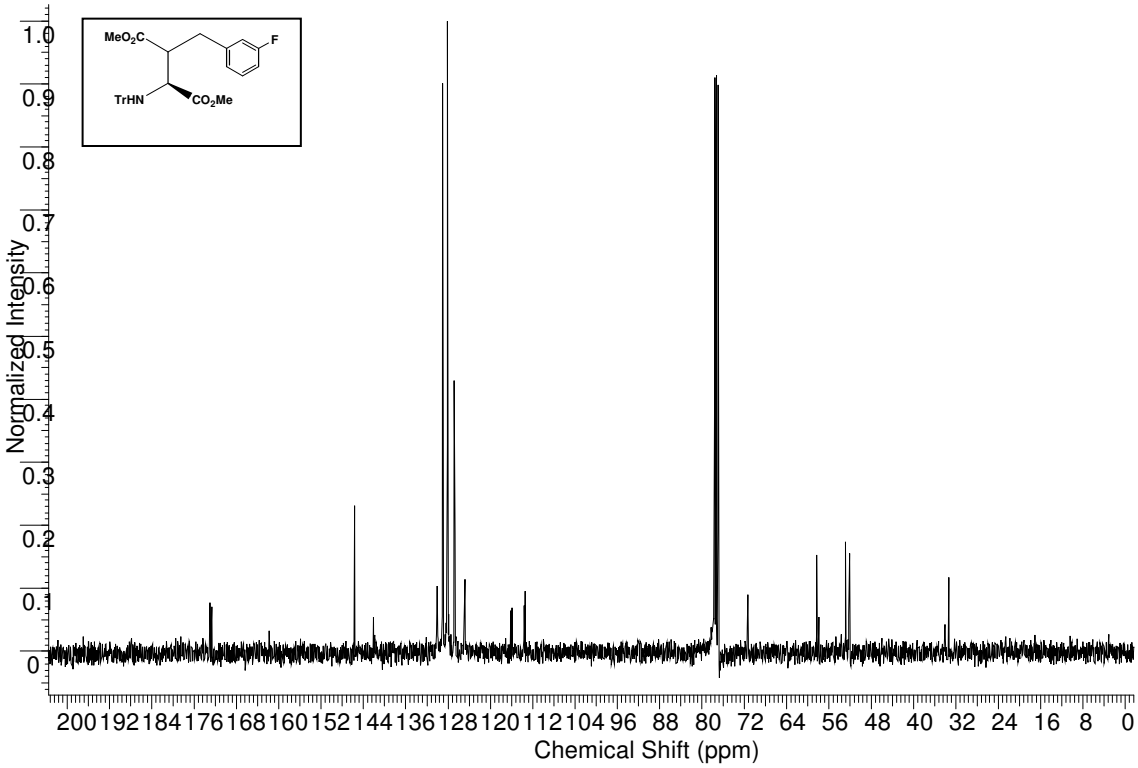

4.10. N-tritylamino dimethyl ester β-3 fluoro-benzylaspartate (3g, *S,S*)

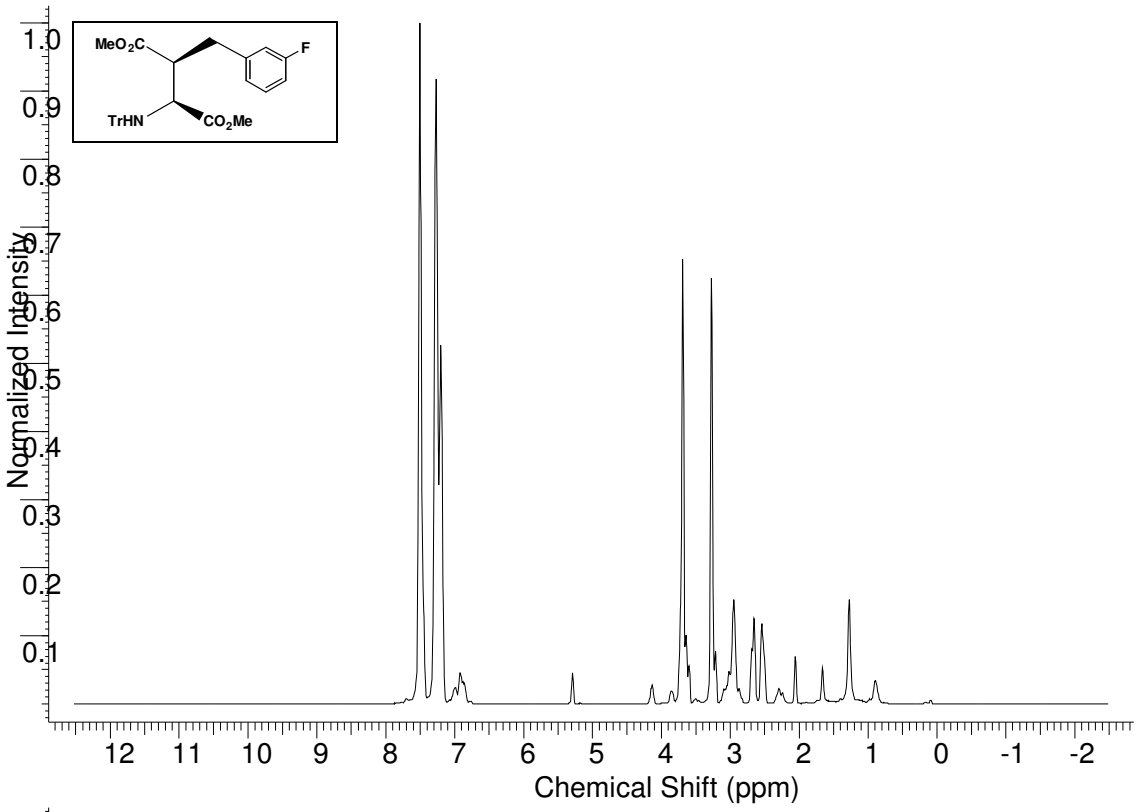

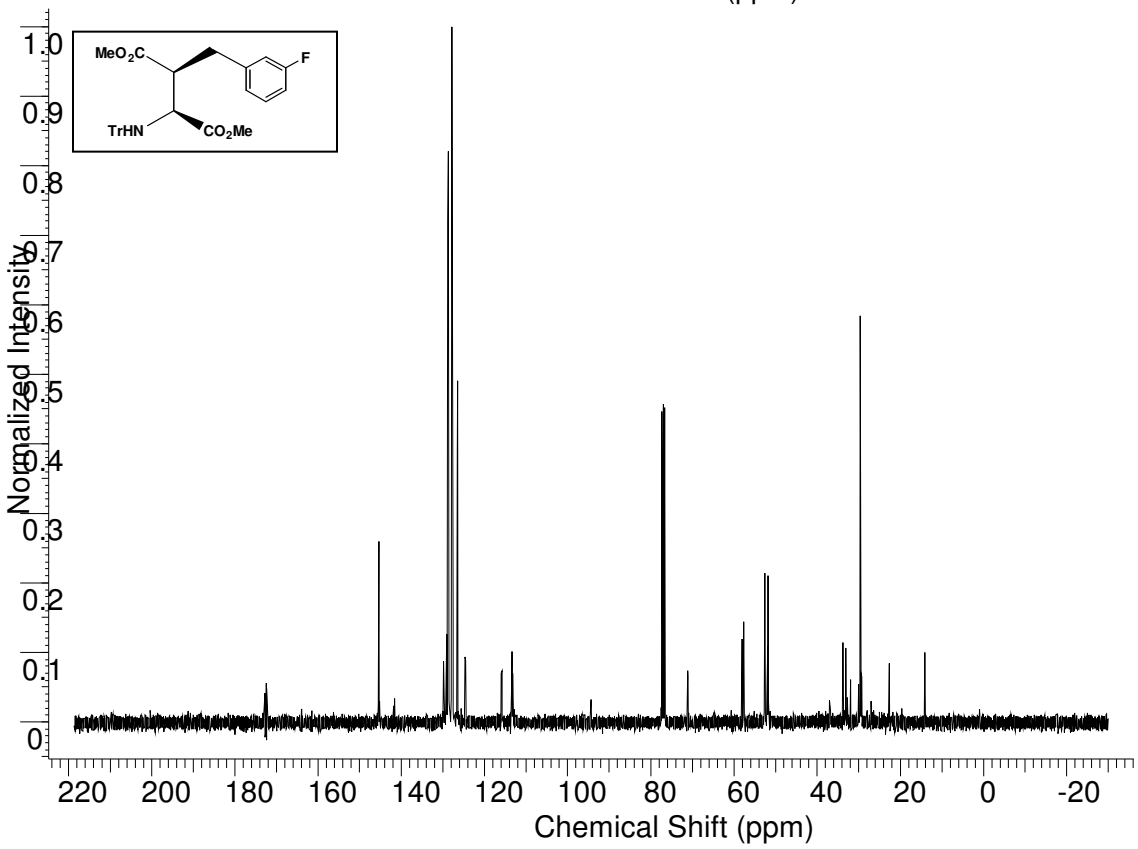

4.11. N-tritylamino dimethyl ester β-3 fluoro-benzylaspartate (3g. *S,R*)

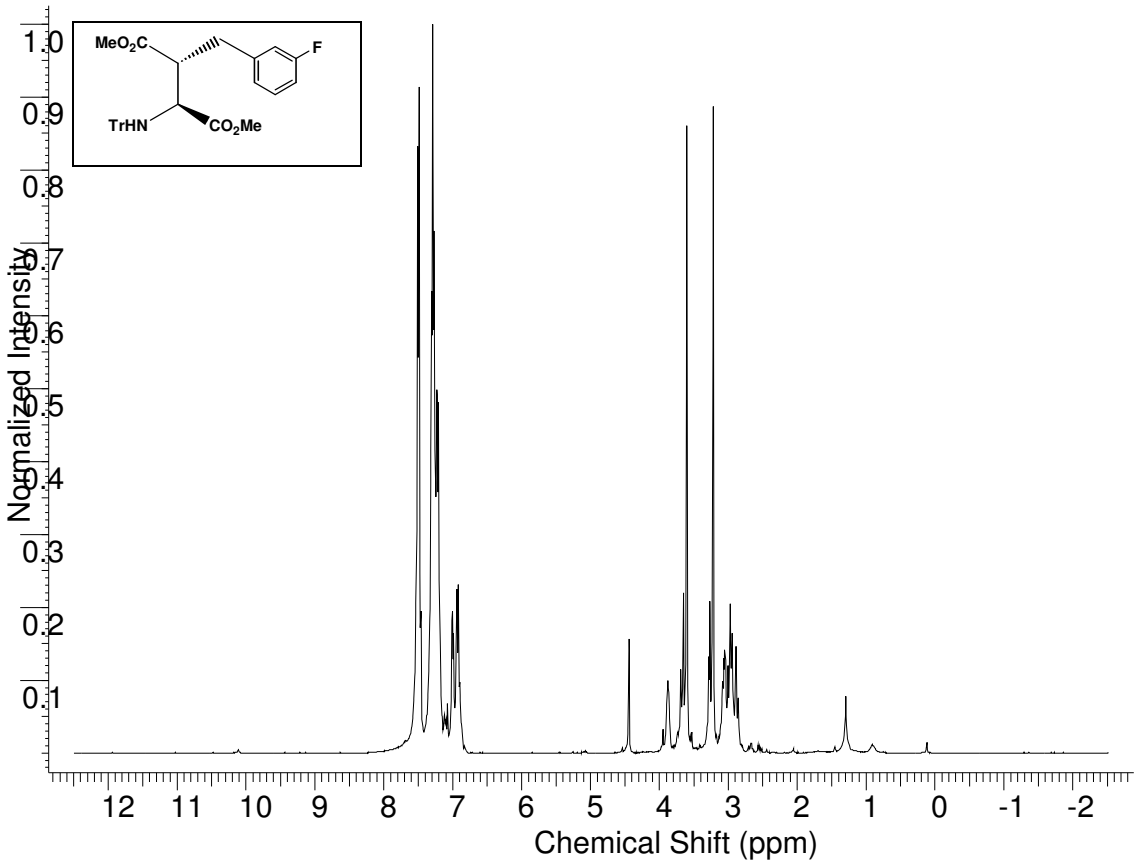

4.12 N-tritylamino dimethyl ester β-4-fluoro-benzyl aspartate (3h)

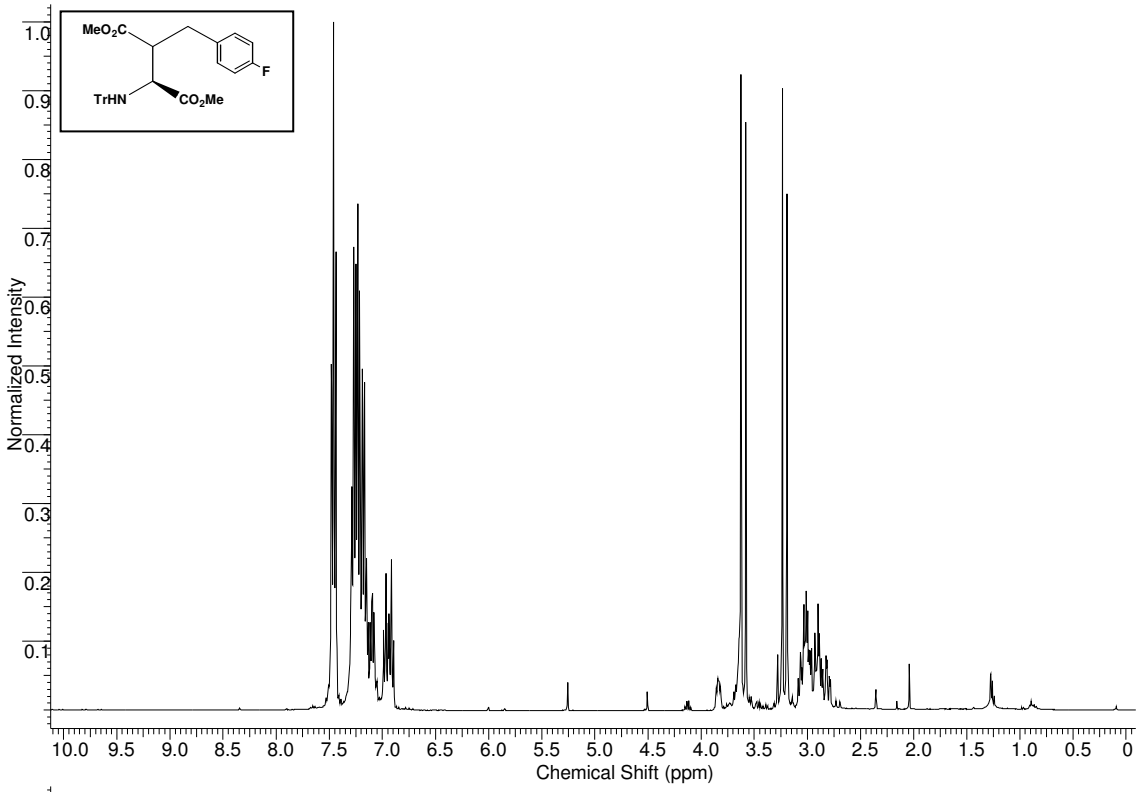

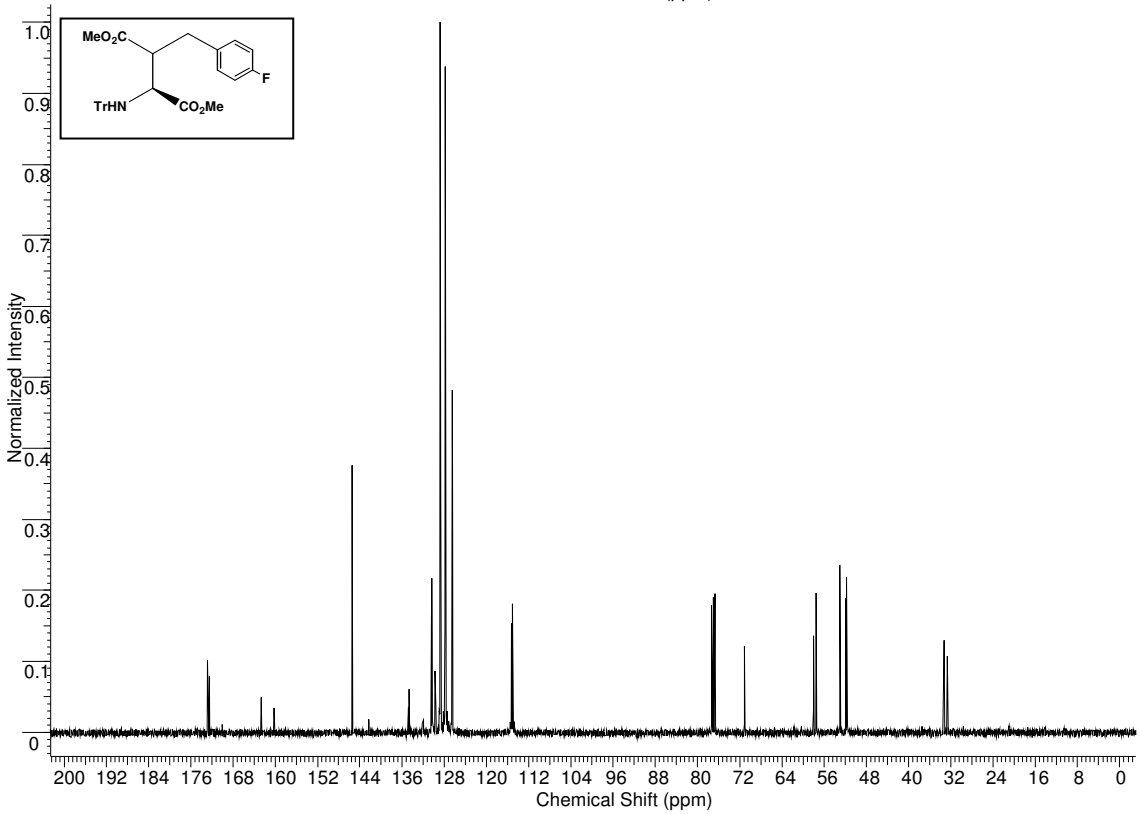

4.13. N-tritylamino dimethyl ester β-3-nitro-benzyl aspartate (3i)

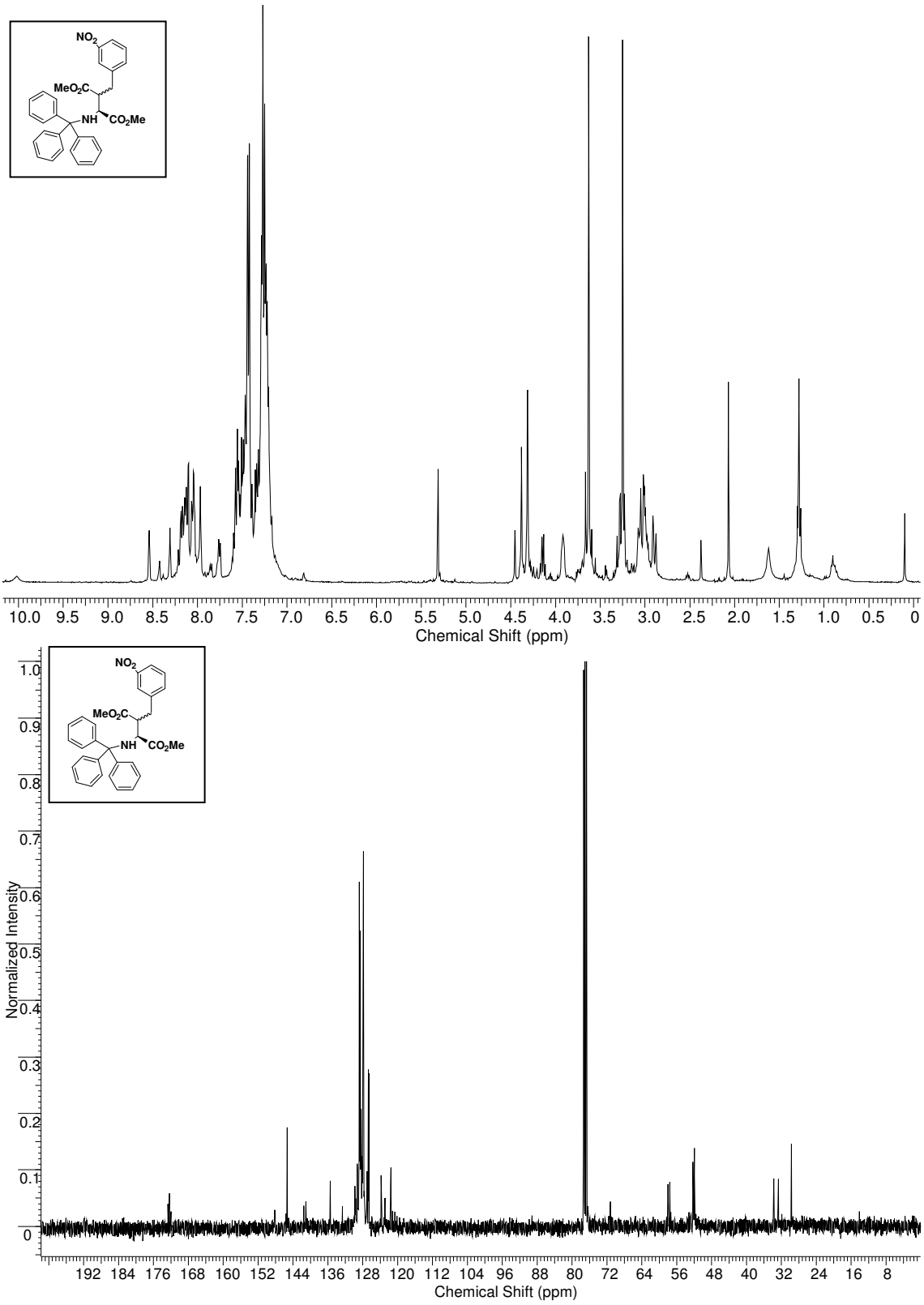

4.14. N-tritylamino dimethyl ester β-3-nitro-benzylaspartate (3i, S,S)

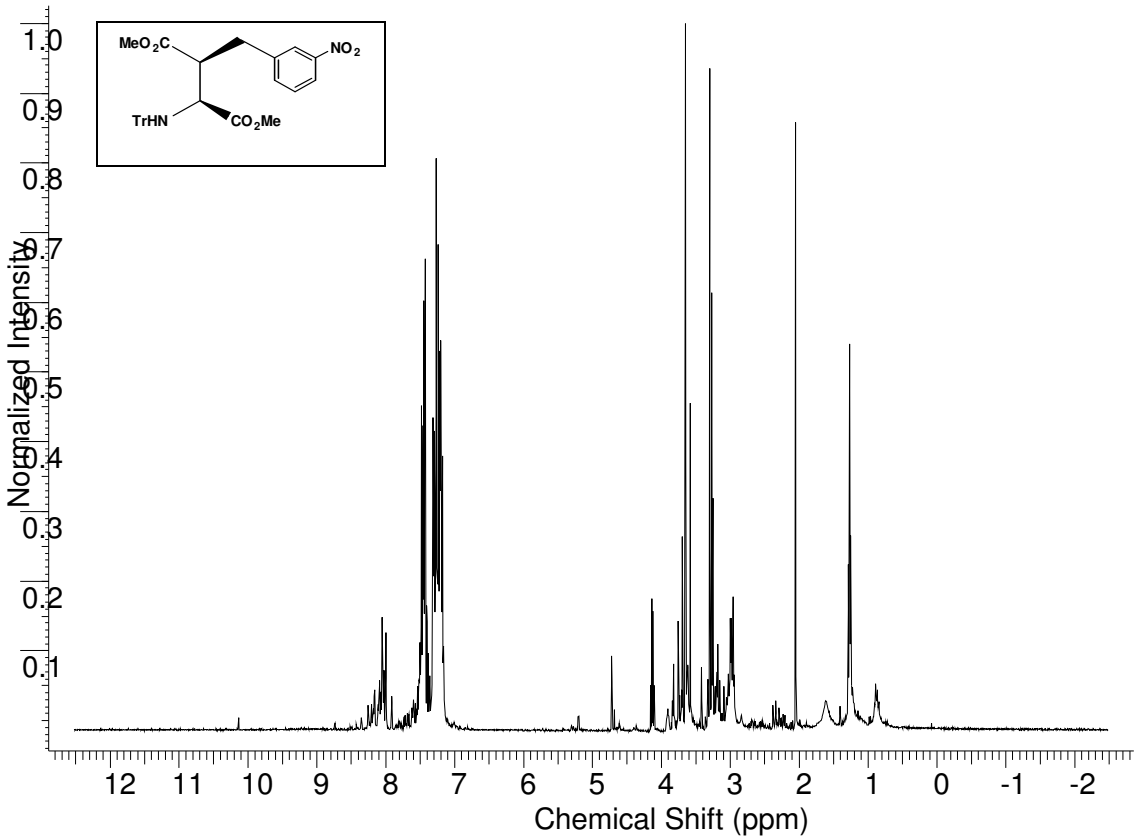

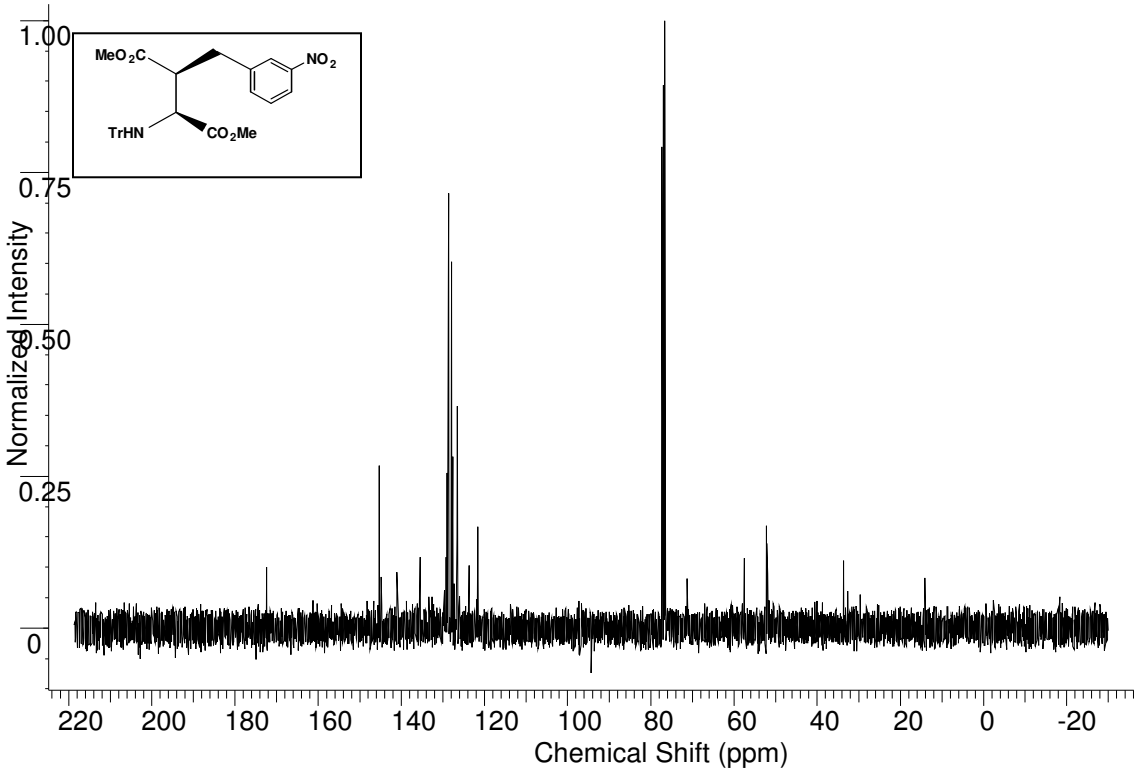

4.15. N-tritylamino dimethyl ester β-P-nitro benzyl aspartate (3j)

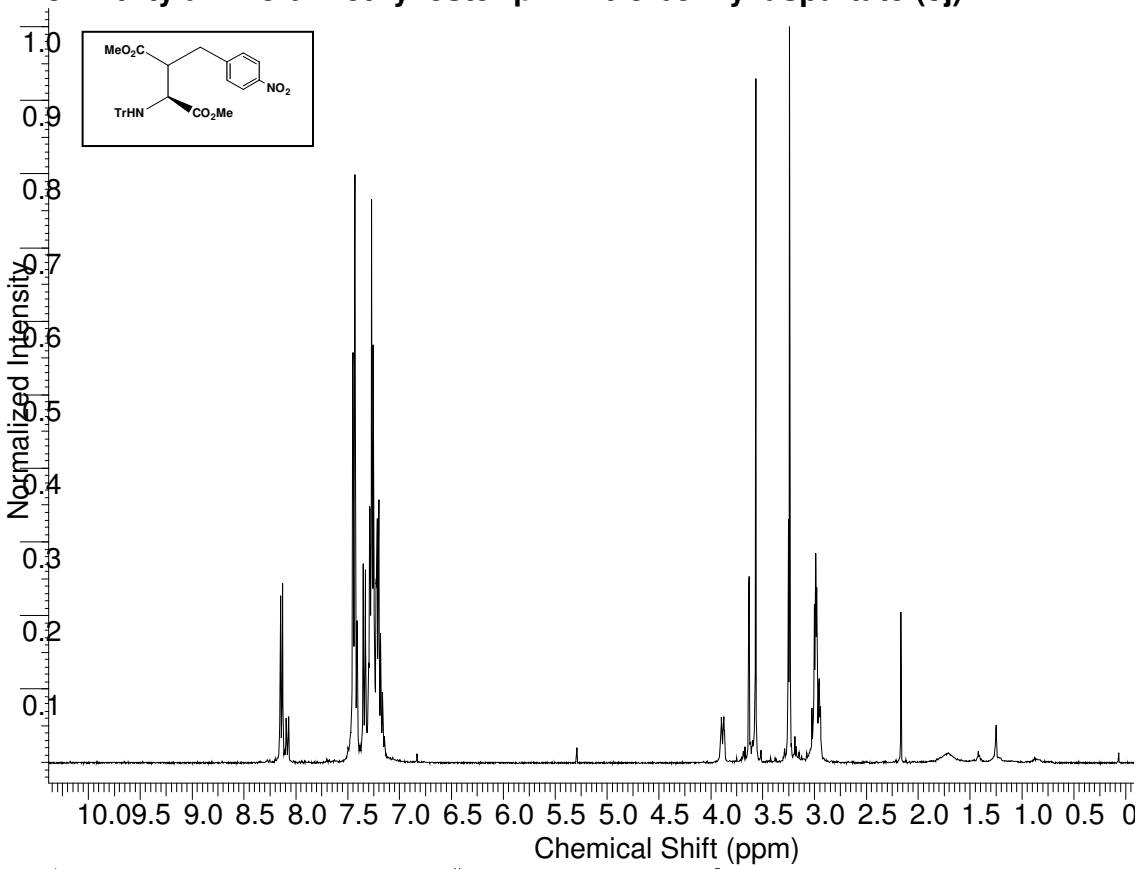

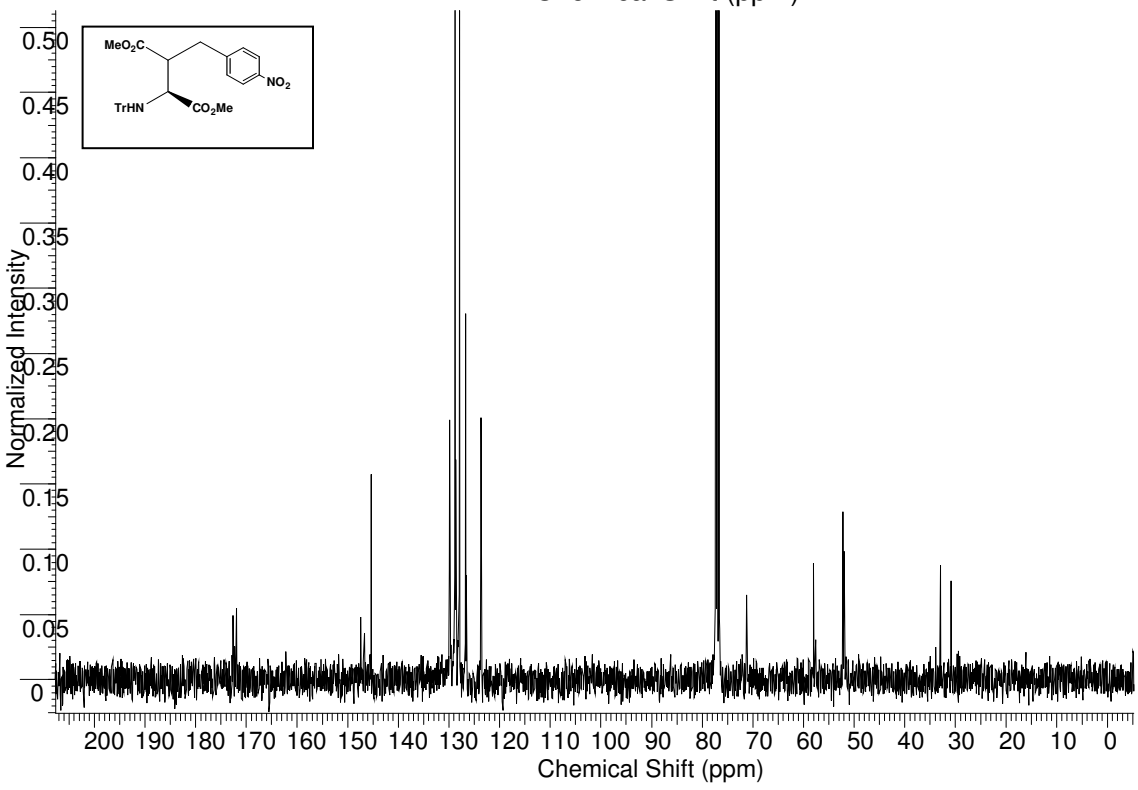

4.16. N-tritylamino dimethyl ester β-3-chloro benzylaspartate

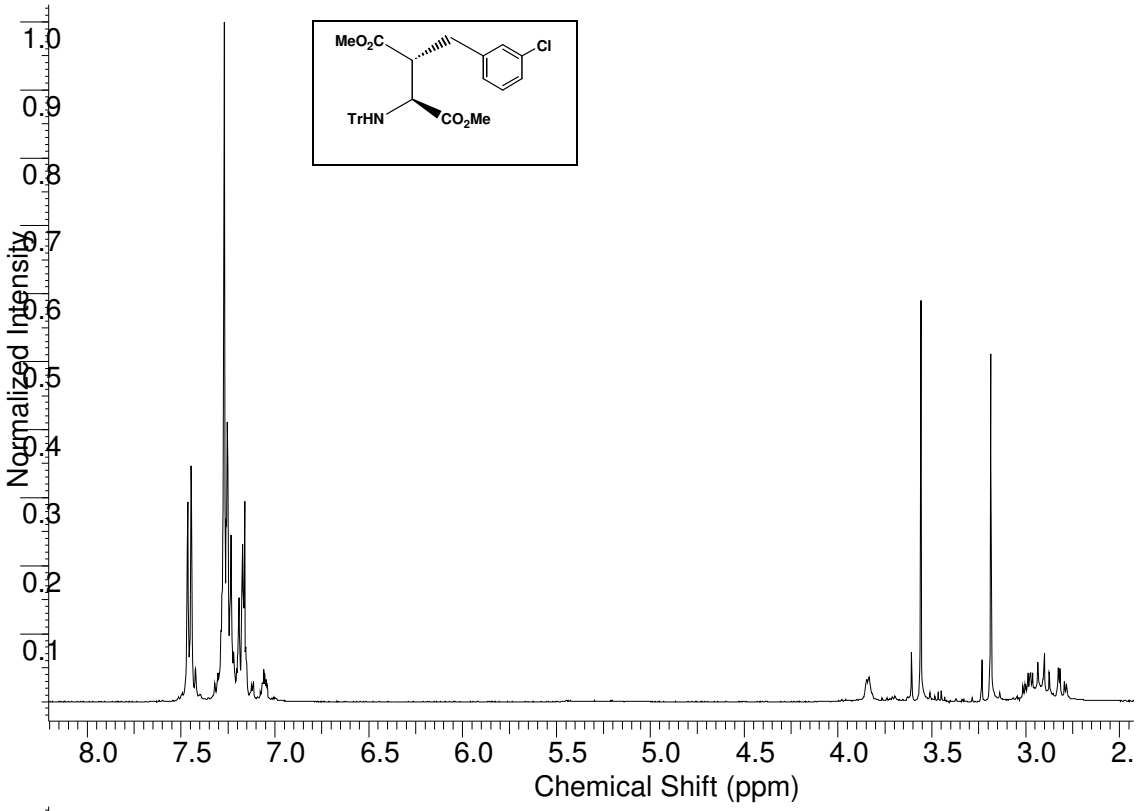

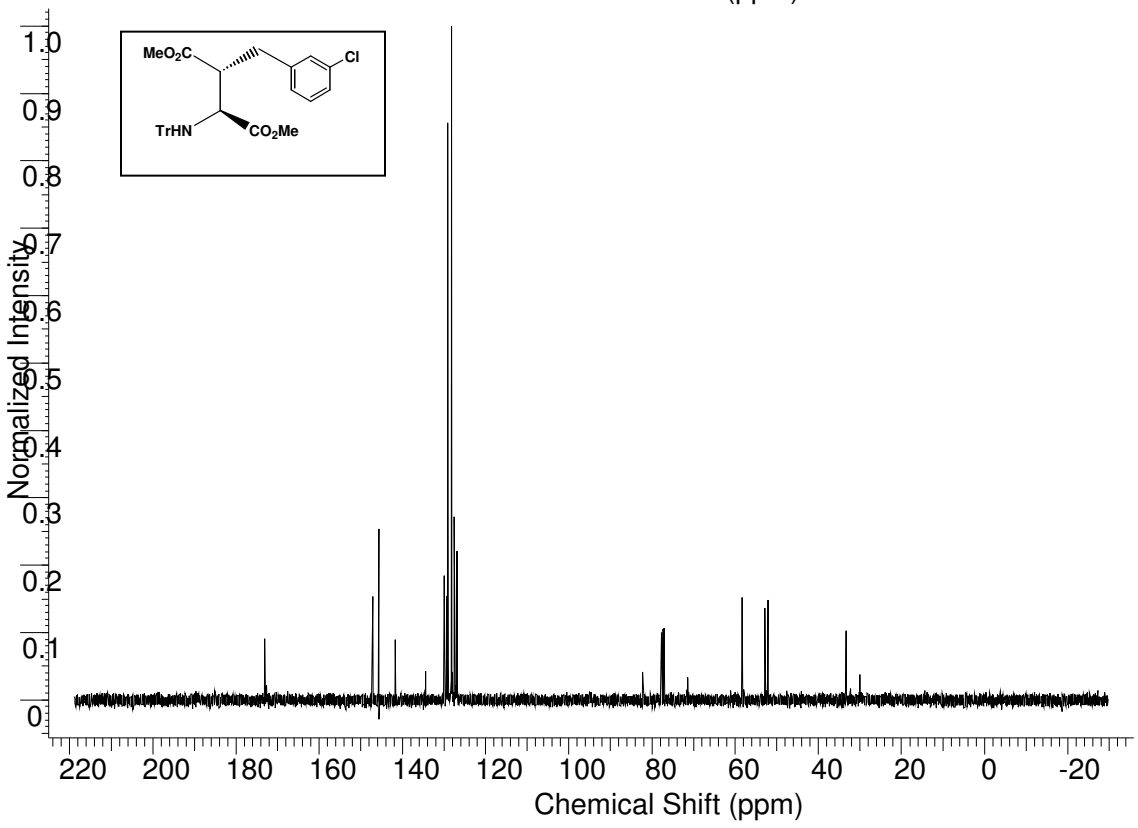

4.18. β-Benzyl aspartate (4A)

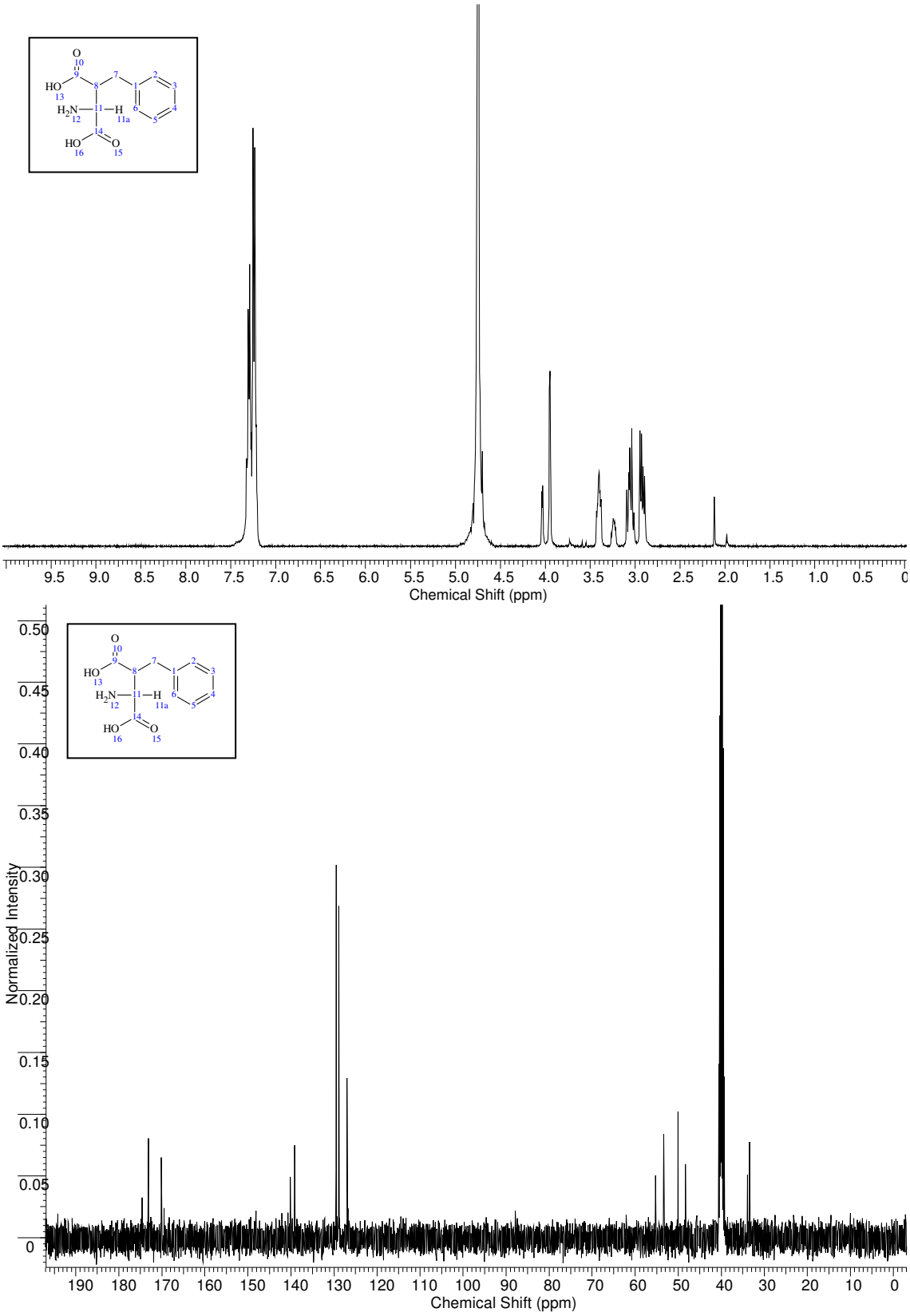

4.19. *S,S* L-β-Benzylaspartate (4A)

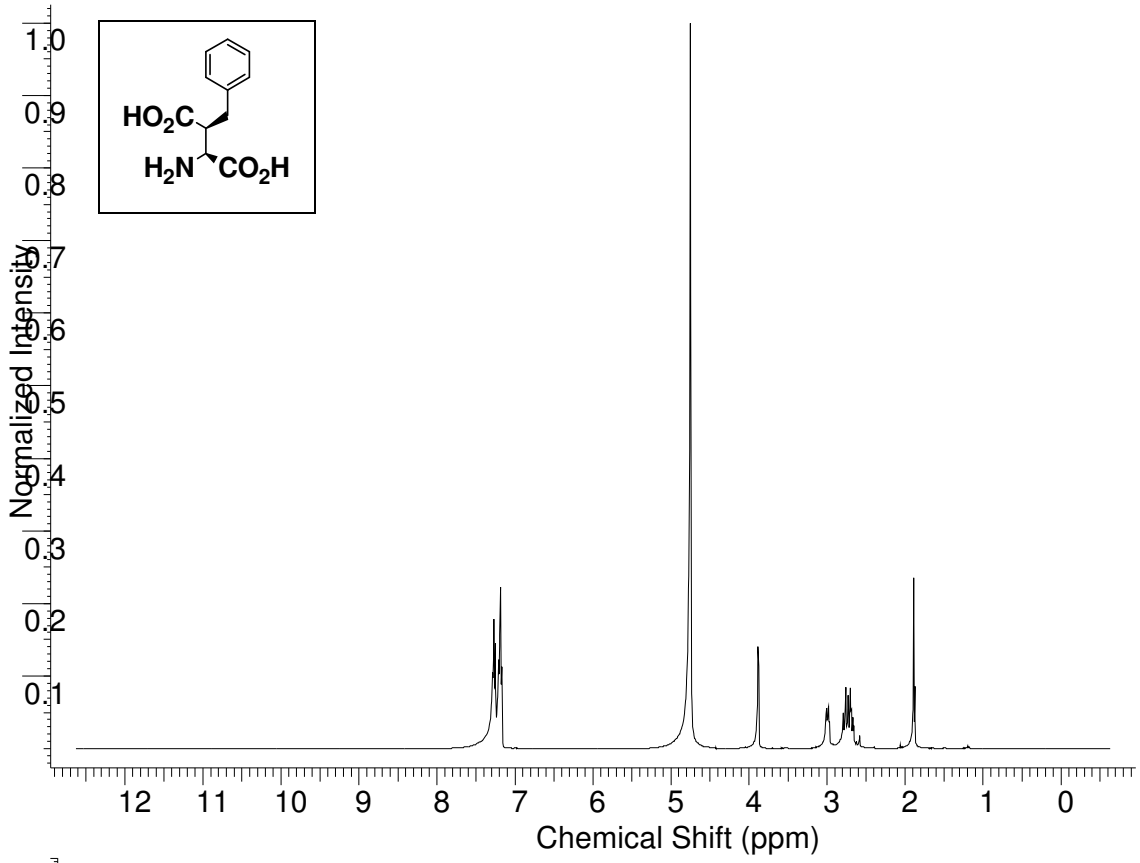

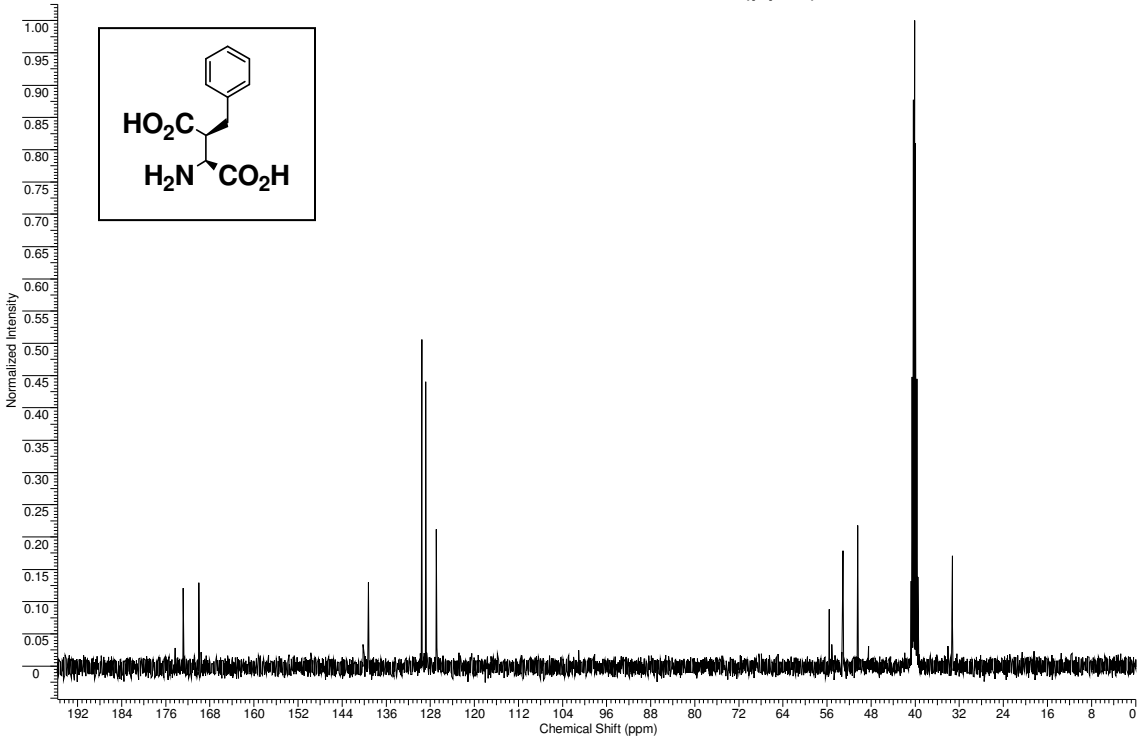

4.20. β-2-Napthyl methyl aspartate (4B)

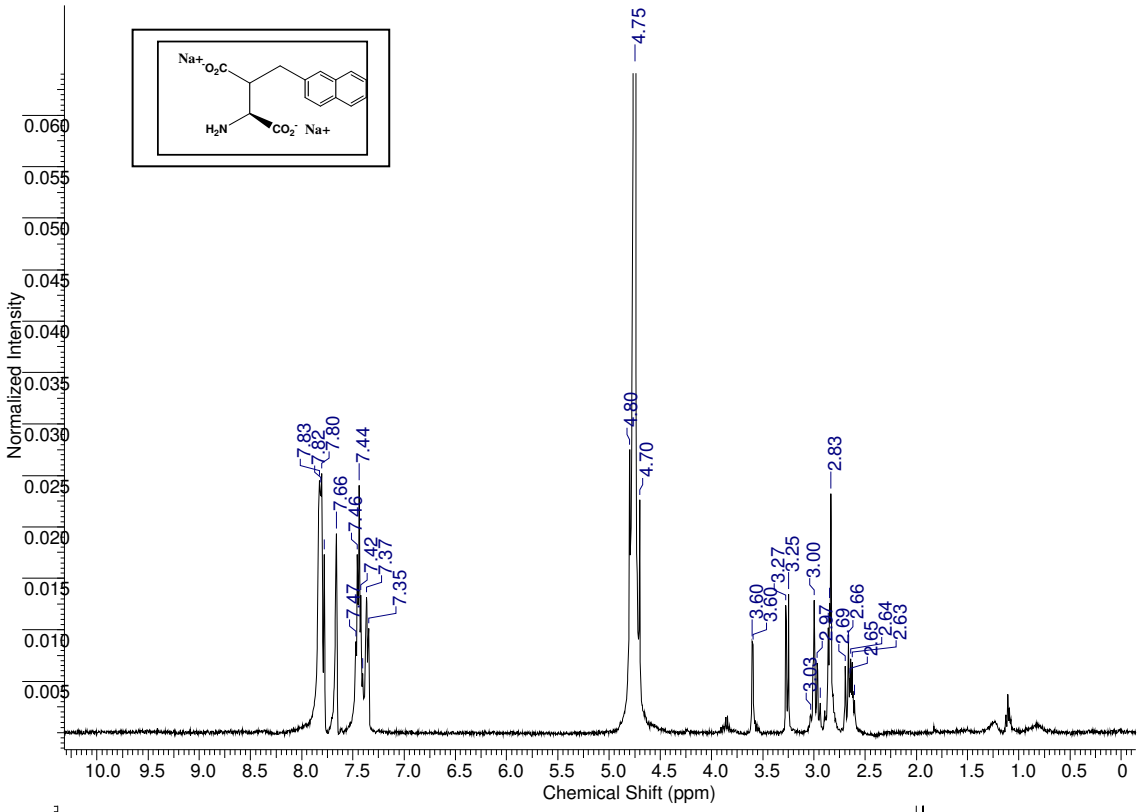

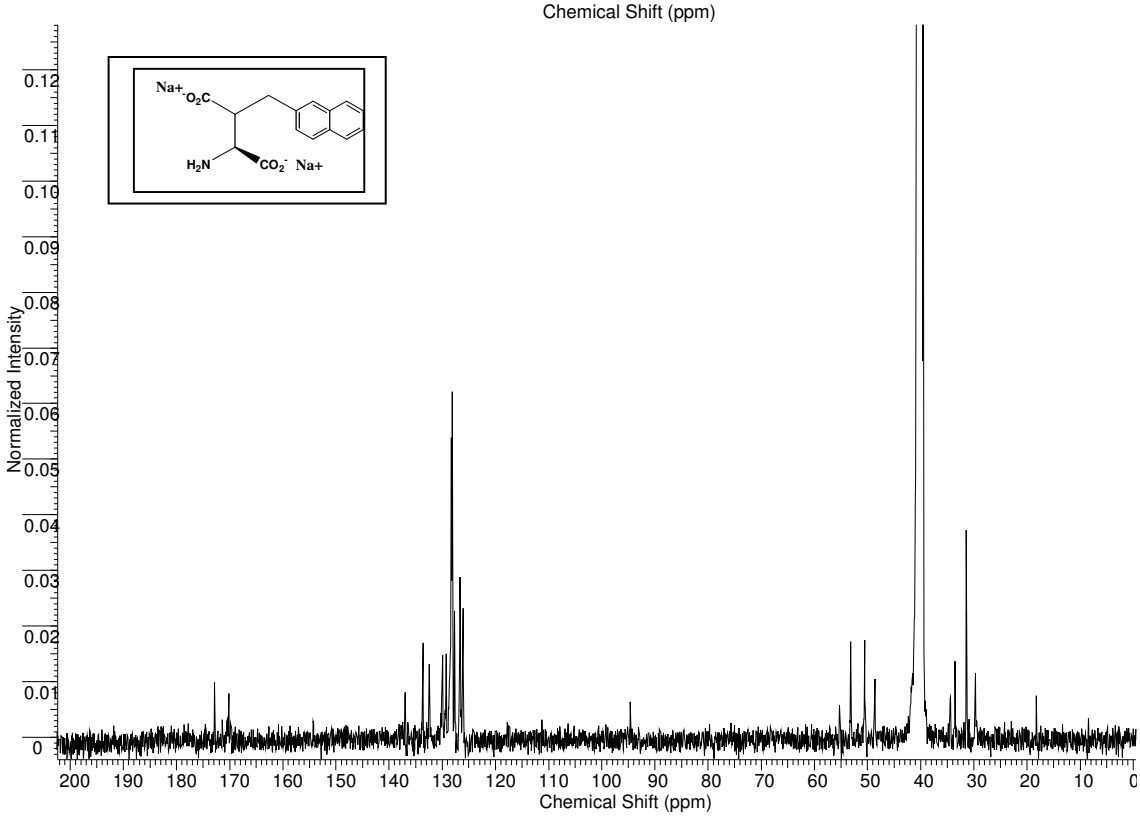

4.21. β-3,5 Dimethyl-benzyl aspartate (4C)

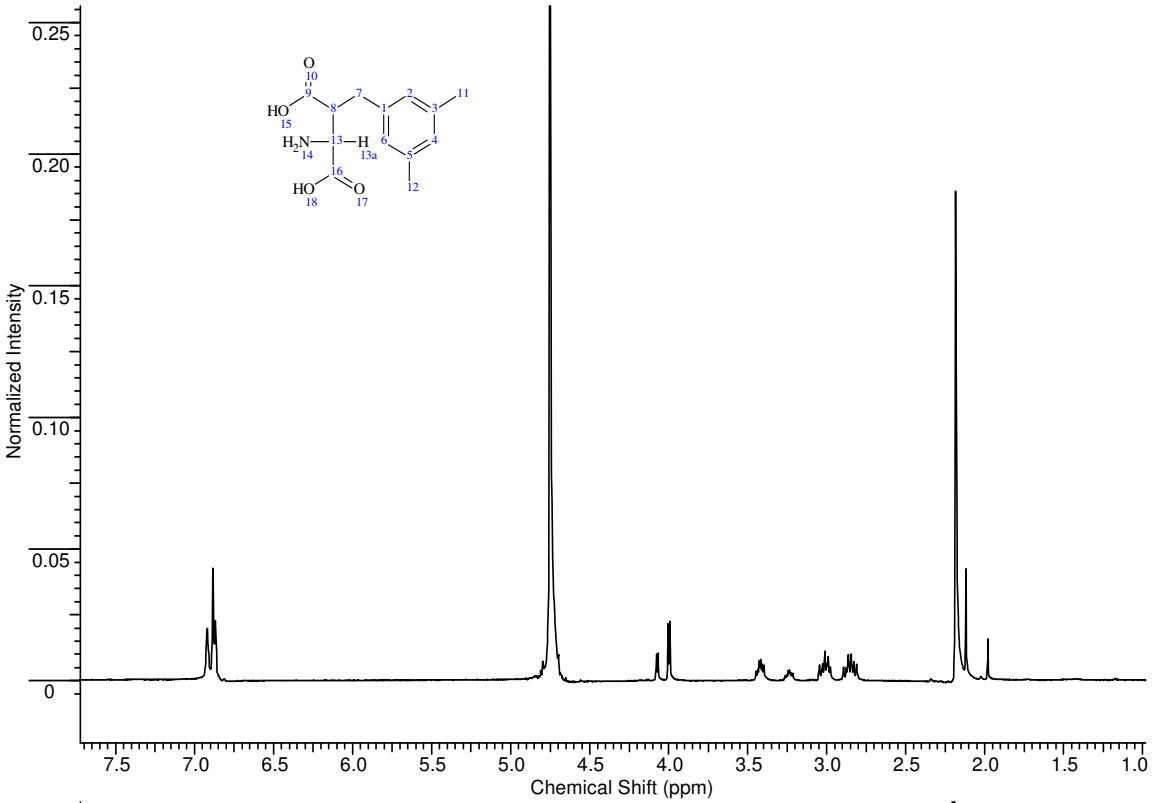

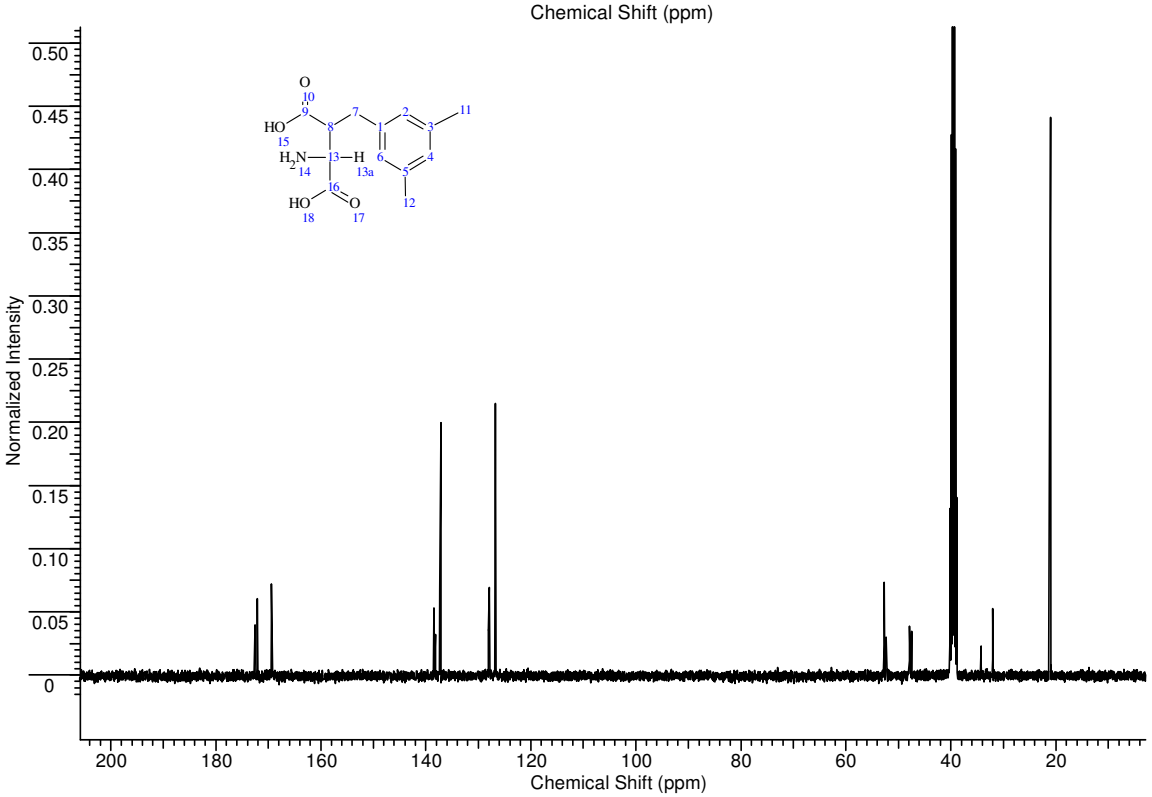

4.22. β-3 Methyl-benzyl aspartate (4D)

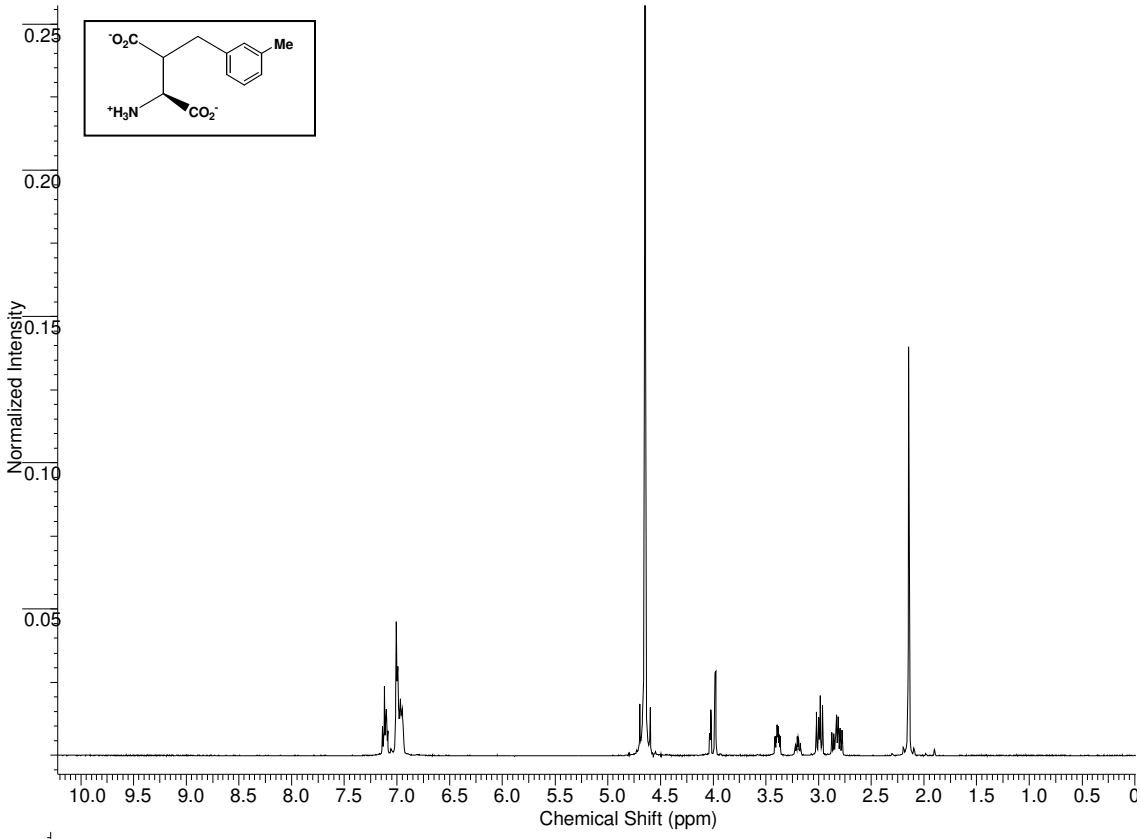

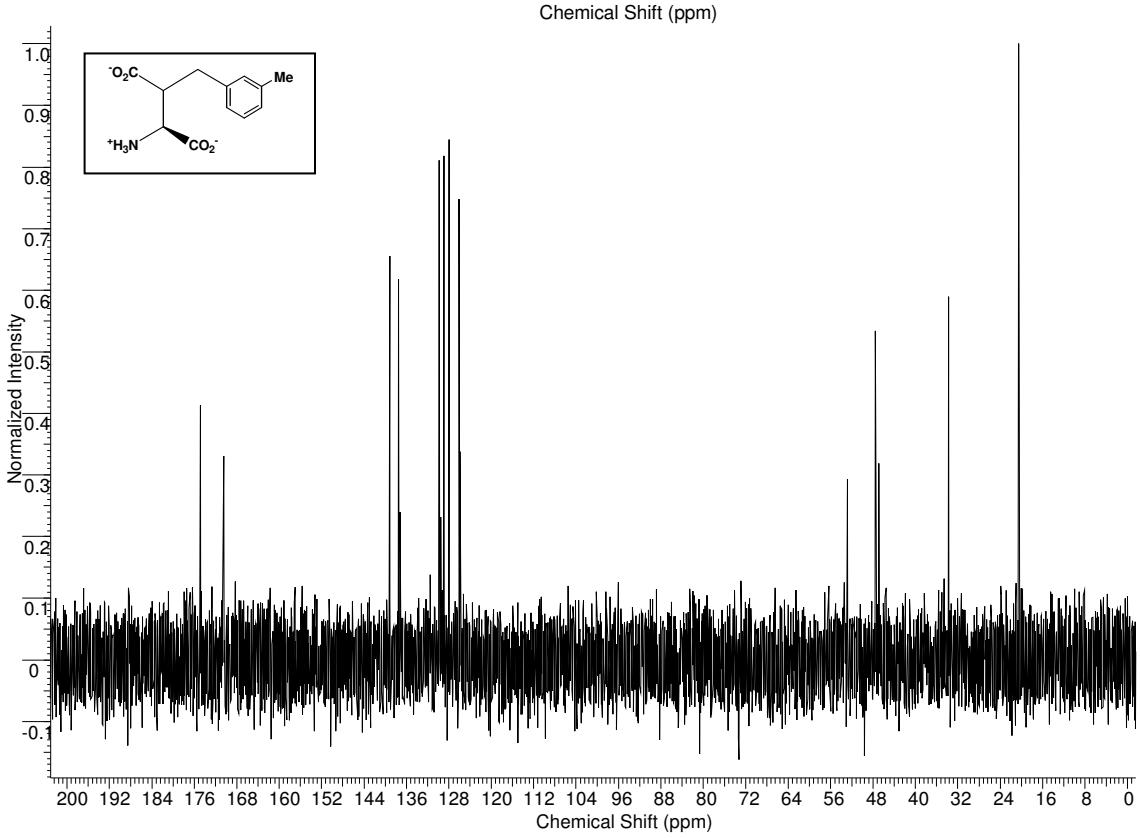

4.23. β-2,6 Dicloro-benzyl aspartate (4E)

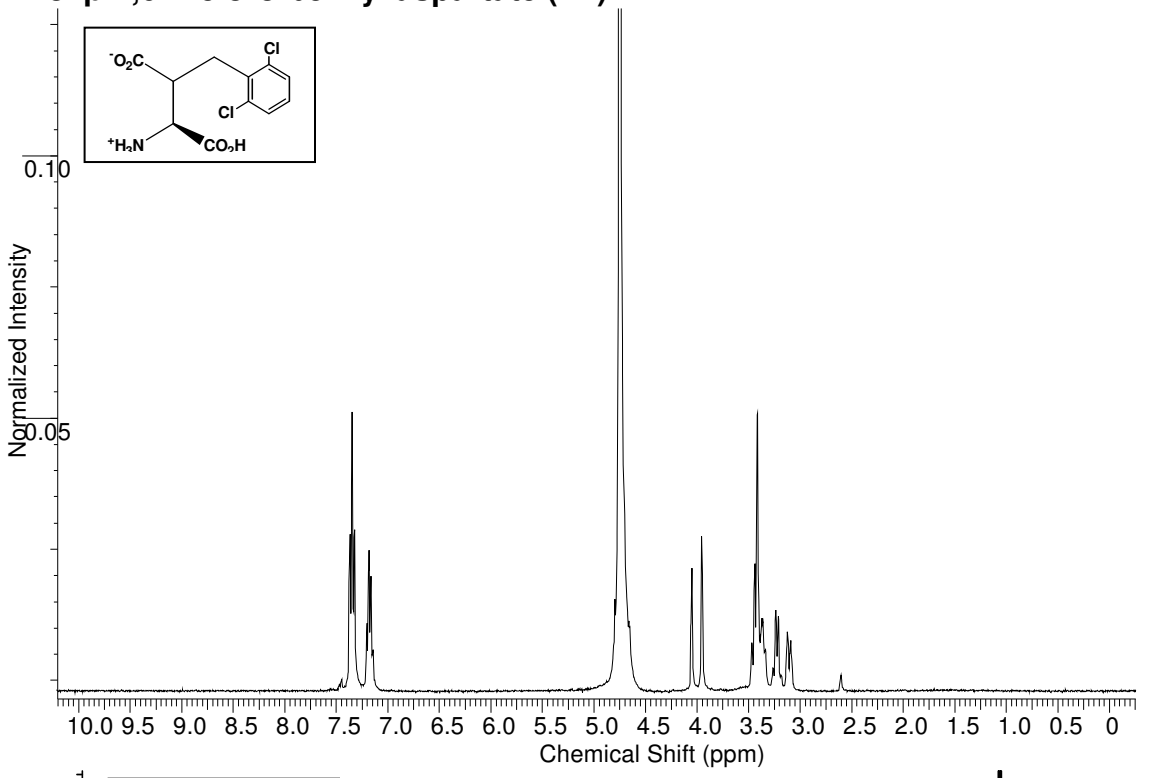

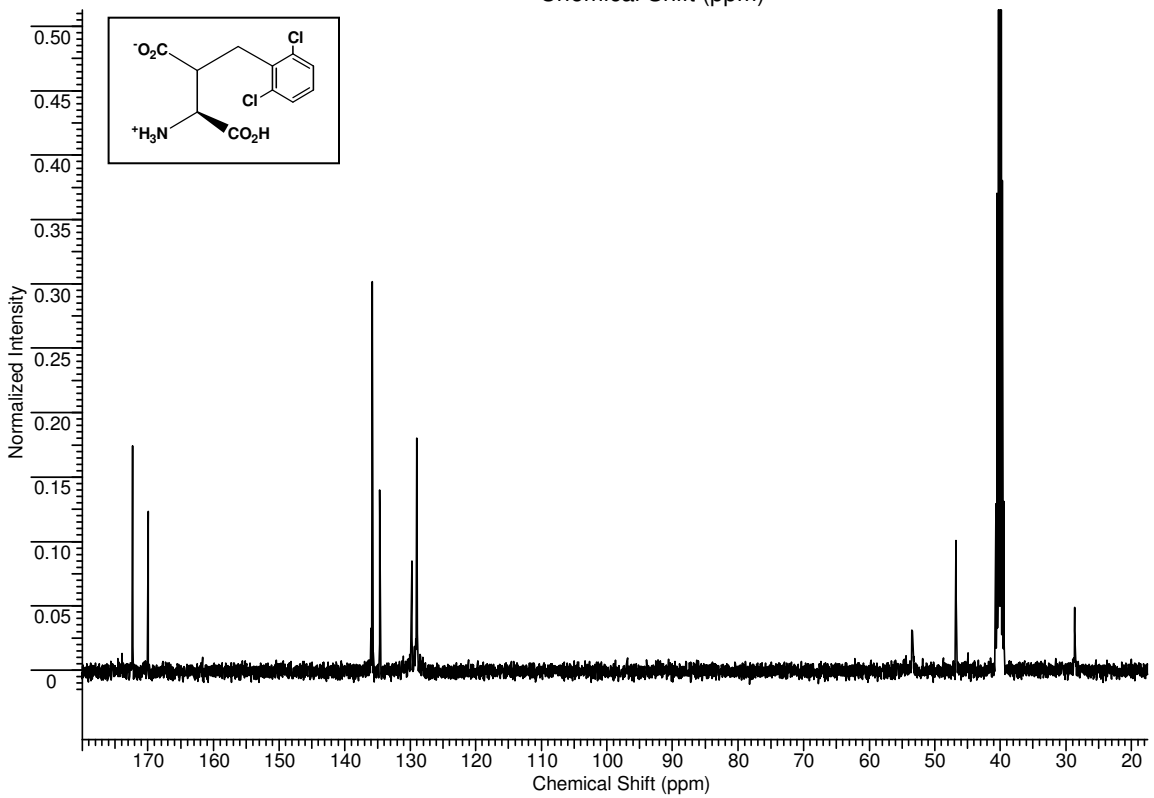

4.24. β-3 Bromo-benzyl aspartate (4F)

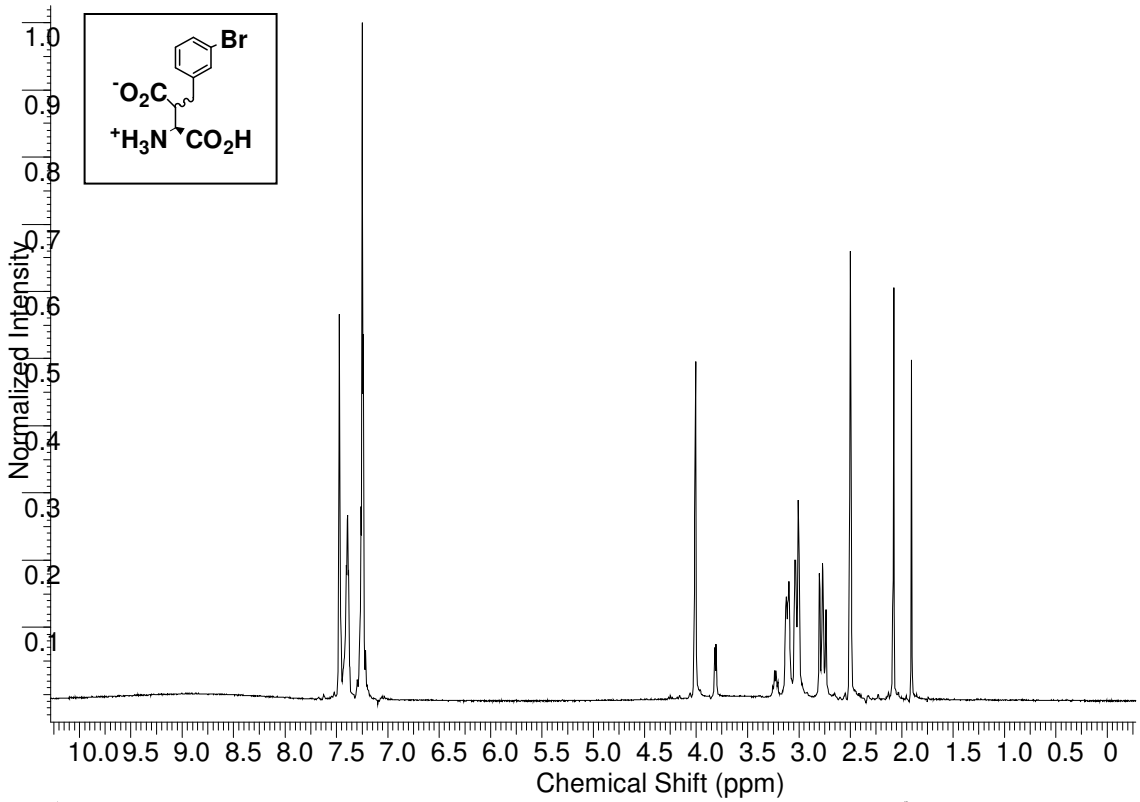

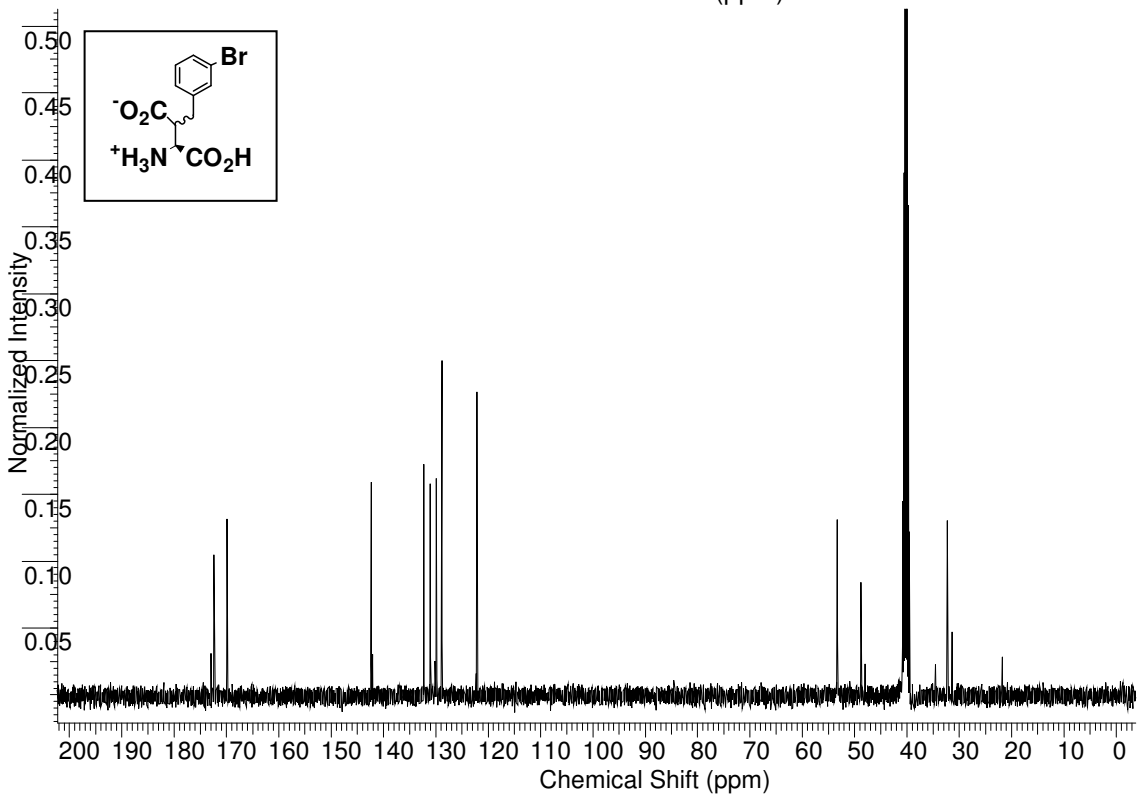

4.25. β-3 Fluoro-Benzyl aspartate (4G)

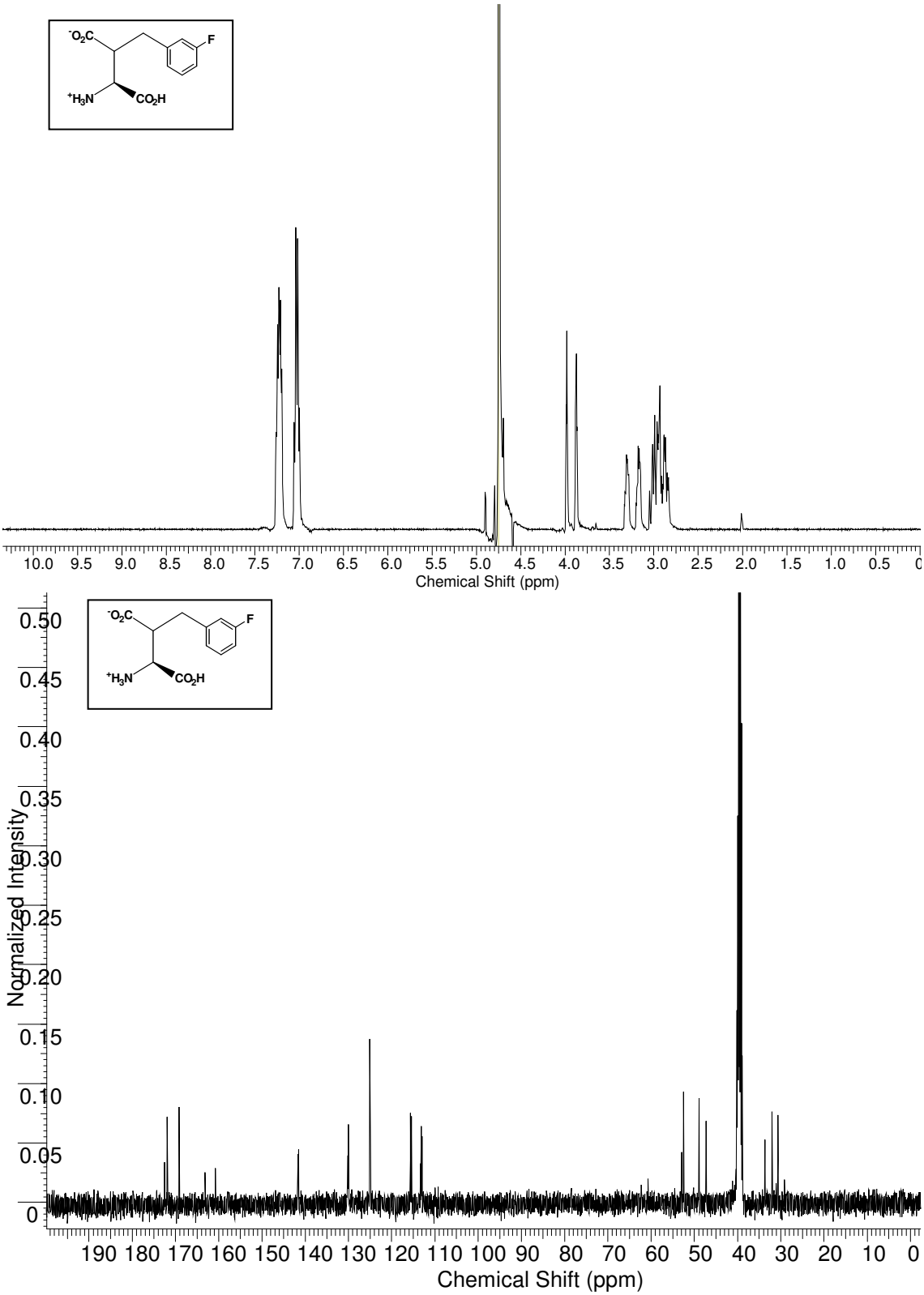

4.26. β-3 Fluoro-Benzylaspartate (4G, S,S)

Spectra a from synthesis with KHMDS, spectra b from HPLC (spectra b. reported).

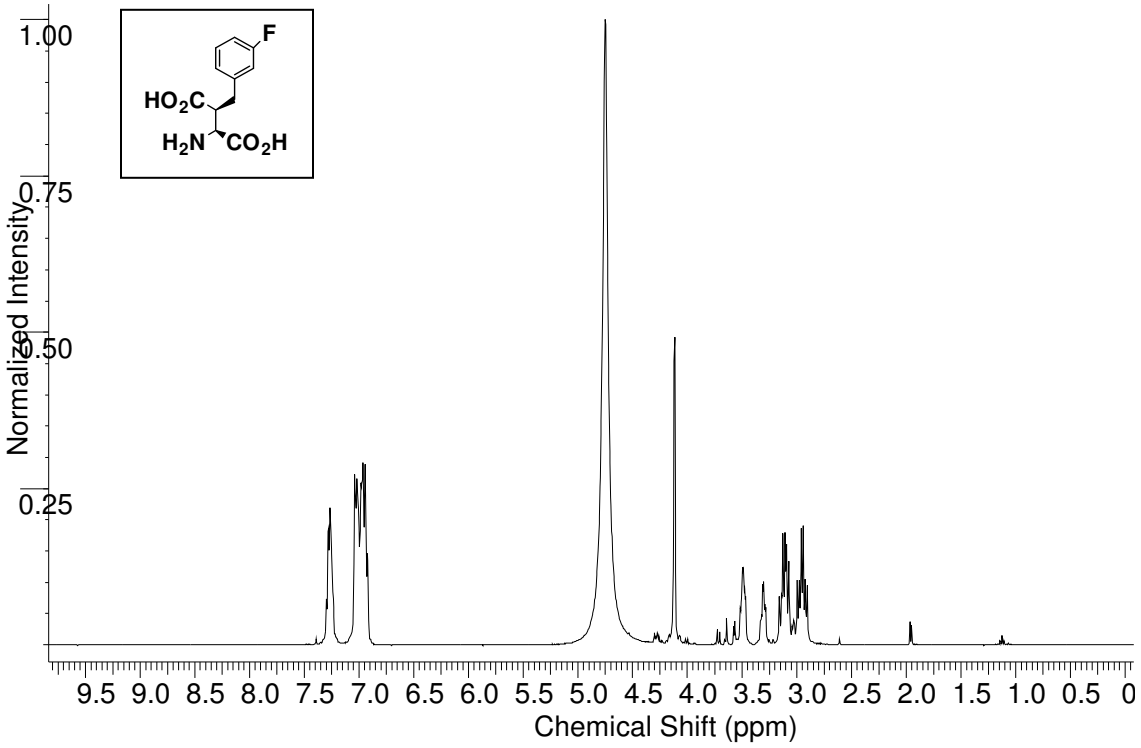

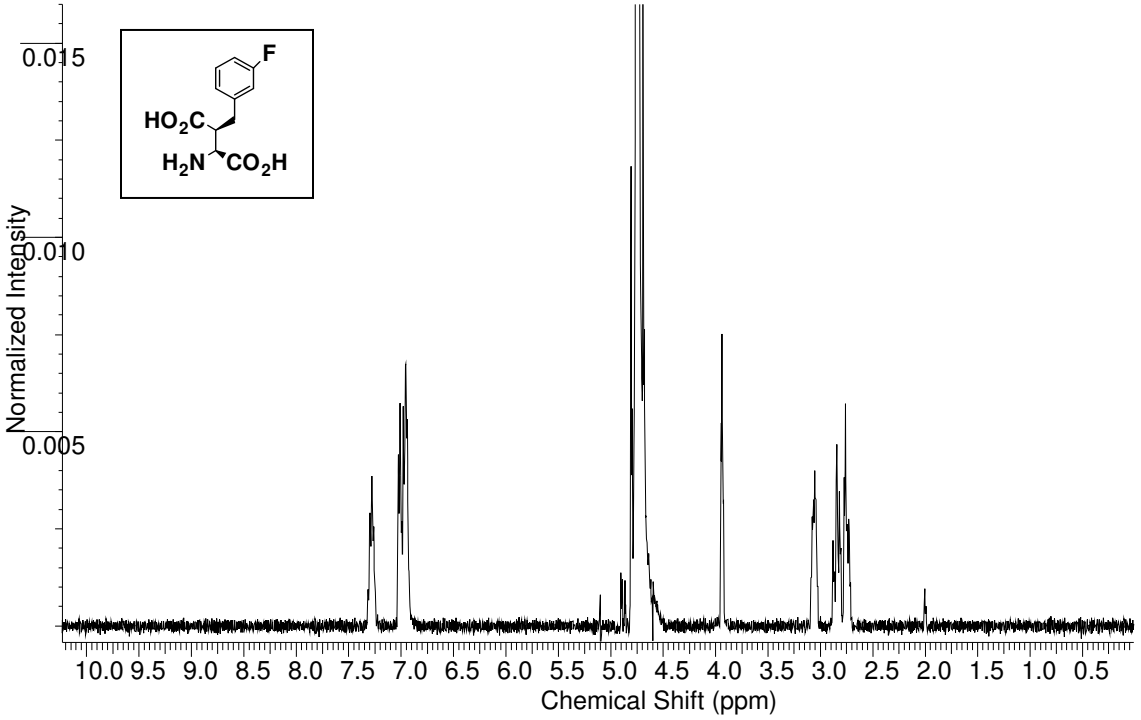

Carbon data from HPLC, spectra reported.

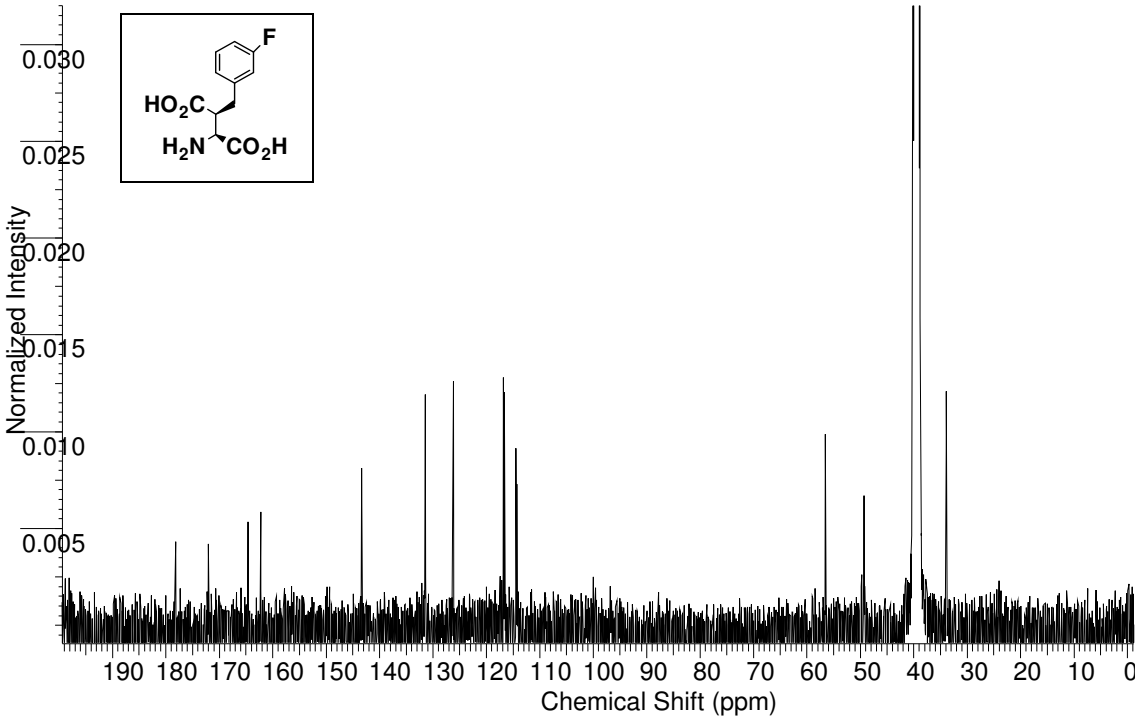

4.27. β-3 Fluoro-Benzylaspartate (4G, S,R)

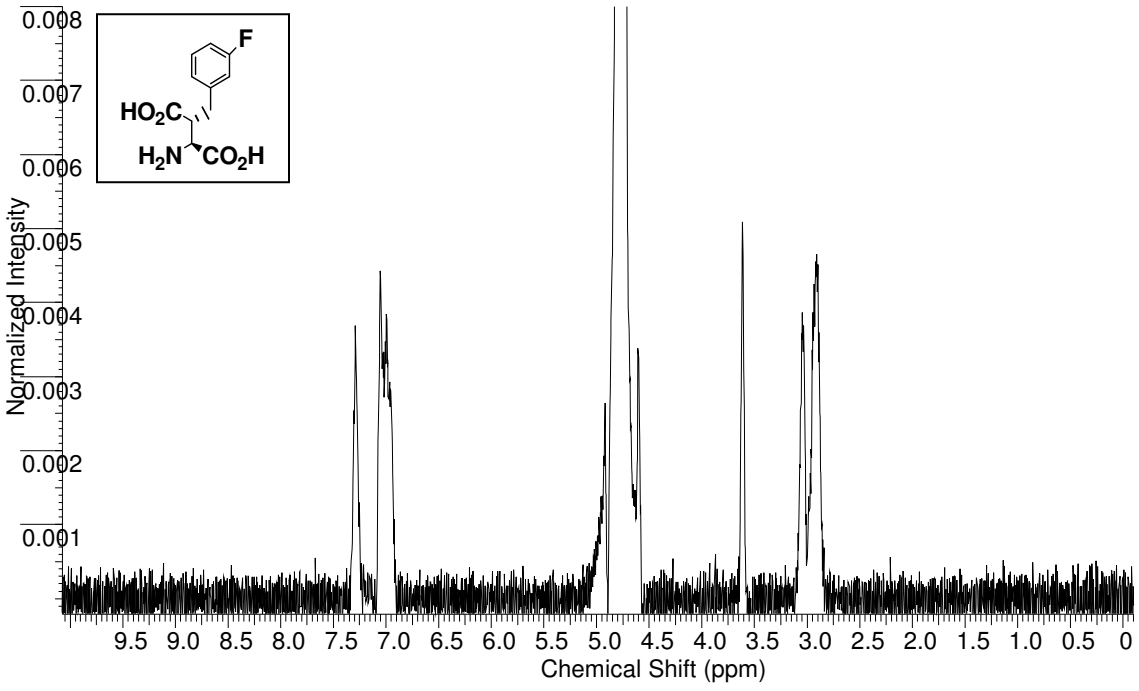

4.28. β-4-Fluoro-benzyl aspartate (4H)

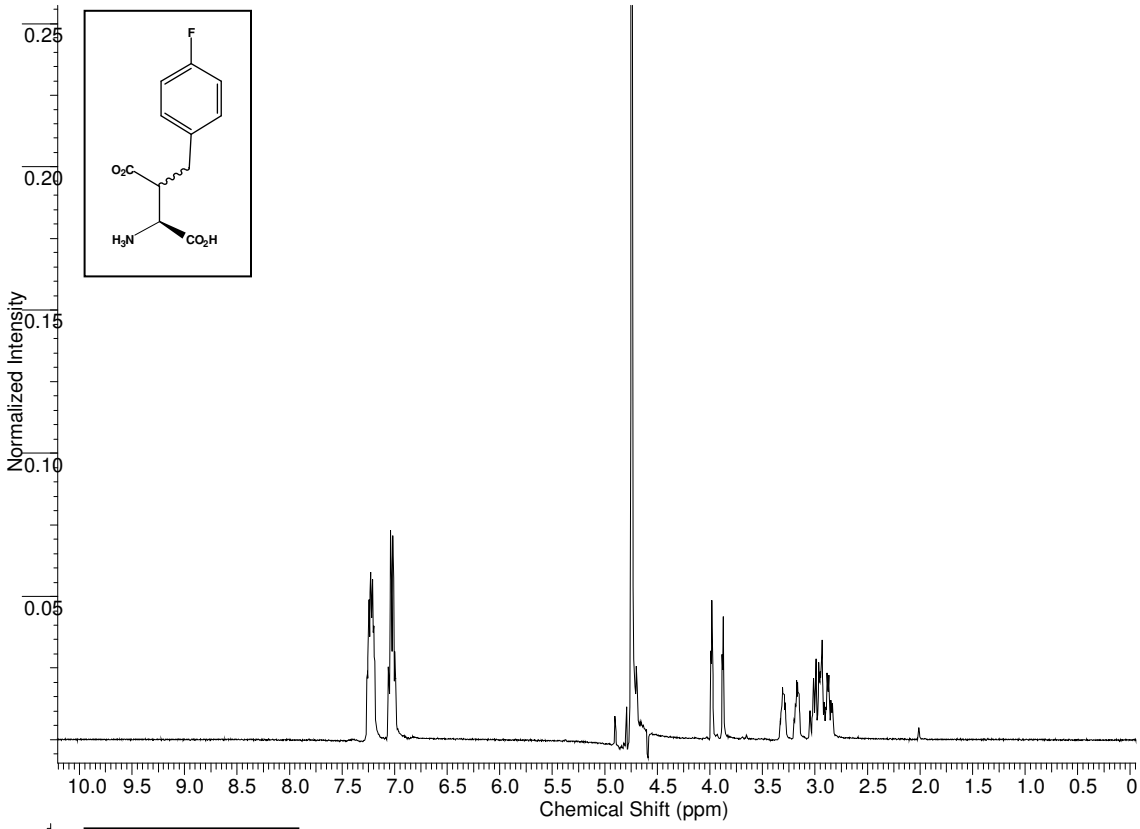

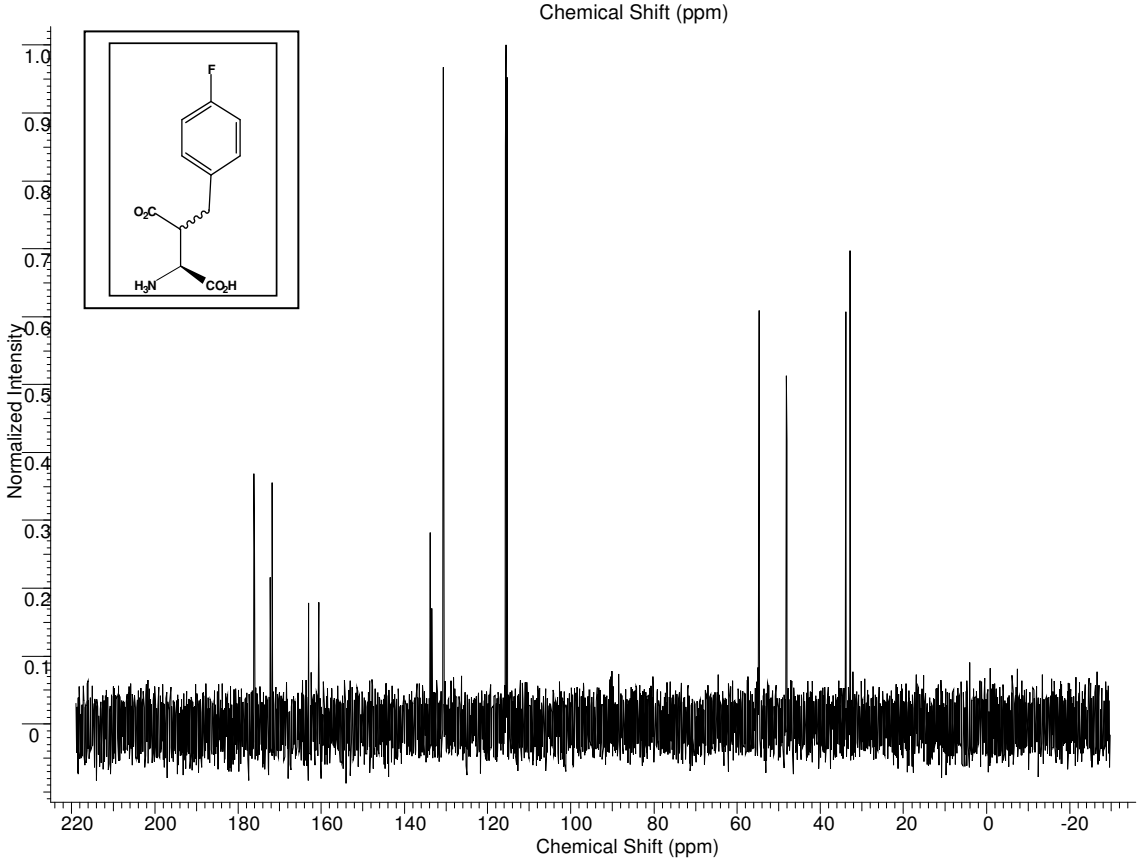

4.29. β-3-Nitro-benzyl aspartate (4l)

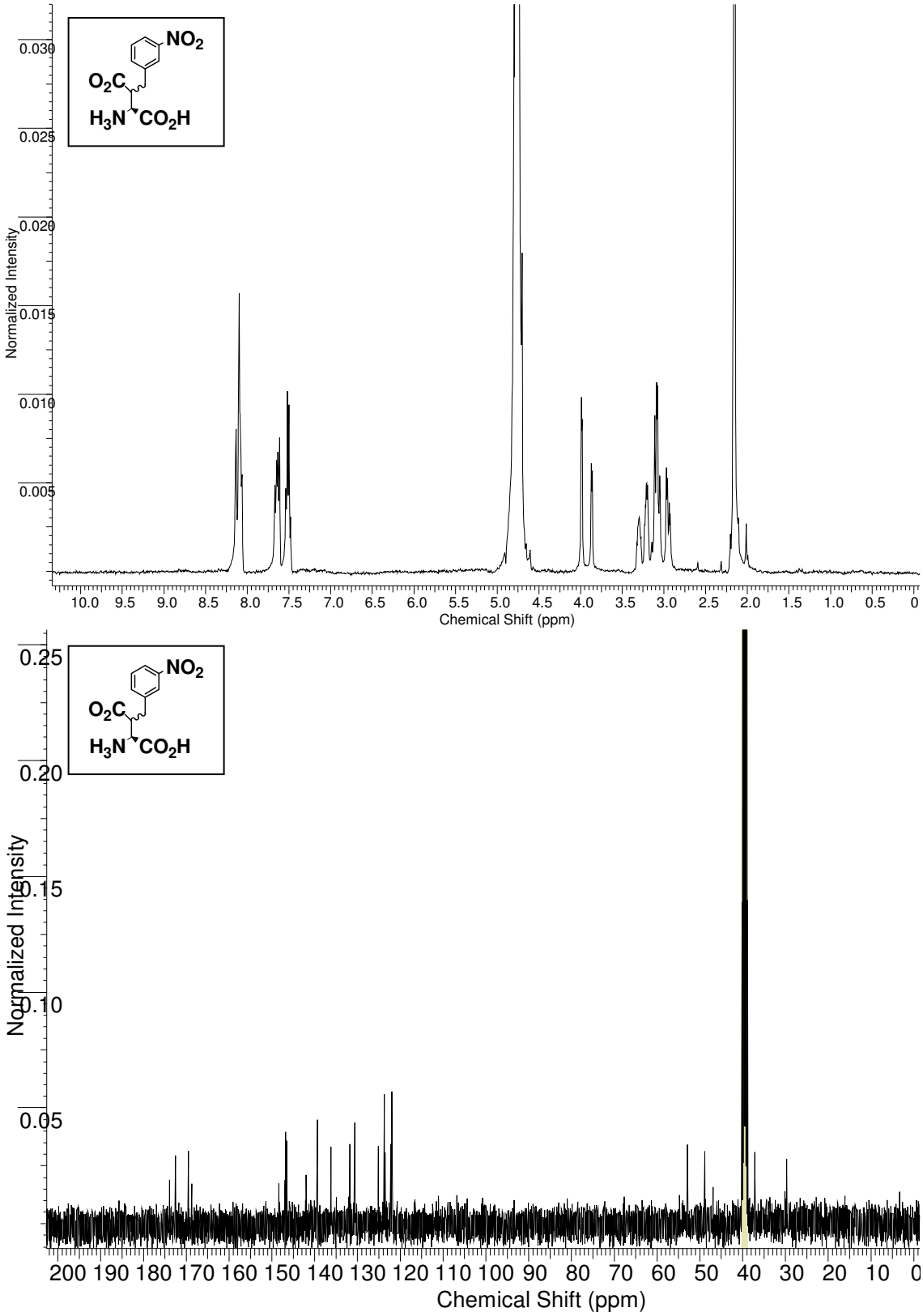

4.30. β-3 Nitro-benzylaspartate (4I, S,S)

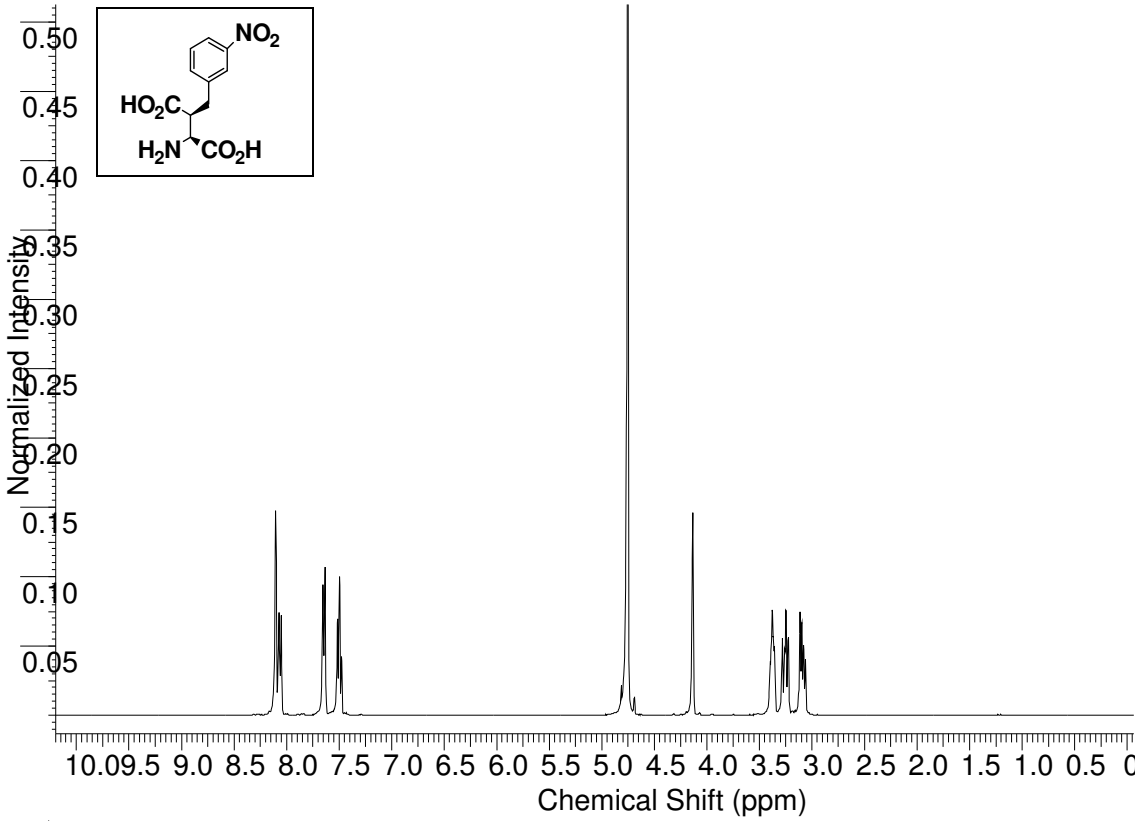

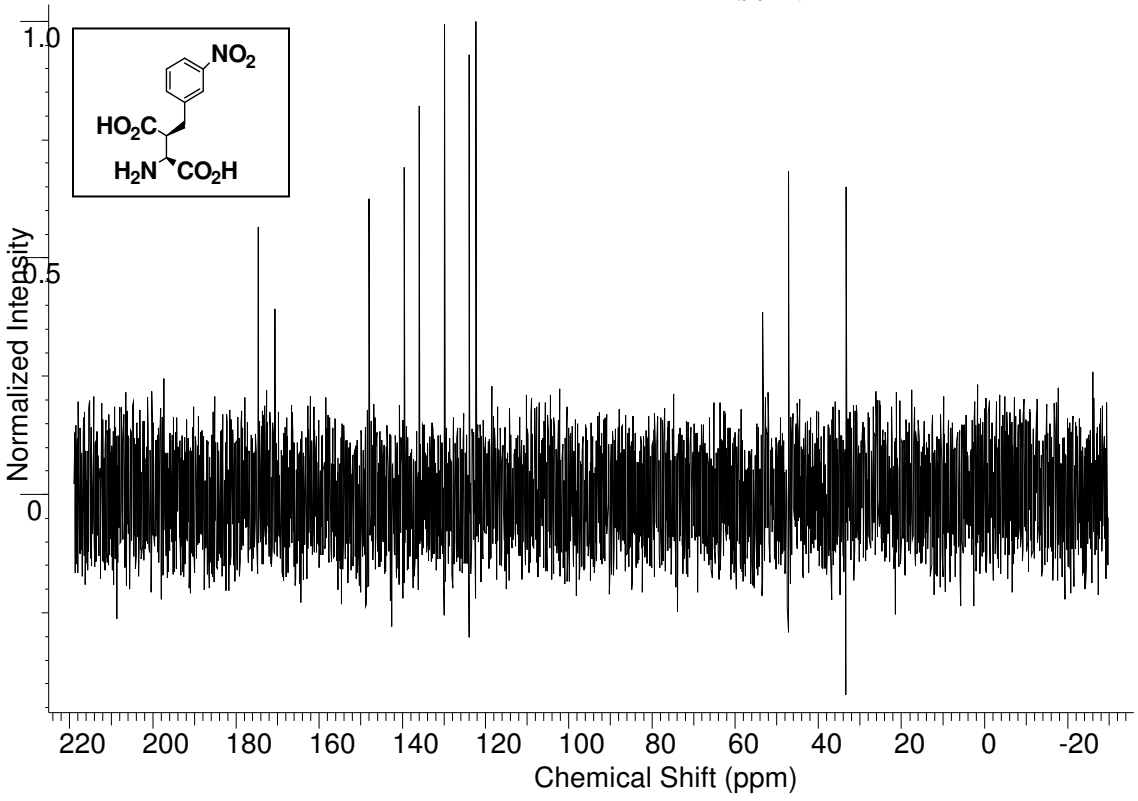

4.31. β-para-nitro-benzyl aspartate (4J)

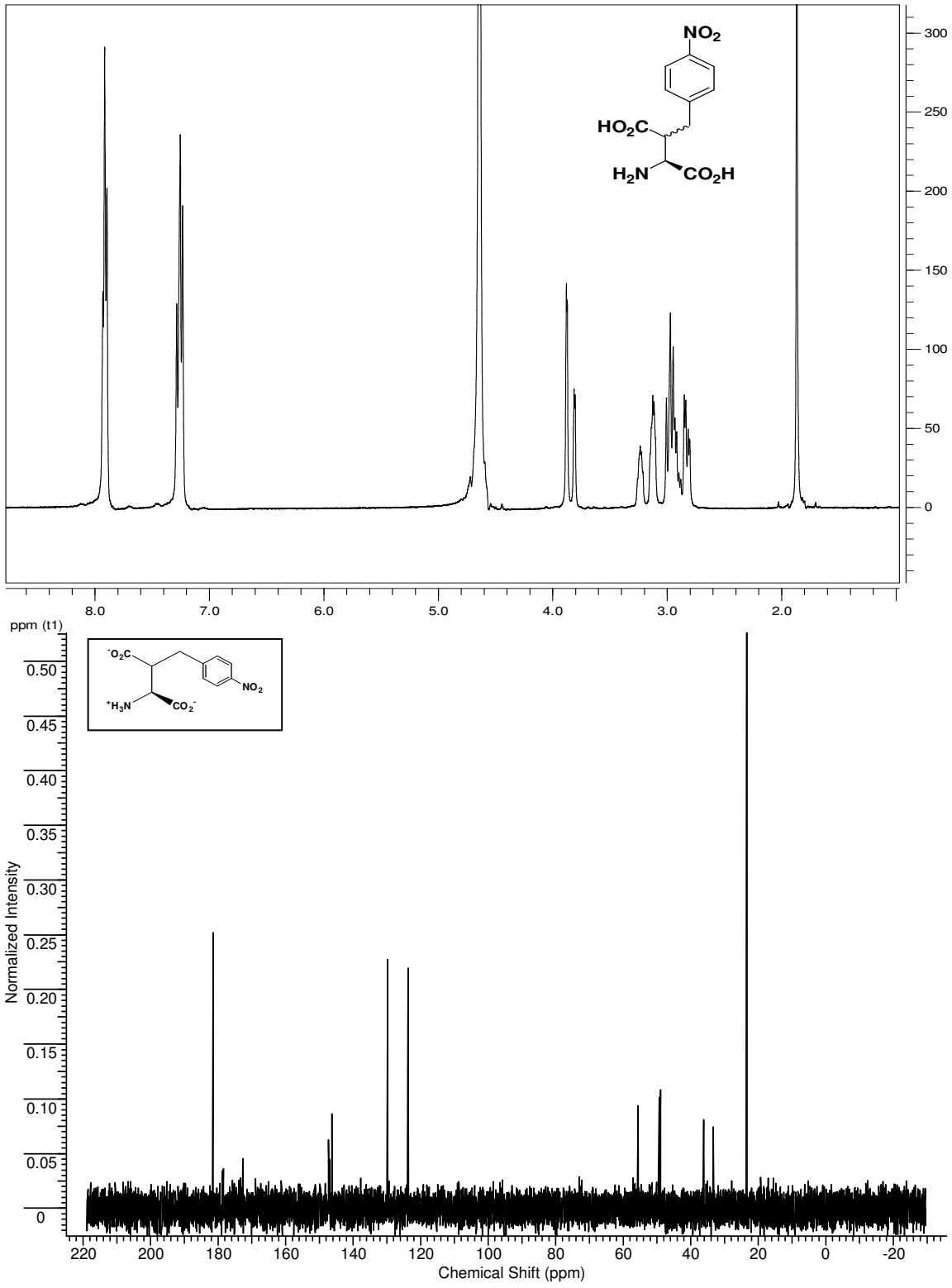

4.32. β-3 Chloro-benzylaspartate S,R